Rijkswaterstaat
Ministerie van Infrastructuur en Milieu

Mapping inland shipping emissions in time and space for the benefit of emission policy development: a case study on the Rotterdam-Antwerp corridor

TU Delft

Mapping inland shipping emissions in time and space for the benefit of emission policy development: a case study on the Rotterdam-Antwerp corridor

by

L.J.M. Segers

to obtain the degree of Master of Science

at the Delft University of Technology

Student number:	4395344	
Supervisors:	Prof. dr. ir. M. van Koningsveld	TU Delft
	Drs. O.C. Koedijk	TU Delft / Rijkswaterstaat
	Dr. Ir. R.G. Hekkenberg	TU Delft
	Ir. P.J. Jonker	Rijkswaterstaat
	Ir. S.E. van der Werff	TU Delft
	Ir. M. Jiang	TU Delft

TU Delft

Preface

This thesis represents the final stage of my study time at the Delft University of Technology. This study has been conducted as the last part of my master, to obtain the Master of Science degree in Civil Engineering, within the master track Hydraulic Engineering. This research was carried out in collaboration with Rijkswaterstaat, by means of a graduate internship.

Everything you have learned during your student days comes together in your master thesis: your substantive and scientific knowledge, of course, but also the skills you developed to take responsibility, to work together, and to be assertive in asking questions and taking decisions. Because you are fully in charge of your own research, which is such a big project, in the beginning it felt like a leap of faith. I started with my thesis when we were just at the start of the COVID-19 pandemic. This resulted in the fact that I have been working from home from the start of my thesis, and only met my fellow students and supervisors in online environments. This took some time getting used to in the beginning, but now we don't know even better. Although everything was online, I have always been able to rely on my supervisors. A fully online graduation also brought numerous advantages: online meetings always made it easy for my entire committee to join, and the communication with my professor went super smoothly via chatting in Teams.

Bringing this research to a good end would certainly not have been possible without the help of others. Therefore I would like to take this opportunity to express my gratitude to the people who have supported and guided me through this process.

First of all, I would like to thank Mark van Koningsveld, the chair of my graduation committee. Because of his great enthusiasm and dedication to the topic, he was able to keep motivating me throughout the process. I would also like to thank Solange van der Werff in particular, who has taken a lot of time for me, when I needed a sympathetic ear, or to help me out with programming issues. I also would like to thank the other committee members, Pieter Jonker, Otto Koedijk, Robert Hekkenberg and Man Jiang. Due to the different backgrounds of the members of the committee, I was able to call on a lot of knowledge and I was able to learn a lot from the input I received.

I would like to close off by thanking my friends and family. It hasn't always been easy during my student days, but I could always fall back on you, and you always continued to support me. I am very grateful for that. I would like to thank Anne and Jacco in particular: without you this would truly not have been possible.

Loes Segers
April 2020

Abstract

The pressure to reduce emissions in the sector of inland shipping is increasing. In the Netherlands, a Green Deal has been drawn up for inland navigation, which defines goals for the upcoming years, concerning CO_2 emissions and environmental pollutants. The increasing pressure gives rise to the question how to get insight into the emission from inland shipping. In the context of CO_2 emissions, the global climate effect is mainly of importance. But considering environmental pollutants such as nitrogen oxides (NO_x) and particulate matter (PM_{10}), the local effect is even more important. This asks for insight into the emission distribution along an inland waterway network. To date, a tool is lacking that is able to map the potential emission of an individual inland ship as a function of time and space. Various studies have been conducted into emissions from inland shipping, but most of these studies concern only rough estimates of total emission levels and are not suitable to down drill the output to the emission of a single inland ship.

The main objective of this study is to develop a method that is able to map the potential CO_2, PM_{10} and NO_x emission levels of inland shipping on a certain waterway network, as a function of time and space. This way, the emission hotspots can be identified. The method is based on a bottom-up approach, that uses the dimensions of a vessel, the sailing speed and the waterway characteristics to calculate the energy consumption and corresponding emissions of a single inland vessel. This method can be used in the support of development and evaluation of emission policies. To illustrate the potential of this method, it is applied to a case study: the inland fleet on the Rotterdam-Antwerp corridor, one of the main transport axes in the Netherlands.

A literature study was conducted to develop this bottom-up method to estimate the emissions of a single ship as function of time and space. This started with estimating the resistance, by subdividing it into different resistance components. Besides the effect of ship dimensions and travelling speed, the additional resistance due to limited water depth has been taken into account. The resistance a ship experiences, determines how much power a ship requires, which can be translated to energy consumption. Afterwards, a literature study is performed to translate the energy to potential emission rates. This is done by means of emission factors, taking into account the engine age and the partial engine load.

Subsequently, the developed method has been applied to observed and simulated data of inland shipping. At first, the method has been applied to observed AIS-data of one day of the Rotterdam-Antwerp corridor. The data set provides a detailed time series with the geographical position of each single ship in the fleet and the ship characteristics. A Fairway Information System (FIS) network has been implemented to take into account the waterway characteristics. By applying the developed algorithms to the dataset, the emissions are computed per ship per timestamp. By summing the emissions on the network, the distribution of potential emissions is mapped along the corridor: this is the 't0 emission scenario', showing the potential emission distributions of one day (2 September 2019, 1928 ship trajectories). The emissions are expressed in gram per meter. Second, a Python model has been developed that simulates this 't0' case. The main reason for developing a model is that the model can be used in support of development and evaluation of emission reduction policies. The developed model uses an origin-destination matrix, resulting from the AIS data, as input to simulate the fleet. The FIS network is used again to account for fairway properties. The model simulates the fleet along the corridor, resulting in a simulated time series. By applying the algorithms to this time series, the emission per ship per timestamp can be computed in the same way as with the AIS data, and the emissions can be summed on the waterway network: the output is the simulated 't0 emission scenario'.

A number of conclusions can be drawn, based on the output of the AIS data and the simulation model. The 't0 emission scenario' resulting from AIS data shows high emission levels around locks (where ships are stationary for some time, but the engine keeps on idling, resulting in accumulation of emissions). Also relatively high emission levels can be indicated on waterway sections with high traffic intensities or high average sailing speeds. The developed model is able to create total emission output that deviates with just 0.3% - 3.8% from the 't0' case. The model is also able to compute a quite similar emission distribution: the emission levels of the model per edge of the network are compared the the emission levels of the same edge in the 't0 emission scenario'. For the majority of the main waterways of the corridor, the model simulation deviates 0-20% from the emission distribution of the 't0' case.

To show the potential of the model to use it for evaluation of emission reduction policies, a first assessment of three alternative measures has been performed: the effectiveness of a 'zero emission policy' at locks, fleet renewal and a speed limit. A 'zero emission policy' at locks has especially a significant local effect: there is no more accumulation at lock areas. Fleet renewal is a promising measure considering environmental pollutants, with a potential emission reduction of 33% of NO_x, and 67% of PM_{10}, when replacing all engines in the fleet older than the year 2007 by new ones. A speed limit can also be an effective measure: a first assessment showed that a speed limit of 12 km/h can lead to a potential CO_2, PM_{10} and NO_x emission reduction of 27, 19 and 24 percent respectively.

There are a number of important limitations of this research. At first, we have not taken into account currents. The developed method is able to incorporate currents, but because of time limitations and no access to the right information, still water has been assumed. This is an appropriate assumption for the majority of the corridor, but some fairways (Western-Scheldt, Eastern-Scheldt, the river Maas) are dealing with currents, and therefore the output of the model is less reliable on these locations. It is recommended for future research to incorporate currents along the corridor and take them into account in the calculations of emissions. Second, the developed model makes use of average speeds. The current model gives a proper initial estimate of the emission patterns, but for further research it is interesting to implement speed variations, to improve the simulation of emission distributions across the network. Third, the model makes use of a lock simulation element, which is only able to handle one ship at the time. To simulate locking processes more properly, and to be able to map the emissions around locks in a better way, development of this lock simulation element is required.

Summarizing, a method was developed that estimates the emissions of a single inland vessel as a function of time and space. This method has been applied to an observed AIS time series of the Rotterdam-Antwerp corridor, to map a 't0 emission scenario', and to a time series resulting from a model simulation. This model is able to simulate the 't0' case, and provides a tool to assess alternative future emission reduction policies.

Abstract (NL)

De druk om emissie te reduceren in de binnenvaartsector neemt toe. In Nederland is een Green Deal opgesteld voor de binnenvaart, waarbij doelen zijn gedefinieerd voor de komende jaren, wat betreft emissie van CO_2 en milieu verontreinigde stoffen. Deze toenemende druk vraagt om inzicht in de emissies van de binnenvaart. In de context van CO_2 emissie is voornamelijk het globale klimaateffect belangrijk. Voor emissie van milieu verontreinigde stoffen zoals stikstof oxiden (NO_x) en fijnstof (PM_{10}) is het lokale effect van groter belang. Hierom is inzicht nodig in de verdeling van emissies over het binnenvaartnetwerk. Tot op heden is er nog geen instrument ontwikkeld dat de potentiële emissie van een individueel binnenvaartschip in kaart brengt als functie van plaats en tijd. Verschillende onderzoeken zijn uitgevoerd waarin wordt gerekend aan de emissies van de binnenvaart, maar de meeste van deze studies beperken zich tot grove schattingen van totale emissielevels en kunnen niet gebruikt worden om de emissie output terug te brengen naar de emissie van een enkel schip.

Het belangrijkste doel van dit onderzoek is een methode ontwikkelen waarbij de potentiële emissie van CO_2, PM_{10} en NO_x in kaart kan worden gebracht op een waterwegennetwerk, als een functie van plaats en tijd. Op deze manier kunnen locaties met hoge emissielevels worden geïdentificeerd. De ontwikkeling van deze methode is gebaseerd op een bottom-up aanpak, waarbij de afmetingen van het schip, de vaarsnelheid en de karakteristieken van de waterweg worden gebruikt om het energieverbruik en bijbehorende emissie van een individueel schip te schatten. Deze methode kan worden gebruikt ter ondersteuning van het ontwikkelen en evalueren van beleidsmaatregelen om emissies te reduceren. Om het potentieel van deze methode te illustreren, wordt de methode toegepast op een case studie: de binnenvaartvloot op de corridor Rotterdam-Antwerpen, een van de belangrijkste transportassen in Nederland.

Een literatuurstudie is uitgevoerd om deze bottom-up methode te ontwikkelen, om zo de emissie van een individueel binnenvaartschip te schatten als functie van plaats en tijd. Dit begint bij het schatten van de weerstand, welke kan worden onderverdeeld in verschillende weerstandscomponenten. Bij deze schatting wordt naast het effect van de afmetingen van het schip en de snelheid, ook rekening gehouden met extra weerstand door limitaties in waterdiepte. De weerstand die een schip ervaart, bepaalt hoeveel vermogen een schip nodig heeft, wat vervolgens vertaald kan worden naar energieverbruik. Hierna is er een literatuurstudie uitgevoerd om het energieverbruik te vertalen naar potentiële uitstoot. Deze vertaling is gebaseerd op zogenaamde emissie factoren, waarbij de leeftijd van de motor en de gedeeltelijke motorbelasting een belangrijke rol spelen.

Vervolgens is de ontwikkelde methode toegepast op geobserveerde en gesimuleerde data van de binnenvaart. Allereerst is de methode toegepast op geobserveerde AIS-data van één dag op de corridor Rotterdam-Antwerpen. Deze data bevat een gedetailleerde tijdreeks met de geografische positie van ieder schip in de vloot en de bijbehorende scheepskarakteristieken. Een netwerk wat resulteert uit een vaarweginformatiesysteem (FIS) is geïmplementeerd, om zo de karakteristieken van de waterweg mee te kunnen nemen. Door de ontwikkelde algoritmes toe te passen op de dataset, kunnen emissies per schip per tijdsstap worden geschat. Door de emissies vervolgens op te tellen op het netwerk, kan de verdeling van de potentiële emissie in kaart worden gebracht langs de corridor: dit is het 't0 emissie scenario', dat de potentiële emissie laat zien van één dag (2 September 2019, 1928 scheepstrajecten). De emissies worden uitgedrukt in gram per meter. Vervolgens is een Python model ontwikkeld dat deze 't0' case simuleert. De belangrijkste reden om een model te ontwikkelen, is dat dit model gebruikt kan worden in de ondersteuning van de ontwikkeling en toetsing van emissiereductie beleid. Het ontwikkelde model maakt gebruik van een herkomst-bestemmingsmatrix, die voortkomt uit de AIS data, en als input wordt gebruikt om de vloot te simuleren. Het FIS netwerk wordt opnieuw gebruikt om de waterweg karakteristieken mee te nemen. Het model simuleert de vloot langs de corridor, wat resulteert in een gesimuleerde tijdsreeks. Door de algoritmes toe te passen op deze tijdsreeks, kan de emissie per schip per tijdsstap worden geschat, op eenzelfde manier als gedaan werd met de AIS data, en kunnen de emissies worden opgeteld op het netwerk: de output is het gesimuleerde 't0 emissie scenario'.

Er kunnen een aantal conclusies worden getrokken, gebaseerd op de output van de AIS data en het simulatie model. Het 't0 emissie scenario' wat voortkomt uit de AIS data, laat hoge emissielevels zien rondom sluizen (waar schepen stationair zijn voor een bepaalde tijd, maar ze de motor laten draaien, wat resulteert in accumulatie van emissie). Ook kun je relatief hoge emissielevels zien op waterweg secties waar de verkeersintensiteit

hoog is of de gemiddelde vaarsnelheid hoog is. Het ontwikkelde model is in staat om totale emissie output te genereren dat slechts 0.3% tot 3.8% afwijkt van de 't0' case. Het model berekent ook een redelijk vergelijkbare emissie distributie: de emissielevels van het model per stukje netwerk zijn vergeleken met de emissielevels van datzelfde stukje netwerk in het 't0 emissie scenario'. Voor het overgrote deel van de hoofdvaarwegen van de corridor, wijkt de modelsimulatie 0-20% af van de emissie distributie in de 't0' case.

Om te laten zien wat de potentie is van het model wanneer je dit gebruikt voor het evalueren van beleidsmaatregelen om emissie te reduceren, is er een eerste toetsing gedaan van drie verschillende maatregelen: de effectiviteit van een 'zero emission policy' bij sluizen, vloot vernieuwing en een snelheidslimiet. Een 'zero emission policy' bij sluizen heeft voornamelijk een significant lokaal effect: er is geen accumulatie meer te zien rondom sluizen. Vlootvernieuwing is een veelbelovende maatregel wat betreft milieu verontreinigde stoffen, met een potentiële reductie van NO_x van 33%, en van PM_{10} van 67%. Een snelheidslimiet kan ook een effectieve maatregel zijn: een eerste toetsing laat zien dat een snelheidslimiet van maximaal 12 km/h kan leiden tot een potentiële CO_2, PM_{10} en NO_x emissie reductie van respectievelijk 27, 19 en 24 procent.

Er zijn een aantal belangrijke limitaties van dit onderzoek. Allereerst is er geen rekening gehouden met stroming. Het is mogelijk om met de ontwikkelde methode stroming mee te nemen, maar door tijdslimitaties en het ontbreken van de juiste informatie, is er stilstaand water aangenomen op de vaarwegen. Dit is een redelijke aanname voor het grootste deel van de corridor, maar een aantal vaarwegen (Westerschelde, Oosterschelde, de Maas) hebben te maken met stroming en daardoor is de output van het model minder betrouwbaar op deze locaties. Een aanbeveling is dan ook om in vervolgonderzoek stroming op de corridor op te nemen, en dit vervolgens mee te nemen in de berekeningen van emissies. Ten tweede maakt het ontwikkelde model gebruik van gemiddelde snelheden. Het huidige model geeft een geschikte eerste schatting van emissiepatronen, maar voor vervolgonderzoek is het interessant om snelheidsvariaties te implementeren, om zo de simulatie van de emissieverdeling over het netwerk te verbeteren. Ten derde maakt het model gebruik van een sluis simulatie element, wat slechts één schip per keer bedient. Om het proces rondom een sluis beter te simuleren, en het in kaart brengen van emissies daarmee te verbeteren, is het ontwikkelen van dit simulatie element een vereiste.

Kort samengevat, is er in dit onderzoek een methode ontwikkeld die de emissie van een enkel binnenvaartschip kan schatten als functie van plaats en tijd. Deze methode is toegepast op een geobserveerde AIS tijdsreeks van de corridor Rotterdam-Antwerpen, om zo het 't0 emissie scenario' in kaart te brengen, en op een tijdsreeks die voortkwam uit een model simulatie. Dit model is in staat om de 't0' case te simuleren, en dient als een instrument om verschillende emissie reductie maatregelen te toetsen.

Contents

1 Introduction

Due to the Paris Agreement of 2015 and national climate plans, the pressure to reduce emissions is increasing. Also the inland shipping sector is under pressure. To reduce emissions, it is important to create a clear picture of where emissions occur. The main goal of this thesis is to develop a method that is able to map the emissions caused by inland shipping over time and space. This way insight is gained into the potential emission distributions. The method can be used for the sake of the development of emission policies. To outline the possibilities of the method, the methodology will be applied to a case study: the Rotterdam-Antwerp corridor, one of the main transport axes in the Netherlands. The CO_2, PM_{10} and NO_x emission distributions will be mapped along the network. Emission hotspots can be identified and it will be demonstrated how the method can serve as a tool to assess future emission reduction policies.

This chapter provides a general introduction on the inland shipping sector in general, and more specifically on inland shipping in the Netherlands and on the Rotterdam-Antwerp corridor. Afterwards we dive into the problem description of this study and the research gap, followed by the definition of the research objective, scope and the research questions that are going to be answered.

1.1. Background information on IWT and the RA-corridor

1.1.1. Inland shipping in general

Inland shipping is transportation of all kind of goods by inland waterways. It is one of the main modes of transportation in the logistic chain and it plays a key role in the transportation of goods in Europe. More than 37,000 kilometres of waterways connect hundreds of European cities and industrial regions. These trade routes over water are highly valuable for industry. The river Rhine is a perfect example to illustrate this: this river is approximately 1000 kilometres long, flowing between Basel and Rotterdam. Due to the Mannheim Convention of 1868, free shipping of the Rhine became a fact, which resulted in economic success of the Rhine region. At the moment, the Rhine is one of the most busy rivers in the world considering freight transport and it is a crucial transport axes in West-Europe (Bureau Voorlichting Binnenvaart, 2017).

Inland waterway transport is a competitive alternative to other modalities like road or rail transport. At first, this is because inland navigation is environmental-friendly compared to its alternatives: it has a relatively low energy consumption per tonkilometer and it has low noise emissions. Secondly, inland shipping is a relatively safe mode of transport, especially when you consider the transportation of dangerous goods (European Commission, 2020a). In the third place, inland waterway transport is characterized by its reliability and major capacity for increased exploitation, compared to other modes of transport which are often confronted with congestion and capacity problems (Bureau Voorlichting Binnenvaart, 2017).

1.1.2. Modal share of inland shipping in Europe and the Netherlands

The modal split, which is the distribution of transportation modes, depends on the industrial activities in the area, but also the geographical location. Across Europe, rail, road, shipping and inland navigation are the main modes of transportation of goods. Underground pipelines are used in case of fixed routes, transporting large volumes of liquids. In case of urgent delivery of small cargo, cargo airlines are preferred.

Because the modal share of inland shipping depends on the geographical location, we see large differences in modal share of inland shipping between different main ports in Europe. Each main port is connected to rail, but the connections by waterways can differ between ports, since these depend on the scale, draught, waterway conditions and dimensions of locks and bridges. For example, rail transport has a large share in the modal split of the port of Hamburg: the River Elbe is not navigable everywhere and some waterway connections are not accessible to larger inland vessels. The ports of Rotterdam and Antwerp, however, are well connected by a

system of waterways: both ports link up directly to the River Rhine, which is a easily navigable connection to the hinterland (Bureau Voorlichting Binnenvaart, 2017). Figure 1.1 shows the differences in modal split between Rotterdam-Antwerp and the two main ports of Germany: Hamburg and Bremerhaven.

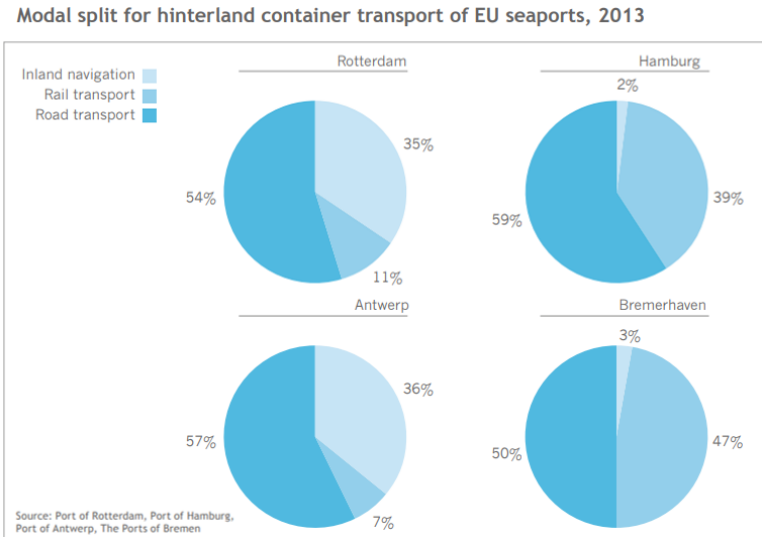

Figure 1.1: Modal split for hinterland container transport of EU ports (Bureau Voorlichting Binnenvaart, 2017)

The Netherlands has a dense network of waterways. Because the Netherlands is located at the delta of several important European rivers (such as the Rhine, Maas and Scheldt), the Netherlands is the gateway to the hinterland of Europe. In addition to the rivers, the Netherlands has several lakes and canals that connect the most important cities. This well-integrated waterway network makes inland shipping an attractive way of transport in the Netherlands (Bureau Voorlichting Binnenvaart, n.d.[b]).

The modal share of inland navigation in the Netherlands is high: currently, 34% of freight transported in the Netherlands is carried by inland shipping (CBS, 2020b). Figure 1.2 represents the modal split per EU country in 2012, which shows that the modal share of inland navigation is by far the highest in the Netherlands. With a fleet of 8000 inland ships, the Dutch fleet is the biggest and most modern fleet of Europe.

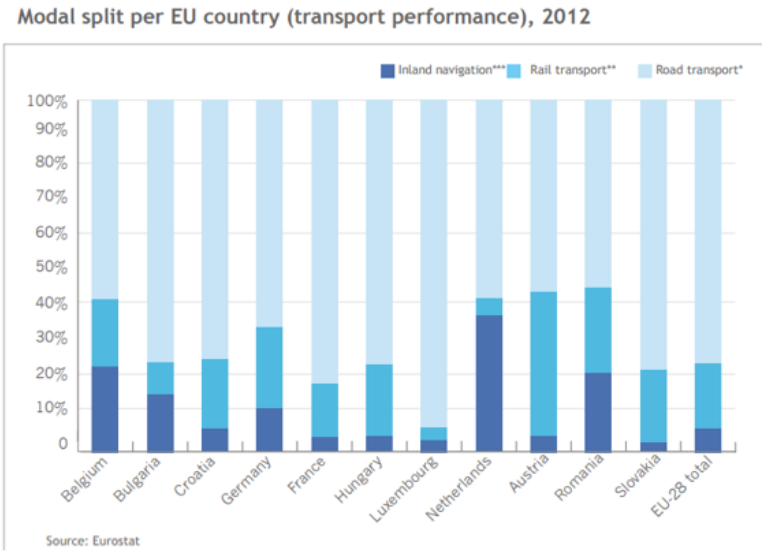

Figure 1.2: Modal split per EU country, based on transport performance in ton km (Bureau Voorlichting Binnenvaart, 2017)

1.1.3. The Rotterdam-Antwerp corridor

The Rotterdam-Antwerp corridor is one of the main transport axes of the Netherlands, especially considering inland navigation. The waterway network forms an important connection between Rotterdam and Antwerp: the transport of goods between these two biggest port of Europe is for 75% covered by inland shipping. This

corridor is important for the Dutch and Flemish economy: all ports within the corridor create (direct or indirect) 440.000 jobs in the region. In addition, the corridor is part of the Dutch-Flemisch Delta, which is seen as the entrance gate to Europe: the ports are well connected to the hinterland and are therefore also of importance for the economy of Europe as a whole (Royal HaskoningDHV, 2018).

The region of the corridor Rotterdam-Antwerp is characterized by its diversity: there are urban regions with a lot of economic activity and high concentration of population on one hand, and agriculture, nature and the vulnerable delta of the river Rhine and Scheldt on the other hand (Royal HaskoningDHV, 2018). The Delta landscape consists of special natural values: the islands of Zeeland and South Holland are located within the transitional area of salt and fresh water, which results in special nature reserve. Therefore, large parts of the Delta are designated as Natura-2000 areas (Royal HaskoningDHV, 2018). Because these nature reserves are located in the region of the corridor Rotterdam-Antwerp, it is even more important to consider the environmental impact of the inland fleet and how this impact can be reduced. Figure 1.3 shows the Nature-2000 areas in the region of the Rotterdam-Antwerp corridor.

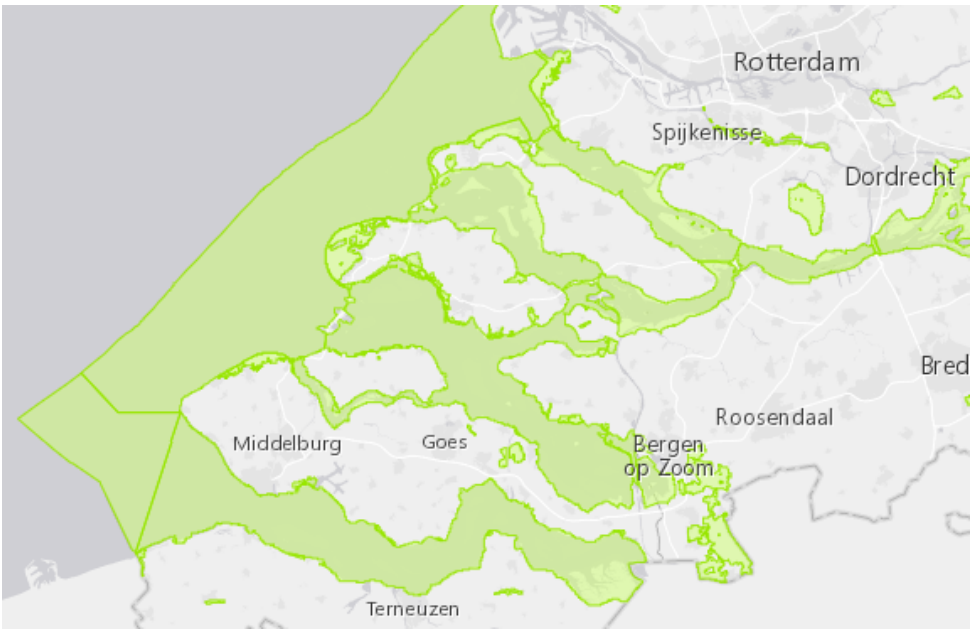

Figure 1.3: Nature-2000 areas in the region of the Rotterdam-Antwerp corridor (Natura2000, 2020)

Figure 1.4 shows the main routes of inland shipping from Rotterdam to Antwerp (and vice-versa) and the different locks on the route. The main fairways on the corridor are the Scheldt-Rhine connection (70.000 inland ships per year) and the Zuid-Beveland canal (44.000 inland ships per year) (Royal HaskoningDHV, 2018).

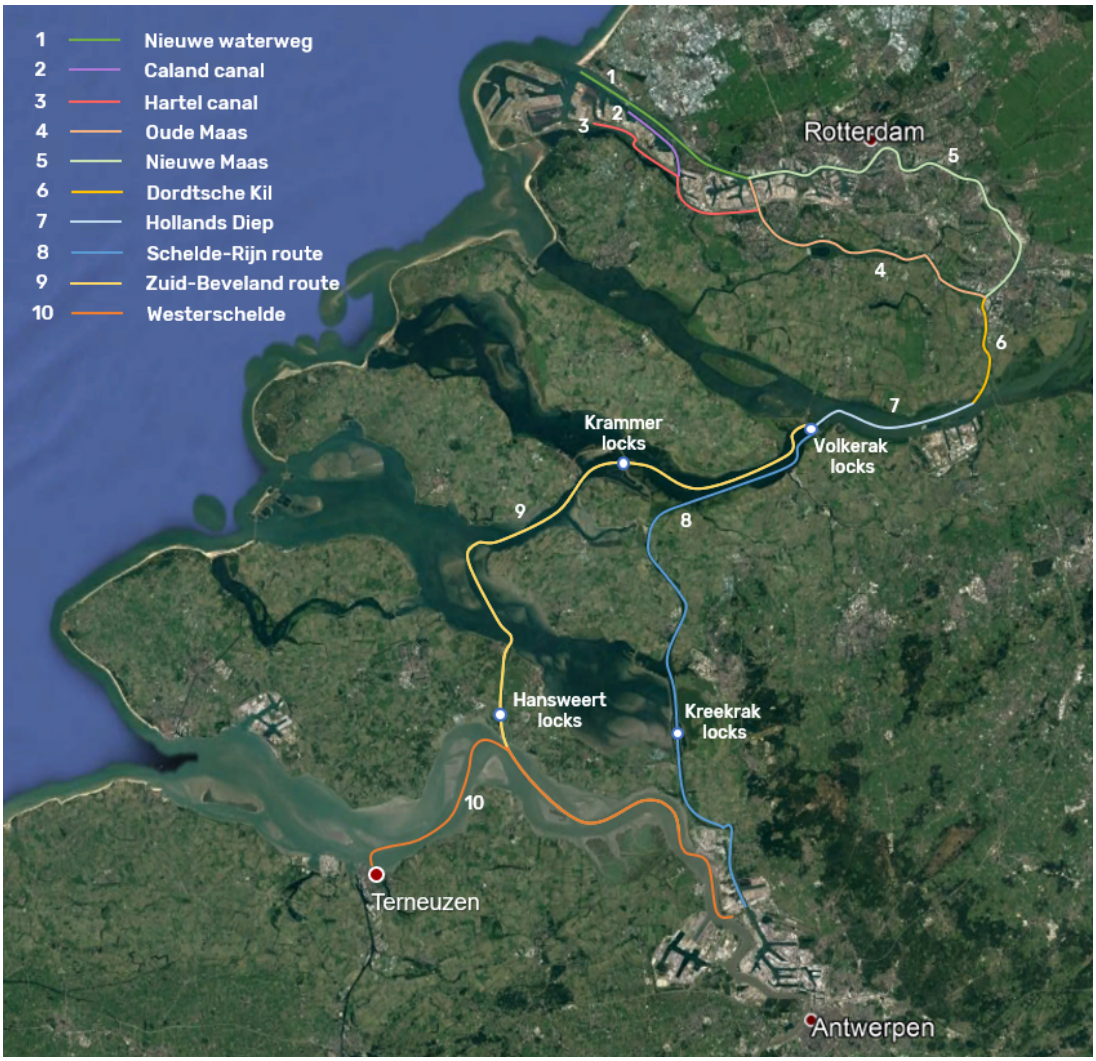

Figure 1.4: Main routes of inland shipping on the Rotterdam-Antwerp corridor

1.2. Problem description

1.2.1. Increasing pressure to reduce emissions

In 2015 the Paris Agreement was adopted: the first universal, legally binding climate agreement. It aims to limit global warming, and one of the key elements is to reduce emissions worldwide (European Commission, 2020b). As a contribution to this agreement, participating countries came up with national climate action plans. In 2019, the Netherlands has submitted a national climate agreement with ambitious goals to reduce emissions (Ministerie van Economische Zaken en Klimaat, 2019). Due to these developments, the pressure to reduce emissions is increasing, also in the sector of inland shipping.

Due to this increasing pressure, a Green Deal has been drawn up for the inland shipping sector. It defines goals and ambitions for inland shipping for the upcoming years, concerning the CO_2 emissions and emissions of environmental pollutants. These objectives are visualized in the timeline in Figure 1.5 and summarized below (Green Deal, 2019):

- 2024: A reduction of CO_2 emissions of at least 20% compared to 2015, and a reduction of environmental pollutants of at least 10% compared to 2015.
- 2030: A reduction of CO_2 emissions of 40% to 50% compared to 2015;
- 2035: A reduction of environmental pollutants of 35% to 50% compared to 2015;
- 2050: To have realized emission-free and climate-neutral inland shipping.

The increasing pressure to reduce emissions from inland shipping gives rise to the question how to get insight into the emissions patterns along an inland waterway network.

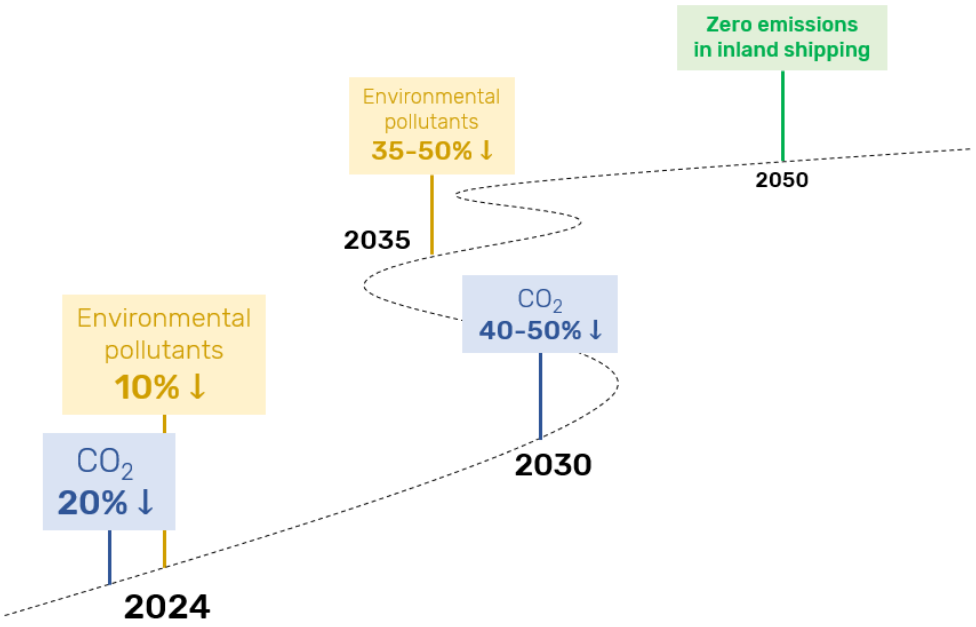

Figure 1.5: Timeline Green Deal goals and ambitions for inland navigation

1.2.2. Contribution of inland shipping to emissions

Although inland navigation is a relative sustainable mode of transport compared to other ways of transportation (in terms of emissions per tonkm), it still significantly contributes to the total emissions resulting from the transport sector: the CO_2 emissions caused by inland shipping are 5% of the total CO_2 emissions resulting from the transport sector in the Netherlands. Considering the environmental pollutants PM_{10} and NO_x emitted, the contribution of inland shipping is even higher: more than 10% of the PM_{10} emissions in the Netherlands resulting from transport can be attributed to inland navigation. For NO_x, this is even more than 12% (CBS, 2020a). Especially because the Rotterdam-Antwerp corridor crosses different Nature-2000 areas, there are strict requirements regarding emissions of environmental pollutants and it makes it even more important to reduce emissions from inland navigation in these areas.

1.2.3. Research gap

To come up with effective solution methods to reduce emission levels in inland shipping, it is important to get insight into the potential emission distribution patterns, with resolution in time and space. Estimating emissions is complex, because the energy consumption and corresponding emissions of inland vessels depend on a large number of factors. The dimensions of a vessel and the sailing speed have a significant influence on the resistance a ship experiences, and so on the required energy and the emission output. In addition, the waterway characteristics are of importance: if a ship is for example sailing in shallow water, this results in an increase of the resistance and so influences the energy consumption of the ship. It is therefore important to look for a method that takes into account both the ship characteristics of a single vessel and the characteristics of the waterway in the computation of emissions.

To date, various studies have been conducted into emissions from inland shipping, but most of these studies concern only rough estimates of total emission levels. Rijkswaterstaat developed the BIVAS model, which is a model that performs network analysis of inland water transport. The model also contains an element that computes different types of emissions from inland navigation. The model computes the total energy consumption on the waterway, and subsequently translates this to emissions (Rijkswaterstaat, 2021b). The method to calculate the energy consumption in the BIVAS model is based on literature of Bolt (2003). This method does depend on the dimensions of the ship and the speed, and it makes an assumption for an increase in resistance due to waterway restrictions. This method is developed to determine results on fleet basis or yearly basis, and therefore works with generalized assumptions, looking at a large number of vessels. Therefore, this method is not suitable to map the energy consumption of a single inland vessel.

Besides BIVAS, there are also other tools to calculate emissions of inland water transport. The National Institute for Public Health and Environment developed the calculation tool AERIUS: with this tool emission calculations

are performed for inland shipping on a yearly basis. The tool distinguishes between stationary ships and sailing ships. The stationary emission calculations take into account the total number of visits at mooring places per year, the average residence time and a stationary emission factor in kg per hour. The emission calculation of sailing vessels takes into account the total number of ship movements per year, the total distance sailed and an emission factor expressed in kg per km (RIVM, 2019). The AERIUS tool more looks at the spreading of emissions. It is a rough estimate of total annual emissions of inland shipping, but does not take into account individual ship characteristics or fairway characteristics. Insight into emission distribution over time and space is lacking.

Another calculation tool is PRELUDE: this tool is developed by TNO, commissioned by the Ministry of Infrastructure and the Environment. PRELUDE is a MS-Excel calculation tool that generates emission data of inland water transport, using the same calculation method as BIVAS, but in a relatively simplified way. The number of ships per year, times an emission factor, times a trend factor, results in a total emission output of a certain year. The calculations are based on weighted averages of number of ships and sailing speeds (Hulskotte, 2013). Although this tool takes into account different emission factors depending on the CEMT class of the waterway, it only maps the total emissions resulting from inland shipping. The tool does not have the capacity to map the emission distribution over time and space for individual ships.

The main goal of this thesis is to get insight into the potential emission distribution of inland water transport, by developing a method that is able to map the emissions of a single ship over time and space along a network. This method will be bottom-up, and takes into account the ship and fairway characteristics. The method will be applied to the case study on the Rotterdam-Antwerp corridor. By mapping the emissions along the corridor, high emission levels can be identified. The method can be used in support of development and evaluation of emission reduction measures.

In previous master thesis work of Vehmeijer (2019), a first step has been made in developing a model that estimates the total CO_2 emissions on the Rotterdam-Antwerp corridor and to compare different alternative scenarios on corridor level. She used this model to identify the impact on CO_2 emission of several infrastructural modifications: (1) increasing bridge heights on the Scheldt-Rhine canal, (2) conversion of the Bathse sluize into a lock and (3) removal of the Kreekrak locks. In addition, she assessed the effect of three different fleet scenario's: (1) a fleet with high-cube containers, (2) standard vessels and departure slots and (3) sea level rise.

Vehmeijer (2019) used relatively rough estimates of the energy consumption of inland ships, based on literature of Bolt (2003), which is also the starting point of the BIVAS model. Appendix A shows the comparison between the resistance calculation method of Vehmeijer and the method developed in this study: it shows that the resistance output of Vehmeijer is relatively high. The calculation method used by Vehmeijer takes into account the ship dimensions and the sailing speed, and includes a term to account for waterway restrictions. This method is suitable when looking at an entire fleet, averaging out disturbances, but less suitable when looking at a single vessel. In addition, Vehmeijer worked with constant vessel speeds and a fixed water depth at the trajectories she investigated. This results in the assumption that the ship's resistance is constant along the route. But to be able map emission distributions along the network, the variation in sailing speed and the waterway characteristics are important. Therefore, the method developed in this research will take the variation in water depth and vessel speed as a starting point.

In addition, Vehmeijer (2019) has drawn conclusions on the total emission of the corridor and the relative impact of different infrastructural modifications and scenarios. Her research focused on CO_2 emissions only, but the pressure to reduce emissions of environmental pollutants is increasing as well. Therefore, this research will focus on a broader spectrum of emissions: CO_2, nitrogen oxides (NO_x) and particulate matter (PM_{10}). In the context of CO_2 emissions, the global climate effect is mainly of importance. But considering NO_x and PM_{10} emissions, the local effect is even more important. Therefore insight is required in where potential high emission levels are located, instead of estimates of total emission levels. These locations can be identified by mapping the potential emission levels of the inland fleet on the corridor, distributed over time and space. To do that in a proper way, a more detailed bottom-up approach is required to calculate emissions: a method will be developed to determine the energy consumption of a single ship, and the corresponding emissions, on trip level.

Where Vehmeijer (2019) looked at an average number of ships on a yearly basis, based on IVS-90 data, and only took the total emission on the corridor into account, this study looks at the variation of emissions over time and space, based on detailed AIS-data: no studies have yet been found linking emissions from inland shipping to AIS data. AIS data provides us detailed information about the (variation in) velocities of inland vessels over

the network, which really improves the calculations of required power of a ship and so of the calculations of emissions.

The main goal of this thesis is developing a bottom-up method that is able to calculate the potential emission of a single ship, distributed over time and space, based on the ship and waterway characteristics. The main advantage of such a bottom-up method is that it gives the possibility to look at emission distributions on trip level, as well as performing these calculations for an entire fleet and look at the total distribution. Such a method makes completely down drilling possible per time and space: you can look at the total emission picture, but you can also completely break it down to single components, per time and space, and analyze which components have the largest impact. Preliminary studies on emissions from inland navigation did not yet allow full down drilling per time and space, which increases the value of developing such a method in this research.

1.3. Research objective and scope

The main objective of this research is to develop a method that is able to map the potential CO_2, nitrogen oxide and particulate matter emission levels of inland shipping on a certain network, as a function of time and space. This way, the main sources of emissions can be identified. The method will be based on a bottom-up approach, that uses the dimensions of a vessel, its velocity and the waterway characteristics to calculate the energy consumption and corresponding emissions of a single inland vessel. By performing these calculations for the entire fleet, the emissions can be summed on the network and the emission distribution can be mapped. This method can be used for the sake of the development of emission policies.

To illustrate the possibilities this method offers, it will be applied to a case study: the Rotterdam-Antwerp corridor, one of the main transport axes in the Netherlands. This brings us to the scope of this research: we will consider inland waterway transport on the Rotterdam-Antwerp corridor, only taking into account freight transport and neglecting recreational craft. Previous research of Vehmeijer (2019) only took into account a part of the Rotterdam-Antwerp corridor (including the Scheldt-Rijn canal and the Zuid-Beveland route). This thesis will focus on the entire corridor, as presented in Figure 1.4. The focus is on CO_2, NO_x and PM_{10} emissions: other types of emissions are not going to be taken into account (which is further elaborated in Chapter 4). The emission distributions will be mapped on the Rotterdam-Antwerp corridor. The diffusion of emissions in the air is not part of this research: the focus will be on the potential locations where emission from inland shipping takes place. This means that the method developed in this study gives no assurance if these emissions are actually emitted. This is because many factors have influence on actual emissions: for example the wind, the position of the exhaust of the engine and if certain emission filters are applied to the exhaust, can have influence on actual emission levels.

1.4. Research questions

To achieve the defined research objective, the following main research question has been defined:

''How to develop a method that can map the CO_2, NO_x and PM_{10} emission potentials of inland shipping on an inland waterway network as a function of time and space, which can be used in support of the development and evaluation of emission policies?"

In order to answer this research question, four sub-questions are formulated. The approach of these sub-questions is further elaborated in the following section.

1. "How to methodologically estimate the energy consumption and emission potential of an individual inland vessel as a function of time and space?"

2. "Can we apply this method on observed AIS data and to what extent can we derive an estimate of emission patterns based the observed fleet (t0 emission scenario)?"

3. "Can we apply this method on simulated data and to what extent can we reproduce the AIS-based t0 emission scenario? What explains the differences between the two outcomes, if any?"

4. "Can we subsequently apply the developed algorithm to simulate alternative emission reduction policies and evaluate the effectiveness of different measures?"

1.5. Approach and methodology

To answer the different sub-questions of this research, the approach and methodology of each question will be discussed.

Sub-question 1: "How to methodologically estimate the energy consumption and emission potential of an individual inland vessel as a function of time and space?"
Based on literature study, a detailed bottom-up method will be developed that is able to estimate the energy consumption of a single inland vessel as a function of time and space. This starts with developing a method to estimate the resistance of a ship, taking into account the effects of the ship dimensions, travelling speed and waterway characteristics. The resistance a ship experiences, determines how much power a ship requires. Subsequently, the energy consumption of a certain inland vessel can be estimated. Afterwards, a literature study is performed to translate the energy consumption method to corresponding emission rates of CO_2, NO_x and PM_{10} of a single inland ship.

Sub-question 2: "Can we apply this method on observed AIS data and to what extent can we derive an estimate of emission patterns based the observed fleet (t0 emission scenario)?"
Rijkswaterstaat provided an AIS-dataset with observed data of the fleet on the Rotterdam-Antwerp corridor. AIS stands for Automatic Identification System: the AIS-dataset provides a detailed time series with the geographical position of each single ship in the fleet and several ship characteristics (vessel type, ship dimensions, velocity). The developed method to estimate the energy consumption and emission potential will be applied to each single ship in the observed data. The data provides the vessel characteristics, and the waterway characteristics are taken into account by implementing a Fairway Information System (FIS) network. The emission calculations can be performed for the entire fleet and the potential emission distributions can be mapped along the network as a function of time and space. This will be the t0 emission scenario.

Sub-question 3: "Can we apply this method on simulated data and to what extent can we reproduce the AIS-based t0 emission scenario? What explains the differences between the two outcomes, if any?'
A Python model will be developed with the goal that the model is able to simulate the t0 emission scenario resulting from the AIS data. The Python package OpenTNSim (Open Source Transport Network Simulation) will be used to simulate the fleet on the network by discrete time simulation. The fleet characteristics are input of this model and are based on analysis of the AIS-dataset (determining the amount of ships, origin-destination, ship characteristics). To take into account the waterway characteristics, the same Fairway Information System (FIS) network is implemented in the model. The fleet simulated by the model will sail on this network. The method to calculate the energy consumption and potential emission of an inland vessel is applied to the time series resulting from the model simulation. The emission rate of each individual vessel is computed per timestamp. Subsequently, the emission output will be summed on the network and the potential emission distributions will be visualized. The t0 emission scenario resulting from the AIS-data serves as validation of this model output and the differences between the model simulation and the t0 emission scenario will be identified and explained.

Sub-question 4: "Can we subsequently apply the developed algorithm to simulate alternative emission reduction policies and evaluate the effectiveness of different measures?"
The reason to develop a model that is able to simulate the t0 emission scenario, is that it can be used as a tool to support the development and evaluation of emission reduction policies. By using a model, alternative measures to reduce emissions can be implemented and simulated. The effectiveness of different future emission reduction policies can be compared and explained. In this study a first step will be made of assessing emission reduction policies, to show that the developed method can be used for this.

1.6. Report outline

This report starts with the Literature, Materials and Methods section (Part I). This part starts with Chapter 2 describing the methodology that will be used to tackle the problem step by step. In Chapter 3 and 4 a literature study is conducted to develop a method to estimate the energy consumption of an inland ship (Chapter 3) and the corresponding emissions (Chapter 4) as a function of time and space. Chapter 5 discusses all the details of the AIS dataset that will be used to map the emissions of the fleet on the Rotterdam-Antwerp corridor. Chapter 6 addresses the most important elements of the model development.

Part II is the results section of this study. In Chapter 7, the 't0 emission scenario' of the Rotterdam-Antwerp corridor will be mapped based on observed AIS data, and a model simulation is performed to simulate this 't0 emission scenario'. In Chapter 8, this model will be used to assess the effectiveness of alternative future emission reduction policies.

Part III is the conclusions, discussion and recommendation section of this thesis. By answering the defined research questions, the main conclusions of this study are drawn in Chapter 9. Chapter 10 reflects on this study and defines the most important limitations, from which a number of recommendations will follow.

I

Literature, materials and methods

2

Method development

The main goal of this thesis is to develop a method that is able to map the emissions caused by inland shipping over time and space. A second objective is that the method can be used in support of the development and evaluation of emission policies.

To map the variation in emissions with resolution in time and space, the following information is required:

- An inland waterway network with fairway properties
- Information about each individual ship in the fleet: per ship, we require its vessel characteristics and a time series that describes the route the vessel sails, containing the geographical position for each timestamp
- Algorithms to estimate the energy consumption and potential emission per ship per time step, taking into account the fairway properties and vessel characteristics

This information is key to the method of this research. This chapter describes the methodology that will be used to tackle the problem step by step.

Methodologically estimate the energy consumption and potential emissions
The basis of this research is the development of algorithms to estimate the energy consumption and potential emissions of an individual inland vessel, as a function of time and space. Figure 2.1 shows how this method will be structured. Following the approach by Vehmeijer (2019), we start with estimating the resistance of a ship. The ship dimensions, sailing speed and waterway characteristics are decisive in these calculations. The resistance can be translated to the power (kW) and the required energy (in kWh). By multiplying the energy with a certain emission factor (in g/kWh, which is dependent on the engine age and the partial engine load), the potential emission of a single vessel can be determined as a function of time and space.

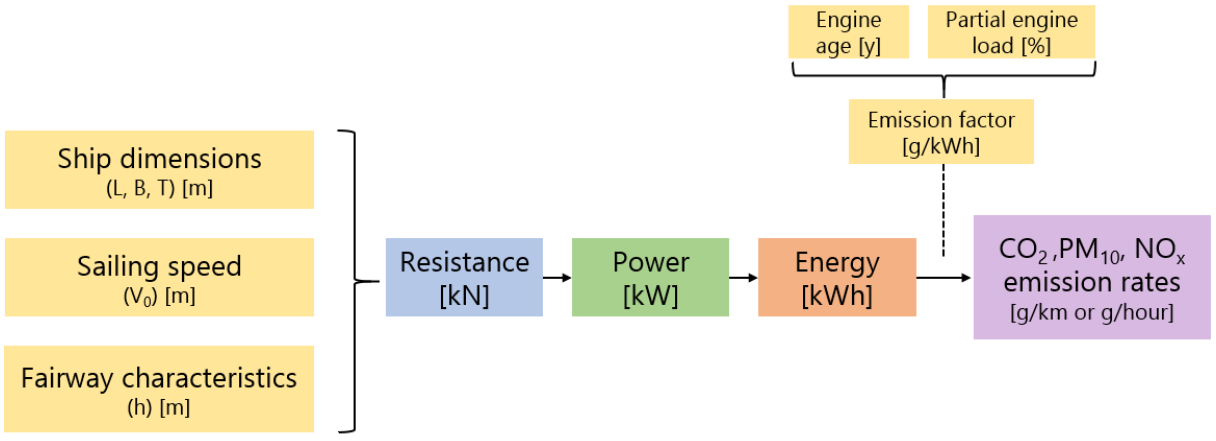

Figure 2.1: Structure of the method to estimate the energy consumption and emissions of a single inland vessel

Connection to an inland waterway network with fairway properties: FIS
To map the emissions of inland shipping on an inland waterway network, we need to incorporate information about the geometry of the fairways. In addition, the water depth, fairway width and currents have influence on the resistance a ship experiences, and so on the energy consumption and potential emissions of a ship. Therefore we want to include fairway properties of the network. We will make use of the dutch Fairway Information Services (FIS), which collects all information from the Dutch waterways in one system. From this online source we can read out a graph, containing the geometry and actual information about the characteristics of the fairways. In this study the focus will be on water depth, but for follow-up research, a FIS network can also offer a solution to include other properties, when the right information is available.

Applying the method to observed AIS data ('t0 emission scenario')
In addition to fairway properties, we require information about each vessel in the fleet. We need information about the vessel type, ship dimensions and sailing speed. In addition, we need information about the route each ships sails over time, which provides the required resolution in time and space.

We are going to use AIS (Automatic Identification System) data to map the fleet. AIS data provides actual information about inland water transport. Rijkswaterstaat provided an AIS dataset containing information about the fleet on the Rotterdam-Antwerp corridor. The data contains a time series of each single ship on the corridor, including information about the geographical position and the vessel characteristics. The time series provides the distance traveled and the time period between two timestamps: with this information the velocity of the ship can be computed per timestamp, which is an requirement of the emission calculations.

AIS data provides detailed information about the geographical positions of vessels. You can show the distribution in space of vessel movements along a cross section of a waterway in quite some detail. But the included fairway properties in the emission calculations and to quantify potential emissions on a waterway section, the AIS data will be connected to the FIS network: although you reduce the waterway sections to one dimension, it offers the possibility to include properties such as variation in water depth in your calculations, and to assign emissions to certain edges on the network.

The AIS data, connected to the FIS network, provides enough information to perform the energy consumption and potential emission calculations. The developed algorithm can be applied to the AIS time series, and the required energy and potential emissions can be computed per ship, per timestamp. We call this output the 't0 emission scenario', which represents the current potential emission distributions over time and space.

Applying the method to simulated model data (simulated 't0 emission scenario')
Besides AIS data, the algorithms will be applied to a time series resulting from a model simulation. A model will be developed that simulates the fleet on the inland waterway network by means of discrete event simulation. The reason to develop this model is because we want to assess the effectiveness of alternative future emission policies.

To simulate the fleet in a proper way, different information about the fleet resulting from the AIS dataset will be used as input for the model: this concerns an origin-destination (OD) matrix, with the characteristics of each ship, the route it sails and the average speed. The python package OpenTNSim (Open source Transport Network Simulation) will be used to simulate the inland traffic based on the OD matrix. The simulation is linked to the FIS network, to take into account fairway properties. The simulation results in a time series, where the algorithms can be applied in the same way as with the AIS data, to compute the energy consumption and emissions per ship per timestamp. This output can be validated with the 't0 emission scenario' output resulting from the AIS data.

Quantify emissions on the network
Due to the link with the FIS network, the emission can be quantified on the network for both the AIS data and the model simulation output. The FIS network consists of a large set of nodes, connected by edges. The emissions on each edge can be summed. This way, the potential emission distributions can be visualized on the network and emission hotspots can be identified.

Simulate alternative emission reduction policies
The developed model can now be used in supporting the development and evaluation of emission policies. The illustrate the possibilities of the method, a first assessment of some alternative emission reduction policies will be performed.

3

Method to estimate energy consumption

The first step in developing a method to estimate the potential emission of an inland vessel, is to estimate the energy consumption of a ship. In this section, different literature will combined to develop a bottom-up method to calculate the required energy. The energy consumption of an inland vessel depends on the required power and the vessel speed. The required power is dependent on the resistance a ship experiences, consisting of different resistance components. The dimensions of the ship, the sailing speed and waterway characteristics have influence on the resistance, and so on the required power and energy.

Figure 3.1 gives an overview of how the total energy required is made up of different components and shows how this chapter is structured. We start with the energy consumption of an inland vessel, which is the product of the required power and the time period considered. The required power can be subdivided into the power needed for hotel systems on board, and the power required for propulsion (Section 3.1). In the determination of the propulsion power, a number of efficiencies have to be taken into account. In addition, the propulsion power depends on the resistance a ship experiences. The total resistance will be drilled down into a number of resistance components, based on literature of Holtrop and Mennen (Section 3.2). When a vessel is in a stationary stage, some assumptions have to be made, which is discussed in Section 3.3. In Section 3.4 of this chapter, the developed method will be illustrated by applying the calculations to a reference vessel. The dependence of the speed and water depth will be mapped. In the final section a sensitivity analysis is performed, to see what happens with the resistance and power output of the method when applying certain changes to input variables.

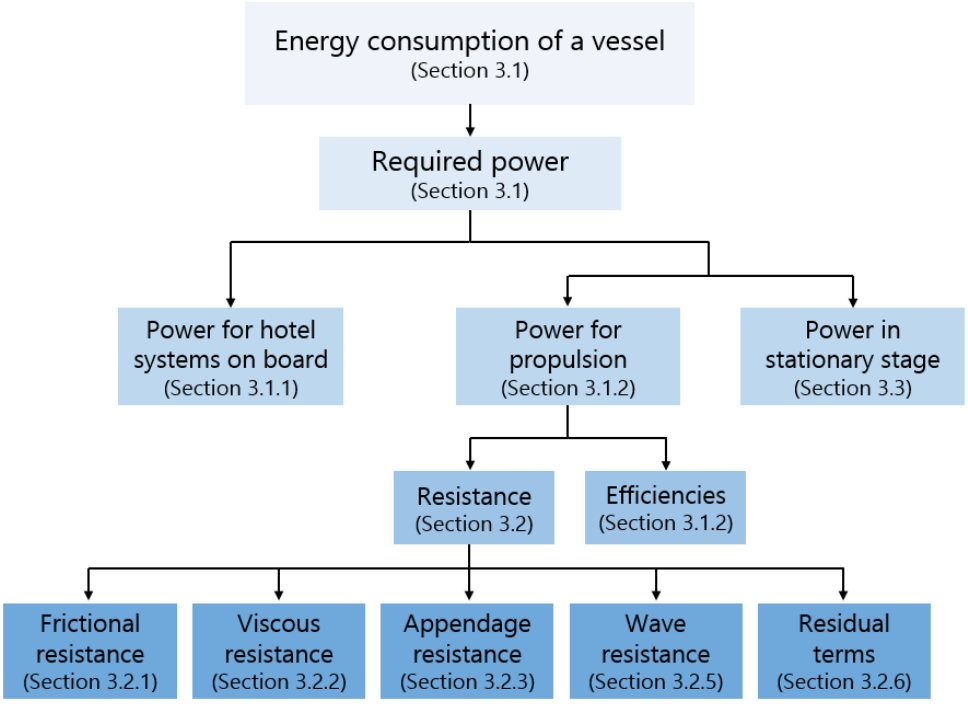

Figure 3.1: Overview of different sections in Chapter 3

3.1. Total required power and energy consumption

The total energy consumption of a ship during a specific time period depends on the total required power:

$$E = P_{tot} * \Delta t \tag{3.1}$$

In which:
E = energy consumption during Δt [kWh]
P_{tot} = total required power [kW]
Δt = time period [hours]

The total required power of a ship can be subdivided into two components: the power required for hotel systems on board, and the power required for propulsion:

$$P_{tot} = P_{hotel} + P_{propulsion} \tag{3.2}$$

With all the power components expressed in kW. Section 3.1.1 elaborates on the power required for hotel systems on board. The power required for propulsion is discussed in Section 3.1.2.

3.1.1. Required power for hotel systems on board

The hotel systems on board require heat and electrical power (think of lighting, heating of cabins) (Toscano and Murena, 2019). The hotel power component (P_{hotel}) takes this required energy into account. In general, this component is relatively low for inland ships, since the scale of these ships is relatively small and there are not so much activities on board of the ship. When vessels become larger, the hotel power component increases. Therefore, the hotel power is estimated as a percentage of the total installed power (taking into account the scale of the ship): the hotel power is estimated to be 5% of the installed engine power (de Vos and van Gils, 2011).

$$P_{hotel} = 0.05 * P_{installed} \tag{3.3}$$

Please note that this component does not take into account the idling of the engine in a stationary stage: this topic is discussed in Section 3.3.

3.1.2. Required power for propulsion

The required power for propulsion depends on several factors. It starts with the resistance of ship that needs to be overcome. The resistance an inland vessel experiences, depends on its dimensions and shape, the velocity of the ship and waterway characteristics. To translate the resistance to total required power, you have to take into account propulsion characteristics and different losses in the system. This section shows step by step which calculations are required to come up with the total required power for propulsion. To illustrate these different steps, Figure 3.2 shows a schematization of a ship, illustrating different power components and efficiencies we are dealing with.

The Effective Horse Power (EHP), or effective power P_e, is the power that is needed to travel with a certain (relative) speed, overcoming its resistance (Watson, 1998). The EHP, delivered by the ship's propellers, can be defined as follows:

$$P_e = V_0 * R_{tot} \tag{3.4}$$

In which:
P_e = effective power [kW]
V_0 = the speed of the vessel [m/s]
R_{tot} = ships resistance [kN]

In Section 3.2 a method is developed, combining different literature, to estimate the total resistance an inland vessel experiences, R_{tot}.

The Delivered Horse Power (DHP), P_d, is the power that is delivered to the propeller. DHP can be expressed as the power required to sail with a certain speed (Effective Horse Power (EHP)) plus the losses at the propeller

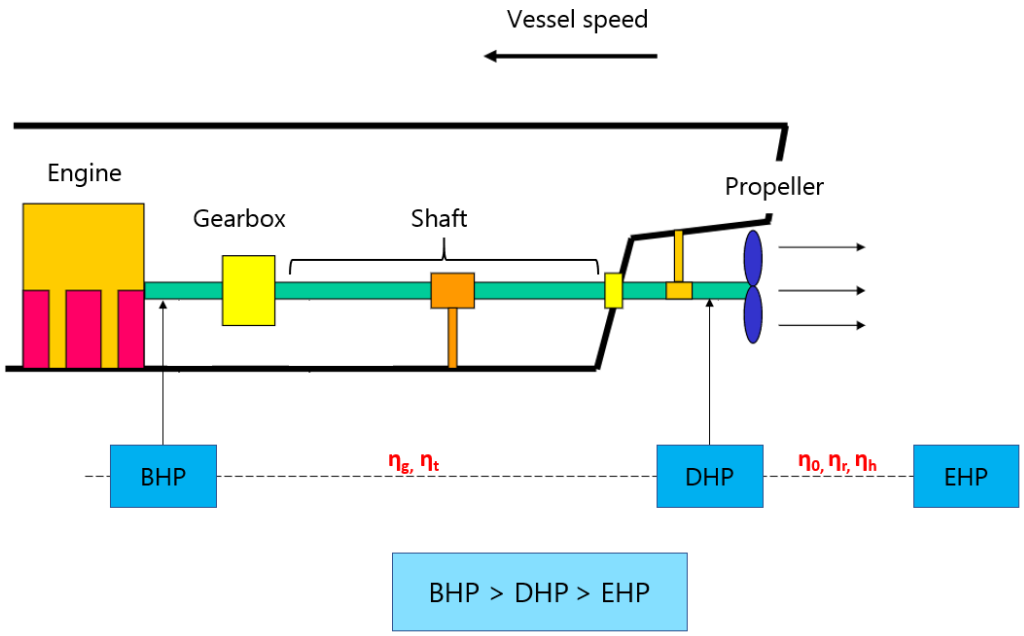

Figure 3.2: Schematization of a ship to illustrate different power components and efficiencies

(open water efficiency of the propeller, relative rotative efficiency and the hull efficiency). Therefore, DHP > EHP. (Watson, 1998):

$$P_d = \frac{P_e}{\eta_0 \eta_r \eta_h} \tag{3.5}$$

In which:
P_d = delivered horse power [kW]
η_0 = open water efficiency of propeller [-]
η_r = relative rotative efficiency [-]
η_h = hull efficiency [-]

The Brake Horse Power (BHP), P_b, is the power required to sail with a certain speed (Effective Horse Power (EHP)) plus the losses at the propeller (already considered in the DHP), shaft and gearbox. Therefore holds that BHP > DHP > EHP. The Brake Horse Power is the total power required for propulsion ($P_{propulsion}$).

$$P_b = \frac{P_d}{\eta_t \eta_g} = P_{propulsion} \tag{3.6}$$

In which:
P_b = brake horse power [kW]
η_t = transmission efficiency (losses in the shaft) [-]
η_g = gearing efficiency [-]

Below, the different efficiencies are further explained and for each of these components a suitable value is assumed or a calculation method is proposed.

Open water efficiency
The open water efficiency of the propeller (η_0) is related to the ratio of the thrust power to the power absorbed by the propeller with no hull in front of it. η_0 especially depends on the vessel speed (V_0), the thrust force (T), the diameter of the screw (D_s) and other design characteristics. Typical values for (η_0) are between 0.55 and 0.70 (MAN Energy Solutions, 2018). A value of 0.6 has been assumed to be on the conservative side.

Relative rotative efficiency
The relative rotative efficiency (η_r) of the propeller accounts for the changes in water flow to the propeller behind the ship, relative to the open water flow conditions. The variations of (η_r) are small with typical values between 0.98 and 1.02 (Hekkenberg, 2013). A value of 0.98 has been assumed.

The hull efficiency
The hull efficiency η_h is determined according to the following formula:

$$\eta_h = \frac{1-t}{1-w} \tag{3.7}$$

In which:
η_h = hull efficiency [-]
t = thrust deduction factor [-]
w = wake fraction [-]

In a literature review of van Terwisga (1989) an empirical method of Papmel is described to determine the wake fraction, which can be found in Appendix C, Section C.1.

Transmission and gearing efficiency
The transmission efficiency (η_t) takes into account losses at the shaft. A common value of 0.98 for η_t is used. Gearbox losses are included with the gearing efficiency η_g. A usual value is 0.96 (Watson, 1998).

3.2. Resistance

The total resistance of an inland vessel determines the total required power and so the energy consumption. This section will discuss how the total resistance can be estimated. There are many different methods to estimate the resistance, and it is quite complex to make a good estimation: the resistance of a ship depends on many variables. In this research, the method of J. Holtrop and G.G.J. Mennen (1982) is used as a basis. Holtrop and Mennen estimate the total resistance by making a clear breakdown into different resistance components:

$$R_{tot} = R_f(1+k_1) + R_{APP} + R_W + R_B + R_{TR} + R_A \tag{3.8}$$

In which:
R_{tot} = total resistance of the ship [kN]
R_f = frictional resistance [kN]
$1+k_1$ = form factor describing the viscous resistance of the hull form in relation to R_f [-]
R_{APP} = appendage resistance [kN]
R_W = wave resistance [kN]
R_B = additional pressure resistance of bulbous bow [kN]
R_{TR} = additional pressure resistance of immersed transom stern [kN]
R_A = model-ship correlation resistance [kN]

In the following sections each individual resistance component will be discussed.

3.2.1. Frictional resistance

The first resistance component considered in Formula 3.8 of J. Holtrop and G.G.J. Mennen (1982) is the frictional resistance, R_f.

As a vessel moves through water, the friction of the water acting on the entire wetted surface of the hull, causes a net force in opposite direction of ship's motion. This is the frictional resistance, which is a function of the wetted surface area (S_T), the velocity profile, surface roughness and water viscosity (United States Naval Academy, n.d.). The effect of viscosity is treated in the next section (Section 3.2.2).

The frictional resistance can be expressed as a function of the dimensionless friction coefficient (Bolt, 2003):

$$R_f = C_f \frac{1}{2} \rho V_0^2 S_T \tag{3.9}$$

In which:
R_f = frictional resistance [N]
C_f = friction coefficient [-]
ρ = density of water [kg/m^2]
V_0 = velocity of the vessel, relative to the water [m/s]
S_T = wetted surface area of the vessel [m^2]

Please note that the V_0 is the velocity of the vessel relative to the water. Relative to the water means that you take into account the current: if a vessel moves with the current, the velocity relative to the water is lower than the actual velocity, resulting in less friction. When the vessel sails against the current, it is a reverse effect: the velocity relative to the water increases, resulting in more friction. This effect is important to consider, but for simplification, we assume in this study that the ship sails on still water.

In the following subsections first a method is proposed to calculate the wetted surface area (S_T) of the vessel. Afterwards a method is elaborated to estimate the dimensionless friction coefficient (C_f), taking into account shallow water effects.

Wetted surface area S_T
There are several ways to calculate the wetted surface area. Since the wetted surface area has a significant influence of the total frictional resistance, a detailed approach of J. Holtrop and G.G.J. Mennen (1982) is used:

$$S_T = L(2T+B)\sqrt{C_M}(0,453+0,4425C_B-0,2862C_M-0,003467\frac{B}{T}+0,3696C_{wp})+2,38\frac{A_{BT}}{C_B} \tag{3.10}$$

In which:
L = length of the vessel [m]
T = draft of the vessel [m]
B = width of the vessel [m]
C_M = midship section coefficient [-]
C_B = block coefficient [-]
C_{wp} = water plane area coefficient [-]
A_{BT} = wet transverse sectional area of the bulbous bow [m^2]

The block coefficient, C_B, expresses the 'fullness' of the ship. It is the ratio between the underwater volume of the ship's hull to the volume of a rectangular underwater block with a length and width equal to these of the ship, and the depth equal to the draft (illustrated in Figure 3.3). The block coefficient is relatively high for inland vessels and is assumed as a constant of 0.85: this is the maximum value of the block coefficient for which the method of Holtrop and Mennen is still applicable.

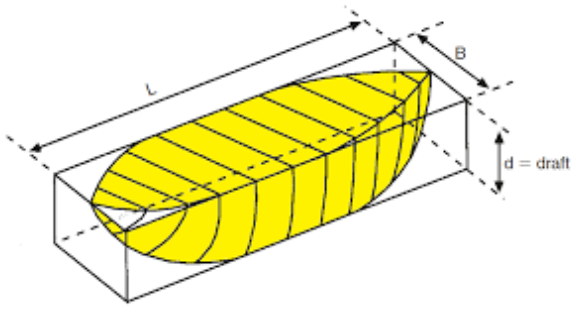

Figure 3.3: Visualisation of block coefficient. The underwater volume of the ship's hull is highlighted in yellow.

The midship coefficient C_M and the water plane coefficient C_{wp} are determined from Schneekluth and Bertram's formula (Saha and Sarker, 2010), and both depend on the block coefficient:

$$C_M = 1,006-0,0056C_B^{-3,56} \tag{3.11}$$

$$C_{wp} = \frac{1+2C_B}{3} \tag{3.12}$$

A_{BT} is the wetted transverse sectional area of the bulbous bow of the ship. Most of the inland ships do not have a bulbous bow. Therefore, we assume A_{BT} to be zero.

Dimensionless friction coefficient C_f
Over the years, several methods have been developed to determine the friction coefficient C_f. The ITTC57 correlation line is a frequently used method to predict the frictional resistance of ships, which assumes no waterway restrictions (depth, width) and so unrestricted flow conditions. The original resistance prediction method of J. Holtrop and G.G.J. Mennen (1982) uses the ITTC57 friction line as starting point.

In reality, inland shipping is usually influenced by waterway limitations. This has influence on the frictional resistance, which leads to decreasing accuracy of the prediction of the ITTC57 correlation line. Therefore, a modification of this correlation line by Zeng et al. (2018) is proposed, taking into account shallow water effects.

Width and depth limitations both have influence on the resistance of inland vessels. This modification focuses on the effects of shallow water, since the effects from the lateral direction are in many cases much smaller than from the vertical direction. For simplification, waterways with no width, but only depth limitations are considered. In these cases, limited water depth mainly affects the bottom area of the vessel. The effects on other parts of the wetted surface are significantly smaller.

Below, the effects of limited water depth are briefly discussed, followed by a fit of the numerical friction line proposed by Zeng et al. (2018) and a proposed method to be able to directly apply the theory to calculate the frictional resistance.

2D flat plate and velocity increase
Inland ships usually have a long parallel midbody with a large flat bottom, which is considered as a 2D flat plate (see Figure 3.4). The velocity of far-field incoming water is V (which is zero when you assume no current). The water underneath the ship is accelerated by ΔV, caused by limited water depth and the displacement of the ship. This acceleration also occurs in deep water, but it is more significant in shallow water.

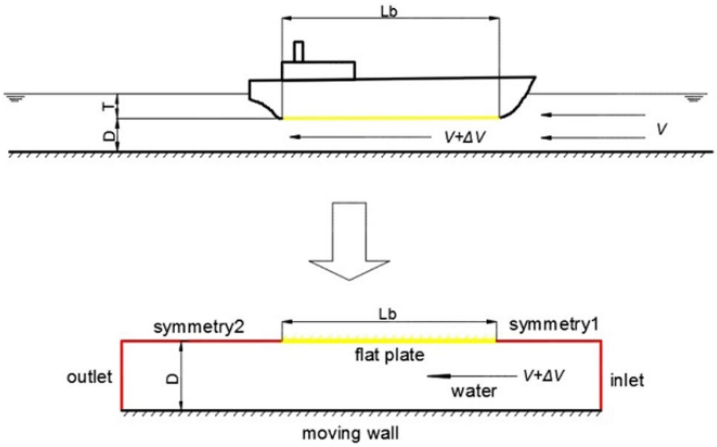

Figure 3.4: Simplification of the bottom of the ship in shallow water (Zeng et al., 2018)

Figure 3.4 shows the following parameters: L_b is the length of the flat bottom (which is from now assumed to be equal to the ship length L). T is the draft of the ship and D is the distance between the flat plate of the ship and the bottom of the waterway.

The physical effects of shallow water on friction
When a vessel sails in shallow water, the flow will be accelerated due to the displacement of the boundary layer. This leads to a thinner boundary layer: this layer decreases when D/L decreases (which means shallower water):

- D = the water depth minus the draft of the ship (= h - T)

- L = the length of the flat plate

Entering shallow water consequently means that the velocity gradient normal to the 2D flat plate increases, which results in an increase of local friction. This means that the total friction, summing the local frictions, is also increased in case of limited water depths and depends on D/L.

Fitting of a numerical friction line
Zeng et al. (2018) proposes a numerical friction line, taking into account the shallow water effects. This friction line is based on Computational Fluid Dynamics (CFD) calculations. He applied a regression analysis, using the method of least squares. The results of the fitting give a function for the total frictional resistance coefficient in deep water ($C_{f,deep}$) and in shallow water ($C_{f,proposed}$).

The deep water (D/L close or greater than 1) friction coefficient only depends on the Reynolds number:

$$C_{f,deep} = \frac{0.08169}{(\log R_e - 1.717)^2} \tag{3.13}$$

The Reynolds number is defined as follows:

$$R_e = \frac{V_0 L}{\nu} \tag{3.14}$$

In which:
V_0 = velocity of the vessel [m/s]
L = ship length [m]
ν = kinematic viscosity [m^2/s]($\approx 1 * 10^{-6}$)

For shallow water conditions (D/L < 1), the friction coefficient depends on the Reynolds number and on D/L:

$$C_{f,proposed} = \frac{0.08169}{(\log R_e - 1.717)^2}\left(1 + \frac{0.003998}{\log R_e - 4.393}\left(\frac{D}{L}\right)^{-1.083}\right) \tag{3.15}$$

This function should approach the deep water friction coefficient when D/L is close to 1. The errors of this fitted friction line are mostly less than 1% (only for D/L = 0.01 it is less than 3%) (Zeng et al., 2018).

Method to apply the modified friction line
The proposed modification of the ITTC57 correlation line can not directly be applied, since a ship also has non-horizontal wetted surfaces that have to be taken into account. Therefore, the following formula is proposed by Zeng et al. (2018):

$$C_f = C_{f_0} + (C_{f,proposed} - C_{f,Katsui})\left(\frac{S_B}{S_T}\right)\left(\frac{V_1}{V_0}\right)^2 \tag{3.16}$$

In which:
C_f = corrected total friction coefficient of a ship in shallow water [-]
C_{f_0} = conventional friction coefficient (ITTC57 correction line) [-]
$C_{f,proposed}$ = proposed friction line in shallow water [-]
$C_{f,Katsui}$ = Katsui's line to calculate the friction coefficient of a flat plate in unrestricted conditions [-]
S_B = area of the flat bottom [m^2]
S_T = area of the total wetted surface [m^2]
V_0 = vessel speed [m/s]
V_1 = corrected velocity, velocity underneath ship's bottom [m/s]

The conventional frictional resistance correlation line, proposed by ITTC57, is defined as follows:

$$C_{f0} = \frac{0.075}{(\log R_e - 2)^2} \tag{3.17}$$

The friction line proposed by Katsui is:

$$C_{f,Katsui} = \frac{0.0066577}{(\log R_e - 4.3762)^a} \tag{3.18}$$

In which 'a' is defined as:

$$a = 0.042612 \log R_e + 0.56725 \tag{3.19}$$

Please note that it is also possible to use another suitable friction line for deep water.

The area of the flat bottom (S_B) can be approximated by multiplying the length and the width of the vessel:

$$S_B = L * B \tag{3.20}$$

The total wetted surface area of the vessel can be approximated by the previous addressed method of J. Holtrop and G.G.J. Mennen (1982) (see Equation 3.10).

To find the average velocity underneath the ship, at the edge of the flat bottom, empirical data is regressed, which results in the following formula (Zeng et al., 2018):

$$V_1 = V_0 + \Delta V = 0.4277 V_0 exp\left(\left(\frac{h}{T}\right)^{-0.07634}\right) \tag{3.21}$$

The uncertainty of this formula is 2.5% and it is only suitable for $\frac{h}{T} \leq 4.0$. If $\frac{h}{T}$ is higher than 4, V_1 is assumed to be equal to V_0.

Zeng et al. (2018) tested Formula 3.16 and it resulted that this proposed method agrees better with the values derived from CFD than ITTC57. It has an uncertainty less than 3%, which makes it a successful method to predict the friction including shallow water effects on the ship's flat bottom.

To give an idea of how the corrected friction coefficient C_f is influenced by the Reynolds number and water depth limitations, the calculations are performed for a reference vessel. We consider a M9 vessel, which is a motor vessel defined in the Rijkswaterstaat vessel type classification (for more information about different vessel types: see Appendix F. The main dimensions of this vessel are a length of 135 meter, a width of 11.75 meter and a draft of 2.75 meter. Figure 3.5 shows the results. The blue lines represent the situations for deeper water, and the red lines show the results of more limited water depths. In general, the friction coefficient is lower for higher Reynolds numbers: you see a significant increase of the friction coefficient when the Reynolds number becomes low. For limited water depths, we see that the friction coefficient is much higher than in case of deep water: the friction line shifts upwards in case of water depth limitations. For low Reynolds numbers, the water depth limitations have even more influence on the increase of the friction coefficient.

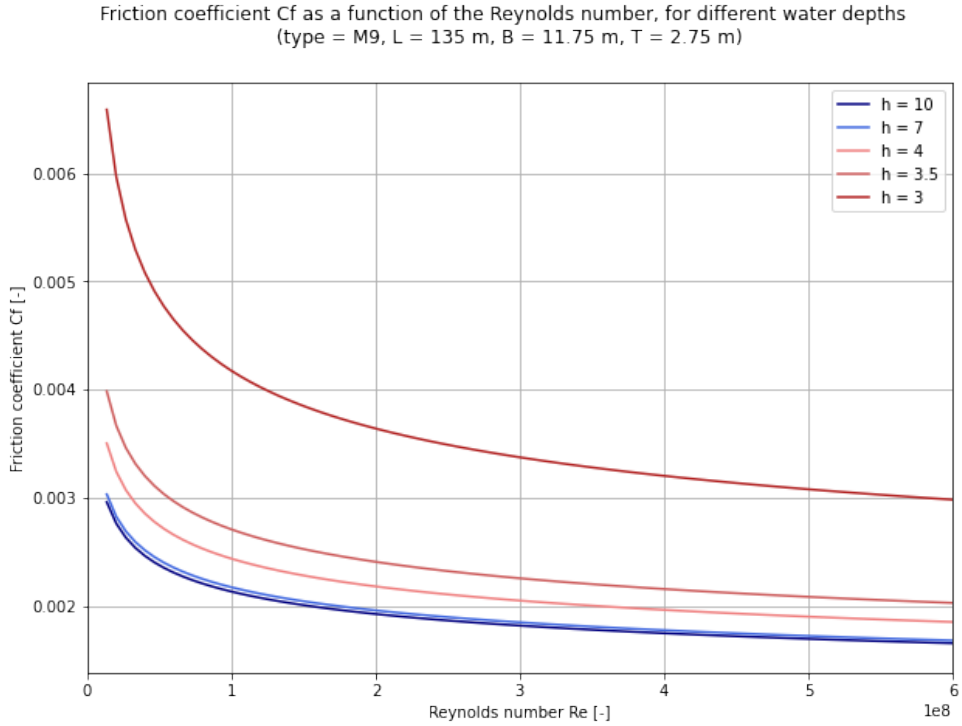

Figure 3.5: Friction coefficient C_f for a reference vessel (M9) as a function of the Reynolds number, for different water depths

By incorporating the dimensionless friction coefficient proposed by Zeng et al. (2018) (Formula 3.16) in Formula 3.9, the frictional resistance R_f term can be determined.

3.2.2. Viscous resistance

The second component considered by J. Holtrop and G.G.J. Mennen (1982) is the viscous resistance component: viscosity is part of the frictional resistance and can be incorporated by introducing the form factor $(1+k_1)$, which is related to the frictional resistance R_f.

Viscosity is a property of a fluid describing the resistance to flow. When there is a lot of interaction between the fluid particles, the viscosity is higher and so the frictional resistance of the ship is higher (higher form factor). Water has a relatively low viscosity, but still it produces a significant viscous resistance force on the ship.

Formula 3.22 proposes a way to estimate the form factor. This formula is a modification of an earlier form factor equation proposed by Holtrop and Mennen (Watson, 1998). The form factor has to be multiplied by the frictional resistance (see Formula 3.8) to take into account the effect of viscosity. The form factor $(1 + k_1)$ can be expressed as:

$$1 + k_1 = 0,93 + 0,487 * c_{14} * (B/L)^{1,068} (T/L)^{0,461} (L/L_R)^{0,122} (L^3/\Delta)^{0,365} (1 - C_p)^{-0,604} \tag{3.22}$$

In which:

c_{14} = coefficient accounting for the specific shape of the afterbody [-]
L_R = parameter reflecting the length of the run [m]
Δ = water displacement [m^3] (see Formula C.2)
C_p = prismatic coefficient [-]

The prismatic coefficient C_p is, just like the block coefficient, a way to indicate the 'fullness' of a ship. It can be expressed as a function of the block coefficient C_B and the midship coefficient C_M (Saha and Sarker, 2010):

$$C_p = \frac{C_B}{C_M} \tag{3.23}$$

L_R is a parameter reflecting the length of the run, so te length of the immersed shaped stern. L_R can be determined according to the following expression (J. Holtrop and G.G.J. Mennen, 1982):

$$L_R = L\left(1 - C_p + \frac{0,06 C_p lcb}{4C_p - 1}\right) \tag{3.24}$$

The value 'lcb' is the longitudinal position of the centre of buoyancy forward (+) or aft (-) of 0.5L as a percentage of L, and can be expressed as a function of the prismatic coefficient (Saha and Sarker, 2010):

$$lcb = -13,5 + 19,4 C_p \tag{3.25}$$

The coefficient C_{14} accounts for the specific shape of the afterbody and depends on the coefficient C_{stern} (Watson, 1998):

$$C_{14} = 1 + 0,0011 C_{stern} \tag{3.26}$$

C_{stern}=-25 to -20 for barge-shaped forms
= -10 for after body with V sections
= 0 for normal shape of after body
= +10 for an after body with U sections and Hogner stern

For simplification, C_{stern} is assumed to be 0, which makes C_{14} equal to 1.

With these values, the form factor $(1 + k_1)$ can be determined according Formula 3.22, taking into account the effect of viscosity on the frictional resistance.

3.2.3. Appendage resistance

The third component proposed by J. Holtrop and G.G.J. Mennen (1982) is the appendage resistance. The appendages of a ship (e.g. rudder, shafts, skeg) result in an additional frictional resistance when a ship moves through the water. It can be expressed as follows:

$$R_{APP} = 0,5 \rho V_0^2 S_{APP} (1 + k_2) C_f \tag{3.27}$$

In which:
R_{APP} = appendage resistance [N]
V = velocity of the ship [m/s]
S_{APP} = wetted area of the appendages [m^2]
$(1 + k_2)$ = appendage resistance factor [-]
C_f = dimensionless friction coefficient (See Formula 3.16) [-]

The wetted area of the appendages of inland ships is estimated to be around 5% of the total wetted area S_T.

The appendage resistance factor $(1 + k_2)$ differs with the type of appendage considering. For simplicity, a constant value of $(1 + k_2) = 2.5$ is used (Holtrop and GGJ Mennen, 1978).

3.2.4. Additional resistance due to limited water depth (Karpov method)

We have seen already that water depth restrictions result in an increase of the frictional resistance: the method of Zeng et al. (2018) was applied in Section 3.2.1 to take into account this effect, by modifying the original friction line and making use of an adjusted increased velocity V_1 underneath the bottom of the ship.

In addition to the frictional resistance, limited water depth has also a significant influence on among other things the wave resistance. When the vessel starts to approach its critical speed, the resistance is increased significantly. In limited water depth, this critical speed is reached must faster, and therefore it is important to consider this effect in the total resistance estimation.

To take this effect into account, the Karpov method is applied (van Terwisga, 1989). With the Karpov method,

the vessel speed V_0 is adjusted: the corrected speed V_2 is determined by the coefficient α^{**}. This coefficient depends on the depth Froude number $F_{n,h}$:

$$F_{n,h} = \frac{V_0}{\sqrt{gh}} \tag{3.28}$$

In which 'h' is the water depth is meters. The corrected vessel speed V_2 is determined according to:

$$V_2 = \frac{V_0}{\alpha^{**}} \tag{3.29}$$

Figure 3.6 shows the course of the coefficient α^{**} as a function of the depth Froude number $F_{n,h}$, for different water depth to draft ratios (h/T). This figure is an approximation of an older figure from 1976 proposed by Basin.

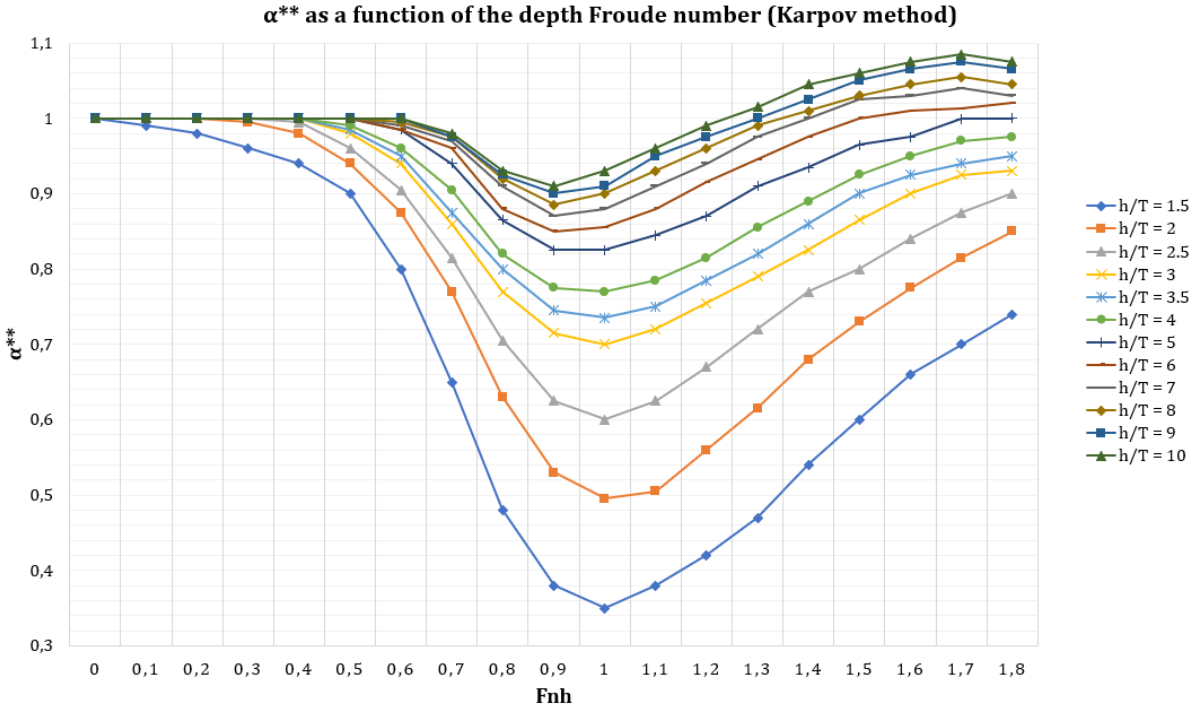

Figure 3.6: Karpov method: estimation of α^{**} based on the depth Froude number $F_{n,h}$, for different h/T ratios

For each h/T curve from Figure 3.6, an 6^{th} order polynomial approximation in Excel is applied, to determine for each depth Froude number the corresponding coefficient α^{**}. These approximation curves are performed for separated depth Froude number ranges, in order to reach a better result. In Appendix B the approximations can be found. The resulting equations are implemented in the model, in order to calculate the corrected velocity V_2, which will be used in the wave resistance and residual resistance components discussed in the next sections.

3.2.5. Wave resistance

The fourth resistance component defined by J. Holtrop and G.G.J. Mennen (1982) is the wave resistance. When a ship moves through the water, it creates waves, which results in additional resistance. As the vessel speed increases, the height of the produced waves increases and therefore the wave resistance becomes higher (United States Naval Academy, n.d.). When approaching limited water depth, the wave resistance increases even more.

For estimating the wave resistance, a distinction is made between different ranges of Froude numbers. The Froude number used in these calculations is based on the corrected velocity V_2, which takes into account the effect of shallow water, as explained in the previous section:

$$F_{n,V_2} = \frac{V_2}{\sqrt{gL}} \tag{3.30}$$

The following wave resistance calculation methods are based on the Holtrop and Mennen method, discussed in literature from Sarris (2003). Different expressions of the wave resistance are defined for Froude numbers lower than 0.4, higher than 0.55 or in between 0.4 and 0.5. The complete elaboration of all parameters in these expressions can be found in Appendix C, Section C.2.

Wave resistance in case F_{n,V_2} < 0.4

$$R_{W1} = c_1 c_2 c_5 \Delta \rho g e^{\left(m_1 F_{n,V_2}^{-0.9} + m_4 cos(\lambda F_{n,V_2}^{-2})\right)} \tag{3.31}$$

In which:
R_{W1} = wave resistance ($F_n < 0.4$) [N]
$c_{1,2,5}$ = coefficients [-]
Δ = water displacement [m^3]
F_{n,V_2} = Froude number, based on V_2 [-]
m_1, m_4 = coefficients [-]
λ = wave-making length [−]

Wave resistance in case F_{n,V_2} > 0.55

$$R_{W2} = c_{17} c_2 c_5 \Delta \rho g e^{\left(m_3 F_{n,V_2}^{-0.9} + m_4 cos(\lambda F_{n,V_2}^{-2})\right)} \tag{3.32}$$

Wave resistance in case 0.4 < F_{n,V_2} < 0.55
In case the Froude number is in between 0.4 and 0.55, a combination of R_{W1} and R_{W2} is used to calculate the wave resistance:

$$R_{W3} = R_{W1} + \frac{(10 F_{n,V_2} - 4)(R_{W2} - R_{W1})}{1.5} \tag{3.33}$$

3.2.6. Residual resistance terms

Finally, the residual resistance terms are taken into account: J. Holtrop and G.G.J. Mennen (1982) define the additional resistance due to presence of a bulbous bow (R_B) and the immersed transom (R_{TR}), and a resistance term accounting for the model-ship correlation (R_A). Since the bulbous bow is most of the time not present at inland vessels, only R_{TR} and R_A are considered.

Resistance due to the immersed transom R_{TR}
Inland vessels often have an immersed transom (newer ships in loaded condition), which results in an additional pressure resistance (R_{TR}) that has to be taken into account. R_{TR} can be determined by:

$$R_{TR} = 0.5 \rho V_2^2 A_T c_6 \tag{3.34}$$

Please note that the corrected velocity V_2 is again used in these calculations, accounting for shallow water effects. The coefficient c_6 depends on the transom immersion Froude number (F_{nT}):

If $F_{nT} < 5$:

$$c_6 = 0.2(1 - 0,2 F_{nT}) \tag{3.35}$$

If $F_{nT} \geq 5$, c_6 becomes 0.

The Froude number based on the transom immersion $F_n T$ is:

$$F_{nT} = V_2 / \sqrt{2 g A_T / (B + B C_{wp})} \tag{3.36}$$

The water plane coefficient C_{wp} can be determined from Formula 3.12. The immersed part of the transverse area of the transom, A_T, is assumed to be 0.2*B*T.

Model-ship correlation resistance R_A
The final resistance term is the model-ship correlation resistance R_A, again taking into account the shallow water effect by applying the corrected velocity V_2:

$$R_A = \frac{1}{2}\rho V_2^2 S_T C_A \tag{3.37}$$

In which:
C_A = correlation allowance coefficient [-]
S_T = wetted surface area [m^2] (Formula 3.10)

The model-ship correlation allowance coefficient takes into account the differences between the resistance which is measured by full-scale experiments and the resistance estimated by model testing (Gillmer and Johnson, 1982). It considers the effect of the hull roughness and the still-air resistance. The correlation allowance coefficient C_A can be found by the following expression proposed by Holtrop and Mennen, discussed in literature of Sarris (2003):

$$C_A = 0.006(L+100)^{-0.16} - 0.00205 + 0.003\sqrt{L/7.5}C_B^4 c_2(0.04 - c_4) \tag{3.38}$$

In which C_B is the block coefficient, which is assumed to be 0.85. c_2 is equal to 1, since this coefficient accounts for the effect of a bulbous bow, which is mostly not present at inland vessels. Coefficient c_4 depends on the ratio T/L: if T/L < 0.04, c_4 = T/L. If T/L > 0.04, c_4 = 0.04.

3.3. Energy consumption during the stationary stage

When vessels have to slow down, for example at locks, the emissions per unit time decrease. But while waiting, the main and auxiliary engines are in general not turned off, but keep on idling. Because the ship is stationary during waiting, and so stays at the same place, the emissions are accumulated at this location. It has been assumed that emissions of an inland vessel during this stationary stage are 15% of the emissions per unit time during average propulsion on the same waterway. This assumption results from an estimation in literature of Hulskotte (2011), and the percentage is based on the energy required for idling of the engine and some occasional steering of the ship. Please note that this assumption is rough and therefore this is a limitation in mapping the emissions in the stationary stage. There is limited data available about this topic and more research is required to improve the estimation of emissions in the stationary stage.

To make an estimate of energy consumption in this stationary stage, a distinction has been made between the Rijkswaterstaat inland vessel classes. For each vessel class, the average velocity is estimated based on 5 days AIS data (2 - 6 September 2019). For more information about AIS data: see Chapter 5. Speeds below 0.2 m / s are not included in the average values. Based on the average velocities and a fixed water depth of 10 meters (for simplification), the required power during a stationary stage is determined for each vessel class: this calculation is based on the same calculation methods as discussed in the previous sections (for the dimensions of each vessel class: See Figure F.1 in Appendix F). The total required power (P_{tot}) resulting from the calculations, is multiplied by 15 percent, to determine the required power in a stationary stage (P_{stat}):

$$P_{stat} = 0.15 * P_{tot} \tag{3.39}$$

Table 3.1 shows the results of these calculations: for each vessel class, the average velocity resulting from AIS data is indicated and subsequently P_{stat} is calculated. The stationary power calculation of vessel type BII-6l (indicated with *) has not been performed, because the available data was not enough to make a good estimation of the vessel velocity: the same stationary power value as for the type BII-6b has been assumed.

3.4. Illustrating energy consumption calculation methods

In this chapter the energy consumption of inland vessels was treated. The energy consumption per unit time depends on the total required power, which can be be subdivided into the power for hotel systems on board and the power required for propulsion. The power required for propulsion depends on the resistance a ship experiences. A subdivision was made based on literature of Holtrop and GGJ Mennen (1978): the resistance was subdivided into frictional resistance, the effect of viscosity, frictional resistance from appendages, wave resistance and residual resistance terms (due go the immersed transom and model-ship correlation). To account

Motor vessels			Barges			Convoys		
Type	V_{mean} **(m/s)**	P_{stat} **(kW)**	**Type**	V_{mean} **(m/s)**	P_{stat} **(kW)**	**Type**	V_{mean} **(m/s)**	P_{stat} **(kW)**
M2	3,51	16	**B01**	3,69	14	**C1l**	2,41	6
M3	3,61	33	**B02**	3,09	12	**C1b**	2,78	9
M4	3,52	23	**B03**	3,53	22	**C2l**	3,79	113
M5	3,81	33	**B04**	3,44	25	**C3l**	3,77	104
M6	3,74	39	**BI**	3,20	29	**C2b**	4,34	104
M7	3,87	51	**BII-1**	3,86	60	**C3b**	2,79	51
M8	3,90	65	**BII-2l**	3,53	83	**C4**	4,22	203
M9	3,99	86	**BII-2b**	3,70	102			
M10	3,94	81	**BII-4**	3,40	113			
M11	3,95	94	**BII-6l**	-	314*			
M12	3,85	103	**BII-6b**	4,37	314			

Table 3.1: RWS inland vessel classification: average speed per vessel class (based on AIS data of 2 - 6 September 2019) and calculated power during stationary stage (P_{stat}).

for shallow water effects, a modification of the friction line proposed by Zeng et al. (2018) was applied, and for the other resistance terms, the shallow water effect was incorporated by using a corrected velocity, proposed by the Karpov method, described in literature of van Terwisga (1989).

This section will illustrate the results of applying the resistance and power calculation methods treated in this chapter to a reference vessel. The RWS vessel class M9 is chosen for these calculations, since there was reference data available to compare the output of the calculations with. For more information about the RWS vessel classes, see Appendix F.

The following characteristics of the M9 motor vessel are used in the calculations:

- The resistance and required power of the vessel is considered in a loaded condition
- L = 135 m, B = 1.75 m, T = 2.75
- The installed power is assumed to be 1750 kW

3.4.1. The different resistance components as function of the velocity

When a vessel speeds up, the resistance increases. The effect of an increased velocity is is greater for one resistance component than for another. This effect is illustrated for in Figure 3.7: the different resistance components have been plotted against the vessel speed, for a fixed water depth (h = 10 meter, deep water). The blue line represents the total resistance the M9 reference vessel experiences for different sailing speeds. You can see an exponential increase when the velocity becomes higher. The other curves represent the separate resistance components discussed: the yellow line shows the effect of frictional resistance, including the viscosity effect, the green line the frictional effect of the appendages, the red line the wave making resistance and the purple line the residual resistance terms (due to immersed transom and model-ship correlation). As you can see, especially the wave making resistance causes the exponential increasing behaviour of the resistance when the sailing speed becomes higher.

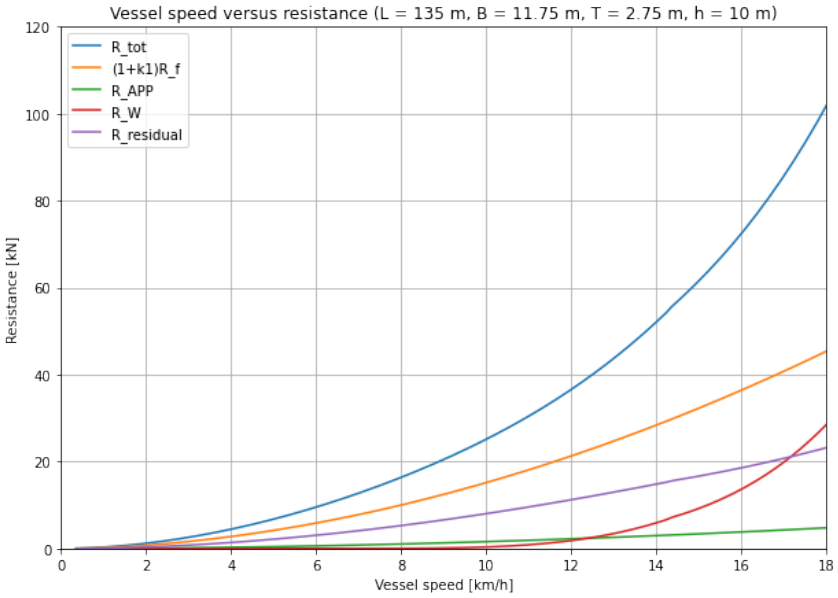

Figure 3.7: Total resistance and different resistance components as a function of the vessel speed

3.4.2. The total resistance for different water depths

Water depth limitations have been considered in the resistance calculation method elaborated in this chapter. When a ship enters shallow water, the resistance increases significantly. To illustrate this effect, the total resistance as function of the velocity is plotted for different water depths (Figure 3.8) for the same M9 reference vessel. The blue lines show the results for relatively deep waters, and the red lines show the effect of more limited water depths. As you can see, in case of limited water depth, the resistance shows a more asymptotic behaviour. This is because the ship is approaching its critical speed (which is $\approx \sqrt{V_0 h}$ in shallow water conditions) (Pompée, 2015), resulting in a significant increase of the wave making resistance. In addition, the frictional resistance increases as well due to limited water depth.

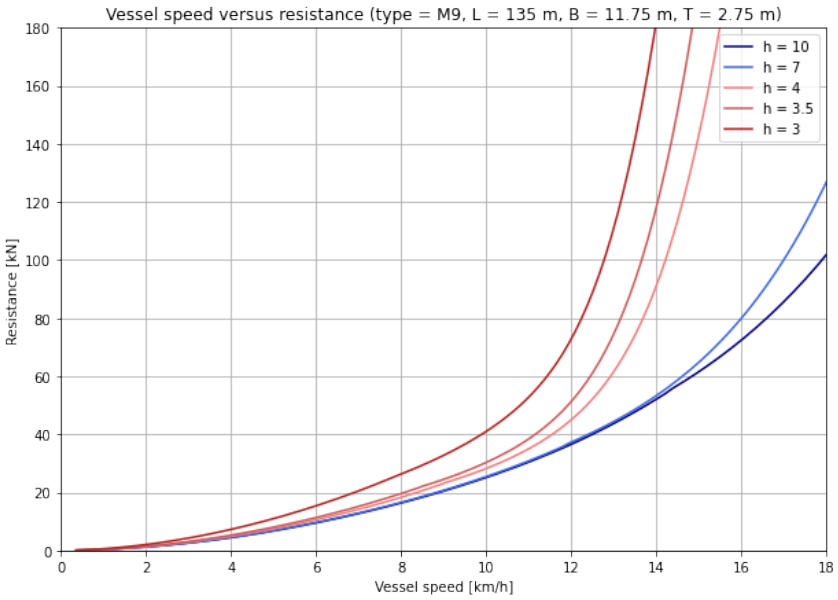

Figure 3.8: Total resistance as a function of the vessel speed, for different water depths

3.4.3. The total required power

The total required power consists of a power component for hotel systems on board, which is assumed to be 5% of the installed engine power, and a power component for propulsion. The power required for propulsion

is related to the resistance of the vessel. Figure 3.9 shows the output of the power calculations for the same reference vessel M9: the power is plotted against the vessel speed, again for different water depths. Also in this figure you see the asymptotic behaviour of the required power when a vessel enters shallower water: the critical speed is reached earlier when you sail in limited water depth. Approaching the critical speed results in an extensive increase of the power.

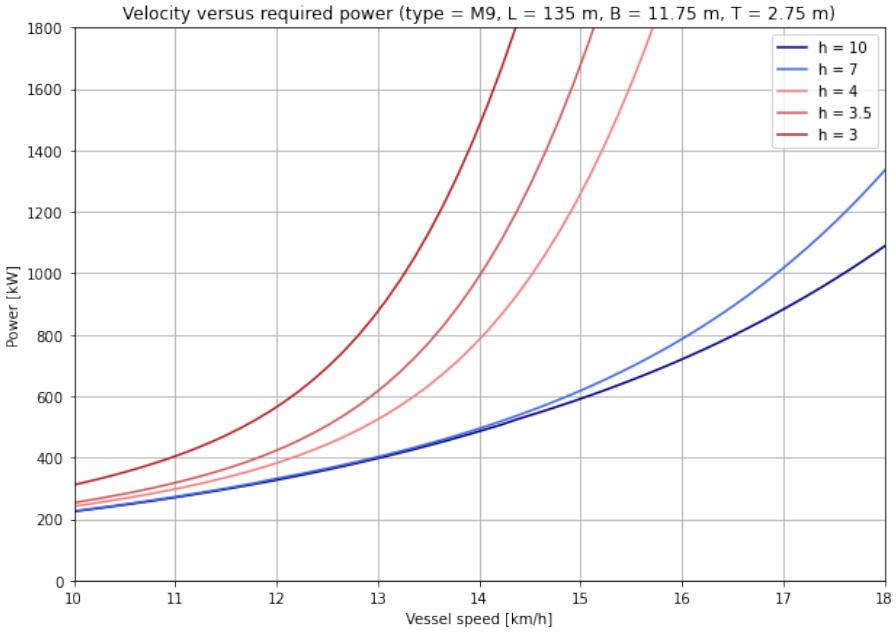

Figure 3.9: Vessel speed versus total required power

Please note that the x-axis of Figure 3.9 starts at 10 km/h (instead of 0 km/h): this was done to be able to directly compare the power output with a reference project. We verify the power output by comparing it to a reference figure presented in the thesis of Hekkenberg (2013): Figure 3.10 shows the results of Computational Fluid Dynamics (CFD) calculations of Zigic (2007). As you can see, the output of the developed power calculation method of this chapter (Figure 3.9) shows comparable behaviour: the deep water curve almost completely matches. Estimating required power in limited water depth is quite complex and therefore these estimates are quite uncertain, but the behaviour is similar in both figures and the asymptotic behaviour is clearly reflected.

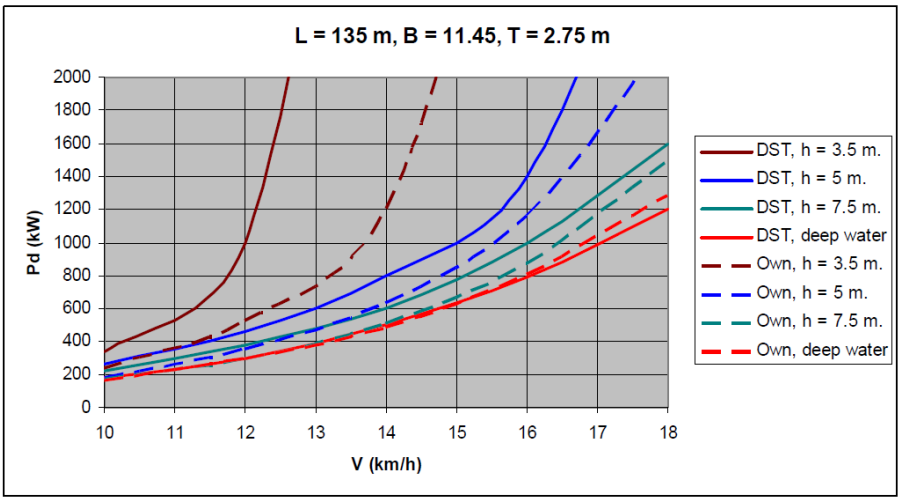

Figure 3.10: Validation figure for power calculations of M9 motor vessel (Hekkenberg, 2013)

3.5. Sensitivity analysis of energy consumption estimation method

A sensitivity analysis has been performed for the most important input variables of the energy consumption estimation method treated in this chapter. It has been tested what happens with the resistance and power output when you apply a certain change to one of the input parameters. The results of this sensitivity analysis is presented in Appendix E. The most important outcomes are listed below:

- The efficiencies have a proportional effect on the power output
- The length and width of a vessel have significant effect on the resistance and power output: for example, when you increase the vessel length (base case: L = 135 m) with 22.2%, the resistance increases with 27.5% and the required power with 21.0%. The relative impact of increased vessel size becomes larger when the absolute length and width values are larger.
- The sensitivity of the draft is limited in case of deep water. The resistance does not decrease significant in case of lower drafts. For example: decreasing a draft by 9.1%, shows only 1 percent reduction of the resistance and power output.
- As discussed before, the block coefficient was set to a fixed value of 0.85. Inland ships have a relatively high block coefficient, especially when you consider barges. The developed method is not suitable for higher block coefficient values than 0.85. The sensitivity analysis also shows this: when the block coefficient is above 0.85, we see an excessive increase of the resistance and power output. For example, when the block coefficient is set to 0.9, which is a 5.9% increase compared to the base case with a block coefficient of 0.85, the resistance of a ship increases with 48.5% and the power output with 37.0% compared to the base case. Above 0.9 the method no longer gives usable output. This is also an important limitation of the method.

4

Method to estimate emissions

In Chapter 3 a method was developed to predict the energy consumption of an inland vessel. In this chapter, a method will be developed that translates the energy consumption to the potential emissions.

How much a ship emits depends on the required energy of the vessel, expressed in kWh. The translation to emissions can be performed with so called emission factors: these emission factors, expressed in g/kWh, depend on many different variables and vary per type of emission. The engine age has a strong influence on the emission factors: the newer the engine is, the lower the emission factors. In addition, the partial engine load is of importance. This is the part of the total installed power that is used at a specific moment in time. When the partial engine load is low, the engine is less efficient and the emission becomes relatively higher. Correction factors have to be applied to general emission factors to take this effect into account.

In this chapter we will first discuss the main emissions resulting from inland shipping. Afterwards we discuss to development of a method to actually calculate these emissions, by means of the determination of emission factors. Subsequently, the emission calculation method is illustrated for a reference vessel: the effect of the velocity, water depth and engine age on the emission rates will be mapped. At the end of this chapter the most important findings of a sensitivity analysis of the method will be presented.

4.1. Main emissions in inland navigation

In the introduction chapter the goals defined in the Green Deal were introduced (Section 1.2 Problem description). Figure 1.5 showed a timeline of the ambitions drawn up in the Green Deal regarding the reduction of emissions from inland shipping. The Green Deal makes a distinction between CO_2 emission (the most important greenhouse gas resulting from inland navigation) and environmental pollutants. In the following sections, the most important emissions caused by inland shipping are discussed in more detail, based on this subdivision.

4.1.1. CO_2 emissions

Carbon dioxide (CO_2) is the main greenhouse gas caused by human activities. In the transport sector, CO_2 is generated during combustion of fuel. The amount of CO_2 emitted is proportional to the consumption of fuel, and depends on the carbon content. CO_2 emissions generated by human activities, including inland shipping, contribute to the enhanced greenhouse effect, which leads to global warming.

The capacity of the transport mode has a significant influence on the CO_2 emission per tonne-kilometer. When a modality is carrying large volumes at once, the fuel per tonne-kilometer is relatively low. Inland shipping has the advantage that it can carry relatively large volumes for the amount of CO_2 that is emitted. The annual figures also show this: the share of inland shipping in the entire CO_2 emissions of the transport sector in the Netherlands was only 5.1% in 2017 (See Figure 4.1), but the inland shipping share in the Dutch transport performance is about 35% (Bureau Voorlichting Binnenvaart, n.d.[a]).

Although inland shipping is a relatively sustainable transport mode concerning CO_2 emissions, the amount of CO_2 emitted is still considerable: the pressure to reduce CO_2 emissions in inland shipping is increasing, and therefore it is relevant to take CO_2 emissions of the inland fleet on the Rotterdam-Antwerp corridor into account.

4.1.2. Environmental pollutants

In this research the following environmental pollutants of inland shipping will be taken into account:

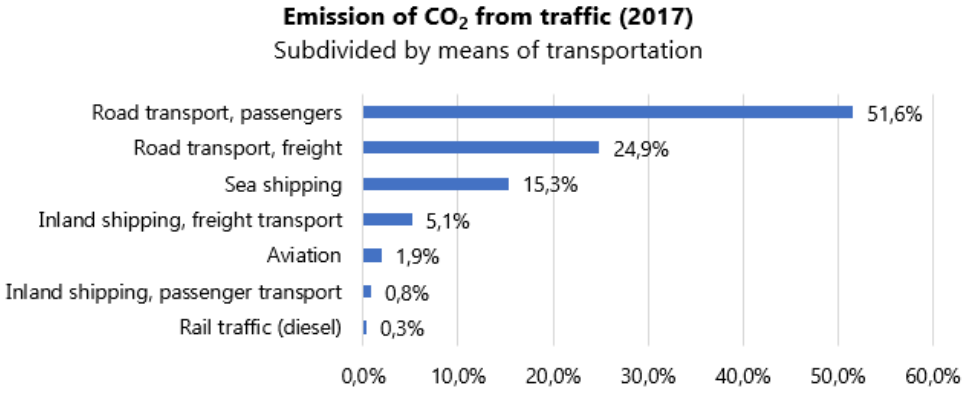

Figure 4.1: Emission of CO_2 from traffic, subdivided by means of transportation (data of 2017) (CBS, 2020a)

- Nitrogen oxides (NO_x)
- Particulate matter (PM_{10})

The focus on NO_x and PM_{10} is based on the relative contribution of inland shipping to the total amount of of that type of emission, caused by mobile sources on or above Dutch territory. Figure 4.2 shows the relative contribution of inland shipping to the main pollutants NO_x, PM_{10} and SO_2 (CBS, 2020a).

As you can see from Figure 4.2, the contribution of inland shipping to the total NO_x and PM_{10} emissions from mobile sources is considerable: for NO_x emissions this was more than 12% in 2018, for PM_{10} this was 10%. Figure 4.2 also shows that the relative contribution of inland shipping to the total amount of NO_x and PM_{10} emissions increased over the years. Please note: this does not mean that the total amount of these emissions caused by inland shipping increased over the years. This can be seen in Figure 4.3: in absolute terms, there is a (slight) decrease over the years in the amount of NO_x and PM_{10} emitted by inland shipping on Dutch territory.

Sulfur dioxide (SO_2) is an important environmental pollutant to consider with regard to health issues and environmental acidification. But the SO_2 emissions caused by inland shipping considerably decreased over the years (Figure 4.3): from 2011, inland shipping uses low sulfur fuel (Bureau Voorlichting Binnenvaart, n.d.[a]). This results in a limited contribution of inland navigation to SO_2 emissions (Figure 4.2). Therefore, the SO_2 emissions on the Rotterdam-Antwerp corridor will not be part of this research.

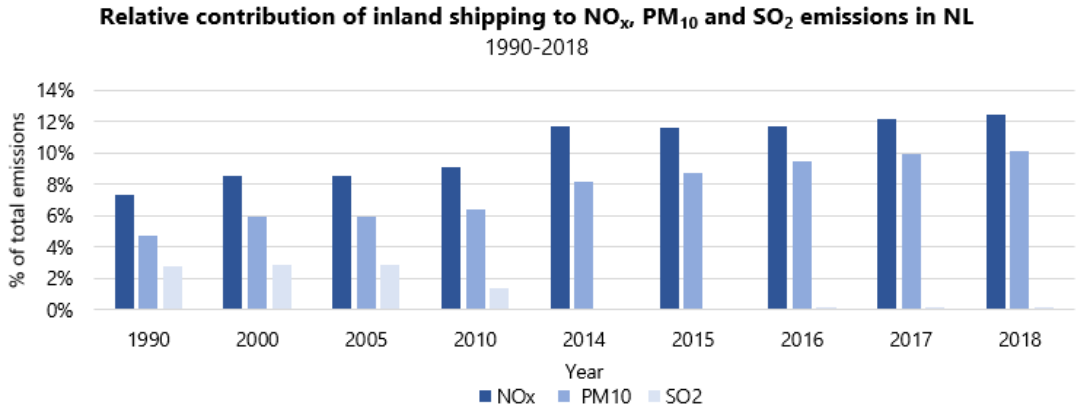

Figure 4.2: Yearly relative contribution of inland shipping to the total amount of emission of the air pollutants NO_x, PM_{10} and SO_2 for the period 1990-2018 (CBS, 2020a)

More background information about NO_x and PM_{10} is provided below, to give an idea of what these environmental pullotants are, how they originate and why it is important to reduce these emissions.

Nitrogen oxides NO_x
Nitrogen oxides are caused by high temperatures and pressures of the engine: nitrogen present in the air then combines with oxygen (Hulskotte and Bolt, 2012). Nitrogen oxides can cause health problems, but also have

impact on nature. Nitrogen oxides deposit in nature, which can disturb the ecological system. This could result in the loss of biodiversity (RIVM, n.d.). Nitrogen oxides are hereinafter referred to as NO_x.

Given the strict nitrogen standards in the Netherlands, the pressure to reduce NO_x emissions is high. Inland shipping causes a large share of theNO_x emissions in the Netherlands: in 2018, inland shipping accounted for 12.5% of the total NO_x emissions from mobile sources on Dutch territory, and these emissions have has remained fairly stable in recent years (Figure 4.3). Therefore, this is an area where is still much to be gained.

There already are various ways to reduce NO_x emissions. An effective way to do this is Selective Catalytic Reduction (SCR). This catalyst removes nitrogen oxides from flue gas: NO_x is converted into harmless water and nitrogen by a chemical reaction, using urea as a catalyst. SCR can reduce nitrogen oxides up to 90% (Bureau Voorlichting Binnenvaart, 2017). However, these kind of innovations are expensive, which prevents skippers from investing. The Green Deal plans to make subsidies available to stimulate these investments, but there is not yet enough money available to green the entire fleet (Rijksoverheid, 2020).

Particulate matter PM_{10}
Particulate matter is a term for small particles in the air, which can be harmful to health. Most of these particles in the air are caused by humans, especially by combustion processes. Soot is part of particulate matter, which is a product of incomplete combustion. Particulate matter is hereinafter referred to as PM_{10}, which refers to particles with a diameter of less than 10 micrometers (Atlas Leefomgeving, n.d.).

The emission of PM_{10} is related to the sulfur content in the fuel. Because inland navigation uses low sulfur fuel since 2011 (Bureau Voorlichting Binnenvaart, n.d.[a]), this resulted in a decrease of the total PM_{10} emissions from inland shipping (see Figure 4.3). The emission of PM_{10} can be reduced even further by using soot filters, but this also requires an investment from the skipper, which does not stimulate the development of reducing particulate matter emissions. The contribution of inland shipping to the total PM_{10} emissions resulting from transport in the Netherlands is therefore still relatively high (more than 10%) and many steps can still be taken to reduce these emissions.

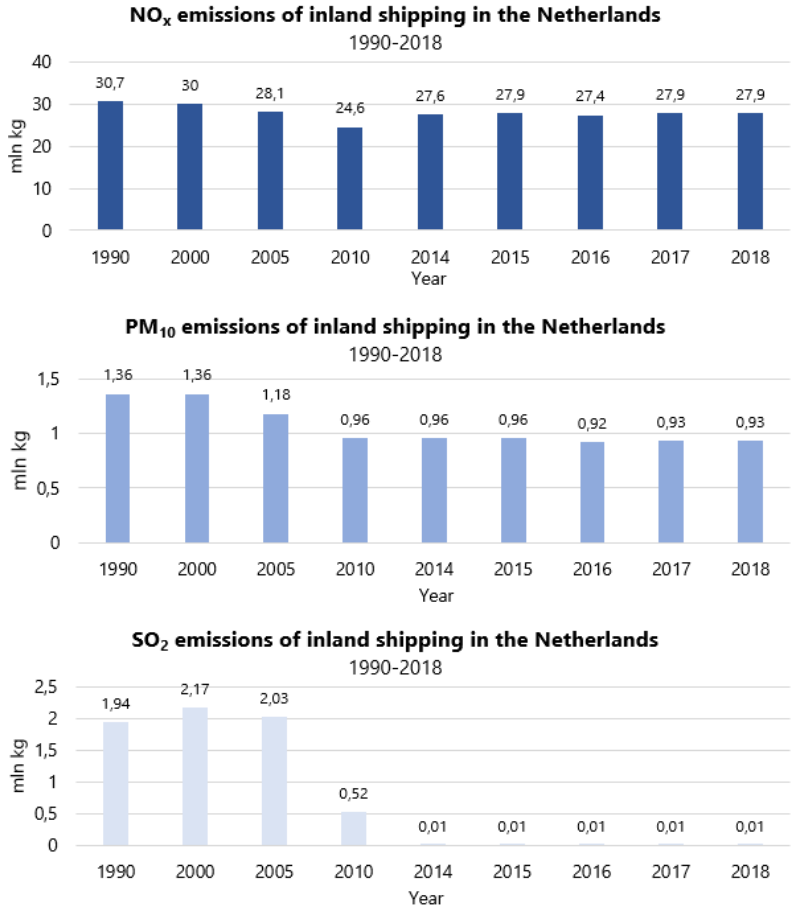

Figure 4.3: Yearly amount of NO_x, PM_{10} and SO_2 emissions caused by inland shipping for the period 1990-2018 (CBS, 2020a)

4.2. Calculating emissions

Now the focus on emission types has been determined, the next step is to elaborate on a method to calculate emissions. In Chapter 3 a method was developed to estimate the energy consumption and total required power (P_{tot}) of inland vessels, depending on the dimensions of the ship, the sailing speed and the waterway restrictions. One of the findings in this chapter was that when you travel with the same speed, significantly more power is required in limited water depth.

In this section, the total power required will be translated to the corresponding emissions. The total emission (in gram) during time span Δt, is the total required power multiplied by this time span (which is the required energy in kWh), multiplied by a certain emission factor (in g/kWh) (Hulskotte and Bolt, 2012):

$$EM_s = P_{tot} \Delta t EF_{tot} \tag{4.1}$$

In which:
EM_s = emission of a single ship during time span Δt [g]
P_{tot} = total required power of an inland vessel [kW]
Δt = time span [h]
EF_{tot} = total emission factor of a certain product [g/kWh]

The total emission factor results from a general emission factor (which depends on the engine age), multiplied by a correction factor (which depends on the partial engine load):

$$EF_{tot} = EF_{general} * C_{correction} \tag{4.2}$$

For each type of emission (CO_2, NO_x and PM_{10}) the total emission factor will be determined, in order to calculate the emission rate for different sailing speeds and water depths. In Section 4.2.1 it is presented how to determine the general emission factors. Section 4.2.2 elaborates on the correction factors that have to be applied to the general emission factors.

4.2.1. General emission factors

Emission factors indicate the rate of how many of a certain product is emitted per unit of energy consumed, expressed in gram per kWh. The emission factors of CO_2, NO_x and PM_{10} are considered in this research. The emission factor of CO_2 is fuel dependent: it depends on the carbon content of the fuel. When the carbon content of the fuel is low, less CO_2 is emitted. The emission factors (NO_x and PM_{10}) are technology dependent, and are therefore more complex to determine.

Engine age dependence

The construction year of the engine has a significant influence on the general emission factor. This is because (1) the preference changed from slow to fast running engines and (2) the technological developments of engines, which results in changes in the emission patterns. Table 4.1 shows actual data of TNO (Ligterink, 2019) regarding general emission factors: for each engine construction year class, the specific fuel consumption is specified, and the corresponding general emission factors of CO_2, PM_{10} and NO_x are shown in the table.

The technology dependent emission factors PM_{10} and NO_x are based on measurements performed by TNO. The fuel dependent emission factor of CO_2 is based on the fuel consumption in Table 4.1. For diesel it holds that 3173 gram CO_2 is produced in the combustion process of 1 kg diesel (CE Delft, 2016). With that information the emission factor of CO_2 has been calculated from the specific fuel consumption (fourth column in the table). From the information in the table it can be concluded that the emission factors for each product are in general significantly lower for newer engine classes.

To determine the emission factors of a vessel with a certain age, the distribution of construction year classes of marine engines has to be determined. This can be performed according to a Weibull-function. The general expression of this Weibull-function is (Ligterink, 2019):

$$f(x;k;\lambda) = \frac{k}{\lambda}\left(\frac{x}{\lambda}\right)^{k-1} e^{(-x/\lambda)^k} \tag{4.3}$$

Construction year classes	Weight class	Fuel consumption [g/kWh]	CO_2 [g/kWh]	PM_{10} [g/kWh]	NO_x [g/kWh]
1900 - 1974	L1 t/m L3	235	746	0.6	10.8
1975 - 1979	L1 t/m L3	230	730	0.6	10.6
1980 - 1984	L1 t/m L3	225	714	0.6	10.4
1985 - 1989	L1 t/m L3	220	698	0.5	10.1
1990 - 1994	L1 t/m L3	220	698	0.4	10.1
1995 - 2002	L1 t/m L3	205	650	0.3	9.4
2003 - 2007 CCR-1	L1 t/m L3	200	635	0.3	9.2
2008 - 2018 CCR-2	L1 t/m L3	200	635	0.2	7
2019 - 2019 CCR-2	L1 t/m L3	200	635	0.2	7
2019 - 20xx stage V	L1	205	650	0.1	2.9
2020 - 20xx stage V	L2 and L3	190	603	0.015	2.4

Table 4.1: General emission factors of CO_2, PM_{10} and NO_x for different construction year classes of marine engines (Ligterink, 2019)

With x is the age (in years) of the engine. TNO determined the the k and λ values of the Weibull-function for weight class L1, L2 and L3, based on the IVR-vesseldatabase and a survey among 350 professional skippers (see Table 4.2). Each RWS vessel class can be assigned to a weight class: Figure F.1 in Appendix F shows an overview of each RWS vessel class, with its characteristics and the corresponding weight class. Figure 4.4 shows the probability density functions of the age of the engine for the three weight classes. The survival function for each weight class is visualized in Appendix D (Figure D.1): the figure shows for a marine engine with a certain age, how many percent of the engines with that age is still active.

Weight class	k	λ
L1	1,3	20,4
L2	1,12	18,5
L3	1,26	18,6

Table 4.2: k and λ values of the Weibull distribution of the construction year classes of marine engines for weight class L1, L2 and L3 (Ligterink, 2019)

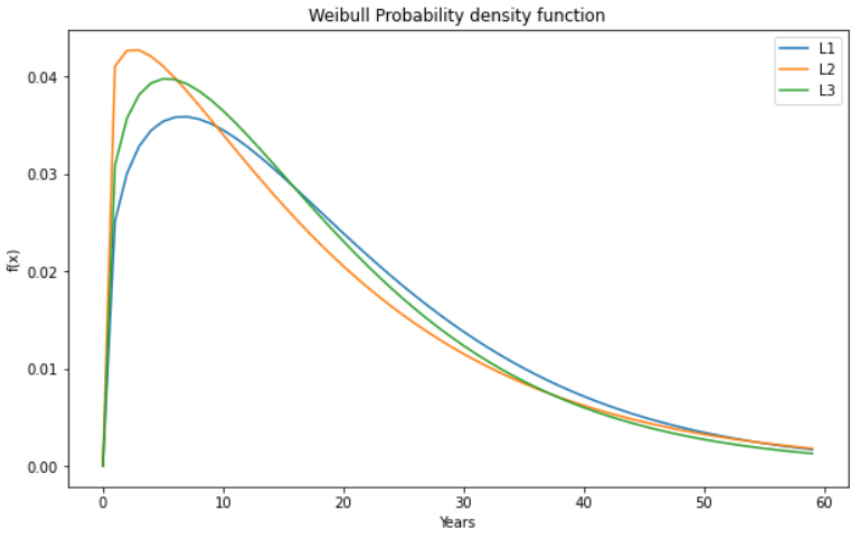

Figure 4.4: Weibull function per weight class, describing the distribution of engine age

With the Weibull-function, it can be computed for each year, how large is the share of engines within each construction year class. Figure 4.5 shows the estimated distribution of the year 2020. Table D.1 in Appendix D shows the corresponding percentages.

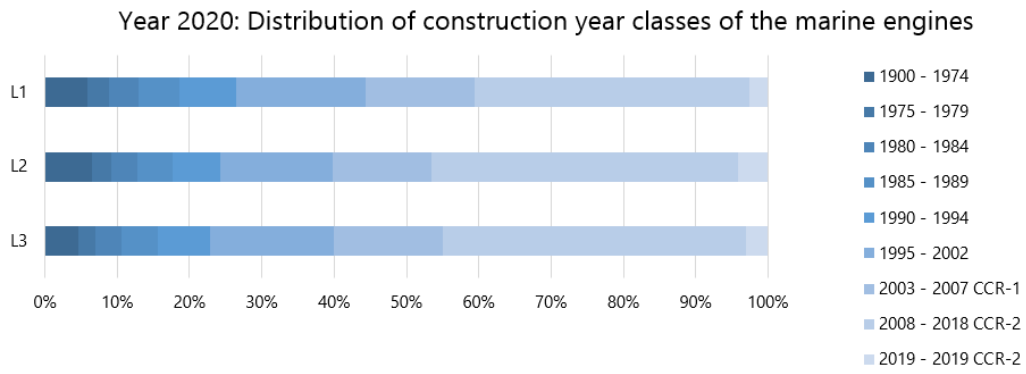

Figure 4.5: Estimated distribution of construction year classes of marine engines of the year 2020

4.2.2. Correction factors: dependency of partial engine load

In a stationary stage or in a stage where a vessel is slowing down or sailing at a slower speed, the partial load of the engine is low: the vessel requires less power, so uses a smaller part of the total installed power of the engine. When the partial engine load is low, the engine is less efficient, which results in higher emission factors. This is mainly caused by the fact that more incomplete combustion occurs, resulting in higher emission levels.

To take this effect into account, the general emission factor (see Table 4.1) has to be multiplied by a correction factor, which results in the 'total emission factor'. TNO provides a table with different partial engine loads and the corresponding correction factors for different combustion products (among other things CO_2, NO_x and PM_{10}), which are presented in Table D.2 in Appendix D. Figure 4.6 shows the correction factors for CO_2, PM_{10} and NO_x (depending on the engine class) as a function of the partial engine load. The figure shows that the CO_2 emission factor is not extremely sensible to low partial engine loads. However, the correction factors of PM_{10} and NO_x can increase significantly in low partial load status of the engine.

The correction factors of NO_x depend on the type of engine class: the CCR-1 and CCR-2 classes correspond to relatively older engine classes (see also Table 4.1), whilst the IWP/IWA classes correspond to the newer 'stage V' classes. The IWP/IWA-v/c-3 class corresponds to smaller vessels with an installed power less than 300 kW. The assumption has been made that vessels from weight class L1 correspond to engine class IWP/IWA-v/c-3. The engine class IWP/IWA-v/c-4 corrresponds to vessels with more power than 300 kW and this engine class is assigned to weight class L2 and L3.

Figure 4.6 shows that the newer engines are more sensible to low partial engines loads considering the emission of NO_x. This is because the catalyst in these engines stays relatively cold when the engine load is low, especially considering bigger ships.

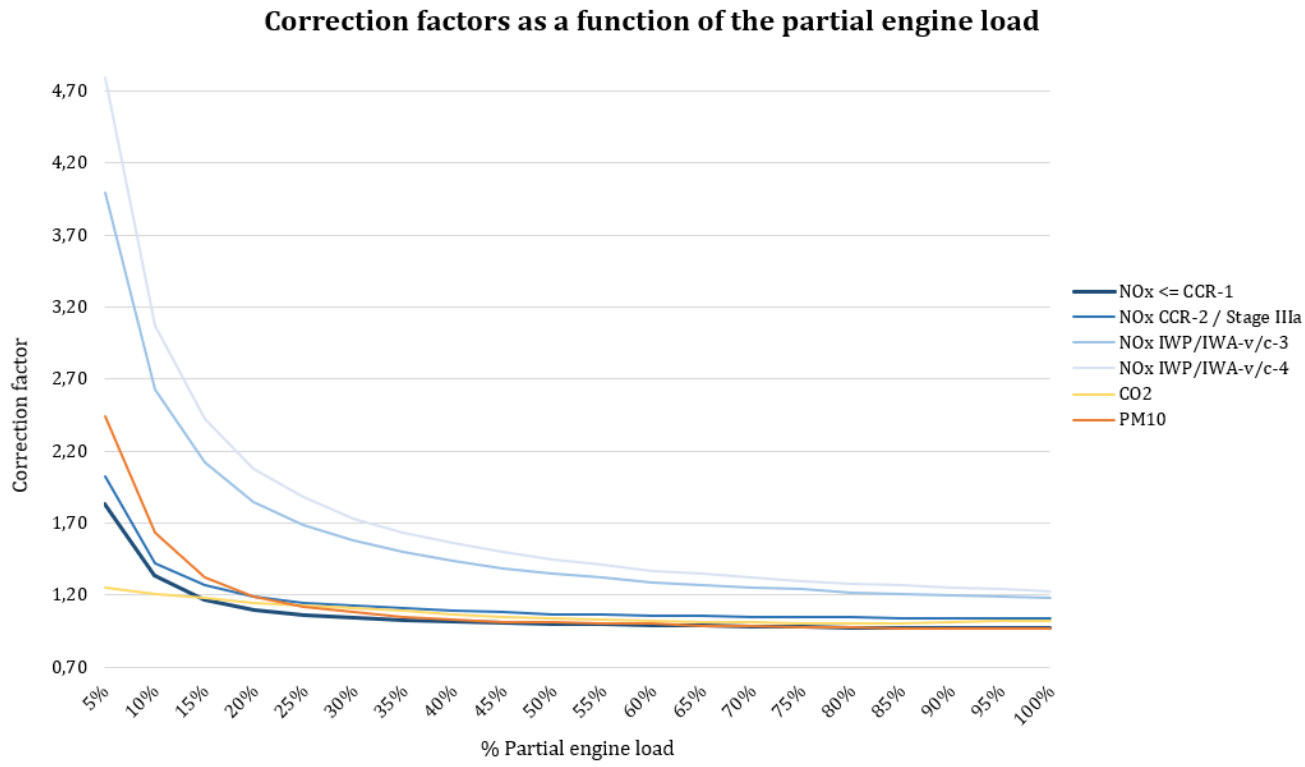

Figure 4.6: Correction factors of the emission factors of NO_x, CO_2 and PM_{10} (Ligterink, 2019)

4.3. Illustrating emission calculation methods

The method to determine the total power required for different ship dimensions, sailing speeds and water depths was elaborated in Chapter 3. The next step was to translate this P_{tot} to emissions, which was elaborated in the previous sections: the total required energy has to be multiplied by an emission factor to determine the total emissions. The emission factor depends on the construction year of the engine and the partial engine load.

In this section, the calculation methods will be applied to a reference vessel: as with the power calculations in Section 3.4, the RWS vessel class M9 has been chosen to illustrate different dependencies of the emission rates (see Appendix F for characteristics of the RWS vessel classes). In the following subsections, the emission rates (in g/km) of the CO_2, PM_{10} and NO_x emissions are mapped for different situations. These emission rates are calculated as follows:

$$EM_{\text{rate}} = P_{\text{tot}} EF_{\text{general}} C_{\text{correction}} / V_{0,\text{km/h}} \tag{4.4}$$

In which:

EM_{rate} = emission rate [g / km]
P_{tot} = total required power [kW]
$EF_{general}$ = general emission factor [g / kWh]
$C_{correction}$ = correction factor [-]
$V_{0,km/h}$ = sailing speed [km/h]

In the following subsections the optimal sailing speed of the reference vessel M9, considering the emission rates, will be visualised. In addition, the effect of different water depths and different engine ages will be treated.

4.3.1. Optimal sailing speed in unrestricted water

The CO_2, PM_{10} and NO_x emission rates (in g/km) of the M9 vessel are calculated for different vessel speeds in unrestricted water (water depth of 10 meters). We assumed that the M9 vessel has an engine constructed in the year 1990. The results are plotted in Figure 4.7. The figure shows that the emission rate grows asymptotically

if you reach a zero speed: the emission rate is expressed in g/km, but if the ship is not running distance (due to zero speed), you divide by zero and the emission rate becomes infinite. Please note that these figures map the emission rates of a sailing vessel: emissions in a stationary stage have to be predicted differently, which was discussed in the previous chapter (Section 3.3). Stationary emission rates of different vessel types are discussed in detail in Chapter 8, Section 8.1.1.

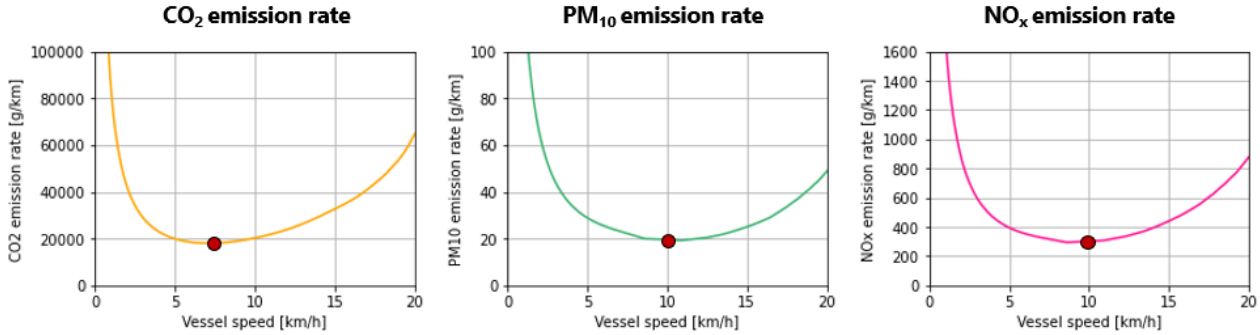

Figure 4.7: Calculated CO_2, PM_{10} and NO_x emission rates of a M9 vessel (in g/km) as function of the vessel speed, for deep water (h = 10 m): the optimal speed for the different curves is marked with the red dot. Construction year of M9 engine: 1990.

The emission rate curves show a parabolic behaviour: at a certain sailing speed, the emission rate has reached a minimum. In each emission rate curve of Figure 4.7, this minimum emission rate is marked with a red dot. We define the corresponding sailing speed as the optimal speed. As you can see, the optimal sailing speed of a M9 vessel, considering the CO_2 emission rate, is around 7.5 km/h, but for the PM_{10} and NO_x emission rates the optimum lies at a higher speed (around 10 km/h). This can be explained by the effect of the correction factors (elaborated in Section 4.2.2). If the sailing speed is relatively low, the partial engine load is low, which causes an increase in the correction factors and so in the emission factors of mainly PM_{10} and NO_x. It also affects the CO_2 emission factor, but to a much lesser extent. This phenomenon means that the engine is relatively less efficient for lower speeds considering the emissions of PM_{10} and NO_x, resulting in the fact that the optimal speed lies a bit higher compared to the CO_2 case.

4.3.2. Emission rates for different water depths

Chapter 3 discussed that more power is required if a ship enters shallower water without reducing its speed: a ship experiences more resistance in limited water depths. We also see this effect in the emission rates: Figure 4.8 shows the CO_2, PM_{10} and NO_x emission rates of a M9 vessel as a function of the vessel speed, for different water depths. Please note again that this picture does not contain information about emission rates in the stationary stage: it provides information about a moving vessel.

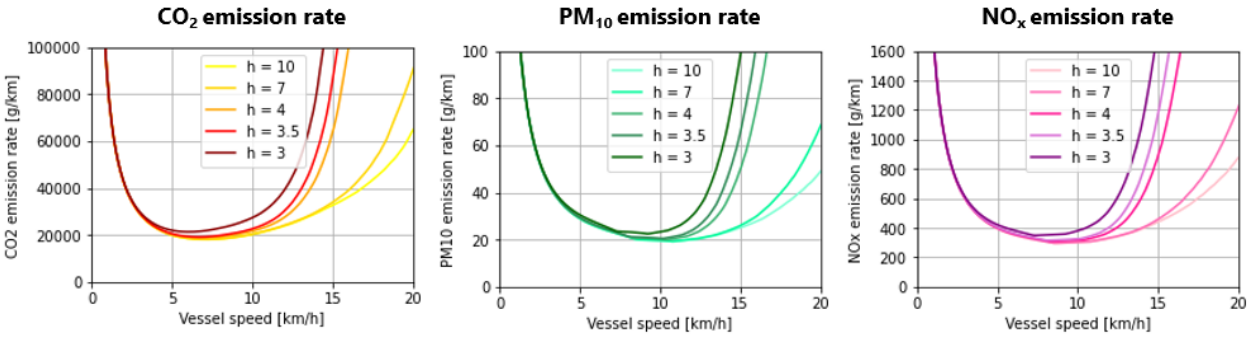

Figure 4.8: Calculated CO_2, PM_{10} and NO_x emission rates of a M9 vessel (in g/km) as function of the vessel speed, for different water depths. Construction year of M9 engine: 1990.

Figure 4.8 shows that in the lower speed ranges, the difference in emission rates between deeper and shallower water are limited. When the speed increases, you see asymptotically behaviour of the emission curves representing shallower water cases. This is the reason why vessels in practise often slow down when they enter shallow water, because they want to avoid extensive fuel consumption.

4.3.3. Emission rates for different engine ages

The emission factors depend on the engine age: due to technological innovation, newer engines are in general more efficient considering emissions (see Table 4.1). This effect is clearly visible when the emission rates are plotted for different construction years of the engine. Figure 4.9 shows the CO_2 emission rate of a M9 vessel for different construction years of the engine (= c_{year}), Figure 4.10 the emission rates of PM_{10}, and Figure 4.11 the emission rates NO_x.

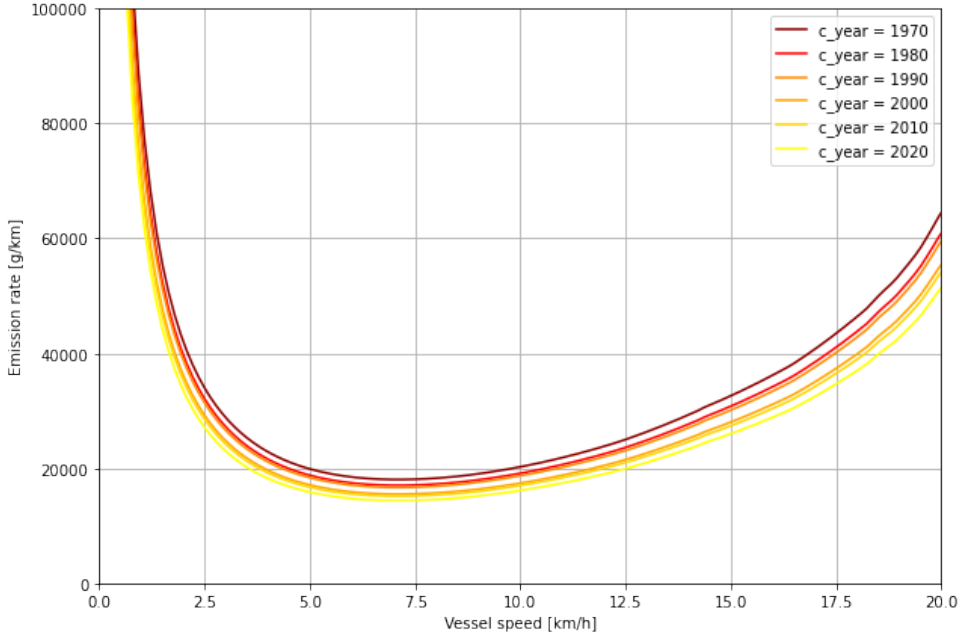

Figure 4.9: Calculated CO_2 emission rate of a M9 vessel (in g/km) as function of the vessel speed, for different construction years of the engine. h = 10 m.

Especially for the particulate matter (PM_{10}) and nitrogen oxides (NO_x) emission rates, you see a significant difference in the emission rates between older and newer engines. Especially for PM_{10}, the emission rates becomes almost zero considering the newest engines. Fleet renewal offers a lot of potential in that regard, because the emission rates of both environmental pollutants can stay limited, also when increasing the sailing speed.

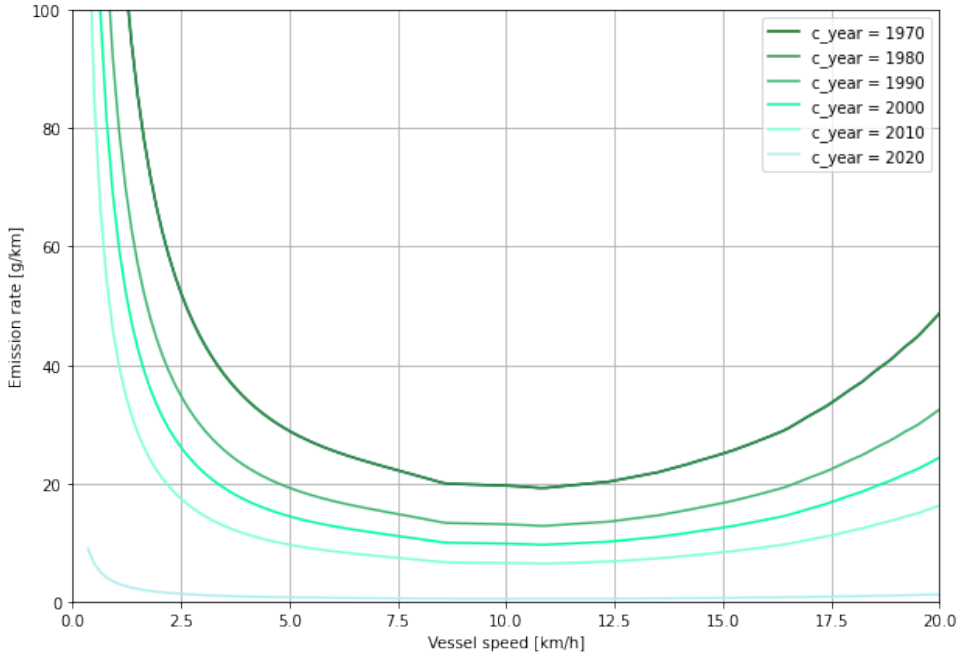

Figure 4.10: Calculated PM_{10} emission rate of a M9 vessel (in g/km) as function of the vessel speed, for different construction years of the engine. h = 10 m.

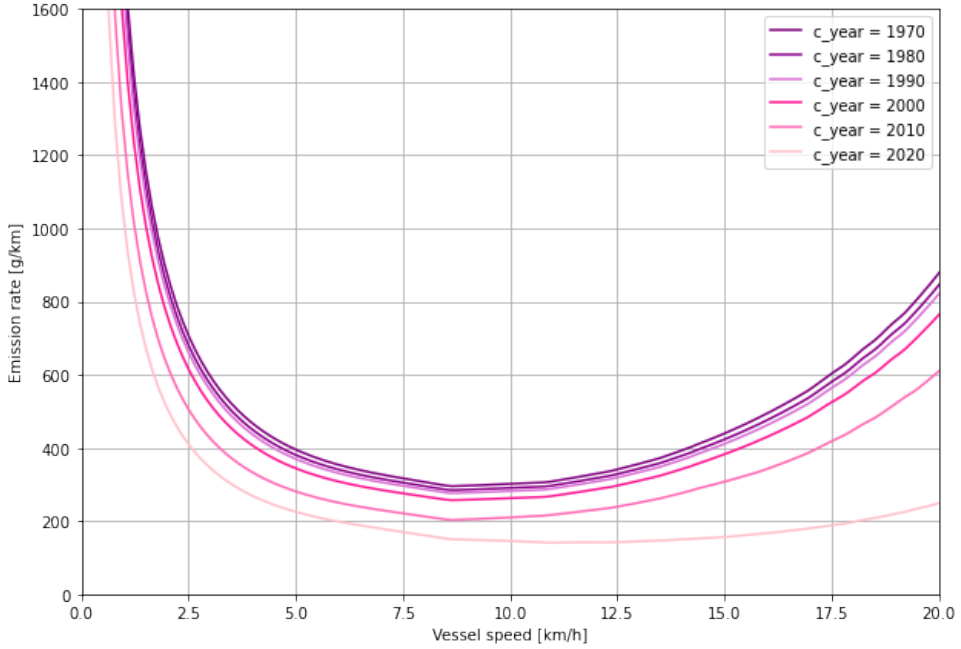

Figure 4.11: Calculated NO_x emission rate of a M9 vessel (in g/km) as function of the vessel speed, for different construction years of the engine. h = 10 m.

4.3.4. Emission rates in gram per hour

Till know we expressed the emission rates in gram per km, since we are interested in the distribution of emissions along the corridor. But on the other side it is also interesting to quantify the emissions per unit time, for example in situations where a vessel is in a stationary stage and does not cover any distance. Therefore, Figure 4.12 and 4.13 show the emission rates for the same reference vessel (M9) expressed in gram per hour. Figure 4.12 shows the emission rates of CO_2, PM_{10} and NO_x for different water depths (with a fixed engine age), and Figure 4.13 shows the emission rates for different engine ages (with a fixed water depth).

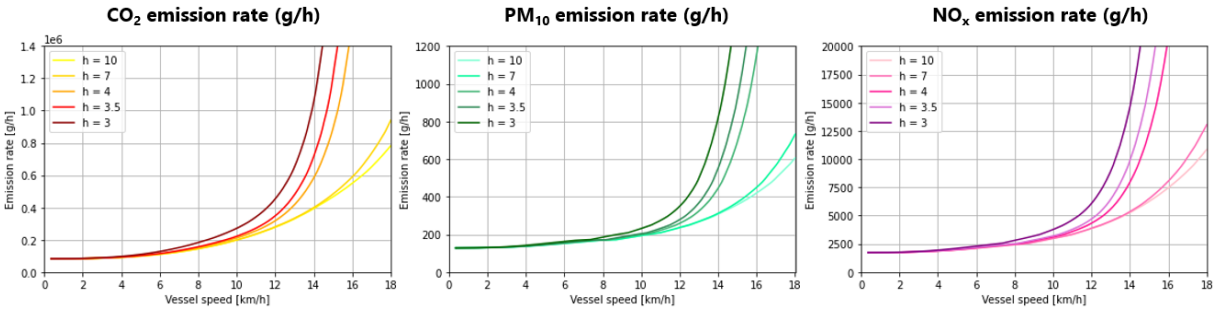

Figure 4.12: Calculated CO_2, PM_{10} and NO_x emission rates of a M9 vessel (in g/hour) as function of the vessel speed, for different water depths. Construction year of M9 engine: 1990.

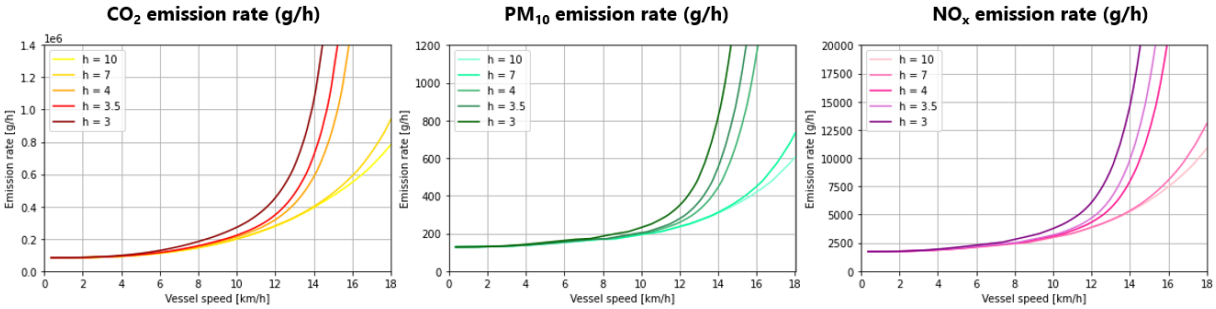

Figure 4.13: Calculated CO_2, PM_{10} and NO_x emission rates of a M9 vessel (in g/hour) as function of the vessel speed, for different engine ages. Fixed water depth of 10 meters.

4.4. Sensitivity analysis of emission estimation method

In the previous chapter, a sensitivity analysis was introduced to see how sensible the resistance and power output is to certain changes applied to input parameters (See Section 3.5). This analysis is also performed for the emission output: see Appendix E. The input parameters with a significant influence on the resistance and power output already have been discussed in Section 3.5. Logically, these results also influence the emission rates. The input parameters that specifically have influence on the emission rates are indicated below:

- A change in the amount of installed power ($P_{installed}$) has especially a significant influence on the particulate matter emission rate.
- Changes in velocity mostly influence the CO_2 emission rate: when increasing the speed of a M9 vessel from 3.5 m/s to 4 m/s, the CO_2 emissions increase by 20.4%. For the PM_{10} and NO_x emissions this is 14.3% and 18.5%.
- The changes in the engine age have a significant influence on the particulate matter and nitrogen emission rates: when the engine of the year 2000 of a M9 vessel is replaced by an engine of the year 2020, this results in a reduction of CO_2, PM_{10} and NO_x emission of 7.2%, 95.0% and 52.4% respectively.

5

AIS: data and approach

In Chapter 3 and 4 a bottom-up method was developed to calculate the energy consumption and potential emissions of a single inland vessel, as a function of ship dimensions, sailing speed and waterway characteristics. One of the goals of this study is to visualize the emission patterns on an inland waterway network (in our case the Rotterdam-Antwerp corridor), to be able to define emission hotspots. For this next step, data is required about the actual fleet on the corridor: how many ships are sailing along the corridor, at which moments in time, which routes do they sail, and what are the ship's characteristics. To find out this information, we will make use AIS data. Rijkswaterstaat provided an AIS dataset, containing three months of data. This chapter will dive into the characteristics of this dataset. In Part II, the results section, the calculation methods of the previous chapters are applied to this AIS dataset, to visualize the emission patterns based on observed data ('t0 emission scenario'), and to use the AIS data as input for the simulation model that will be developed to support the development and evaluation of emission reduction policies.

In this chapter, a general introduction of AIS data is provided and the characteristics of the dataset will be discussed. Subsequently, by means data analysis, the fleet and corridor characteristics will be mapped. It will be explained how important missing data is added to the dataset and how the dataset is enriched with information that is important for the emission calculation method.

5.1. General introduction to AIS data

AIS stands for Automatic Identification System. This system was originally developed for sea shipping, but is now also indispensable for inland shipping. The AIS system provides better identification of vessels, which increases safety and efficiency of shipping. The main purpose of the information system is to enable good communication between skippers and between ships and traffic control centers. From 1 december 2014 it is mandatory for most of the inland ships sailing on the Rhine to have an AIS system on board and to use it (Rijkswaterstaat, 2014).

AIS is an accurate and practical way of exchanging information. The AIS consists of a transponder on board, equipped with a GPS (Global Positioning System) and VHF (Very High Frequency) system. Automatic Identification Systems continuously send signals containing information about the position and velocity of the ship, and several ship characteristics, and is able to receive the information of other vessels (Bureau Telematica Binnenvaart, 2009). Ships are visible from a distance of at least 5 kilometer, which makes it possible to anticipate on time when encountering other ships on the route. Especially in situations with less overview, for example in bends or at crossings, safety is enhanced. AIS enables skippers to plan and make decisions more independently, and the waterway can be managed more efficiently.

In this study, the AIS data is used for another purpose: this data can be used to map the actual fleet on the Rotterdam-Antwerp corridor, to provide insight in the emission levels of inland shipping. The data provides a time series of inland ships on the corridor, including information about the geographical position, the type of vessel, its dimensions and the sailing speed. This information can be used to apply the energy consumption and emission calculation methods: for each time step for each ship, the consumed energy of that time step can be computed, as well as the corresponding potential emission rates. This information can be used later on to map the emission patterns on the corridor, based on actual data.

5.2. The dataset: characteristics

Rijkswaterstaat provided an AIS dataset of the Rotterdam-Antwerp corridor, containing three months of data: August, September and October 2019. This period was chosen to include the influence of different seasons

(summer and fall), because seasonal changes can possibly have influence on waterway characteristics and so on the inland fleet distribution. A conscious choice was made for the period of the end of 2019, so that this still provides an up-to-date picture of the inland shipping sector, but to deliberately not include the effect of the COVID-19 pandemic in this study. The AIS data is requested for the geographic area shown in Figure 5.1.

Figure 5.1: Geographical area of the AIS dataset

In this section some relevant characteristics of the AIS data-set will be highlighted. First, the relevant parameters of the rough AIS data will be discussed in Section 5.2.1. Subsequently, data analysis is applied, to obtain more information about the fleet and the corridor characteristics. This information is relevant to explain certain outcomes in the results section of this study. Section 5.2.2 shows the characteristics of the fleet distribution on the Rotterdam-Antwerp corridor: common vessel types are specified and the distribution of ship dimensions and vessel speed will be presented. In Section 5.2.3 the locks on the network will be analyzed, and Section 5.2.4 discusses the characteristics of specific waterway sections on the corridor.

5.2.1. Parameters AIS data

AIS data consists of a large set of parameters. Not all parameters are relevant for this study. The parameters that will be used are briefly elaborated in this section. Figure 5.2 illustrates how the AIS data looks like: the table shows 5 logs of 'testship-1006', presenting the relevant parameters.

newtimestamp	shipname	vesseltypeERI	latitude	longitude	sog	speed	length	width	draughtInland
2019-08-04 03:59:30+00:00	testschip-1006	8020	51.899250	4.486580	1.3	0.710366	110.0	11.0	1.5
2019-08-04 03:59:51+00:00	testschip-1006	8020	51.899170	4.486380	1.8	0.873326	110.0	11.0	1.5
2019-08-04 04:00:09+00:00	testschip-1006	8020	51.899086	4.486120	2.2	1.195495	110.0	11.0	1.5
2019-08-04 04:00:29+00:00	testschip-1006	8020	51.898972	4.485750	2.7	1.688953	110.0	11.0	1.5
2019-08-04 04:00:49+00:00	testschip-1006	8020	51.898796	4.485415	3.0	1.704806	110.0	11.0	1.5

Figure 5.2: Example of AIS dataframe, presenting the relevant parameters of 5 logs of testship-1006

Shipname

In the AIS data the shipname is logged, which is a unique identification of that specific ship. This is static information, which means that it will not change after the installation of the Automatic Identification System on board. The dataset used in this study, provided by Rijkswaterstaat, does also contain shipnames, but these are anonymized. This means that each individual ship has a unique name (for example 'testship-100'), which is not the real name of that ship, but it makes it possible to identify the sailing pattern of specific ships. In this way, you can for example determine the outward and return routes of a ship.

VesseltypeERI
The parameter 'VesseltypeERI' is a international way of logging the vessel type. ERI stands for Electronic Reporting International and the 'VesseltypeERI' is a four digit number that specifies different types of vessels in inland shipping. When the first digit is an '8', it considers inland vessels. For this research, only inland vessels are considered, and therefore other types of inland waterway navigation (e.g. recreational craft) have been filtered out. In Figure G.1 in Appendix G an overview is given of the inland vessel VesseltypeERI codes.

In this study, the Rijkswaterstaat inland vessel classification is used as a basis to classify different types of inland vessels. The Rijkswaterstaat document 'Richtlijnen Vaarwegen 2020' serves as the main guideline for this (Koedijk, 2020). This classification distinguishes between motor vessels, barges and convoys. Within these three subgroups a number of vessel types are classified, based on the dimensions of the vessel and related to the CEMT-classes, that specify the dimensions of the waterway and the maximum size of a vessel that can navigate that fairway. See Appendix F for an overview of the RWS inland vessel classification.

The 'VesseltypeERI' uses another classification and therefore a translation has been made to subdivide the vesseltypeERI's into the three subgroups of motor vessels, barges and convoys. The vesseltypeERI's linked to each subgroup are also specified in Appendix G, Table G.1.

Timestamp
The Automatic Identification Systems log the information of a ship over time. For each log, the timestamp is specified: it logs the specific date and time of that moment, in an accuracy of seconds. Knowing the timestamp of the next log, the Δt of the time step can be computed. A common Δt of each time step is around 20 - 30 seconds. The Δt is of importance to compute the speed of the vessel, which is discussed below.

Latitude and longitude
For each timestamp along the route of a ship, the latitude and the longitude of the ship are logged, forming the geographical position of the ship at that timestamp. Between two timestamps, the sailed distance can be computed.

Speed over ground
The AIS also logs the 'sog' (see Figure 5.2), which means 'speed over ground'. The sog indicates the sailing speed of the ship relative to the ground, expressed in knots. Because practice shows that the logged sog contains quite a few errors, the speed is also calculated from the time and geographical information. The geographical position of two subsequent time steps can be used to compute the distance in between these two points, Δx. The Δt can be calculated from two subsequent timestamps, which makes it possible to compute the speed: V_0 = Δx / Δt. This speed, expressed in m/s, is also indicated in Figure 5.2 (column 'speed'). This speed will be used in the emission calculations later on.

It is good to mention that this calculated speed still considers the speed over ground. In the energy consumption and emission calculation methods developed in Chapter 3 and 4, we make use of the speed relative to the water, but for simplicity we assumed there are no currents. In that case is the speed relative to the water, equal to the speed over round. But on certain inland waterways, there are currents. Due to complexity of currents and lack of actual data about currents on the corridor, we do not take this into account and we will calculate with the speed over ground. Using the speed over ground in the calculations is an important limitation of the method.

Ship dimensions: length, width, draft
The last three columns of Figure 5.2 contain the 'length', 'width' and 'draughtInland'. The length and width of the ship speak for themselves. The 'draughtInland' represents the draft of the ship at inland waters. The AIS data also contains a 'draughtMarine', which specifies a different draft in case of large open waters, but since we consider inland waters of the Rotterdam-Antwerp corridor, this information is disregarded.

The dimensions of the ship will be used as input for the emission calculations. The length and the width of inland vessels will be used to specify the ship types according to the RWS inland vessel classification (discussed

later on).

The information about the draft in the AIS data is in many cases incomplete and if there is information available, the accuracy of this data is questioned. This information is entered manually by the skipper himself and often contains errors (for example drafts of almost 0 meters, or very high drafts of 5 meters or higher). This is why it was decided to make an estimate of the draft ourselves. The method to do this is further explained in Section 5.3.

Also the information about the length and width of the ship is not always complete in the AIS dataset: since this is important information to perform the nergy consumption and emission calculation, a method is developed to supplement the missing infromation. This also explained in Section 5.3.

5.2.2. Fleet distribution

To give an idea of the characteristics of the inland vessels sailing along the Rotterdam-Antwerp corridor, this section illustrates some fleet characteristics of the AIS dataset. The different vessel types in the dataset are considered, as well as the common ship dimensions and the velocity distribution.

The characteristics that will be shown in this section will be based on an AIS dataset of 9 days (1 - 9 September 2019). This dataset of 9 days has been chosen because it gives reliable average output: if you only look at one day, the characteristics will vary, but this variation is filtered out by viewing a larger dataset. The dataset is limited to 9 days because the analysis requires a lot of computing time. The chosen 9 days (1 - 9 September) are compared to other datasets of 9 days and this selection appears to be representative. Please note that the distributions that are shown in this section are not statistical validated, but they give a first impression of the distribution of characteristics of the fleet.

Vessel types

The AIS parameter VesseltypeERI gives an indication about what kind of vessel we are considering. Figure 5.3 illustrates the variation of VesseltypeERI's in a dataset of one day.

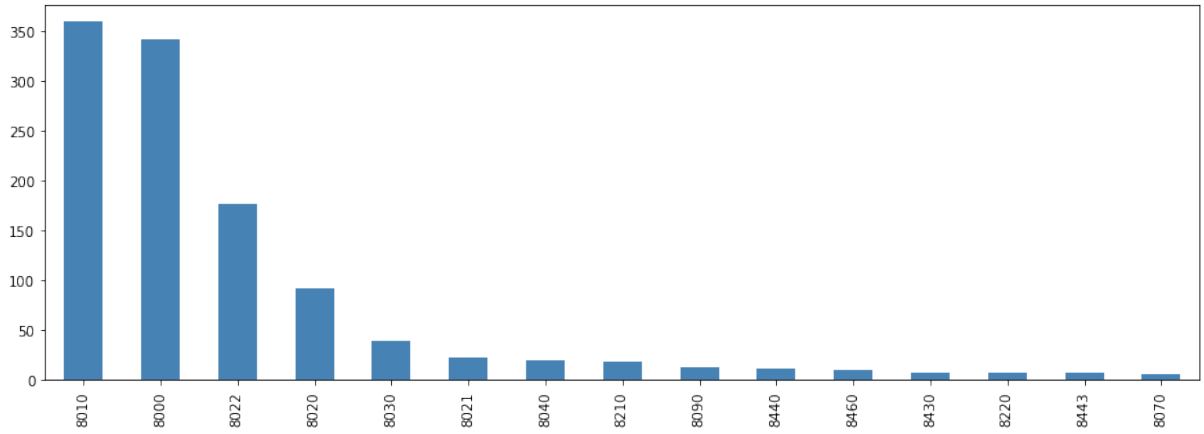

Figure 5.3: Bar chart: variation of vesseltypeERI of AIS data of one day (2 September 2019)

Figure 5.3 only shows the vesseltypeERI's with 5 or more vessels in the dataset. The vesseltypes that are displayed are defined in Table 5.1. For the definition of all vesseltypeERI's: see Appendix G, Figure G.1.

8010	Motor freighter	**8210**	Pushtow, one cargo barge
8000	Unknown vessel	**8090**	Motor freighter pushing one or more frreighters
8022	Motor tanker, liquid cargo, type C	**8440**	Passenger ship
8020	Motor tanker	**8460**	Maintenance vessel
8030	Container vessel	**8430**	Pushboat single
8021	Motor tanker, liquid cargo, type N	**8220**	Pushtow, two cargo barges
8040	Gas tanker	**8443**	Cruise ship

Table 5.1: VesseltypeERI definitions of vessel types displayed in Figure 5.3

Based on the VesseltypeERI we can subdivide the vessels, as in the RWS vessel classification, in the subgroups

motor vessels, barges or convoys. In a lot of cases the VesseltypeERI gives us no information about the vessel type: in that case the vessel type is indicated as 'unknown'. Figure 5.4 gives the distribution, based on 9 days of AIS data (1 - 9 September 2019). As you can see from the figure, the vessels in the dataset are mostly identified as motor vessels.

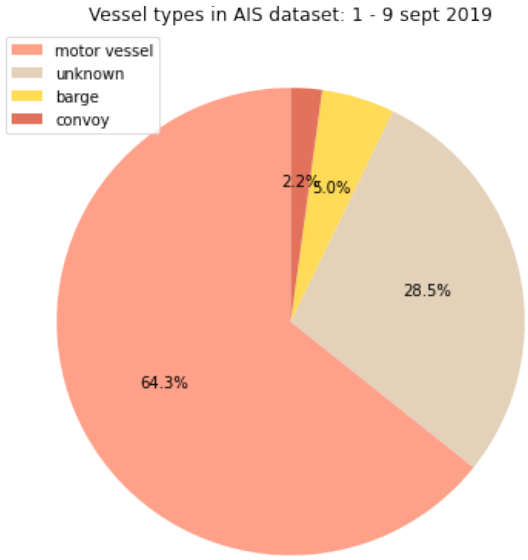

Figure 5.4: Pie chart: vessel types in the AIS data of one day (1st of August 2019), based on the given VesseltypeERI's

Based on the ship dimensions (discussed hereafter) and the VesseltypERI, the RWS vessel type can be estimated. The approach of this estimation method is further discussed in Section 5.3.1. Figure 5.5 shows the variation in RWS vessel classes in the AIS dataset of 9 days (1 - 9 September 2019). The 20 most common vessel types are shown in the figure. Please note that the 'M0' vessel types are filtered out (small shipping), which is further discussed in Section 5.3.5.

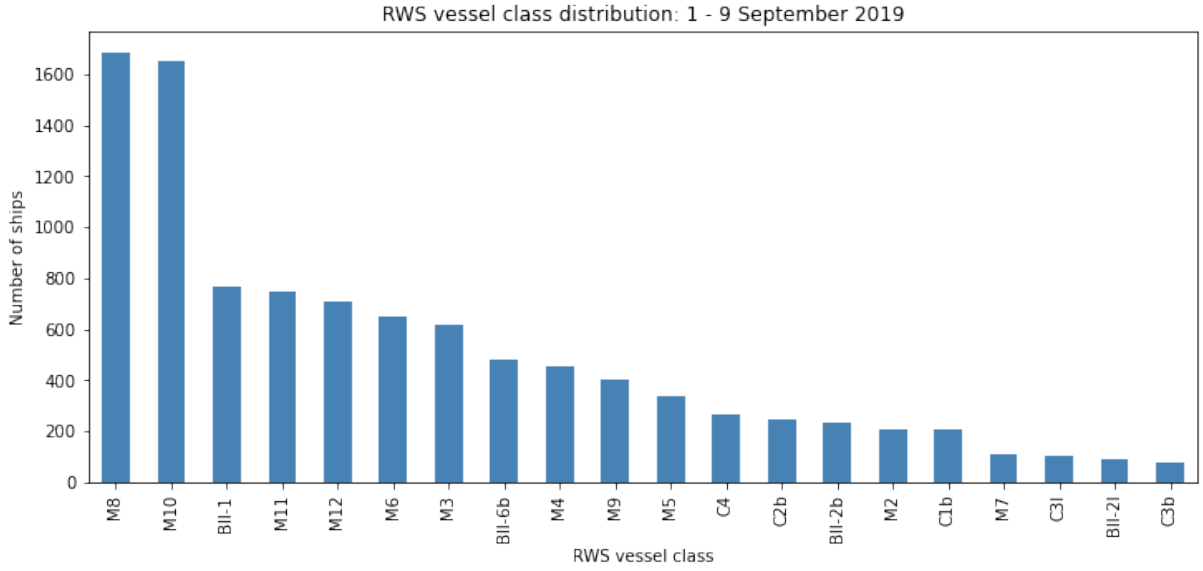

Figure 5.5: Bar chart: Variation of RWS vessel classes in the AIS data of 9 days (1 - 9 September 2019)

Figure 5.5 shows that the M8 motor vessel ('Groot Rijnschip') is the most common ship type, closely followed by the M10 motor vessel ('Maatgevend schip 13.5 * 110'). It has been estimated that the most common barge is the BII-1 type ('Europa II duwstel'). Also the largest motor vessel types M11 ('Maatgevend schip 14.2 * 135')

and M12 ('Rijnschip max') frequently occur according to these estimates. The M6 type ('Rijn-Herne schip L<= 86 m') and M3 type ('Hagenaar') motor vessels are the somewhat smaller motor vessels that are quite common on the corridor. The barge type 'BII-6b' is a pushtow with six cargo barges, which is the largest barge type in the dataset. This barge type is only able to sail on waterways with CEMT class VIc, which is the largest waterway classification. This means that BII-6b ships are not able to sail on a large part of the Rotterdam-Antwerp corridor: Figure 5.6 shows the CEMT classes of each waterway section on the Rotterdam-Antwerp corridor. The fairways marked in yellow are the only waterways where these large barges can sail. For more information about the Rijkswaterstaat inland vessel classification: see Appendix F.

Figure 5.6: Specified CEMT class of each waterway section on the Rotterdam-Antwerp corridor (Rijkswaterstaat, 2009)

Ship dimensions

To give an idea of the distribution in ship dimension, Figure 5.7 shows the distribution of length of the vessels in the fleet. This length distribution is based on 9 days of AIS data. Although the variation in the length is quite large, we see some peaks as well: these peaks can be explained by the dimensions of common ship types. The peak around a length of 80 meters can be explained by the usual length of M5 and M6 motor vessels. The most common ship types, the M8 and M10 motor vessels, usually have a length of around 110 meters, which explains the second and largest peak. We also sea a peak around 135 meters length: this is a common length of M9, M11 and M12 motor vessels.

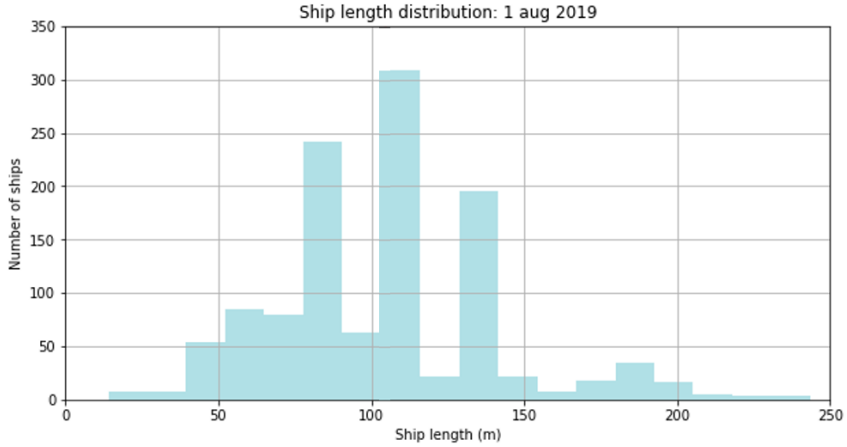

Figure 5.7: Distribution of ship lengths of AIS data of 9 days (1 - 9 September 2019). Average length: 105 m

Velocities

Figure 5.8 gives an overview of the speed variations in the AIS dataset. As discussed before, the speed from the AIS dataset is the speed over ground.

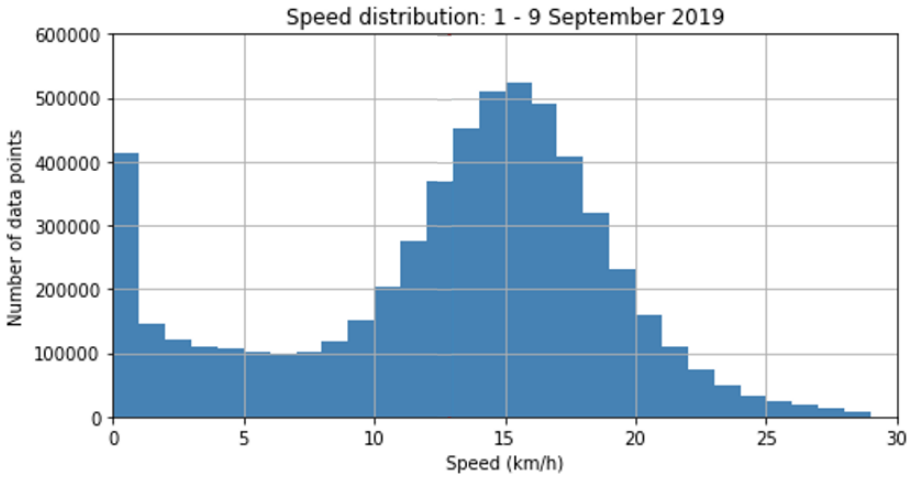

Figure 5.8: Distribution of vessel speeds of AIS data of 9 days (1 - 9 September 2019)

The velocity of inland vessels varies a lot: it depends on the type of ship considered, the waterway characteristics (depth or width restrictions, currents), the traffic intensity and sailing policies. Figure 5.8 shows a peak near 0 km/h: this can be explained by vessels that are slowing down and/or waiting. Another peak can be indicated around 15 km/h, which represents a common velocity when a vessel is on the way. The average speed of the dataset (represented by the red vertical in the figure) is 12.9 km/h.

5.2.3. Lock analysis

Figure 1.4 in the introduction chapter showed a clear overview of the Rotterdam-Antwerp corridor, including the main commercial shipping locks on the corridor. From north to south, these are the following locks:

- Volkerak locks: located in the Volkerakdam between Hollands Diep and Volkerak
- Krammer locks: located in the Philipsdam, which separates the fresh water of the Volkerak-Zoommeer from the salt water of the Oosterschelde
- Hansweert locks: located at the Zuid-Beveland canal
- Kreekrak locks: located at the Scheldt-Rhine canal

In order to properly model the locking process in a later stage (Chapter 6), it is important to analyze the locking process, to have an indication of how long a lock passage approximately takes. Therefore, the AIS data around each lock has been analyzed separately.

Creating trajectories with Movingpandas

Before we can analyse locks, ship trajectories have to be created from the AIS data. The Python package MovingPandas has been used to do this. For each ship, the MovingPandas tool reads the route of that ship from the AIS dataset, which forms one single trajectory.

We know from the analysis of certain trajectories that ships can be stationary for a while: for example when loading or unloading in a port, or when ships have to wait for a lock. When this waiting time is not so long, vessels will not turn off their engine and the engine keeps on idling. It is important to take that effect into account, considering the potential emissions that will accumulate at a waiting location. Practice shows that when skippers have to wait longer than approximately 30 minutes at a lock, they will moor and switch off their engine. Therefore, it has been decided to cut the created trajectories. MovingPandas provides a tool, where you can set that you cut a trajectory when a ship is stationary for more than 30 minutes. This means that the route of a ship is splitted when, for example, a ship is waiting at a lock for more than 30 minutes: when a ship arrives at the lock, the trajectory stops, and a new trajectory continues when the waiting time of that ship is over and the ship can pass the lock. This way, you take into account that a ship turns off the engine while waiting, so the emissions during that waiting time will not be included.

Lock passing times

For the main locks on the Rotterdam-Antwerp corridor, the passage times have been analyzed. The passage

time of a lock is based on the time it takes to get from the outer ports on one side of the lock, to the outer ports on the other side of the lock. Figure 5.9 illustrates this: the passage time is based on the time it takes to sail from A to B or vice versa. This includes the sailing time, waiting time and the time for the actual locking process.

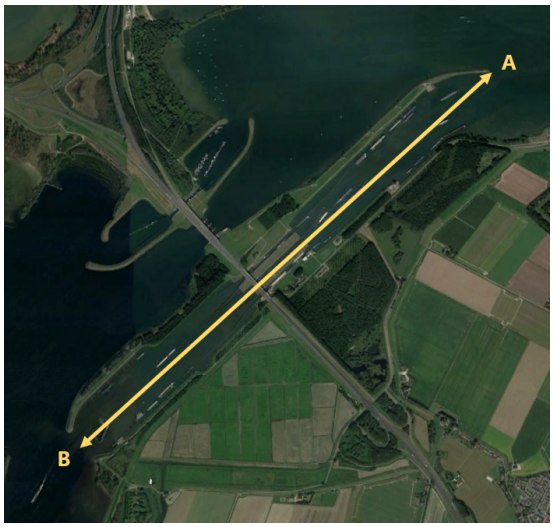

Figure 5.9: Basis of the determination of the lock passing time: the time it takes to get from the outer ports on one side of the lock, to the outer ports on the other side of the lock (so from A to B, or vice versa)

The following figures (Figure 5.10 - 5.13) show the passage time distribution of each lock, based on the AIS data of 9 days (1 - 9 September 2019). Exceptional outliers are removed from the data. The number of lock passages and the average duration of passing the lock are indicated below each figure. The analysis of the lock passing times is based on the lock passages of the (splitted) ship trajectories created with the MovingPandas python package.

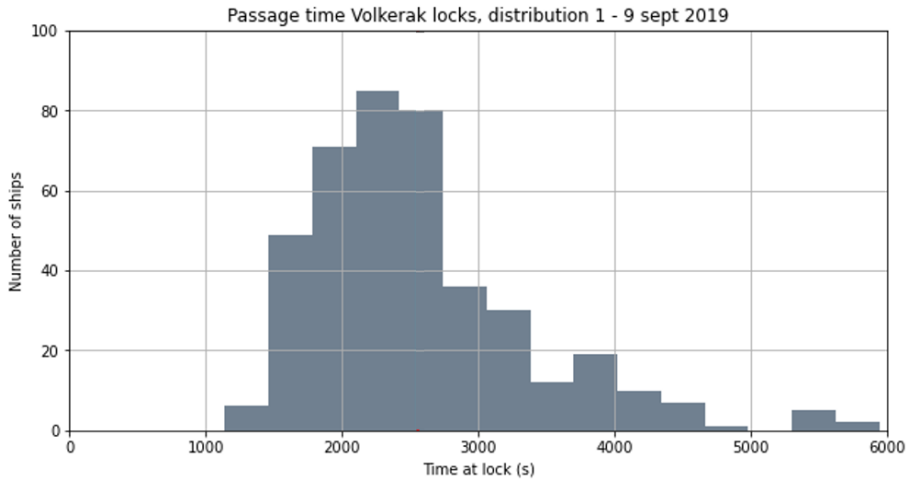

Figure 5.10: Distribution of passing time Volkerak locks of 9 days of AIS data (1 - 9 September 2019). N = 1123 ships. Average duration = 2558 s.

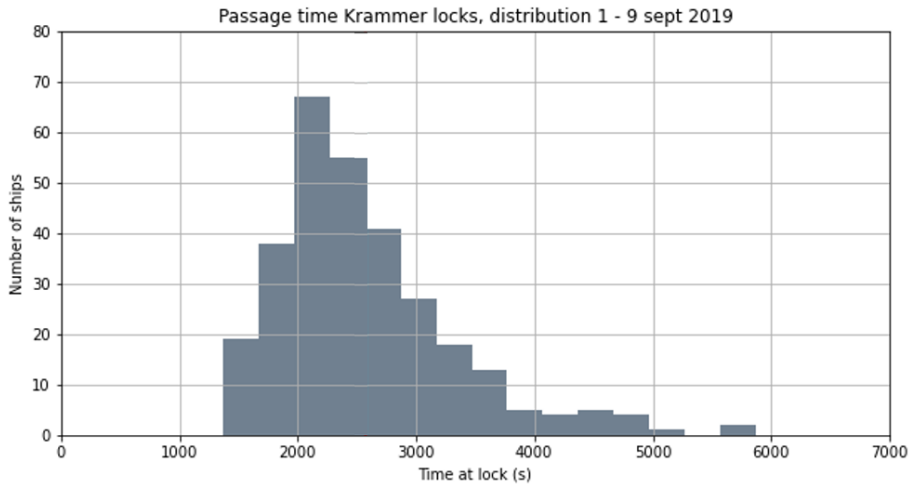

Figure 5.11: Distribution of passing time Krammer locks of 9 days of AIS data (1 - 9 September 2019). N = 507 ships. Average duration = 2571 s.

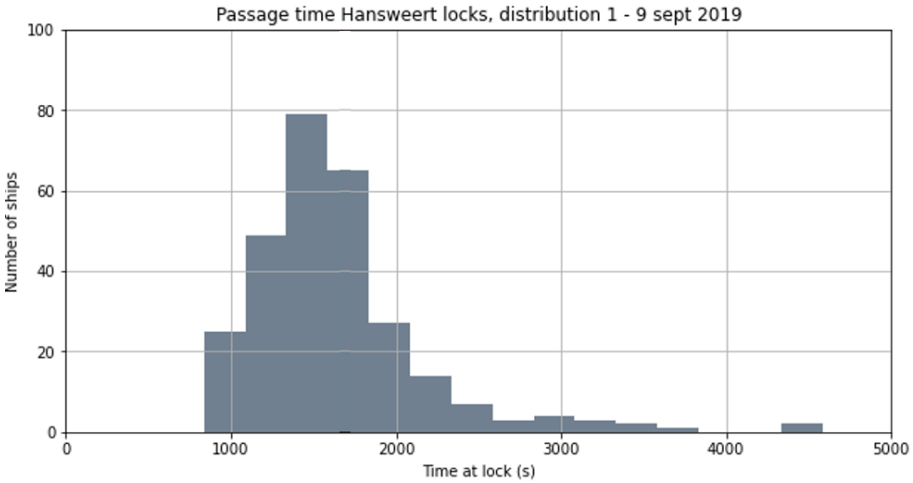

Figure 5.12: Distribution of passing time Hansweert locks of 9 days of AIS data (1 - 9 September 2019). N = 518 ships. Average duration = 1668 s.

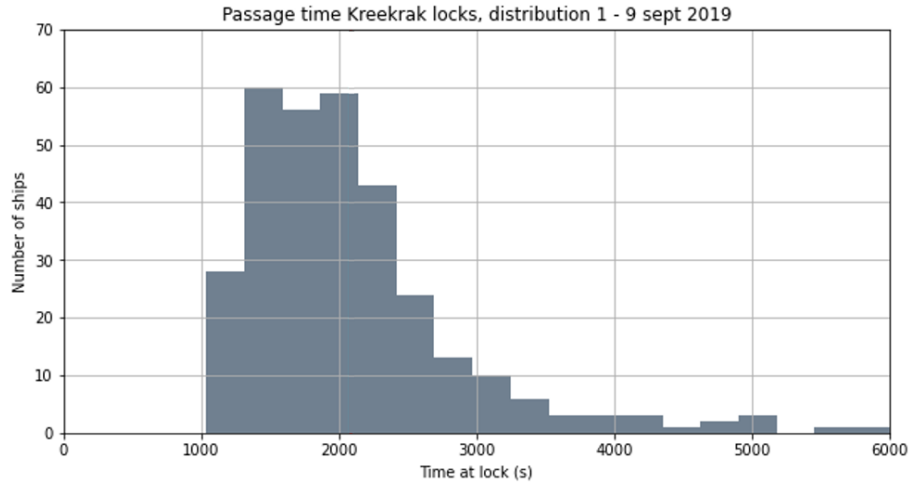

Figure 5.13: Distribution of passing time Kreekrak locks of 9 days of AIS data (1 - 9 September 2019). N = 756 ships. Average duration = 2085 s.

5.2.4. Corridor specifications

To be able to draw the right conclusions in the results section of this study about the reason why certain waterway sections are dealing with relatively higher of lower emission levels, it is important to map the characteristics of different trajectories on the corridor. In this section, we will define the traffic intensity of the important trajectories on the corridor, as well as the speed variations of these waterways.

Figure 5.14 shows the variation in traffic intensity along the Rotterdam-Antwerp corridor: per crucial waterway section, the number of crossings per day (in both directions) has been counted and is visualised in the figure. The figure shows that the Nieuwe Maas and Oude Maas are dealing with a comparable traffic intensity. At the Dortsche Kil the traffic intensity increases a bit, and at Hollands Diep the number of crossings is the highest. In southward direction, we see that the Scheldt-rhine route is dealing with more traffic than the Zuid-Beveland route. The Westerscheldt part of the Zuid-Beveland route has to do with some more traffic, because the traffic between Antwerpen and Terneuzen also makes use of this part of the trajectory.

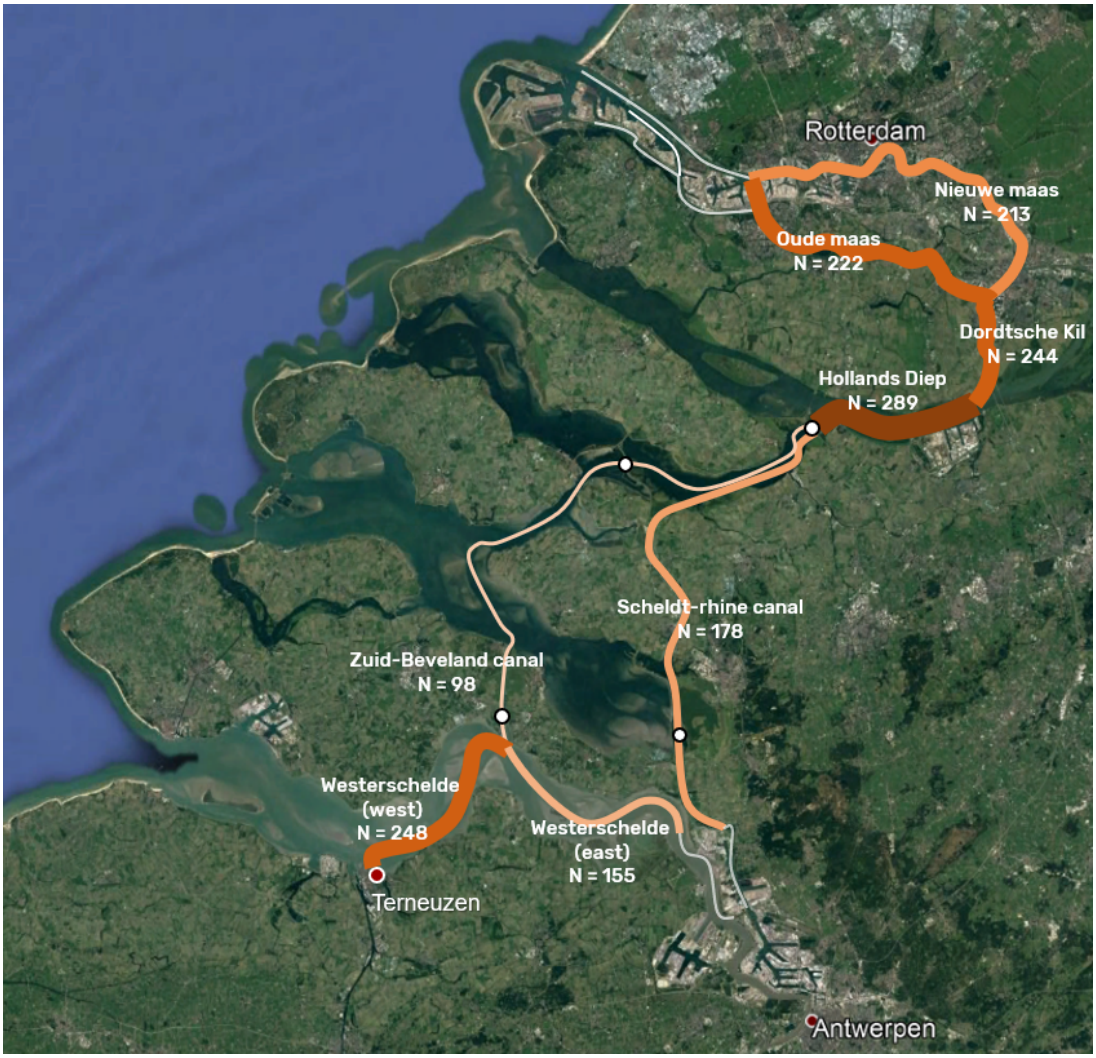

Figure 5.14: Traffic intensity on the Rotterdam-Antwerp corridor, based on an AIS dataset of one day (2 September 2019)

The average velocity varies on the corridor. Table 5.2 shows the average velocity per waterway section. The average velocity on the Nieuwe Maas, Dordtsche Kil, Hollands Diep, Scheldt-rhine canal and Zuid-Beveland canal are quite comparable. The average velocity on the Oude Maas lies somewhat higher. The Westernscheldt has significantly higher average velocities. This is an important aspect to consider, since the sailing speed of vessels has a signifacant influence on the energy consumption and emissions.

Waterway section	Average velocity (m/s)
Nieuwe maas	3,71
Oude maas	4,09
Dordtsche Kil	3,86
Hollands Diep	3,84
Scheldt-rhine canal	3,85
Zuid-Beveland canal	3,88
Westerschelde (east)	4,72
Westerschelde (west)	4,46

Table 5.2: Average velocities on different waterway sections on the Rotterdam-Antwerp corridor (based on AIS data of 2 September 2019)

5.3. Data enrichtment

5.3.1. Estimation of the RWS vessel class

As discussed before, the vesseltypeERI gives information about the ship type. On the basis of these identification codes, it can be determined if we are dealing with a motor vessel, barge or convoy. This subdivision is in line with the RWS inland vessel classification. RWS distinguishes a number of ship types within these three subgroups.

It is desired to determine the RWS vessel class for each ship in the AIS dataset, because this gives us information to estimate the installed power ($P_{installed}$) and the weight class ($L1, L2 or L3$) of the ship. This information is needed to perform the emission calculations.

For a large part of the dataset, the ship length, width and draft is known. Based on especially the length and width of a ship, a python code has been developed to estimate the RWS vessel class. The Richtlijnen Vaarwegen 2020 gives ranges of vessel length and width for each vessel class (Koedijk, 2020). This information is used to subdivide the ships in the right class. For example: considering a motor vessel, and the vessel width is in between 5.10 m and 6.70 m, it can be concluded we are dealing with a motor vessel type 'M2'. A specific python code has been developed for the motor vessels, barges and convoys. In addition, a code has been developed for unknown ship types, which is a more complex estimation method since less information is available. In Appendix F the python codes are presented (Figure F.2 - F.6).

When the RWS vessel class has been determined for each ship in the AIS dataset, the corresponding installed power and weight class can be assigned to that vessel. Information about which installed power and weight class corresponds to which RWS vessel class, is shown in Figure F.1 in Appendix F.

5.3.2. Determine the construction year of the engine

The construction year of the engine determines the emission factor: older engines are less clean and therefore generate more emissions. In Chapter 4, Section 4.2.1 it was explained that the general emission factors depend on the engine age. In Table 4.1 the general emission factors were shown for different construction year classes.

The engine age is not logged in the AIS data, and therefore we have to make assumptions. Section 4.2.1 elaborated on a Weibull-function (Formula 4.3) that can generate the engine age. This function is based on a IVR-vesseldatbase and a survey among 350 skippers. The 'k' and 'λ' values that determine the Weibull-function, vary per ship weight class (L1, L2, L3) (see Table 4.2). The weight class can be, as discussed in the previous section, derived from the RWS vessel class. A python code has been developed to generate a construction year of the engine, each time we identify a new ship in the dataset.

5.3.3. Draft estimation

As discussed before in Section 5.2.1 about the different parameters in the AIS dataset, the information about the draft in the AIS data is in many cases inaccurate or incomplete. For almost half of the raw data, no draft is available or the draft is set equal to 0. Considering the available data, you are dealing with many uncertainties: the data is manually filled in by the skipper and contains errors. Of the part of the data that does contain information about the draft and is not equal to zero, almost 30% considers draft data that is lower than the minimum draft specified for the considered vessel class. Almost 26% contains greater drafts than maximum drafts at loading rates of 85%. Therefore, it has been decided to not use the draft information from the AIS dataset, but develop a method to estimate the draft data based on the information you have.

In the previous section it was explained how a method was developed to estimate the RWS vessel class based

on the information of length and width. The document 'Richtlijnen Vaarwegen 2020' defines a minimum and a maximum draft per vessel class. This information is used as starting point to estimate the draft of a ship. CE Delft (2020) published information about the loading rate of different vessel classes, which means to which extent the ship is loaded on average in a loaded condition: these values vary from 65% to 70%. In addition, CE Delft provides information about what percentage of the travelled kilometers a specific ship class sails on average in loaded condition: these values vary from 70% to 85%. This information is all summarized in Figure F.1 in Appendix F.

To estimate the draft of a ship in the AIS dataset, we first have to estimate if the ship is loaded or unloaded. This starts with drawing a random number for each ship between 0 and 1 (based on a uniform distribution). This number determines if the ship sails in loaded condition, or unloaded condition. For example: a ship sails 85% of the sailed kilometers in loaded condition, and so 15% in unloaded condition. When the drawn random number is 0.15 or smaller, the ship is assumed to be unloaded, and if the random number is higher than 0.15, the ship is assumed to be loaded.

If the ship is loaded, the following expression is applied to estimate the draft:

$$T_{loaded} = T_{min} + (T_{max} - T_{min}) * R_{loaded} \tag{5.1}$$

T_{loaded}= the draft in loaded condition [m]
T_{min} = the minimal draft of the specified RWS vessel class [m]
T_{max} = the maximum draft of the specified RWS vessel class [m]
R_{loaded}= loading rate (to which extent the vessel is loaded) (also depending on the RWS vessel class)

For the values of T_{min}, T_{max} and R_{loaded}, specified per RWS vessel class, is again referred to Table F.1 in Appendix F.

If the ship is unloaded, the draft has been determined as follows:

$$T_{unloaded} = T_{min} + (T_{max} - T_{min}) * 0.25 \tag{5.2}$$

The unloading rate is set to 0.25: this is chosen because of the applicability of the energy consumption methods. By calculating with the minimal draft values, the algorithms are less accurate. Especially for bigger ships with a minimal draft value, the calculation method gives more outliers than we desire. Therefore, it has been chosen to increase the degree of loading a bit in the 'unloaded case' (by assuming a loading rate of 25%), to still get reliable model output. For ships with a length larger than 180 meters, an even stricter assumption has been made for the draft: if the estimated draft is lower than 3 meters, it is set to 3 meters.

It is good to mention that this method to estimate the draft contains a lot of uncertainty, which is a limitation of this study. For follow-up research, it is interesting to include IVS-Next data that provides accurate information about drafts, measured at locks. This data can be a good starting point of a better estimate of the draft of each ship.

5.3.4. Filling in missing information

For quite a few data points, the AIS dataset is missing important information. This mainly concerns the dimensions of the vessel. To perform the energy consumption and emission calculations, the information about the dimensions of the ship is important: the length, width and draft of the ship determine the resistance the ship experiences. Therefore it is important to find out to which extent the missing information can be complemented. We already performed an estimate of the drafts of the ships, so this section focuses on filling in missing ship length or width information.

When both the length and width of the ship are lacking, the choice has been made to filter these datapoints from the dataset: you do not have enough information to make a good estimation of the dimensions. This concerns about 6-7% of the data.

When only the length, or only the width is lacking, a python code has been developed to estimate the RWS vessel class we are dealing with, based on the information that is given: when the RWS vessel class is estimated, we can assume a certain value for the missing length or width.

5.3.5. Outlier detection and filtering the data

To avoid exceptional outcomes in the energy consumption and emission calculations, it is important to detect outliers in the AIS data upfront and filter the outliers from the dataset. In addition, information about vessels that are not within the scope of this research are filtered out as well.

In general, the geographical position is logged quite well by the Automatic Identification System (AIS). Combining the geographical information with the timestamp, the velocity can be calculated. But sometimes errors can occur in the log of the geographical position, which can result in exceptional velocities. Since the velocity of a vessel has a large influence on the emissions, it is important to filter extreme velocities. It has been decided to remove data points from the dataset with speeds above 8 m/s.

This study focuses on inland shipping. For this reason, recreational craft is disregarded. Based on the VesseltypeERI it was already possible to filter out a part of the recreational craft AIS data, but since a lot of vessels in the dataset have an unknown vessel type, an extra filter is applied to filter out small shipping: vessels that belong, based on their dimensions, to the RWS vessel class 'M0' (vessels with a length smaller than 38 meters and/or a width smaller than 5 meters) are filtered from the dataset. In addition, sea shipping is also not part of the scope, and therefore large sea vessels are also filtered out of the dataset: all ships that are bigger than the restrictions set by the largest CEMT class (VIc, six barge pusher) are filtered out. This means that all ships are removed that have a length larger than 270 meters, and/or a width larger than 34.2 meters.

6

Model set-up

The developed method to calculate the energy consumption and potential emission of inland ships as a function of time and space, will not only be applied to AIS data: in addition, a model will be developed that simulates the inland shipping fleet and the corresponding potential emission patterns. The reason for building a model, is to be able to use the developed method of this study in support of development and evaluation of alternative emission reduction policies.

The model will be developed making use of Open source Transport Network Simulation (OpenTNSim). This is a python package that offers us the tools to simulate an inland fleet on an inland waterway network. In this chapter the most important elements of the model development will be highlighted.

6.1. General introduction

To simulate the inland fleet on the corridor and map the potential emission patterns, different information is required as input for the model. Figure 6.1 shows the model outline.

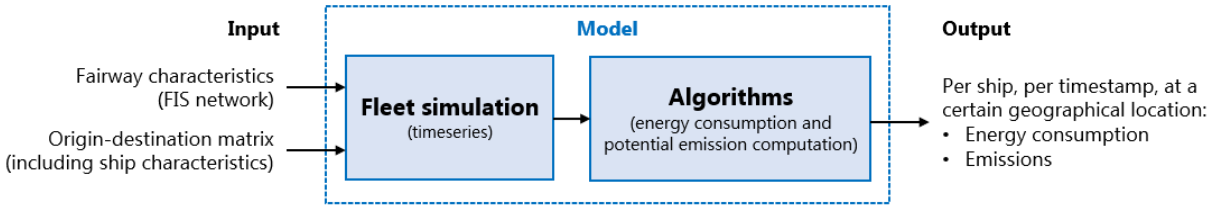

Figure 6.1: Model outline

At first, we need information about the fairway properties: a Fairway Information Services (FIS) network will be used for this, which is a graph that contains actual information about the fairway (geometry, waterway restrictions), obtained from an online source. Secondly, to incorporate the fleet characteristics, an origin-destination (OD) matrix, obtained from AIS data, will be used as input for the model. This OD matrix describes the route of each vessel trajectory, the time at which the ship starts to travel the route and it contains the vessel characteristics, such as the ship dimensions and average velocity. The required input of the model (FIS network and fleet characteristics) is discussed in more detail in Section 6.2.

With the fairway characteristics and OD matrix as input of the model, the simulation of the fleet can be performed. This results in a time series of each individual ship, sailing along the network. Now the developed algorithms to estimate the energy consumption and potential emissions of a vessel (discussed in Chapter 3 and 4) come into play: the algorithms are applied to the simulated time series of the fleet. This results in the following output: per ship, per timestamp, at a certain geographical location, the energy consumption and potential emission is computed. With this information, the potential emission patterns resulting from the modelled fleet simulation can be mapped on the network.

The most important model elements used in the simulation will be discussed in Section 6.3. At the end of this chapter (Section 6.4), the model output will be validated: a validation is performed on the basis of practical data of fuel consumption of different types of inland vessels.

6.2. Model input

6.2.1. Fairway characteristics (FIS)

The simulated ships have to sail along a certain waterway network. We therefore need the geometry of the fairways on the Rotterdam-Antwerp corridor. In addition, the algorithms to estimate emissions take into account fairway properties. Therefore the characteristics of each waterway section are important input of the model.

To obtain the required fairway characteristics, we make use of a FIS (Fairway Information Services) network. This network contains actual fairway information from Vaarweginformatie.nl (2020). With this information, a network can be created, which represents in our case the waterway network of the Rotterdam-Antwerp corridor. The Python package NetworkX has been used for this. NetworkX creates a graph, based on the provided fairway information. A graph is a collection of nodes and edges (edges are sections between pairs of nodes). The inland waterway network of the Rotterdam-Antwerp corridor is basically subdivided in small pieces of waterway (the edges), each with a start point and an end point (the nodes). The graph created in this project is of the type 'DiGraph', which is a directed graph. This means that all connections can be traversed in a certain direction. In our case it concerns a directed graph with two-way traffic (NetworkX, 2020).

The FIS network contains the geographical positions of the nodes on the network, and information about among other things the CEMT class, constraints in ship dimensions, the geometry and the length of the waterway sections (edges). In addition, the TU Delft is working on linking the bathymetry (position of the bottom) to the FIS network. A first version of this bathymetry has been included in this study. This bathymetry is obtained from another online source of Rijkswaterstaat (2021a). For a large part of the edges the bathymetry is specified, but there are edges without information of the bathymetry. For the edges that were missing information, a bathymetry has been assumed based on the bathymetry of the surrounding edges. In Appendix H, Figure H.1, the bathymetry has been visualized on the corridor.

The developed method to estimate potential emissions uses the water depth as an input variable: in more limited water depths, the energy consumption and potential emission of a ship is higher when sailing with the same speed. That is why we would like to include the water depth in the FIS network. The water depth can be defined by the difference between the bathymetry and the water level. The water level is not yet specified in FIS and therefore this information is obtained separately. From waterinfo.rws.nl, data was obtained of the water levels w.r.t. NAP, at several measuring points along the Rotterdam-Antwerp corridor (Rijkswaterstaat, 2021c). In Appendix H, Figure H.2 shows the measurement locations used. For each point, 3 months of water level data was requested (August 2019 - October 2019): an average water level has been determined per measurement location. Subsequently, the average water levels were assigned to the corresponding locations on the FIS network. For the intermediate edges with no information about the water level, assumptions have been made based on the water level of near edges. The water level variation along the network has been visualized in Appendix H, Figure H.3.

The water depth variations along the inland waterway network can now be obtained by the difference of the bathymetry level and the water level. Figure 6.2 shows the visualization of the obtained water depths along the Rotterdam-Antwerp corridor, expressed in meters. The defined water depth ranges in the figure are chosen to visualize variations, but in reality each edge has a unique water depth specified with which we calculate. These water depths will be used as input of the developed algorithms to estimate the energy consumption and potential emissions of inland vessels as a function of time and space. Per ship, per timestamp, the water depth of the waterway section where the vessel is currently sailing, is read. Based on that water depth, the emission is determined for the corresponding timestamp.

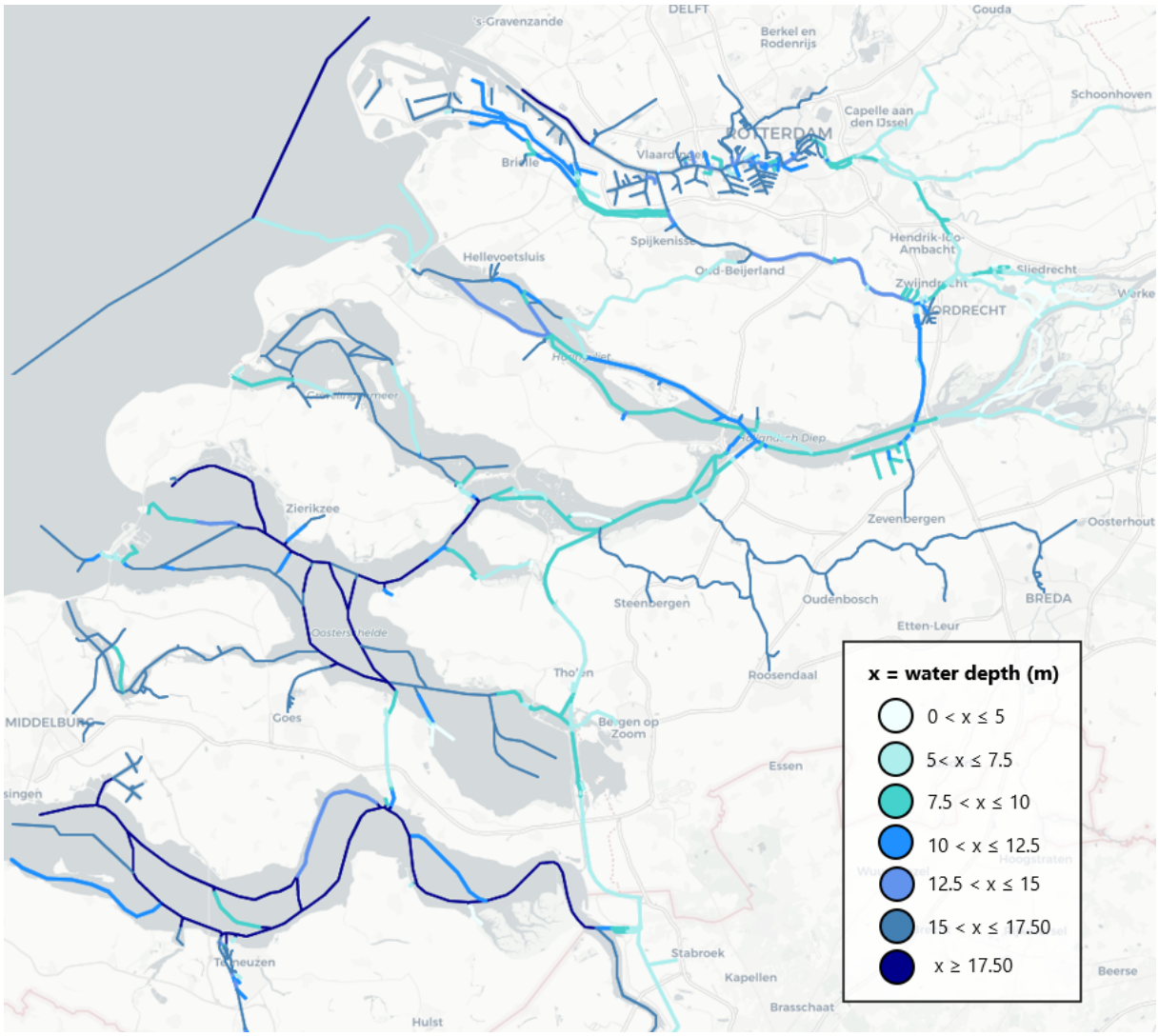

Figure 6.2: Water depth variations along the corridor, expresseed in meters, based on the variations in bathymetry and water level

6.2.2. Fleet definition: origin-destination matrix

To define the fleet that will be simulated by the model, an origin-destination (OD) matrix is created based on AIS data (in Chapter 5 more information was provided about the characteristics of the AIS dataset). This OD-matrix is input of the OpenTNSim model.

The OD-matrix is created as follows. The AIS data is translated to ship trajectories: these created trajectories are routes sailed by individual ships. Such a route is splitted when a ship is stationary for more than half an hour (e.g. when a ship is loading / unloading in a port, or has to wait for a lock, moors and turns off the engine). For each trajectory, the geographical information of the start point (origin) and end point (destination) of the ship has been determined. In addition, the characteristics of the vessel that sails that trajectory are defined: this considers the shipname, RWS vessel class, length, width, draft, installed power and weight class. In addition, the average velocity of the ship on the considered trajectory is calculated. Table 6.1 gives an overview of the information that is in the OD-matrix, showing the first few lines of the total matrix.

Not all vessels start to sail at the same time. To be able to simulate the fleet over time in proper way, we need some information about when vessels start to sail its trajectory. Therefore, a time difference is calculated between the start of the day that will be simulated (00:00), and the moment the vessel of the trajectory considered starts sailing. This time lag, logged is seconds, is presented in the last column of Table 6.1 (time diff).

shipname	latitude origin	longitude origin	latitude destination	longitude destination	length (m)	width (m)	draft (m)	RWS class	P_installed (kW)	L_w	average speed (m/s)	time diff (s)
testschip-1035-2	51,351	4,292	51,328	4,305	110	12	2,16	M10	2400	3	3,245531	36281
testschip-1036	51,328	4,309	51,695	4,466	110	12	2,16	M10	2400	3	3,668065	69513
testschip-1038	51,682	4,395	51,880	4,270	135	12	2,00	M11	2400	3	4,12705	13040

Table 6.1: Overview of information in the origin-destination matrix, which is used as input for the OpenTNSim model

The origin and the destination of the vessel trajectory already give some information about the path a ship is going to sail, but does not yet contain information about certain route choices. For example, when a vessel sails from Rotterdam to Antwerp, it can possibly sail via the Oude Maas or Nieuwe maas, passing the Volkerak locks and then again have another route choice to sail via the Zuid-Beveland canal or the Scheldt-rhine canal. To incorporate this information, it has been analyzed for each vessel trajectory, if it crosses one of these waterway sections that are crucial in defining the route of the ship. Table 6.2 shows this additional information added to the OD-matrix: when a ship crosses a certain waterway section (Nieuwe maas, Oude maas, Maassluis, Scheldt-Rhine or Zuid-Beveland), the value '1' is assigned to that column. If not, the value is 0. How the route is exactly created in the model based on this information, is further discussed in Section 6.3.3 'Path finder'.

shipname	Nieuwe maas	Oude maas	Maassluis	Scheldt-Rhine	Zuid-Beveland
testschip-1035-2	0	0	0	1	0
testschip-1036	0	0	0	0	1
testschip-1038	0	1	0	0	0

Table 6.2: Overview of additional information in the origin-destination matrix, containing information about certain waterway sections that are crossed, which are crucial in defining the route of the ship

6.3. Simulation elements

6.3.1. Discrete event simulation

There are different methods to perform a model simulation of a system. In our case the system we are modelling is the inland shipping fleet on the Rotterdam-Antwerp corridor. In order to clearly explain which simulation method is used in this research and why, the basis of various methods is explained first. You can roughly distinguish between three types of simulation methods: continuous simulation, discrete time simulation and discrete event simulation. Continuous simulation means that the state of the system you are modelling continuously varies in time. Discrete time simulation shows the system changes at fixed, regular points in time. Discrete event simulation describes the system by means of a sequence of events, at random time intervals, at which the system state changes (Resing, 2013).

The OpenTNSim model developed in this study makes use of discrete event simulation (DES). This means that the simulation of vessels contains of a series of events taking place over time: the model assumes that the vessel state is not changing between two events. The vessels sail over a simulated waterway network, which is a network of nodes, connected by edges (explained in more detail in Section 6.2.1). Each time a vessel reaches a certain node, this is considered as an event in the system: each edge contains its own fairway properties, and the variation is important in the calculations of energy consumption and emissions. Therefore, at each node, the information of the vessel is logged. Table 6.3 shows the logged information of one simulated vessel sailing along the network. The table gives information about the logged state message of a vessel, the timestamp of that event and the geometry of the node.

Message	Timestamp	Geometry
Start sailing	2020-09-26 05:13:47	POINT (4.45569170148355 51.8867707898306)
Sailing from node 8865264.0 to node 8865997.0 start	2020-09-26 05:13:47	POINT (4.45569170148355 51.8867707898306)
Sailing from node 8865264.0 to node 8865997.0 stop	2020-09-26 05:21:05	POINT (4.442904032788873 51.88817035853807)
Sailing from node 8865997.0 to node 8860787.0 start	2020-09-26 05:21:05	POINT (4.442904032788873 51.88817035853807)
Sailing from node 8865997.0 to node 8860787.0 stop	2020-09-26 05:21:56	POINT (4.443546464708546 51.88732157071014)
Sailing from node 8860787.0 to node 8864192.0 start	2020-09-26 05:21:56	POINT (4.443546464708546 51.88732157071014)
Sailing from node 8860787.0 to node 8864192.0 stop	2020-09-26 05:24:21	POINT (4.445253511808803 51.88488128924134)
Sailing from node 8864192.0 to node 8860954.0 start	2020-09-26 05:24:21	POINT (4.445253511808803 51.88488128924134)
Sailing from node 8864192.0 to node 8860954.0 stop	2020-09-26 05:27:21	POINT (4.447407858697834 51.88187825836479)
Stop sailing	2020-09-26 05:27:21	POINT (4.45569170148355 51.8867707898306)

Table 6.3: Log of discrete events of a single vessel in the OpenTNSim model simulation

The vessel of Table 6.3 is sailing from one node to another. It logs a message if it starts to sail from a certain node, and when it stops to sail at the subsequent node. The model works with a constant sailing speed. With the information about the timestamp and the geometry, the energy consumption and emission calculations can be performed: the time difference between to events can be computed (Δt), as well as the sailing distance between two nodes (Δx). With this information, the initial velocity V_0 can be computed. By knowing the ship dimensions and waterway characteristics, the energy consumption of the inland vessel can be calculated for each timestep, followed by the emission calculations.

6.3.2. Locks

The time a vessel needs to pass a lock, is equal to the sum of the waiting time, the operating time and possible demurrage time. These passing times vary per lock, as well as other lock characteristics, such as the number of lock chambers and the length and width of such a chamber. In addition, these passing times are dependent on the traffic intensity. To be able to simulate the locking process in a proper way, we have to make a reasonable assumption regarding to the passing times of the different locks on the Rotterdam-Antwerp corridor. These assumptions are based on the AIS data analysis: in Section 5.2.4 the average passing time of each lock has been determined. These outcomes are rounded off and summarized in Table 6.4.

	Average passing time (s)
Volkerak locks	2560
Krammer locks	2570
Hansweert locks	1670
Kreekrak locks	2090

Table 6.4: Average passing time per lock on the Rotterdam-Antwerp corridor, based on 9 days of AIS data (1 - 9 September 2019)

The OpenTNSim package contains a class that describes the locking processes. The average passing times resulted from the AIS data, are implemented for each lock in the model: it has been assumed that 50% of this total passing time results from waiting till you can enter the lock, and 50% of the time has been assigned to the locking process (opening and closing of the doors, entering and leaving the lock and the levelling process). Another important input value of the lock element in the model, is on which side of the lock the water level in the lock itself is levelled with at the start of the simulation. The northward side of each lock has been chosen in all cases.

It is important to note that the lock simulation element is quite limited: a single lock element can only allow one ship to pass at a time. This is why it has been decided to implement more lock elements on the network than there are in reality. This way, excessive waiting times in the model simulation are avoided.

To test if the locking process is well simulated by the model, a test case have been performed at the modelled Volkerak locks. Two vessels are simulated (see Figure 6.3): the first vessel sails through the Volkerak locks from A to B, and the second vessel from B to A.

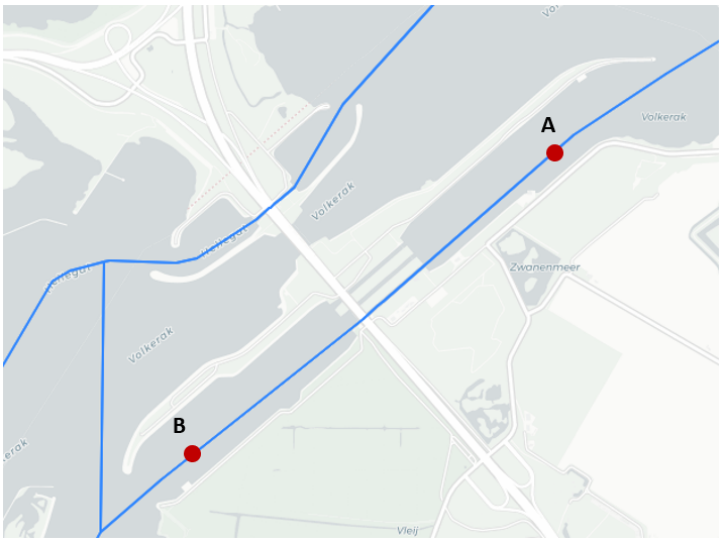

Figure 6.3: Overview Volkerak locks: two points, A and B are indicated. Test vessel 1 is sailing from A to B. Test vessel 2 is sailing from B to A.

Figure 6.4 shows the vessel log tables of the two test vessels. In the log tables, the first column 'message' shows what the vessel is doing (sailing from one node to another, passing the lock, waiting in the line-up area), with the corresponding timestamp (second column). The last column 'value' shows the additional time (in seconds) assigned to the considered vessel during the locking process.

Vessel 1: A to B

	Message	Timestamp	Value
0	Start sailing	2020-09-26 00:00:00.000000	
1	Sailing from node 8862498.0 to node L42863_A s...	2020-09-26 00:00:00.000000	0
2	Sailing from node 8862498.0 to node L42863_A stop	2020-09-26 00:10:25.190040	0
3	Passing lock start	2020-09-26 00:10:25.190040	0
4	Passing lock stop	2020-09-26 00:32:15.190040	1310
5	Sailing from node L42863_B to node B34113_A start	2020-09-26 00:32:15.190040	0
6	Sailing from node L42863_B to node B34113_A stop	2020-09-26 00:32:47.852939	0
7	Sailing from node B34113_A to node B34113_B start	2020-09-26 00:32:47.852939	0
8	Sailing from node B34113_A to node B34113_B stop	2020-09-26 00:32:50.536606	0
9	Sailing from node B34113_B to node 8868426.0 s...	2020-09-26 00:32:50.536606	0
10	Sailing from node B34113_B to node 8868426.0 stop	2020-09-26 00:40:13.948284	0
11	Stop sailing	2020-09-26 00:40:13.948284	

Vessel 2: B to A

	Message	Timestamp	Value
0	Start sailing	2020-09-26 00:00:00.000000	
1	Sailing from node 8868426.0 to node B34113_B s...	2020-09-26 00:00:00.000000	0
2	Sailing from node 8868426.0 to node B34113_B stop	2020-09-26 00:07:23.411678	0
3	Sailing from node B34113_B to node B34113_A start	2020-09-26 00:07:23.411678	0
4	Sailing from node B34113_B to node B34113_A stop	2020-09-26 00:07:26.095345	0
5	Sailing from node B34113_A to node L42863_B start	2020-09-26 00:07:26.095345	0
6	Sailing from node B34113_A to node L42863_B stop	2020-09-26 00:07:58.758245	0
7	Waiting in line-up area start	2020-09-26 00:07:58.758245	0
8	Waiting in line-up area stop	2020-09-26 00:29:48.758245	1310
9	Passing lock start	2020-09-26 00:29:48.758245	0
10	Passing lock stop	2020-09-26 00:51:38.758245	1310
11	Sailing from node L42863_A to node 8862498.0 s...	2020-09-26 00:51:38.758245	0
12	Sailing from node L42863_A to node 8862498.0 stop	2020-09-26 01:02:03.948284	0
13	Stop sailing	2020-09-26 01:02:03.948284	

Figure 6.4: Vessel log of 2 test vessels passing the Volkerak locks from another direction

There are three lock chambers at the Volkerak locks, which means that the two vessels in this test case do not have to wait for each other. But the water level at the locks at the start of the simulation has been levelled with the northward side of the lock, so with the water level at location A. This means that the second vessel, sailing from B to A, has to wait till the water level in the lock that will be used by that vessel has been levelled, before that vessel can enter. The first vessel, sailing from A to B, can enter the lock directly.

The first vessel log table in Figure 6.4 confirms that the first test vessel does not have to wait before it can enter the lock: the water level does not have to be levelled, and the vessel can directly enter the lock. The passing time of that vessel is only 1310 seconds, which is 50% of the average passing time of the Volkerak locks (see Table 6.4). The other 50% of the passing time is not assigned to this vessel, since the vessel does not have to wait. The second table in Figure 6.4 shows the log of the second test vessel, sailing from B to A. It confirms that the vessel first has to wait before it can enter the lock (see message 7: 'Waiting in line-up area start'), because the water level inside the lock has to be levelled with the water level at the southward side of the lock. 50% of the average

passing time (1310 seconds) is assigned to this waiting time, and the other 50% to the locking process.

6.3.3. Path finder

In Section 6.2.2 it was discussed that an origin-destination (OD) matrix , resulting from the AIS data, is used as input for the OpenTNSim model to simulate the fleet. The OD matrix defines for each ship trajectory (route) the start point (origin) and end point (destination) of a vessel, with its ship characteristics and average speed. In addition, it is logged if the considered ship trajectory crosses certain waterway sections, in order to define the right route. How this route is exactly defined in the model, is discussed in two steps: (1) finding a path between two geographical points, and (2) how to take into account intermediate points.

(1) Finding a path between two points

Each edge has a certain distance, which is important information considering the route choice of each vessel in the model. In case there are no waterway restrictions in height, width or depth, a vessel will choose the shortest route between two specified points. This shortest route is determined with the Dijkstra shortest path algorithm, which is part of the NetworkX package. A path is a series of different edges connected to each other (NetworkX, 2020). The Dijkstra algorithm requires two points (start point, end point), and a certain weight, which is in this case the length of the edges.

> **The Dijkstra algorithm**
> The Dijkstra algorithm is a systematic way to find the shortest route from a certain starting point, to each node in the network. Step by step the algorithm runs through all nodes, starting with the nearest node. It is an iterative procedure, in which the 'temporary' shortest paths are improved step-by-step, making use of a smart label procedure (Tijms, 2008).

(2) Finding a path with intermediate points

In case the considered ship trajectory crosses a certain waterway section that is crucial in defining the route, the path determination becomes a bit more complex. These crucial waterway sections (Oude Maas, Nieuwe Maas, Maassluis, Zuid-Beveland canal and Scheldt-rhine canal) are defined as separate columns in the OD-matrix: a value of '1' is assigned if the ship trajectory crosses that waterway section. For these trajectories the paths are cut up. For example, if a ship crosses one crucial waterway section, a first path is created from the start point (origin) to the first intermediate point, and a second path from the intermediate point to the end point (destination). Afterwards, the paths output is summed up and duplicate nodes are removed. In case more than one intermediate points have to be considered, the north or south direction of the ship has been taken into account to determine the correct order of intermediate points.

6.4. Validation of model output

Based on the input characteristics of the model described in this chapter (FIS network and OD matrix) the simulation of the inland fleet on the corridor can be performed. This results in a simulated time series, on which the developed algorithms can be applied, and the energy consumption and potential emissions can be calculated per ship per time step. But to find out whether this output sufficiently corresponds to practice, it is important to validate the model results.

There are a lot of uncertainties in measuring emissions of inland shipping, which results in lack of data to validate the emission output. In order to be able to validate the model output in a proper way, it has been decided to validate the fuel consumption. Practical data on fuel consumption of inland ships is available, which is an effective way of comparing and validating the fuel consumption generated by the OpenTNSim model. Table 6.5 shows data of a survey performed by Rijkswaterstaat in 2003 among 100+ inland skippers, who indicated their type of motor vessel, sailing speed (in km/h) and the corresponding fuel consumption (in L/hour). This data has been compared to the fuel consumption resulting from a simulation performed by the OpenTNSim model: this simulation was performed for each ship type that was also considered in the survey, with the corresponding velocity. Since the RWS survey data gave no information about waterway characteristics, the model calculations have been performed for different water depth. Information about the engine age is not available, so the construction year of the engine has been assumed to be the year 2000. In the last column of the table the number of conducted RWS surveys per ship type is indicated.

Ship type	V_loaded (km/h)	Fuel consumption survey (L/hour)	Fuel consumption OpenTNSim (L/hour) h = 15 m	h = 9.5 m	h = 6.25 m	Engine age (assumption)	N surveys
M1	11,4	29	17	18	19	2000	24
M2	13,6	51	43	45	49	2000	19
M3	13,9	58	54	56	61	2000	9
M4	14,7	83	74	77	81	2000	10
M5	15,8	115	100	104	127	2000	9
M6	15,6	154	113	119	152	2000	21
M8	16,5	189	188	207	272	2000	17

Table 6.5: Validation of fuel consumption output of OpenTNSim model: validated by a survey conducted by Rijkswaterstaat (2003) for different types of motor vessels

Table 6.5 shows that the fuel consumption resulting from the model simulation is quite similar to the fuel consumption from the practical data of the survey. It has to be noted that the survey data is an indication the skippers gave about their fuel consumption with a certain sailing speed, but this is not officially measured data. However, given the uncertainties in prediction the energy consumption of inland ships, these correspondences between model output and practical data provide valuable confirmation that the model can make a reasonably good estimate.

In addition to this direct comparison with practical data, it is also important to look at the spread in the model output. Therefore, the fuel consumption distribution of the model simulation of one day (2 September 2019 in this case) has been mapped for different vessel types. Figure 6.5 shows the distribution of different motor vessel types, and Figure 6.6 of barges and convoys. Only the ship types with 25 or more ships in the data set of the modelled day are shown, to give a representative picture of the distribution of the fuel consumption. Below each figure, the number of ships (N), mean fuel consumption and mean velocity of that ship type (on 2 September 2019) is noted. The spreading in the figures is mainly due to velocity differences between the vessels and differing water depth: if a vessel sails with a relatively high sailing speed in relatively limited water, this can lead to much higher fuel consumption output compared to a same vessel with a much smaller speed, sailing in deep water. The absolute differences are higher in case of larger inland vessels.

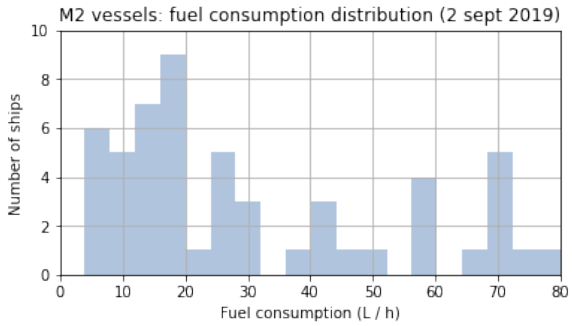

(a) Class M2: N = 45, Mean fuel c. = 33 L/h, V_{mean} = 12.2 km/h

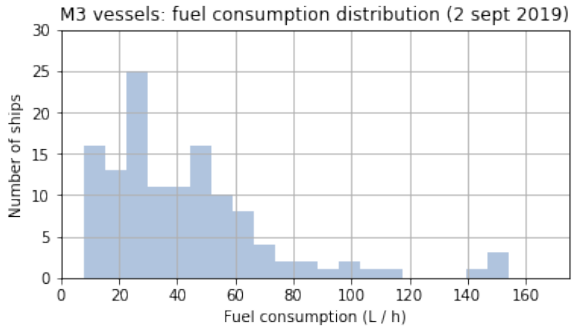

(b) Class M3: N = 110, Mean fuel c. = 50 L/h, V_{mean} = 12.7 km/h

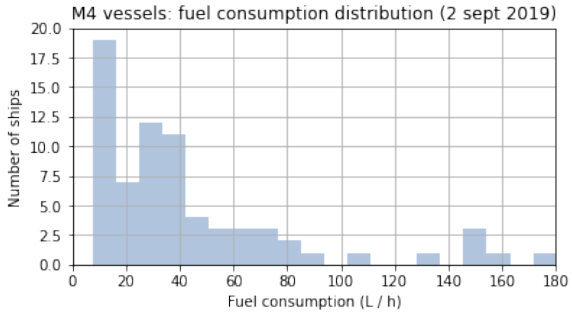

(c) Class M4: N = 64, Mean fuel c. = 54 L/h, V_{mean} = 11.8 km/h

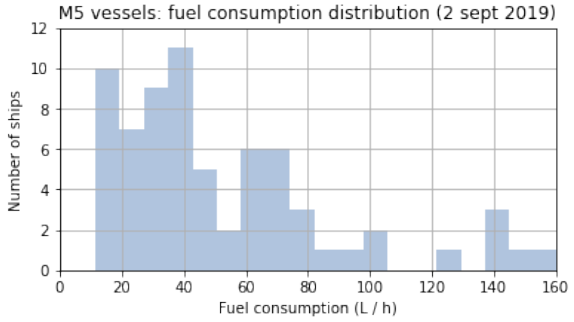

(d) Class M5: N = 63, Mean fuel c. = 60 L/h, V_{mean} = 12.8 km/h

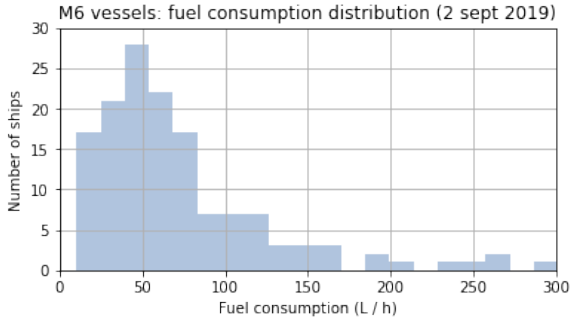

(e) Class M6: N = 133, Mean fuel c. = 76 L/h, V_{mean} = 12.6 km/h

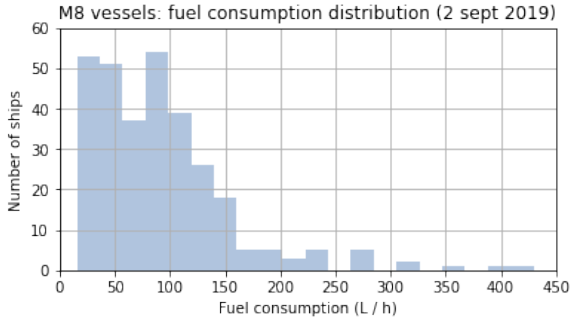

(f) Class M8: N = 263, Mean fuel c. = 92 L/h, V_{mean} = 12.4 km/h

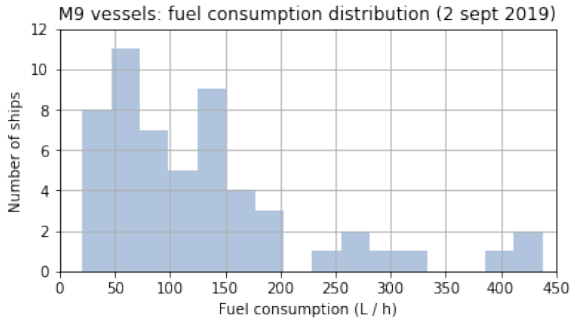

(g) Class M9: N = 62, Mean fuel c. = 140 L/h, V_{mean} = 13.3 km/h

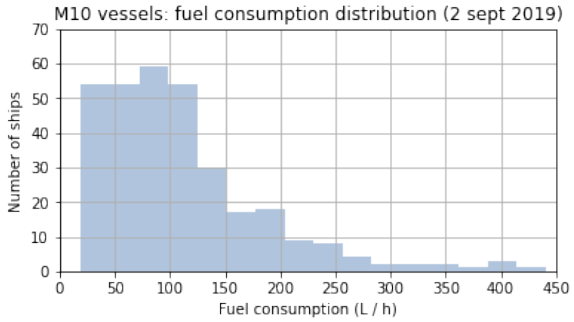

(h) Class M10: N = 281, Mean fuel c. = 112 L/h, V_{mean} = 12.6 km/h

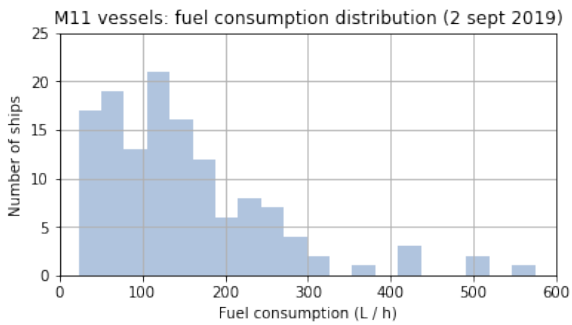

(i) Class M11: N = 127, Mean fuel c. = 145 L/h, V_{mean} = 13.2 km/h

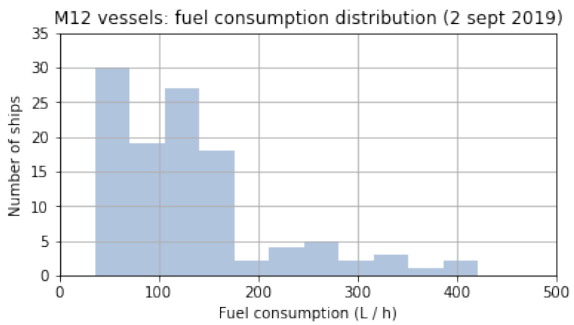

(j) Class M12: N = 105, Mean fuel c. = 132 L/h, V_{mean} = 11.3 km/h

Figure 6.5: OpenTNSim model simulation of 2 September 2019: Fuel consumption distributions of different types of motor vessels

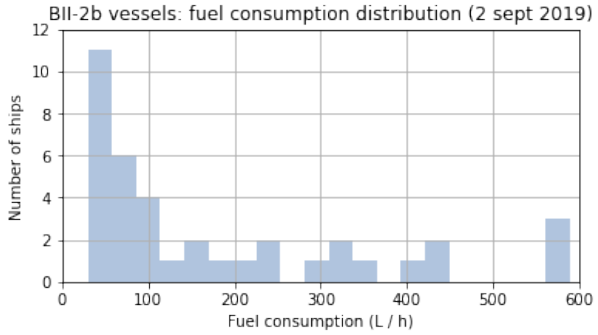

(a) Class BII-2b: N = 36, Mean fuel c. = 191 L/h, V_{mean} = 11.8 km/h

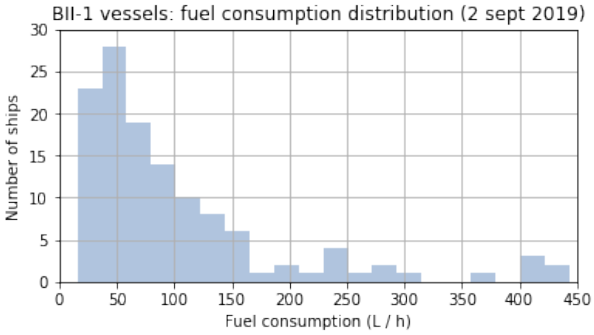

(b) Class BII-1: N = 110, Mean fuel c. = 103 L/h, V_{mean} = 12.4 km/h

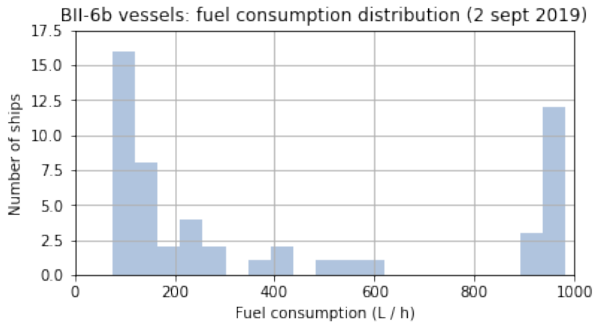

(c) Class BII-6b: N = 52, Mean fuel c. = 403 L/h, V_{mean} = 13.2 km/h

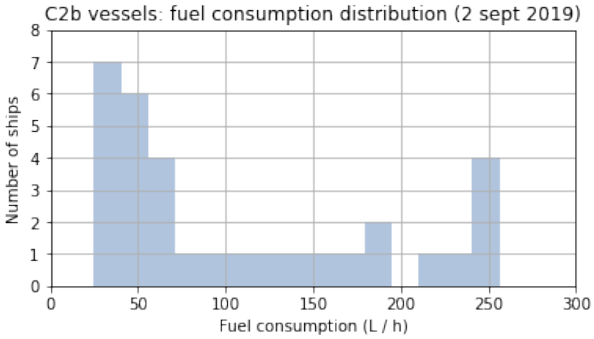

(d) Class C2b: N = 26, Mean fuel c. = 113 L/h, V_{mean} = 13.5 km/h

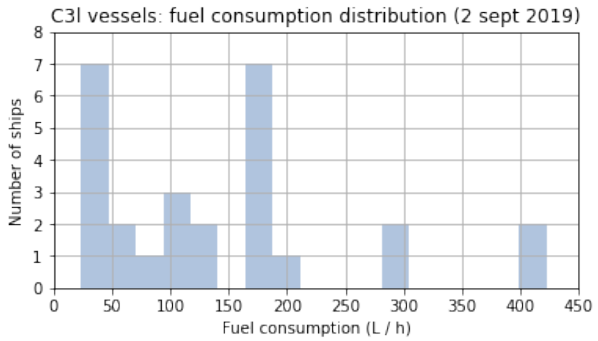

(e) Class C3l: N = 28, Mean fuel c. = 129 L/h, V_{mean} = 11.8 km/h

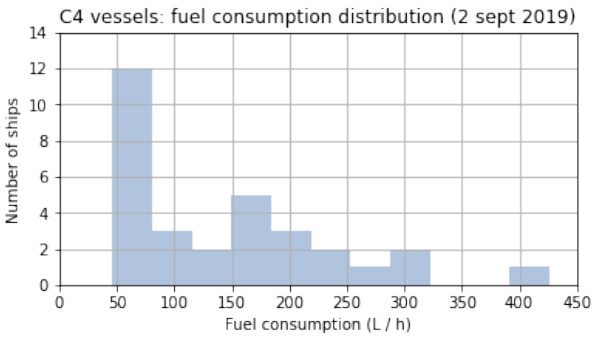

(f) Class C4: N = 34, Mean fuel c. = 216 L/h, V_{mean} = 12.03 km/h

Figure 6.6: OpenTNSim model simulation of 2 September 2019: Fuel consumption distributions of different types of barges and convoys

II

Results

7

Current emission patterns on the corridor

In the literature, materials and methods part of this study (Part I), a method was developed to estimate the energy consumption and potential emissions of a single inland ship, as a function of time and space. In addition, Rijkswaterstaat provided an AIS dataset with observed data of the fleet on the Rotterdam-Antwerp corridor, which has been analyzed to obtain fleet characteristics. Subsequently, a model has been developed that is able to simulate the fleet.

In this chapter, the potential emission patterns of the inland fleet on the Rotterdam-Antwerp corridor will be mapped. This starts with the application of the developed algorithms to the observed AIS data. Based on this output, the potential emission levels will be visualized on the inland waterway network: this is the 't0 emission scenario', which is discussed in Section 7.1. Subsequently, the developed model will be used to simulate the fleet, and the algorithms will be applied to the modelled time series to simulate the 't0 emission scenario' resulting from the AIS data. This model output will be addressed in Section 7.2. This output will be compared to the AIS 't0 emission scenario' in Section 7.3, to determine whether the model is capable of simulating the emission patterns in a proper way.

7.1. Emission patterns based on AIS data (t0 emission scenario)

The AIS dataset contains an observed timeseries of each individual vessel in the fleet, sailing on the Rotterdam-Antwerp corridor. This data provides information about the vessel dimensions, sailing speed and the route of the vessel (geographical position) as a function of time. But beside the vessel characteristics, the fairway properties have also influence on the resistance of a ship, and so on the potential emissions. First we will map the emission patterns without including variation in fairway properties in the calculations: a fixed water depth along the network will be assumed. It provides a first visualization of emission distributions along the network, which is discussed in Section 7.1.1. Afterwards, the AIS dataset will be connected to the FIS network (Fairway Information Services). This way, the fairway properties can be included in the calculations and the potential emission levels can be quantified on the network. This will be addressed in Section 7.1.2.

7.1.1. AIS emission patterns with a fixed water depth

To map the potential emission patterns along the Rotterdam-Antwerp corridor, the developed algorithms to estimate the energy consumption and emission of a single vessel as a function of time and space, are applied to the AIS timeseries. There is no connection to the fairway properties yet, so for the first step, we assumed a fixed water depth of 10 meters along the corridor. Per ship, per timestamp, the CO_2, PM_{10} and NO_x emissions (expressed in gram per meter) have been computed. This output of each timestamp is connected to a certain geographical location on the network. With this information, the emission patterns can be visualized on the network, making use of a Python tool called 'datashader': this tool is able to create graphics of large datasets in a relatively quick and flexible way. The visualizations of potential emission distributions of CO_2, PM_{10} and NO_x are presented in Figure 7.1.

The emission heatmaps in Figure 7.1 clearly show where the high emission levels are located on the fairway network. When waterway sections are marked with a darker color, this means relatively higher emission levels. For example, high emission levels can be indicated at the Volkerak, Krammer, Hansweert and Kreekrak locks (for the specification of the corridor: See Figure 1.4). This can be explained by the fact that ships slow down when they approach a lock, possibly have to wait before they can enter the lock and are also stationary during the locking process. But in this stationary stage, in most of the cases the engine is not turned off but keeps on idling. The ship is still emitting, but stays at the same place, which results in accumulation of emissions at the lock locations.

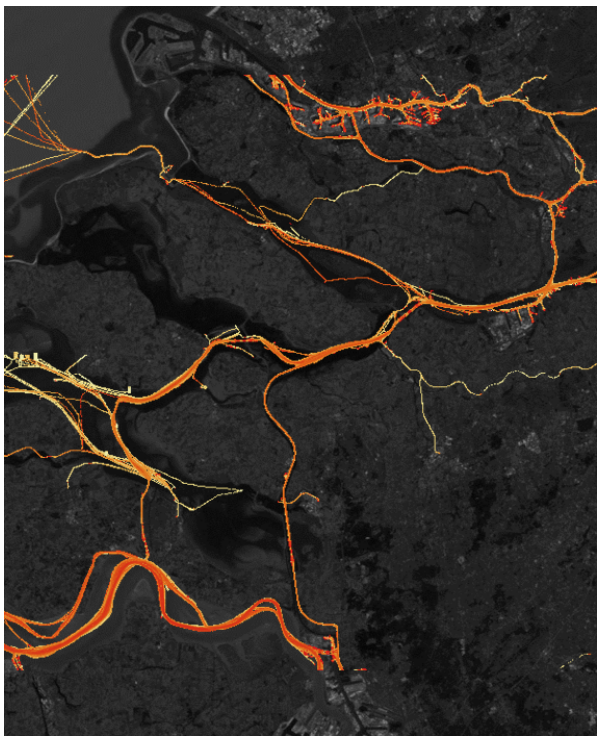

(a) CO_2 emission heatmap of one day resulting from AIS data

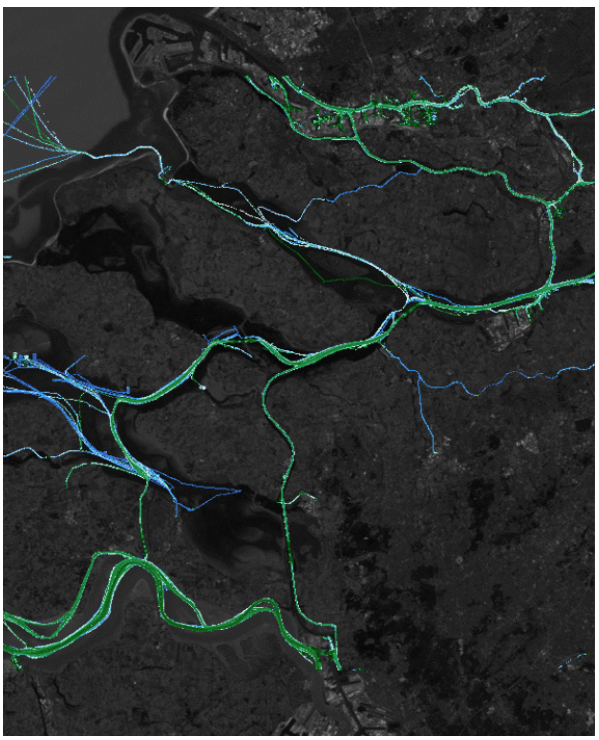

(b) PM_{10} emission heatmapof one day resulting from AIS data

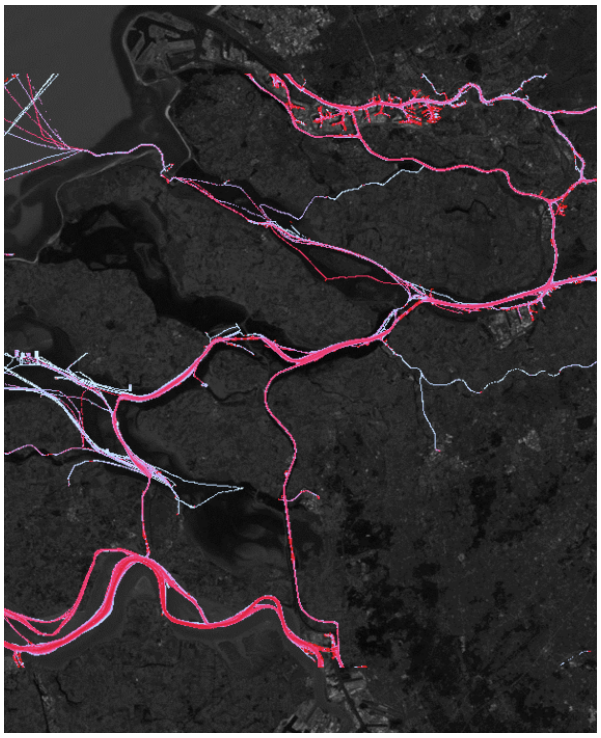

(c) NO_x emission heatmap of one day resulting from AIS data

Figure 7.1: Emission heatmaps of one day (2 Sept 2019) on the Rotterdam-Antwerp corridor, created with the datashader tool in Python. The heatmap is based on the emission levels expressed in gram per meter.

The Botlek region, near the Port of Rotterdam, also shows high emission levels. This can be explained in the same way as the high emission levels at locks: when these ships depart or arrive at their berth in the Botlek, the engine is idling, but you have to sail with reduced speeds and you possibly have to wait for other incoming or outgoing traffic. This results in accumulated emission at the berth spots in the harbour area.

In addition, high emission levels can be identified at the Western-Scheldt. This waterway is dealing with high traffic volumes, but since we only consider the inland shipping on the waterway, this does not explain the high emission levels. Which does provide an explanation, is the analysis of the sailing speeds on the Western-Scheldt: in Section 5.2.4, Table 5.2 showed that the average velocities on the Western-Scheldt are much higher than on the other inland fairways considered. The velocity of a vessel has a significant influence on the emission output, which results in higher emission levels on the Western-Scheldt.

It is also important to consider that currents and tides can play an important role on the Western-Scheldt: these effects have not been taken into account in the calculation methods. We calculate with a vessel speed relative to the water, but we assumed still water on the corridor, which means that the speed relative to the water becomes equal to the speed relative to the ground. AIS data provides the speed relative to the round, and therefore we calculate with that speed. Assuming still water on the corridor is a reasonable assumption for most of the inland waterways on the network. But there are exceptions, such as the Western-Scheldt. The Western-Scheldt is an estuary, dealing with tide and currents, which makes the performed calculations less reliable.

7.1.2. AIS emission patterns when connected to FIS network network

In the previous section, no variations in fairway properties were incorporated in the emission calculations. The visualizations were based on a fixed water depth of 10 meters along the whole fairway network. But the fairway properties have a significant influence on the energy consumption and emissions of inland vessels. Therefore, we want to connect the fairway properties to the AIS data, by means of a FIS (Fairway Information Services) network. This is a graph, containing a collection of nodes, connected by edges (the waterway sections). Each edge contains information about the considered waterway section. FIS is also used in the model simulation (discussed hereafter). A detailed explanation of FIS was given in Section 6.2.1.

Besides the benefits of incorporating fairway properties, another advantage of connecting the AIS data to FIS, is that it gives the ability to sum the emissions on each edge of the network and quantify them. This way, you can easily compare different scenarios. This quantification was not possible in the datashader visualization of the emissions in Section 7.1.1.

Van der Werff (2021) developed a Python code to project the AIS data onto the graph of the FIS network. In order to do this, individual ship trajectories are identified using the Python package MovingPandas. For each trajectory, an output table is created that contains in each row, the name of the edge in the FIS graph, the ship data, and its travelling time, speed and distance required to move from the start node to the end node of the edge. This is done by first creating a distance matrix for each AIS position entry and each node in the FIS graph. Based on the minimum distances, the number of nodes and edges to be considered in the rest of the procedure is reduced drastically. Next, paths are formed of closest nodes and edges, and finally the ship travel data is assembled for each edge it crosses.

The output table created with the projection of the AIS data onto the graph of the FIS network, provides per ship, per edge on the graph, the information needed for the algorithms: the ship dimensions, speed, water depth, and the resolution in time and space. For each row in the table, the energy consumption and emissions can be computed. Because we know which emission takes place at which edge on the graph, the emission can be summed on each edge, and this way the potential emission levels can be quantified on the network. This results in the 't0 emission scenario'. The 't0' potential CO_2 emission patterns of one day of AIS data (2 Sept 2019) are visualized in Figure 7.2. The results of PM_{10} and NO_x are presented in Appendix I, Figure I.1 and I.2.

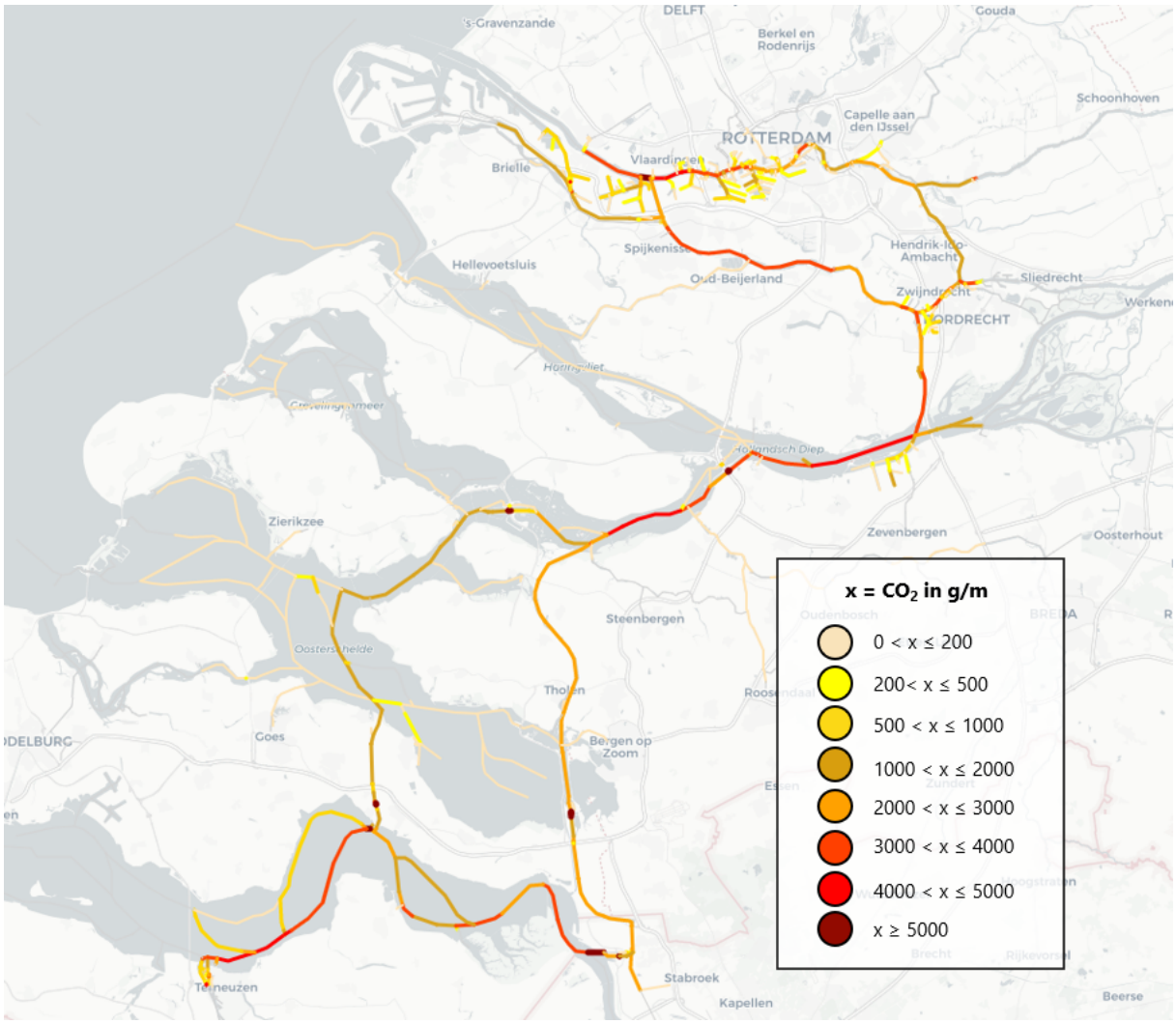

Figure 7.2: AIS 't0 emission scenario': potential CO_2 emission levels of one day (2 Sept 2019) on the Rotterdam-Antwerp corridor

Figure 7.2 shows emission hotspots around lock locations, just as the emission heatmaps in Section 7.1.1. A number of waterways have higher emission levels, such as Hollands Diep and the western part of the Western-Scheldt (See Figure 1.4 for specifications of the corridor). This can be mainly explained by a higher traffic intensity of inland shipping on these waterway sections: in Section 5.2.4, Figure 5.14, the traffic intensity along the corridor was considered.

It is important to address that the potential emission output is less reliable at fairways dealing with currents and/or tides. For the case study on the Rotterdam-Antwerp corridor, this mainly considers the Western-Scheldt, and also a part of the Maas and (to a lesser extent) the Eastern-Scheldt. As discussed before, the developed calculation method to estimate the energy consumption of a ship, assumes still water: therefore the speed relative to the water, becomes equal to the speed over ground. AIS data provides the speed over ground, which results in less reliable output at the fairways with currents. For a large part of the corridor, currents are less significant, and for these parts, still water is a reasonable assumption.

Besides the distributions of emission along the corridor, the total output of the AIS 't0 emission scenario' has also been quantified. Table 7.1 shows the average fuel consumption and average required power of the considered day (2 Sept 2019). In addition, the total fuel consumption (L) and emissions (in g) are presented in the table.

7.2. Emission patterns based on model simulation (simulated t0 scenario)

In the previous section we applied the developed algorithms to an observed AIS time series of the fleet on the Rotterdam-Antwerp corridor, to calculate the energy consumption and potential emissions per ship as a

	AIS t0 emission scenario
Average fuel consumption [L/h]	110
Average required power [kW]	446
Total fuel consumption [L]	545868
Total CO2 emission [kg]	1551610
Total PM10 emission [kg]	712,61
Total NOx emission [kg]	19966

Table 7.1: AIS 't0 emission scenario' output: Average fuel consumption and power; Total fuel consumption and potential emissions of one day (2 Sept 2019)

function of time and space. This output gives a good overview of the current potential emission patterns on the corridor.

But in the context of reducing emissions, we do not only want to get insight into current emissions patterns, but we also want to assess alternative future emission reduction policies. For that reason, we developed a model with the goal that it is able to simulate the current 't0 emission scenario', to subsequently implement alternative measures (Chapter 8) and see what the potential impact is on the emission levels.

In Chapter 6 the development of the model was addressed. The model makes use of an origin-destination (OD) matrix as input, which has been obtained from the observed AIS data. The OD-matrix describes each individual ship in the fleet, including the ship dimensions, vessel class, the time the ship starts to sail, the route it sails and average vessel speed along the trajectory. To take into account fairway characteristics, we make use of the FIS network, just like with the AIS data (for more details about FIS, read Section 6.2.1).

Based on the vessel characteristics from the OD-matrix and the fairway properties from FIS, the model simulates the inland fleet on the Rotterdam-Antwerp corridor, based on discrete event simulation. This results in a time series of each inland ship travelling along the network. The developed algorithms are applied to this simulated time series, to compute the energy consumption and potential emission per ship per time step. It is known per time step on which edge of the waterway network the ship is sailing: this way, the emissions can be summed up on each edge of the network, and subsequently be quantified and visualized. This simulation is performed for the same day (2 September 2019) as considered in the AIS 't0 emission scenario'. The output of this model simulation is called the simulated 't0 emission scenario'.

Figure 7.3 shows the visualization of simulated 't0 emission scenario' of the CO_2 emission distribution along the Rotterdam-Antwerp corridor. In Appendix I, Figure I.3 and I.4, the model result of the PM_{10} and NO_x emissions is given. The total model output of the simulated 't0 emission scenario' is summarized in Table 7.2. At the first glance, the model output looks quite similar to the AIS 't0 emission scenario'. In Section 7.3, the results of the AIS output and the model output will be compared, to determine whether the model is able to properly simulate the 't0 emission scenario'.

	Model simulation t0
Average fuel consumption [L/h]	119
Average required power [kW]	482
Total fuel consumption [L]	530730
Total CO2 emission [kg]	1547533
Total PM10 emission [kg]	685,86
Total NOx emission [kg]	19546

Table 7.2: Model output of simulated 't0 emission scenario': Average fuel consumption and power; Total fuel consumption and potential emissions of one day (2 Sept 2019)

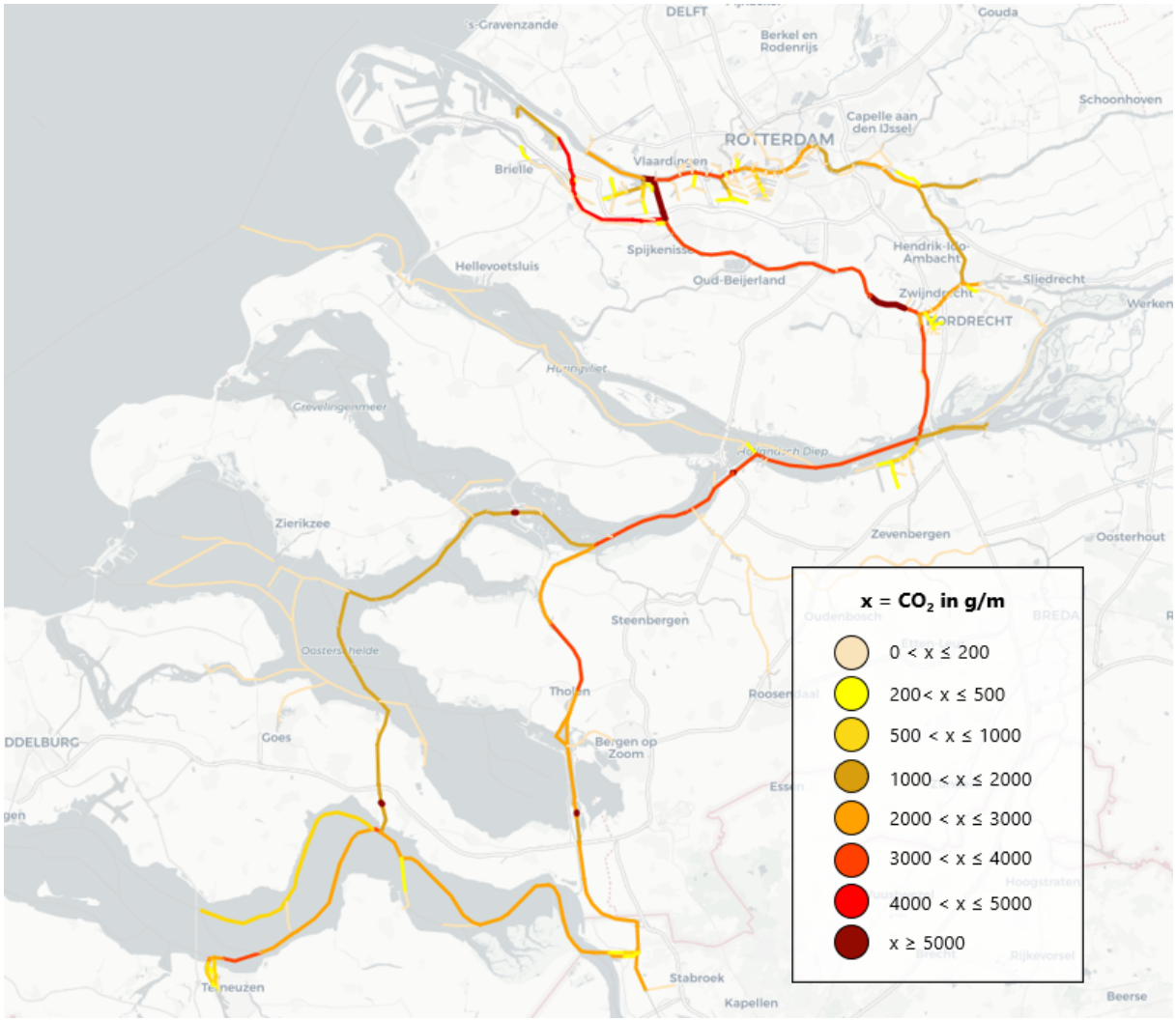

Figure 7.3: Model output, simulated 't0 emission scenario': potential CO_2 emission levels of one day (2 Sept 2019) on the Rotterdam-Antwerp corridor

7.3. Comparison t0 emission scenario: AIS versus model output

In the first section of this chapter, we visualized the current potential emission patterns of inland shipping on the Rotterdam-Antwerp corridor based on AIS data: the 't0 emission scenario'. Subsequently, we modelled the fleet and simulated this scenario. To quantify to which extend the model simulation corresponds to the AIS 't0 emission scenario', the output will be compared.

Table 7.3 shows the total output of 't0 emission scenario' resulting from observed AIS data, versus the output of the model simulation. The table specifies the average fuel consumption, average required power and total fuel consumption and emissions of one day, on the Rotterdam-Antwerp corridor. The last column shows the difference between the AIS output and the model simulation output. This shows that, despite the simplifications of the model, the model is able to compute a very comparable total output. The average fuel consumption and required power is slightly higher in the model ($\approx$ 8%). This difference may be explained by the fact that the model works with average speeds: a ship has contact speed, except when it is stationary in front of a lock. The AIS data works with speed variations, and therefore it also takes into account time steps where a ship has a lower speed or is stationary for a bit. This can result in a lower average fuel consumption and required power. The total fuel consumption and emission output of one day matches even better: the difference between the AIS output and the model is a few percent.

	AIS t0 emission scenario	Model simulation t0	Difference
Average fuel consumption [L/h]	110	119	8,2%
Average required power [kW]	446	482	8,1%
Total fuel consumption [L]	545868	530730	-2,8%
Total CO2 emission [kg]	1551610	1547533	-0,3%
Total PM10 emission [kg]	712,61	685,86	-3,8%
Total NOx emission [kg]	19966	19546	-2,1%

Table 7.3: Output of AIS 't0 emission scenario', compared to model simulation output: Average fuel consumption and power; Total fuel consumption and potential emissions of one day (2 Sept 2019)

The total output of the model simulation matches with the 't0 emission scenario' resulting from the observed AIS data. But we are also interested in to which extent the model is able to simulate the emission distribution along the network in a proper way. Therefore, a difference map has been created: for each edge on the graph of the FIS network, the emission output (in g/m) of the AIS 't0 emission scenario' has been compared to the model simulation output. The absolute percentage difference per edge has been computed, and visualized on the network, to see on which parts of the corridor the model simulates the 't0 emission scenario' well, and on which parts there is room for improvement.

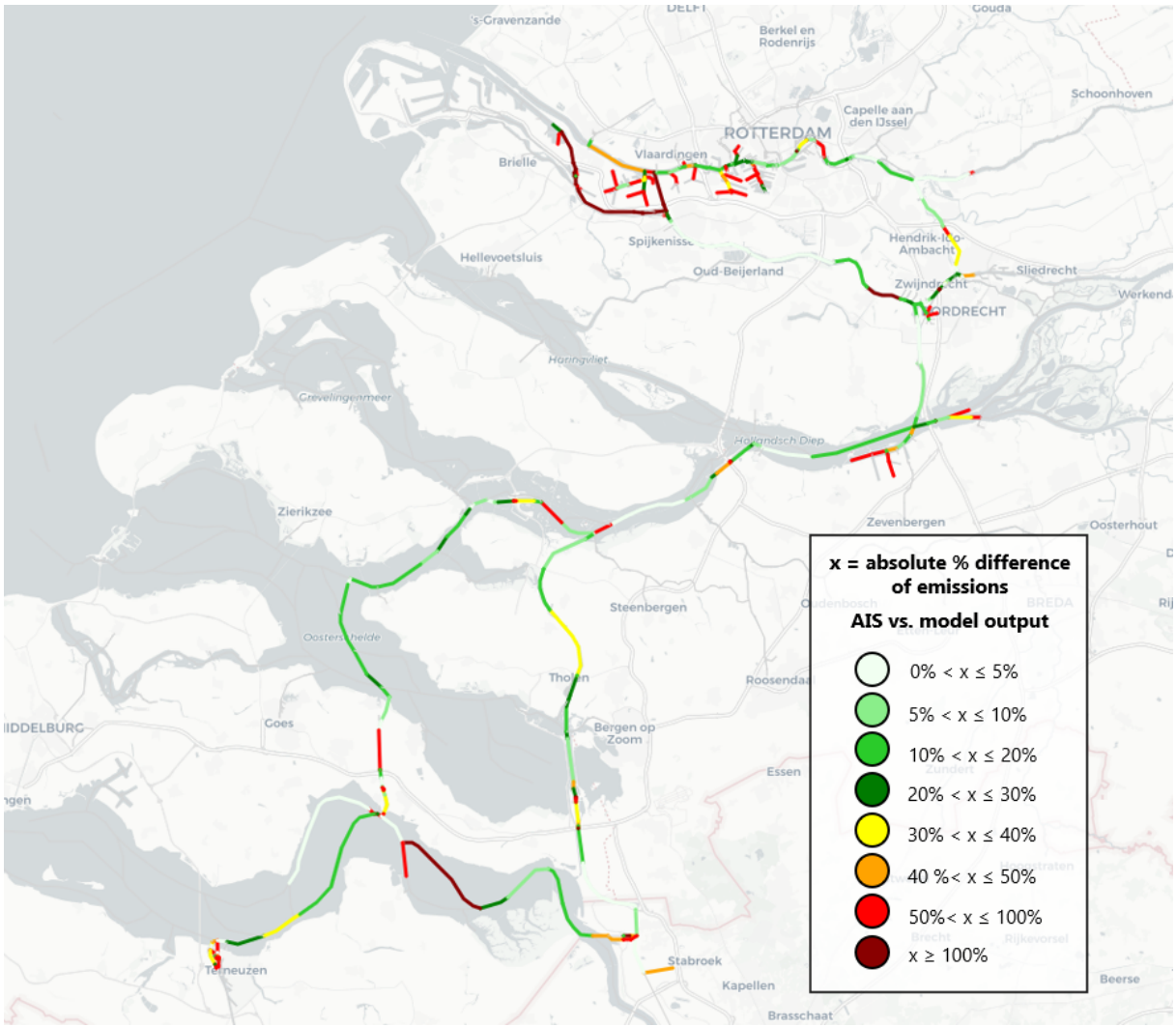

Figure 7.4: AIS 't0 emission scenario' compared to model simulation: difference map, showing the absolute percentage differences of the emission distribution on each waterway section of the fairway network

It appears from the difference map that around locks the absolute percentage difference between the model output and the AIS output is quite high. This can explained by the fact that the AIS data contains a lot of

information about velocity variations. When a vessel is approaching a lock, it will slow down and it possible has to wait before it will enter the lock. Accumulation of emission will take place in front of the lock. Due to detailed information in the AIS data about the geographical position and the extent of slowing down of a ship, the visualization of the emission on the FIS network around locks is more detailed in case of the AIS data: the emission is distributed along a few edges in front of a lock. The model, on the other hand, works with average velocities and therefore details about slowing down when approaching the lock are not simulated. In addition, the lock element is linked to one single edge of the FIS network. When the vessels in the model are stationary because they are waiting for the lock, this means that they are stationary on one single edge, and all the emissions that are assigned to the locking process are assigned to that edge. This results in high emission levels on a relatively small piece of waterway network. This is the reason that the distribution of potential emissions around locks of the model output does not match so well with the distributions resulting from AIS data.

We also see high absolute percentage differences in the Botlek harbor area. This can be explained in the same way as the mismatch at locks: AIS data provides a lot more information about velocity variations, and in and around harbour areas the velocity of the ship will differ a lot. This effect is not captured in the model simulation, because it works with average velocities.

In addition to differences between the AIS and model output resulting from velocity, it is also possible that differences along the fairway network arise because of the limitation of mimicking the exact routes in the model. The origin-destination (OD) matrix, obtained from the AIS data, provides information about each ship trajectory in a data set of one day. The vessel characteristics are defined, as well as information about the route: the origin, destination, and possible crucial intermediate route points are specified (read Section 6.2.2 for more information). Based on this information, the model uses the Dijkstra algorithm to find the shortest route of the ship (see Section 6.3.3). Although most routes are covered in this way, it is not possible to include all exact route details from the AIS data by this method. It is therefore possible that the number of ships sailing on a particular waterway may be higher or lower in the model simulation than the AIS data describes. This can result in differences between the emission distributions of the AIS data and the model.

We have now approached the deviations, but the difference map in Figure 7.4 also shows quite some similarities. On a large part of the main waterways on the Rotterdam-Antwerp corridor (Nieuwe Maas, Oude Maas, Dortsche Kil, Hollands Diep, Zuid-Beveland route, Scheldt-Rhine canal), the model is able to simulate the potential emission distribution of the AIS 't0 emission scenario' quite well. The largest part has an absolute percentage difference between 0 and 20%. On these main waterways, ships will not vary much in speed: this is a possible explanation for quite similar emission distributions of the AIS and model output on these fairways.

8

Assessment of emission reduction policies

In the previous chapter, it appeared that the developed model that simulates the inland fleet on the Rotterdam-Antwerp corridor, is able to properly simulate the 't0 emission scenario' resulting from the AIS data. The main objective of developing a model was that it can be used as a tool in the support of development and evaluation of emission reduction policies. In this chapter, the developed method of this study will be used for that purpose: a first assessment will be performed of alternative measures to reduce emissions.

In the first section of this chapter, the emissions at locks will be addressed: what does the situation look like in the case of zero emission policy at locks? As a second policy assessment, we will be looking at fleet renewal: newer engines are much cleaner, which could have a large impact on emissions in inland shipping. This is addressed in Section 8.2. Finally, a very first assessment of the impact of speed limits will be adressed in Section 8.3.

8.1. Emission reduction at locks

The 't0 emission scenario' presented in Chapter 7 showed that the potential emission levels are quite high in the area around locks: ships are slowing down when approaching a lock and possibly have to wait before they can enter the lock. When a ship has to wait for a long time (longer than ≈ half an hour), skippers will in practice be mooring and will turn off their engine for some time. This scenario is included in both the AIS 't0 emission scenario' and the model simulation, by cutting a ship trajectory when a ship is stationary for half an hour or longer. The timestamps during this stationary stage are cut from the data in this way, and a follow-up vessel trajectory is created when the ship starts to sail again. Although a part of these skippers will turn off their engines when they have to wait for some time, the emissions at locks are still significantly high. This local level of emissions is mainly of importance considering environmental pollutants such as particulate matter and nitrogen oxides, because this has an impact on the local nature and health of the environment.

The pressure to reduce emissions in inland shipping is increasing. Due to the high emission levels at locks, the question rises how the get insight into the emissions in these areas. First of all, we will look at the emission rates of different vessel types, with different engine ages, at locks (Section 8.1.1). This gives insight into where is room for improvement. Subsequently, a 'zero emission policy' at locks will be implemented in the model, to simulate and quantify what the impact would be, if you for example oblige skippers to sail on batteries and / or to connect to shore power when they have to wait for some time. The result is discussed in Section 8.1.2.

8.1.1. Emission rates at locks

To quantify emission rates at locks, you have to distinguish between different ship types (bigger ships emit more) and different engine ages (newer engines are cleaner). In this section, the emission rates are quantified for a number of vessel types, in a stationary stage (so when they are waiting at a lock). We will focus on the emission rates of PM_{10} and NO_x, since the local effect at locks is of importance. The CO_2 emission rates at locks are given in the Appendix J.

Figure 8.1 and 8.2 show the stationary emission rates of PM_{10} and NO_x (expressed in gram per hour) of different ships, varying the construction year of the engine. For the corresponding numbers: see Table J.1 in Appendix J. The different ship types are based on the Rijkswaterstaat vessel classification: for more information about this classification and the characteristics of these ships, see Appendix F.

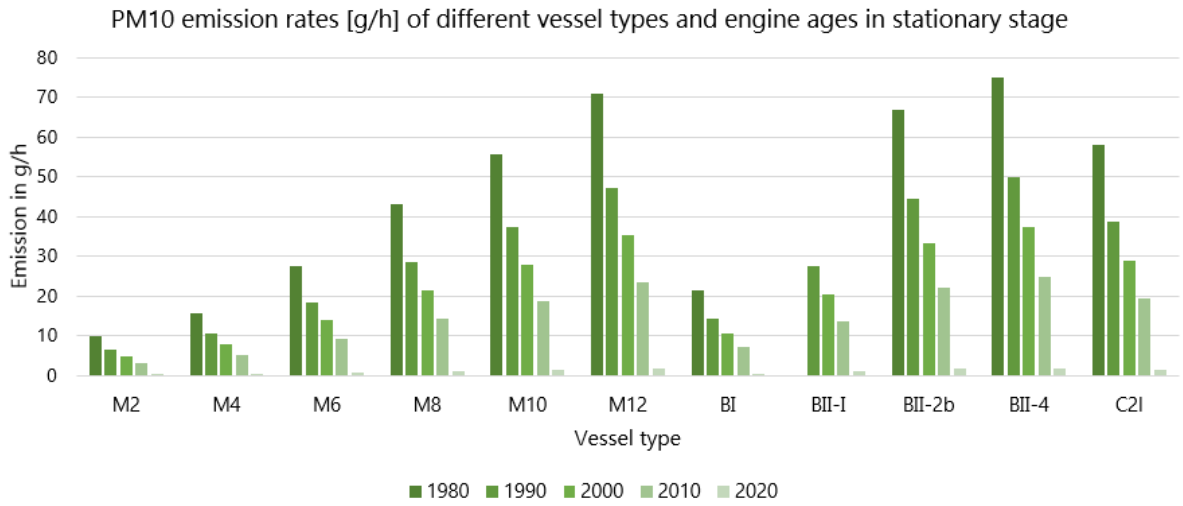

Figure 8.1: PM_{10} emission rates (in g/h) of different vessel types and engine ages in a stationary stages

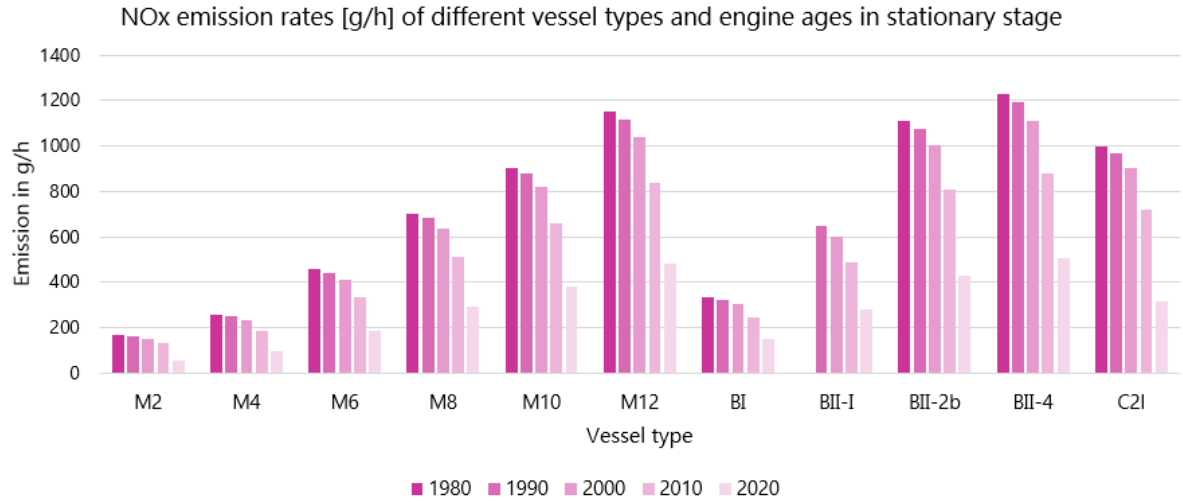

Figure 8.2: NO_x emission rates (in g/h) of different vessel types and engine ages in a stationary stages

The method developed in this study to estimate emissions of a single inland vessel, uses the vessel speed as an important input parameter. In a stationary stage, the vessel speed becomes zero, but the engine keeps on idling, and so the emission rates will not become zero. Therefore, an assumption has to be made for the energy consumption in a stationary stage: the starting point is that the energy consumption of an inland vessel in the stationary stage is approximately 15 percent of the energy consumption in the average propulsion stage. This was discussed in more detail Section 3.3. The stationary emission rates in Figure 8.1 and 8.2 are based on this assumption. The emission rates show that for bigger ships with an older engine, the emission of PM_{10} can amount to 70 g/h or more. For NO_x this is 1100 g/h or more. It also shows that larger ships emit a significant amount, and that a newer engine has a large impact on the emissions of environmental pollutants.

These emission rates give an indication of how much emission potentially takes place at locks, expressed in gram per hour. To quantify how much a ship emits at at a specific lock on the Rotterdam-Antwerp corridor, you have to take into account how much time the lock passage takes. From the AIS data, the lock passing times have been analyzed (see Section 5.2.3 for more details). For the main locks on the corridor, the average passing times are summarized in Table 8.1.

	average passing time	
	seconds	hours
Volkerak	2558	0,711
Krammer	2571	0,714
Hansweert	1668	0,463
Kreekrak	2085	0,579

Table 8.1: Average passing time per lock, determined from AIS data

By multiplying the emission rate of a ship (in gram per hour) by the average passing time of a specific lock, the potential emission of that single ship at the considered lock can be quantified. Figure 8.3 and 8.4 show the PM_{10} and NO_x emissions (in gram) of different types at the Volkerak, Krammer, Hansweert and Kreekrak locks. A fixed engine age of 1990 has been chosen to visualize the differences between the locks. The results of the emissions of other engines ages at these locks are given in Table J.2 - J.5 in Appendix J.

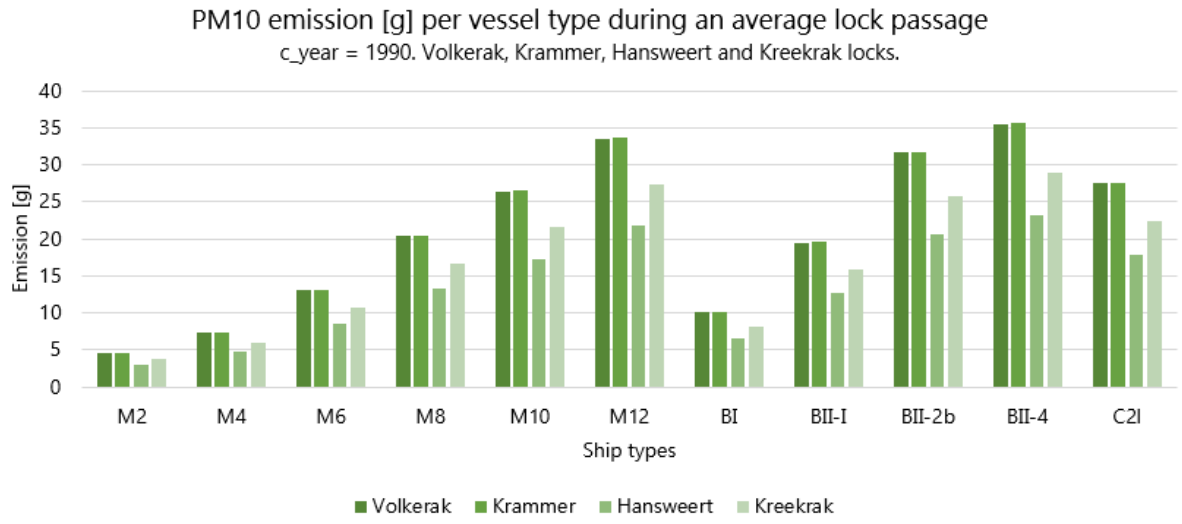

Figure 8.3: PM_{10} emissions during one average lock passage at different locks, for different vessel types with c_{year} = 1990.

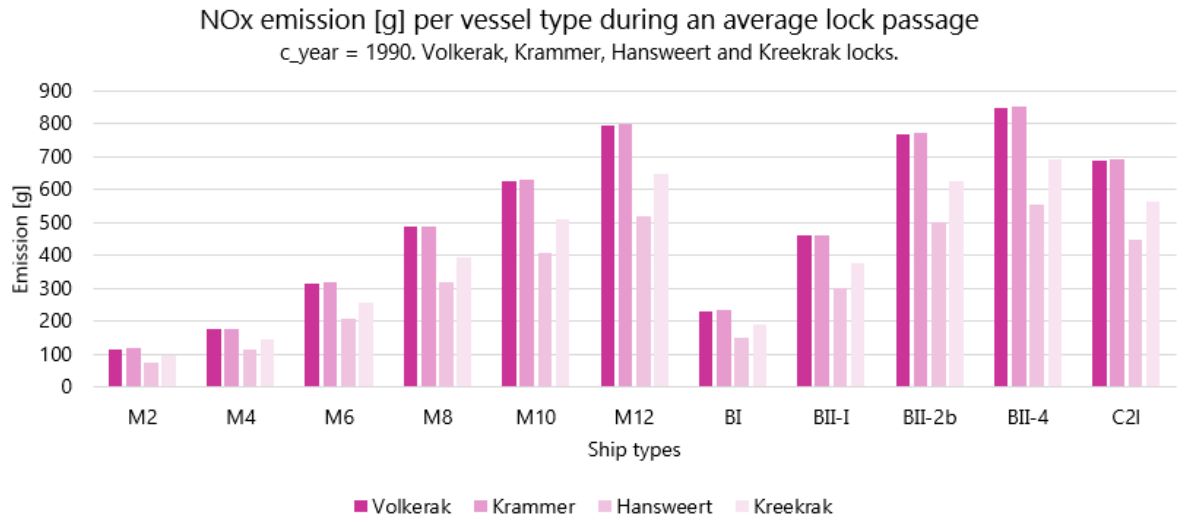

Figure 8.4: NO_x emissions during one average lock passage at different locks, for different vessel types with c_{year} = 1990.

8.1.2. Zero emission policy at locks

Due to the pressure to reduce emissions, the inland shipping sector is developing. In the coming years, higher requirements will be set for emissions from inland shipping, which is why there is a demand for alternative solutions to reduce emissions. For example, one seeks for solutions to tackle emissions at locks.

For solutions at locks, you can for example think of shore power: this a system which can be installed at waiting areas, where vessels can moor, shut down their engine and connect to the shore power system, which provides electrical power from the shore-side. This reduces emissions during the waiting periods. But the question is whether ships will actually moor and connect to the shore power system, if the waiting time is not significantly long enough. Another development that is going on is the technology of hybrid vessels: these ships can be partially electrically powered, which results in less (local) emission. When vessels will make use of an electrical engine / battery in lock areas, this could have significant impact on the local emission levels.

More research is needed to properly map out the applicability of various technologies for reducing emissions at locks. However, the developed model does provide the opportunity to perform an initial assessment. To illustrate this, a 'zero emission policy' has been implemented in the model, to see what the effect would be if skippers for example are required to sail on a battery around a lock, or have to use other technologies to avoid emissions in these areas, such as shore power.

The 'zero emission policy' at locks is implemented in the model as follows. During the model simulation, the information of the stage of each vessel is logged over time (discrete event simulation). The model logs for example when a vessel is stationary at a lock: this is the case while waiting before the ship can enter the lock, and during the locking process. The fuel consumption and emission during these stationary stages is set to zero. Figure 8.5 shows the model output of the potential PM_{10} emission distribution along the network, in case of zero emission at locks. As you can see, at the main lock locations at the corridor (Volkerak, Krammer, Hansweert and Kreekrak), we do not see any accumulation of emission anymore in these areas. The model output of the CO_2 and NO_x emissions in case of a 'zero emission policy' at locks, can be found in Appendix I, Figure I.5 and Figure I.6.

However, considering the effect on the total emission of one day on the Rotterdam-Antwerp corridor, a measure such as 'zero emission policy' at locks does not have that much effect: Table 8.2 shows the total fuel consumption and emissions of one day of the model simulation of the 't0 emission scenario' versus the scenario with zero emissions at locks. The emission reduction is only a few percent. Such a measure therefore has no significant effect on the overall picture, but when you consider the local effect of emissions around locks, such a measure can make a significant contribution.

	Model simulation t0	**Model simulation zero emissions at locks**	**Reduction**
Average fuel consumption [L/h]	119	119	0%
Average required power [kW]	482	482	0%
Total fuel consumption [L]	530730	524613	-1,2%
Total CO2 emission [kg]	1547533	1527257	-1,3%
Total PM10 emission [kg]	685,86	668,95	-2,5%
Total NOx emission [kg]	19546	19152	-2,0%

Table 8.2: Output of model simulation: simulated 't0 emission scenario' versus policy of zero emission at locks. Effect on average fuel consumption and power, and on total fuel consumption and potential emissions.

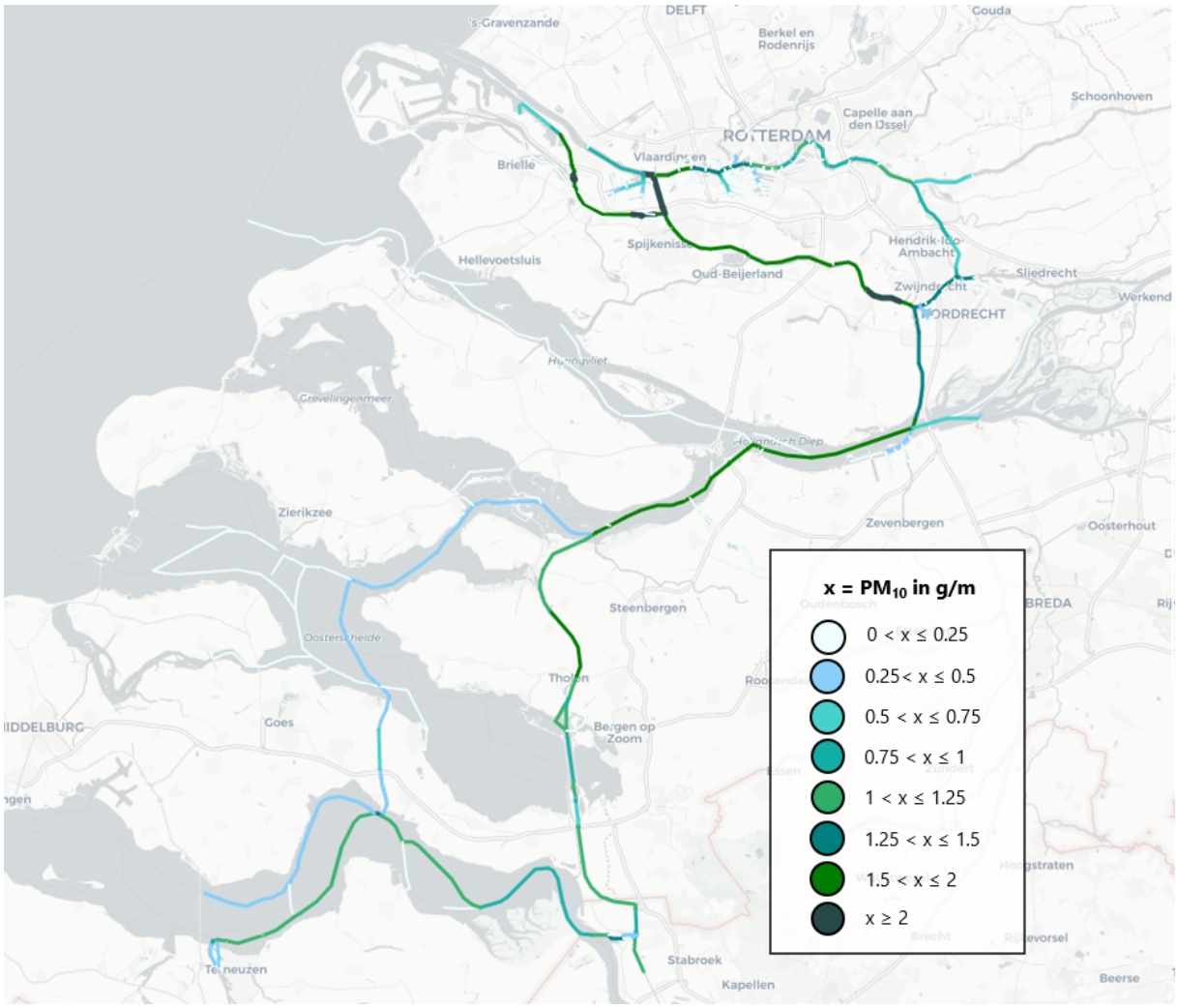

Figure 8.5: Model simulation: zero emission policy at locks. Map shows potential PM_{10} emission levels of one day (2 Sept 2019) on the Rotterdam-Antwerp corridor

8.2. Fleet renewal

In Chapter 4 it has been discussed that the age of the engine has a lot of influence on the emission of an inland ship. Due to technological development of the engines of inland vessels over the years, engines became much cleaner and more efficient. At first, the newer engines are more economical and therefore require less fuel per kWh, which has a direct influence on the CO_2 emissions. Secondly, the technological developments are having a significant effect on the emission factors of particulate matter (PM_{10}) and nitrogen oxides (NO_x): Table 4.1 in Chapter 4 showed that the PM_{10} emission factor of larger ships decreased by 95% from the CCR1 engine class (construction year 2003 - 2007) to the newest Stage V engine class (construction year 2020 or later). For NO_x this is 74%.

With this information in mind it, buying a new engine as an inland skipper seems to be quite attractive. But the newest Stage V engines require large investments, which avoids skippers from investing. Fleet renewal in the near future, with the purpose to reduce emissions and align with the goals defined in the Green Deal, will therefore require a large amount of subsidies to stimulate skippers to invest. It was recently decided that the dutch Ministry of Infrastructure and Water Management will spend 11.7 million euros to support inland skippers and shipping companies in making their fleet more sustainable, which is mainly intended for the purchase of newer engines (Ministerie van Infrastructuur en Waterstaat, 2021).

Fleet renewal is therefore a current theme in the transition towards more sustainable inland shipping. Therefore, this section will provide insight into the effectiveness of fleet renewal on the potential emission distributions on the Rotterdam-Antwerp corridor.

We will first address the estimated current age distribution of the fleet, which has been used in performing the 't0 emission scenario'. This estimation is based on literature of TNO, who defined a Weibull function describing the current engine age distribution of different weight classes of inland vessels (Ligterink, 2019). This Weibull distribution was based on the IVR-vesseldatabase and a survey among 350 professional skippers (see Figure 4.4 in Section 4.2.1). We applied this Weibull function to our fleet of one day (2 September 2019) in the AIS data, as well as in the model simulation. Each ship has been allocated a construction year of its engine in this way. Figure 8.6 shows the estimated distribution of engine ages in the fleet.

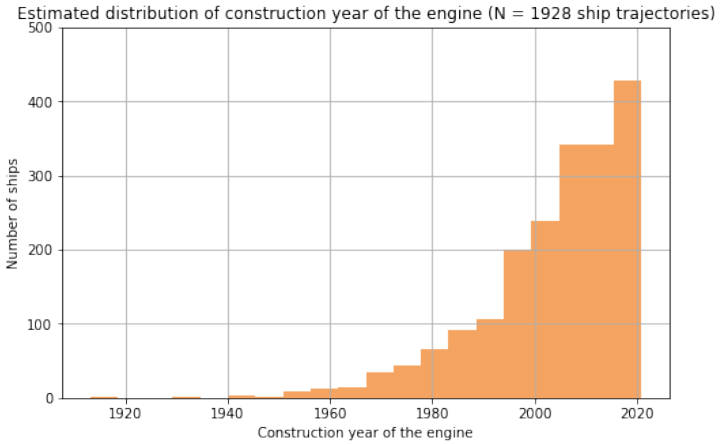

Figure 8.6: Estimated distribution of construction year of the engine (fleet of 1 day, 2 September 2019, N = 1928 ship trajectories)

To assess the effectiveness of fleet renewal policy, the estimated distribution of construction year of the engines is now manipulated in the model: engines which are constructed in the year 2007 or earlier (so engines of the CCR1 classification or older) are replaced by the newest Stage V engines. This means for the particular simulation of 2 September 2019, that about half of the engines are replaced by new ones. The potential emission patterns of CO_2, PM_{10} and NO_x resulting from the model simulation with this fleet renewal are shown in the Appendix I, Figure I.7, I.8 and I.9.

To quantify the impact on the total fuel consumption and emission output of one day on the Rotterdam-Antwerp corridor, Table 8.3 summarizes the total results of the 't0 emission scenario' compared to the scenario with fleet renewal. The last column shows the potential reduction of fuel consumption and emissions. These results show that the effect on the total fuel consumption and CO_2 emissions is quite limited: this fleet renewal may lead to a 5% reduction. Newer engines do not significantly effect the emission factors of CO_2. This is in contrast to the potential effect on the total PM_{10} and NO_x emissions: this fleet renewal can possibly lead to a total PM_{10} emission reduction of 67% and a NO_x reduction of 33%.

	Model simulation t0	**Model simulation fleet renewal**	**Reduction**
Average fuel consumption [L/h]	119	113	-5%
Average required power [kW]	482	482	0%
Total fuel consumption [L]	530730	504898	-5%
Total CO2 emission [kg]	1547533	1471233	-5%
Total PM10 emission [kg]	685,86	229,37	-67%
Total NOx emission [kg]	19546	13182	-33%

Table 8.3: Output of model simulation of one day (2 Sept 2019): simulated 't0 emission scenario' versus fleet renewal scenario (all engines from the year 2007 or older are replaced by new Stage V engines). Effect on average fuel consumption and power, and on total fuel consumption and potential emissions.

We now addressed the impact of fleet renewal on the total output, but we also want to map the effect on the emission distribution along the inland waterway network. For this reason, difference maps are created, showing the absolute differences between the 't0 emission scenario' and the fleet renewal scenario, in emissions distributions along the network, expressed in gram per meter.

Figure 8.7 shows the difference map of CO_2 emissions on the corridor. From the total emission output it already resulted that newer engines have a less significant effect on the CO_2 emission factors, and this also appears

from Figure 8.7. The absolute reduction in emissions of CO_2 per waterway section is limited: for the largest part of the corridor this is less than 200 g/m.

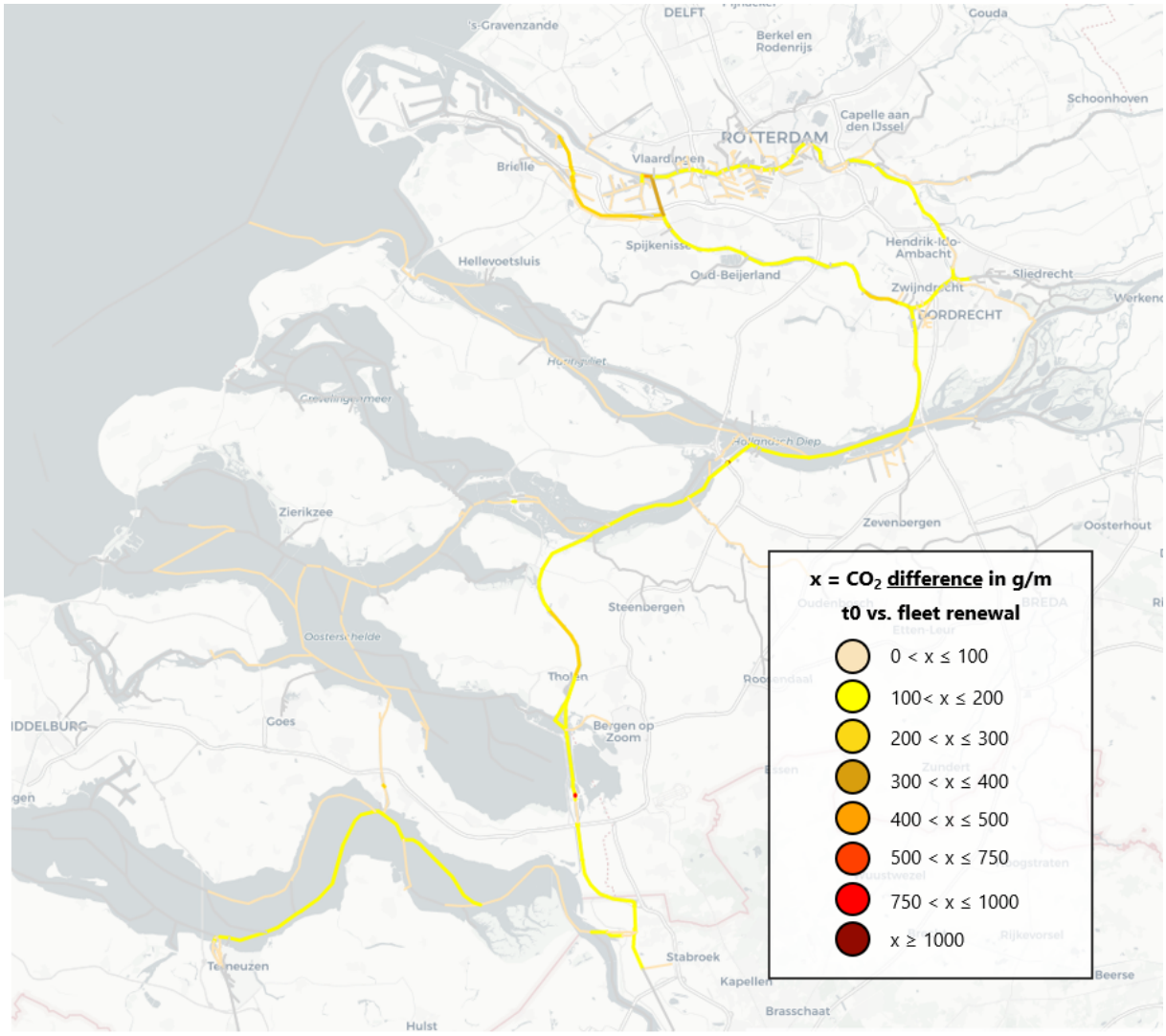

Figure 8.7: CO_2 difference map: t0 model simulation vs. fleet renewal (all engines from the year 2007 or older are replaced by new Stage V engines). Per waterway section the absolute emission reduction in g/m is specified.

Figure 8.8 and 8.9 show the difference maps of the emission levels of PM_{10} and NO_x. It shows how much of these emissions from inland shipping can potentially be reduced (expressed in g/m) per waterway section, when a fleet renewal policy will be practised. These figures show that mainly for particulate matter, but also for nitrogen oxides (to a lesser extent), fleet renewal can result in large absolute reduction of emissions levels along the corridor. The absolute difference is higher on waterways which were dealing with relatively higher emission levels in the 't0 emission scenario', because of higher average speeds on that fairway or due to high traffic intensities. A measure such as fleet renewal therefore has more effect on these waterways in absolute terms.

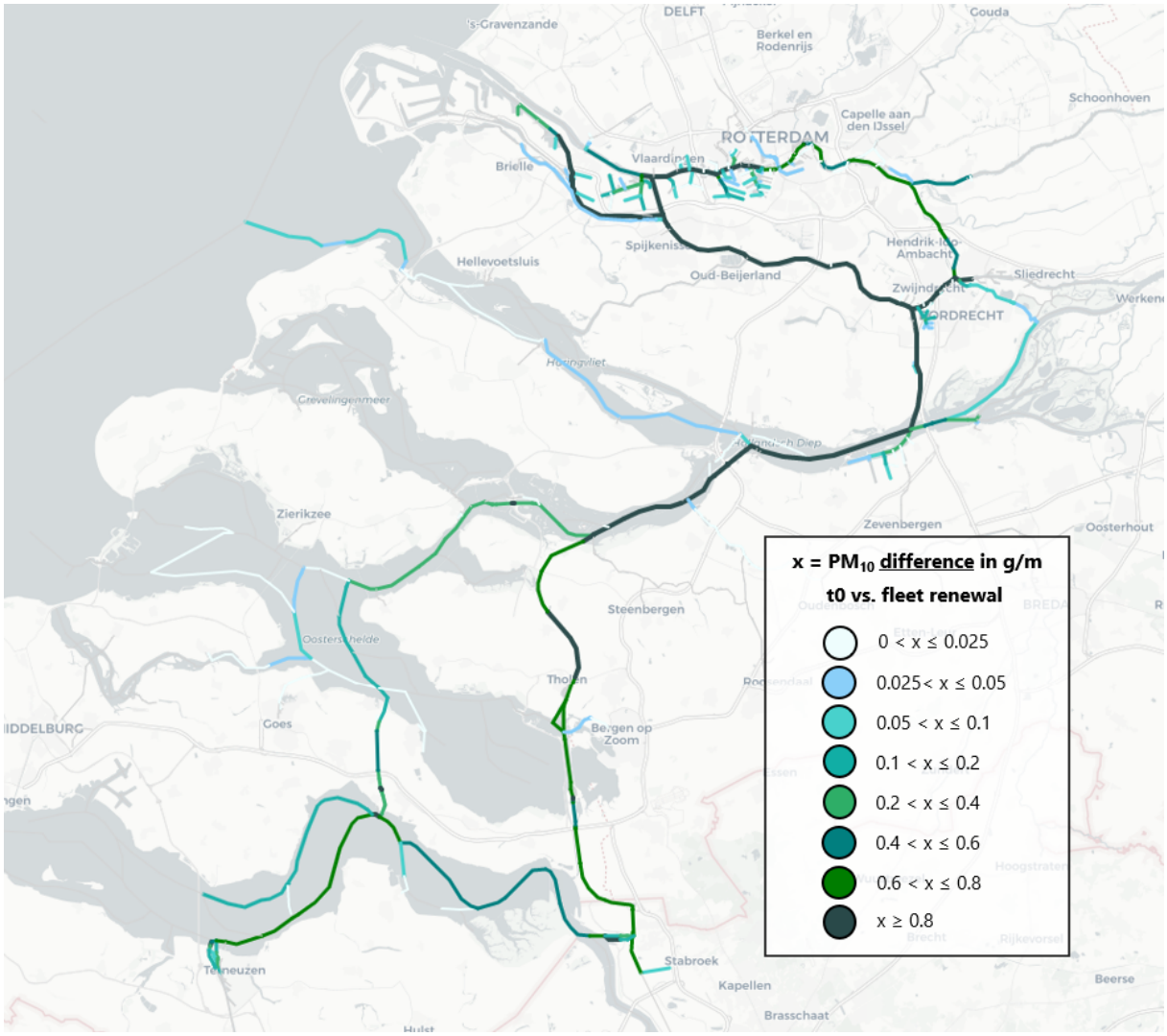

Figure 8.8: PM_{10} difference map: t0 model simulation vs. fleet renewal (all engines from the year 2007 or older are replaced by new Stage V engines). Per waterway section the absolute emission reduction in g/m is specified.

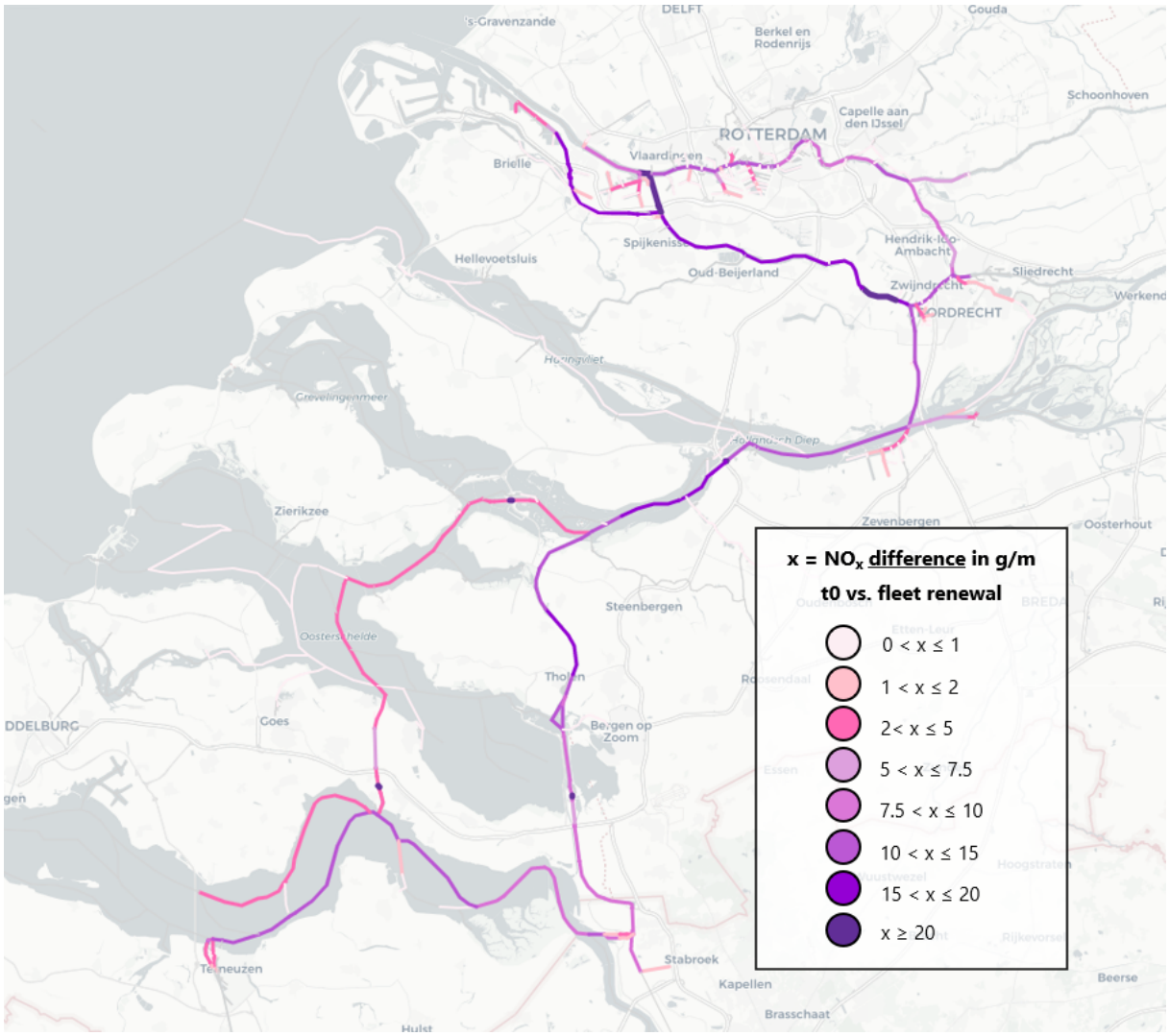

Figure 8.9: NO_x difference map: t0 model simulation vs. fleet renewal (all engines from the year 2007 or older are replaced by new Stage V engines). Per waterway section the absolute emission reduction in g/m is specified.

8.3. Speed limit

The sailing speed of inland vessels is one of the most determining factors in the energy consumption and emission calculations. The relationship between the speed and the required power is exponential, and when a vessel sails in shallow water, this relationship will even show asymptotic behaviour. This behaviour is also reflected in the emission output.

For this reason it seems effective to look for measures related to speed. In this section, the effectiveness of a speed limit will be assessed. The average speeds in the origin-destination matrix resulting from AIS data, which is input of the model, will be manipulated to provide a first assessment: at first, all average speeds above 12 km/h are set to a maximum speed of 12 km/h. This means that the simulated fleet in the model will only contain ships with an average speed of 12 km/h or lower. The implementation of this policy resulted in a reduction of the average speed of 56% of the ship trajectories in the model.

Please note that this is a very first assessment of a speed limit. In reality the problem is much more complex: commercial inland vessels usually have to meet certain sailing schedules and time slots at ports. Imposing a speed limit is a measure with a lot of impact and will not be immediately applicable. This study only provides a first indication of the effectiveness of such a measure. In addition, it is important to note that this model assessment only provides a global overview of the potential impact, since the model works with an average velocity per ship. For example, ships with an average velocity below 12 km/h will not be affected by this measure in the model, but in reality they will possibly sail with a speed above 12 km/h at some spots along their routes.

The potential emission distributions of CO_2, PM_{10} and NO_x resulting from the model simulation with a speed limit of 12 km/h, are presented in Figure I.10, I.11 and I.12 in Appendix I. The total fuel consumption and emission output of the scenario with a speed limit of 12 km/h is compared to total output of the 't0 emission scenario' in Table 8.4.

	Model simulation t0	**Model simulation speed limit 12 km/h**	**Reduction**
Average fuel consumption [L/h]	119	66	-45%
Average required power [kW]	482	268	-44%
Total fuel consumption [L]	530730	362735	-32%
Total CO2 emission [kg]	1547533	1127010	-27%
Total PM10 emission [kg]	685,86	552,9	-19%
Total NOx emission [kg]	19546	14852	-24%

Table 8.4: Output of model simulation of one day (2 Sept 2019): simulated 't0 emission scenario' versus scenario with speed limit of 12 km/h. Effect on average fuel consumption and power, and on total fuel consumption and potential emissions.

The results from Table 8.4 show that the effect of implementing a speed limit has a significant effect on the fuel consumption as well as on the emissions: the potential reduction in total fuel consumption is 32%, and the potential total emission reduction of CO_2, PM_{10} and NO_x is 27%, 19% and 24% respectively. Since the required power (and so the fuel consumption and emissions) depend exponentially on the vessel speed, a strict speed limit quickly results in a significant reduction of emissions. This significant reduction is also explained by the fact that this speed limit reduced the average speeds of more than half of the ship trajectories in the model.

To also quantify the impact of a speed limit on the distributions of emission levels along the Rotterdam-Antwerp corridor, again difference maps have been created. These difference maps show the absolute differences between the 't0 emission scenario' and the scenario with a speed limit of 12 km/h. The difference maps of the CO_2, PM_{10} and NO_x emission distributions are presented in Figure 8.10, 8.11 and 8.12. The absolute reduction of emissions per waterway section, due to the speed limit, are expressed in gram per meter. You can see that the absolute differences are greatest on the waterways where there is normally a lot of traffic, and on the parts where the average speed of ships is relatively higher (see Section 5.14 about the details of traffic intensity and average speeds on several waterways on the corridor).

To quantify what happens if you apply a less strict speed limit, the simulation was also performed for a speed limit of 13 km/h. This measure affected the average speed of 46% of the ship trajectories. The total output is presented in Table 8.5. It shows that a speed limit of 13 km/h still significantly affects the total fuel consumption and emission output of the simulation of one day.

	Model simulation t0	**Model simulation speed limit 13 km/h**	**Reduction**
Average fuel consumption [L/h]	119	76	-36%
Average required power [kW]	482	309	-36%
Total fuel consumption [L]	530730	394273	-26%
Total CO2 emission [kg]	1547533	1208560	-22%
Total PM10 emission [kg]	685,86	569,25	-17%
Total NOx emission [kg]	19546	15599	-20%

Table 8.5: Output of model simulation of one day (2 Sept 2019): simulated 't0 emission scenario' versus scenario with speed limit of 13 km/h. Effect on average fuel consumption and power, and on total fuel consumption and potential emissions.

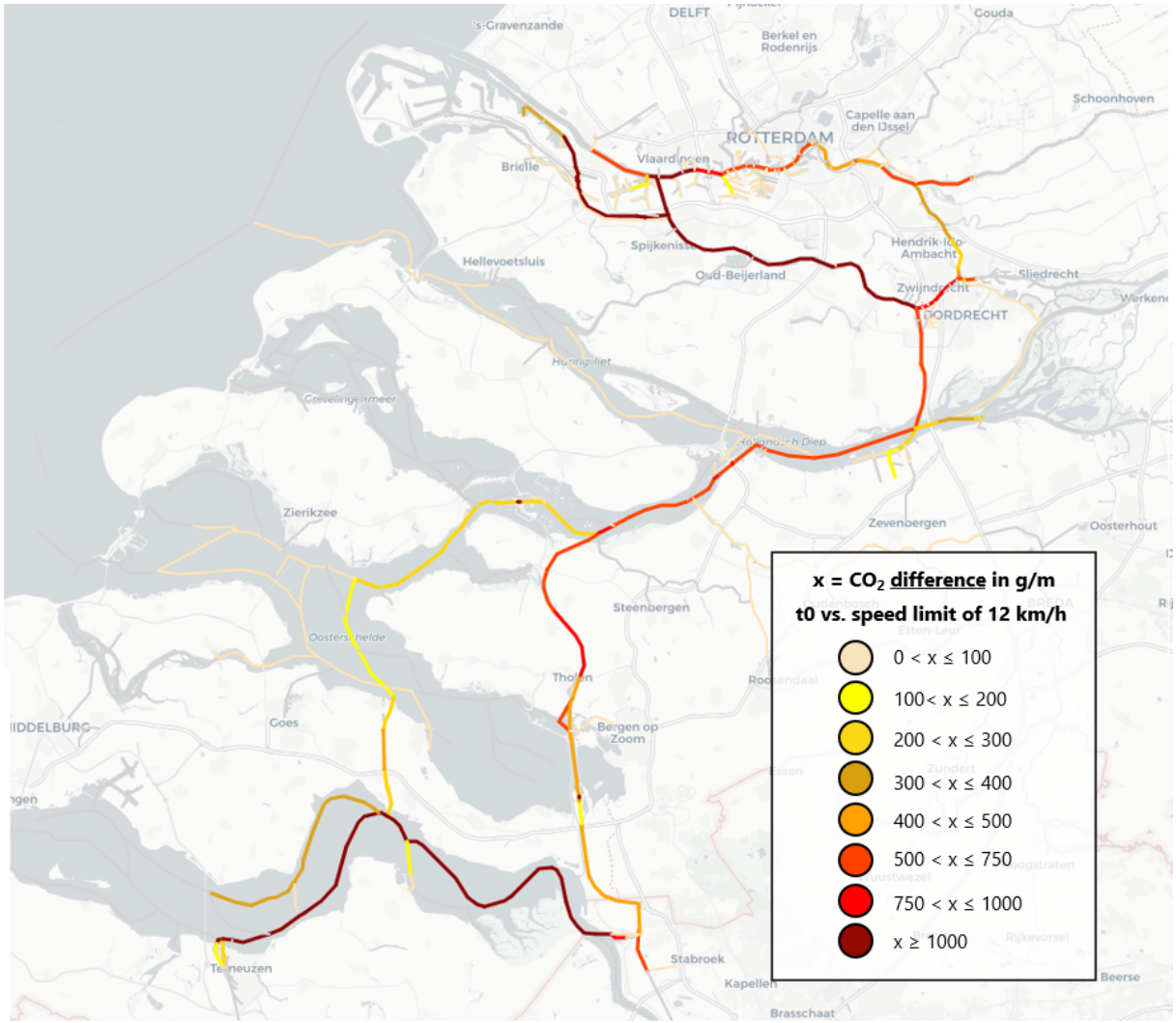

Figure 8.10: CO_2 difference map: t0 model simulation vs. speed limit of 12 km/h. Per waterway section the absolute emission reduction in g/m is specified.

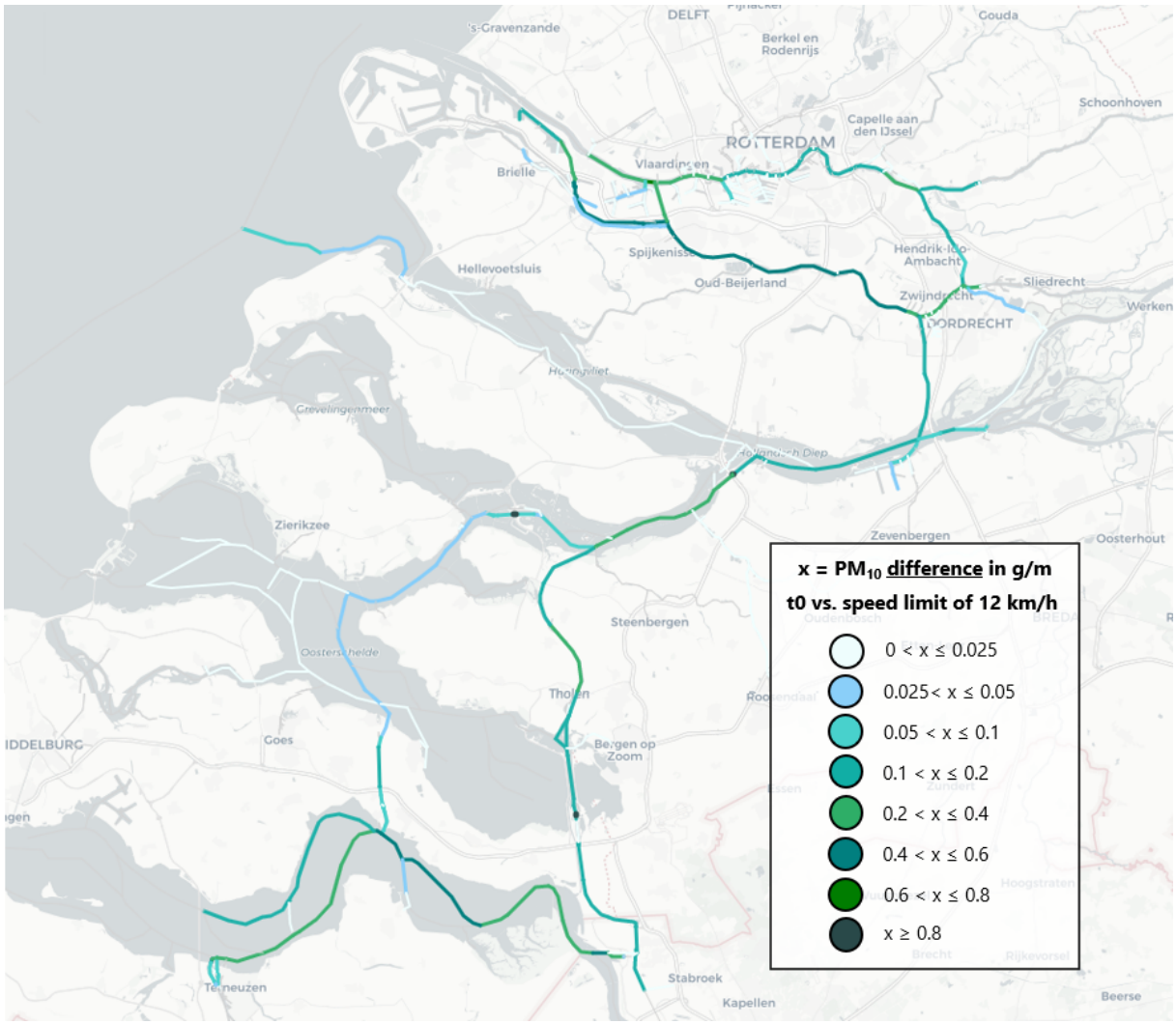

Figure 8.11: PM_{10} difference map: t0 model simulation vs. speed limit of 12 km/h. Per waterway section the absolute emission reduction in g/m is specified.

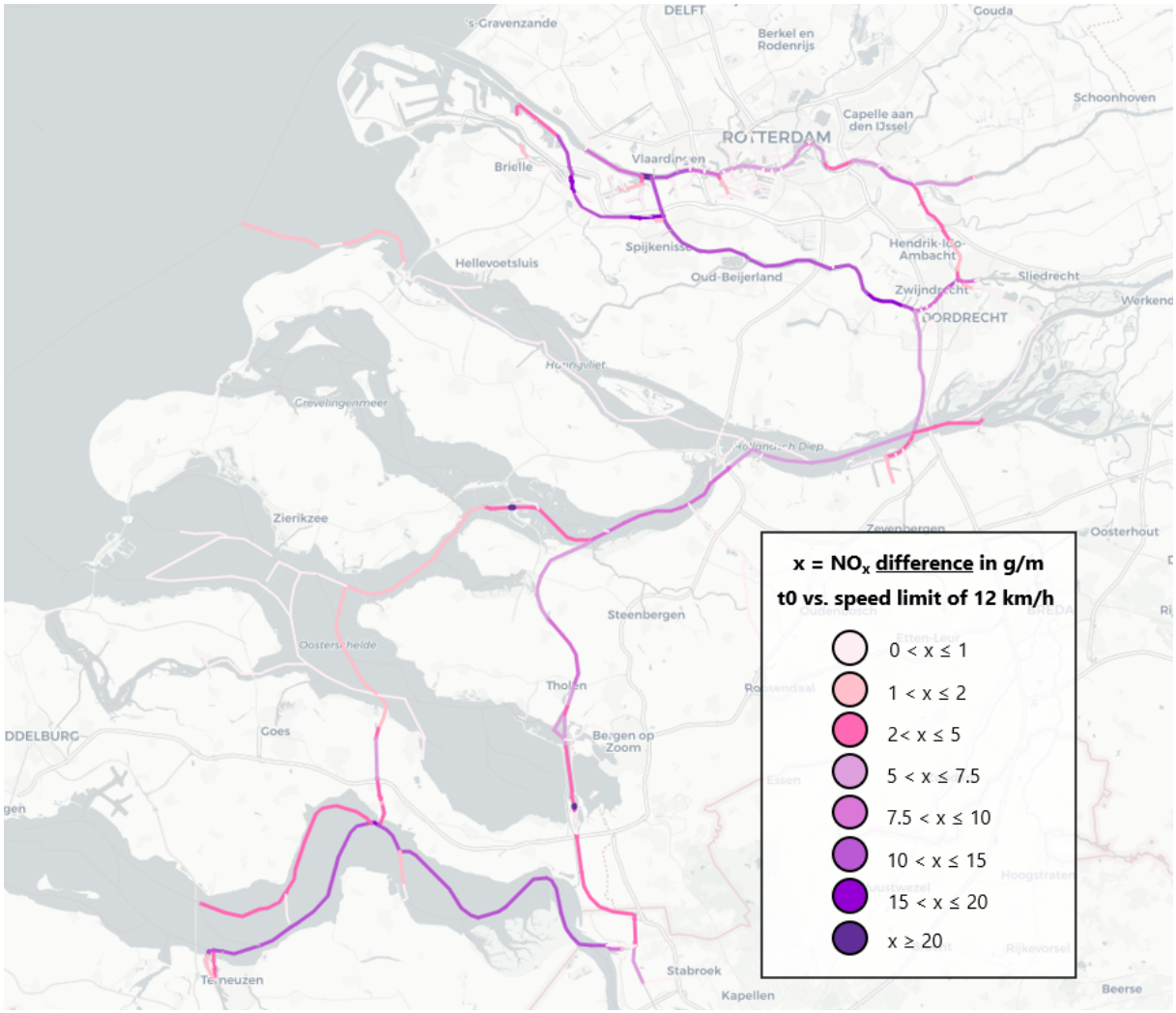

Figure 8.12: NO_x difference map: t0 model simulation vs. speed limit of 12 km/h. Per waterway section the absolute emission reduction in g/m is specified.

III

Discussion, conclusions and recommendations

9
Discussion

In this chapter, we reflect on the results of this study. The most important limitations will be addressed. For this discussion we will make the following subdivision: we start with the limitations of the developed method to estimate emissions, followed by a discussion of the AIS data limitations. Subsequently, the limitations of the model and the assessment of emission policies will be addressed.

9.1. Limitations of the method

In Chapters 3 and 4 a method was developed to estimate the energy consumption and emissions of inland shipping. By combining different literature, an algorithm was developed that is able to calculate the CO_2, PM_{10} and NO_x emissions of a single inland vessel as a function of time and space, with the ship dimensions, vessel speed and water depth as important input parameters. Estimating emissions is quite a complex problem, and therefore some assumptions had to be made.

The initial velocity of the vessel is a key parameter of the method: this velocity is the velocity relative to the water. This means that, when you are dealing with currents and you sail against the current, the velocity relative to the water is higher than the velocity relative to the ground. When sailing with the current it works the other way round. For simplicity, it has been assumed that there are no currents on the corridor, and therefore that the velocity relative to the water is equal to the velocity relative to the ground. The estimated velocity is based on spatial displacements in the AIS data, and thus represents the speed over ground. Due to unavailability of required information about currents and time limitations, it has been chosen to not take into account currents in this thesis. On a large part of the Rotterdam-Antwerp corridor, inland waterways have not much to do with currents. On those waterways the assumption of still water is quite appropriate. But there are parts that are dealing with significant currents and in some cases also tides: this mainly concerns the Western-scheldt, the Eastern-scheldt and the river Maas. This results in less reliable output of the method on these waterways.

The developed algorithm is able to take into account the effect of water depth limitations: the resistance significantly increases when a vessel enters shallow water, which translates to higher fuel consumption and emission rates. The method assumes no width restrictions of the waterway. The focus is on shallow water, since the effects from the lateral direction are in many cases much smaller than from vertical direction (Zeng et al., 2018). But there are cases where the effects of the restrictions in width could become significant: think of narrow channels, for example. In these cases, the developed method becomes less suitable and you have to take into account an increased resistance due to restrictions in water width.

Besides the additional resistance due to width restrictions of the waterway, there can also be an increase in resistance when vessels are passing each other. In such cases, less water is available along the waterway cross section where the vessels are passing, and so there is less room for the reverse flow to flow back past the ship. This causes in an increase in the resistance of both ships, but this is quite a complex problem and depends on many factors. The developed algorithm does not take this effect into account.

In addition to estimating the energy consumption and emissions of a sailing vessel, we also have considered the stationary stage (e.g. when a vessel is waiting in front of a lock). It has been assumed that the energy consumption of a vessel in a stationary stage is 15% of the energy consumption of the average propulsion stage of that same vessel, sailing on the same waterway. This assumption is based on an estimate of Hulskotte (2011), but it is a rough estimate and there is lack of literature available to come up with a more detailed estimate. In addition, there is no empirical data available to validate the output of the method in the stationary stage. In further research it would be valuable to collect empirical data of the fuel consumption of inland vessels in a stationary stage, to validate the method for emissions of vessels that are not moving, but do not turn off their

engine.

A final limitation that is important to address is the applicability of the developed algorithms. From the sensitivity analysis resulted that the method is applicable for block coefficients of 0.85 or lower. Inland vessels such as barges are very block-shaped and can sometimes have a higher block coefficient than 0.85, which would result in higher resistance. However, the current algorithm, gives excessive results when using higher block coefficients. Additionally, the algorithm becomes also less reliable when we consider very large vessels with relatively small drafts. In these cases, the wave resistance component creates outliers in the output. It has therefore been decided to assign a greater draft than the minimum draft to large unloaded ships, in order to avoid excessive values. These limitations in applicability of the algorithms are important to consider and can possibly be improved in future research.

9.2. Limitations of the AIS data

Rijkswaterstaat provided an AIS dataset of the fleet on the Rotterdam-Antwerp corridor. We applied the developed algorithms to the AIS time series, to calculate the potential emission of a ship per timestamp. AIS is an accurate way of logging information in shipping, but is also has its limitations.

An important limitation of AIS is that information is regularly missing in the data. For example, some of the AIS data is missing information about the length or width of a ship. When the length or the width was given, we made an estimation of the missing variable making use of the Richtlijnen vaarwegen (Koedijk, 2020). But when the information of both the length and the width is lacking, you do not have enough information to estimate the dimensions of the ship. Since the dimensions are input of the developed algorithms to estimate potential emissions of inland vessels, we cannot do anything with this data. For that reason, this data has been filtered out from the dataset. This comprised around 6-7 percent of the data.

Information about the draft in the AIS data is in many cases inaccurate or incomplete. For almost half of the raw data, no draft is available or the draft is equal to 0. Considering the available data, there are many uncertainties: the data is manually filled in by the skipper and contains errors. Of the part of the data that does contain information about the draft and is not equal to zero, almost 30% considers draft data that is lower than the minimum draft specified for the considered vessel class. Almost 26% contains greater drafts than maximum drafts at loading rates of 85%. Therefore, it has been decided to not use the draft information from the AIS dataset, but develop a method to estimate the draft data. This estimate is based on the drafts specified per vessel class, and the average loading rates. This is a limitation of this study, since it is quite a rough estimate of the draft distributions. For further research it would be valuable to include more detailed information about the draft of ships in the AIS data.

The parameter VesseltypeERI in the AIS dataset provides information about which type of vessel we are considering. But for a large part of the ships in the data, the vessel type is unknown. For that reason we classified the ships based on the RWS vessel type classification: an estimation of the vessel class was performed based on the ship dimensions. The small M0 motor vessels were filtered out of the dataset: this is small shipping and we assumed that most of these vessels are recreational vessels, which are not within the scope of this research. Due to lack of information about the vessel types, this is a rough assumption and therefore a limitation of this study.

Besides the missing data, the data also contains in some cases outliers considering the velocity of the vessels. The velocity is computed based on the travelled distance and the corresponding time. But sometimes the log of the geographical position contains some errors. When a geographic location is logged that is further away than where the ship actually is, the distance traveled appears to be a lot longer and this causes an error in the speed. Therefore, outliers in the velocity (> 8 m/s) are filtered out of the dataset, to avoid outliers in the energy consumption and emission output. But it is important to consider this results in less useful data, which is a limitation.

9.3. Limitations of the model

Besides using AIS data to map emissions of inland shipping, a model was developed to simulate the fleet and the potential emissions. The main goal of building a model was that it can be used as a tool to support development and evaluation of emission reduction policies. The model is a simplification of reality, and we had to make various assumptions for the model development.

An origin-destination (OD) matrix was created from AIS data, of the vessels sailing along the Rotterdam-Antwerp

corridor during one day. This OD matrix served as input for the model, describing the vessel characteristics. AIS data contains a lot of information about velocity variations, but simulating this in the model is quite complex. For simplicity, we computed an average velocity of each ship trajectory in the OD matrix. This results in a constant vessel speed per vessel in the model simulation, which is an limitation of the model. In reality, vessels will for example slow down in limited water or when approaching a lock, and will increase their vessel speed at wide fairways with deep water. This has a relation to the resistance and so the energy consumption and emissions, which is not incorporated in the model. In the model only a reduction of the vessel speed has been taken into account if the underkeel clearance of a vessel becomes quite small, which avoids outliers in the required energy when a vessel is sailing with a relatively high average speed through shallow water. In order to map the distribution of emissions along an inland waterway network even better, it is valuable to implement velocity variations in the model in further research.

The OD-matrix describes the start point, end point and possible intermediate route points of a ship trajectory. This way, the shortest path along the network could be determined making use of the Dijkstra shortest path algorithm. Although this is a reasonably good method for guiding vessels from the AIS data to the correct route, it is not able to simulate all the route details that are described by AIS data. It therefore does not provide 100% certainty that the simulated ship is sailing exactly the same route as the ship from the observed AIS data, which is a limitation of the model.

The model makes use of the Python package OpenTNSim, which stands for Open source Transport Network Simulation. This package is used to simulate inland water transport along a fairway network. The package contains an element that simulates the locking process: you can implement a lock element on a fairway network and specify the number of lock chambers and the average passing time of the lock. But at the moment, the capacities of this simulation element is limited: a single lock element can only allow one ship to pass at a time. This is why it has been decided to implement more lock elements on the network than there are in reality. This way, excessive waiting times in the model simulation are avoided. In further research it would be valuable to have a more accurate simulation of the lock elements in the model.

The modelled fleet is projected onto the FIS (Fairway Information Services) network, just like the AIS 't0 emission scenario'. The FIS network provides information about the geometry of the inland waterway network, and information about fairway properties. The water depth is an important input variable of the developed method to estimate emissions. To map the water depth variation across the FIS network, the difference between the bathymetry and water level has been computed per waterway section. The bathymetry was recently connected to the FIS network, but this information was still under development and therefore not complete. The water level was obtained by ourselves, using several measuring locations of the water level from an online source. Although mapping the water depth based on the bathymetry and these water levels is a proper first estimate, there is room for improvement because assumptions had to be made for missing data.

To validate the output of the model, we made use of practical data about the fuel consumption of different vessel types, sailing with a certain speed. We compared this data with the fuel consumption of the same ship with the same speed, simulated in the model. The model output appeared to correspond quite well with the practical data. We assumed this model validation as sufficient. But there is lack of data available to validate the emission output: the actual emission is quite complex and depends on many factors. This makes it impossible to validate the emission output in a proper way. The emission output of this study gives an indication of where high emission levels are located, but the absolute numbers resulting from the model contain uncertainties, which is a limitation of the model.

9.4. Limitations of assessment of emission policies

The goal of the model development was to create a tool that supports the development and evaluation of alternative measures to reduce emissions. We assessed the effectiveness of different policies, but this considers a very first investigation of these measures. The main objective of this research was to provide a suitable method to map emission patterns on a inland waterway network, and ensure this method provides tools to assess alternative measures to reduce emissions. But more research is needed to provide full insight into the effectiveness of packages of measures.

This can be explained by means of one of the assessed policies: a speed limit of 12 km/h. For all vessels in the model simulation, having a higher average speed than 12 km/h, their average speed was set to 12 km/h. Since the model is working with average speeds, this is a limitation of this assessment: the ships with an average speed lower than the speed limit are not affected by the policy. But in reality, their speed varies over time,

and on some locations on the corridor, their speed will above the speed limit. This could not be taken into account in the assessment. In addition, implementing a speed limit in practise is much more complex. Commercial skippers have to deal with sailing schedules and time slots at ports. More research is required into the applicability and effectiveness of such a measure.

10
Conclusions

In this chapter, we summarize the results of this research, taken into account the limitations discussed in Chapter 9. We look back on the research questions defined in Chapter 1 and will address how these questions are answered by this study.

We formulated four sub-questions that we wanted to answer when defining the main objectives of this thesis. These four questions will be addressed, to draw the most important conclusions resulting from this research.

"Sub-question 1. How to methodologically estimate the energy consumption and emission potential of an individual inland vessel as a function of time and space?"
By means of literature study, a detailed bottom-up method was developed to estimate the energy consumption and potential emission of a single inland ship, as a function of time and space. This bottom-up method starts with estimating the resistance a ship experiences. The resistance was subdivided into different components, based on literature of Holtrop and GGJ Mennen (1978): frictional, viscous, appendage, wave and residual resistance. The method of Holtrop and Mennen estimates the resistance based on the ship dimensions and the vessel speed.

We did not only want to account for the vessel characteristics in this bottom up method, but also for the fairway characteristics: think of currents, shallow water or width restrictions of the waterway. It was decided to focus on water depth limitations only: due to time limitations and no available data about currents along the corridor, it was decided to neglect currents and assume still water on the corridor. For a large part of the Rotterdam-Antwerp corridor the assumption of no currents is reasonable. Effects from width restrictions are in many cases much smaller than from vertical direction, so therefore only the water depth has been taken into account. Based on literature of Zeng et al. (2018), a modification was applied to the frictional resistance term to account for shallow water effects. In addition, the Karpov method was implemented to account for the shallow water effect on the wave resistance and residual resistance terms.

The resistance (kN) can be translated to total power (kW), by multiplying it with the vessel speed and taking into account several efficiencies. The total required energy (kWh) can be computed by multiplying the calculated required power with the time period (in hours) that a vessel is sailing.

For the translation from energy to potential emissions, we made use of so called emission factors, expressed in gram per kWh. The emission factors of CO_2, particulate matter (PM_{10}) and nitrogen oxides (NO_x) were determined based on literature of TNO (Ligterink, 2019). The age of the engine and partial engine load play an important role in this.

By combining all the literature, algorithms were developed that estimate the energy consumption and potential emissions of a single inland vessel, as a function of time and space. These algorithms require the ship dimensions, vessel speed, water depth and engine age as main input variables. The method is applied to a reference vessel and some conclusions can be drawn from the output. At first, the output of the algorithm shows that larger ship dimensions result in higher resistance and so in higher emissions. Second, older engines result in much more emissions of environmental pollutants compared to the newest engines: considering a M9 vessel, for example, the emission of particulate matter is 95% smaller for an engine from the year 2020, compared to an engine from the year 2000. For nitrogen oxides this is 52.4%. Besides the ship dimensions and the engine age, the vessel speed has a lot of influence: when a vessel increases it speed, the energy consumption and emissions increase exponentially. In shallow water, the critical velocity is reached earlier, and the energy consumption shows asymptotically behaviour when approaching the critical velocity. Finally, the method has been validated by means of a reference figure of the power output, obtained from the thesis of Hekkenberg (2013): in deep water the output almost completely matches. In shallow water there is a lot of uncertainty,

but the behaviour of the power output of the developed algorithms and the reference of Hekkenberg (2013) is similar.

''Sub-question 2. Can we apply this method on observed AIS data and to what extent can we derive an estimate of emission patterns based the observed fleet (t0 emission scenario)?"
The developed algorithms estimate the energy consumption and potential emission of a single inland ship, as a function of time and space. Therefore these algorithms are suitable to apply to an observed AIS time series.

The AIS (Automatic Identification System) data describes the route of each individual vessel in the fleet over time. In addition, it provides information about the vessel dimensions and vessel type. Besides these vessel characteristics, the sailing speed of the vessel can also be computed per ship per timestamp: the travelled distance between two timestamps (Δx) can be computed (based on the geographical information), as well as the time period between two timestamps (Δt). The velocity, V_0, equals Δx / Δt.

In short, the AIS dataset provides us the input parameters about the vessel characteristics and velocity, needed for the calculation methods. In addition, it provides the resolution in time and space of each individual vessel in the fleet. But the developed algorithms do not only account for vessel characteristics and speed, but also for the limitations in water depth. To incorporate fairway properties in the method, the AIS data is connected to the FIS (Fairway Information Services) network. FIS is an only source, containing actual information about the geometry of the fairway and its properties. This information can be loaded in the form of a graph. This graph is a collection of nodes, connected by edges: the edges represent parts of waterways. By connecting the AIS data to FIS, the fairway properties can be taken into account as input of the developed algorithms to estimate emissions, and it gives us the possibility to quantify the output on the fairway network.

Combining this information, the developed algorithms can be applied to the AIS data. Per ship, per timestamp, the information about the vessel characteristics, speed and the fairway information of the waterway section where the ship is currently sailing, is specified. This is input of the algorithm, which results in the energy consumption (in kWh) and potential emissions (in g) per ship, per timestamp. These calculations are performed for the entire fleet. Due to the connection to the FIS network, the emissions can be summed up on each edge of the waterway network. By dividing the total emission by the length of the edge, the potential emission levels can be quantified along the inland waterway network, expressed in gram per meter. The potential emission patterns were subsequently visualized on the corridor, and the emission hotspots could be identified. This output was called the 't0 emission scenario'. The output of the 't0 emission scenario' shows high emission levels around locks and in port regions: these are locations where ships are stationary for a longer period. Ships are slowing down and/or have to wait in these areas, but when the waiting time is limited, they will not turn off the engine. This results in accumulation of emission.

The 't0 emission scenario' shows that observed AIS data is suitable for applying the developed method, in order to derive emission patterns of an inland shipping fleet as a function of time and space, and visualize this on an inland waterway network. The output clearly shows variations in emission levels: AIS data provides detailed information about the resolution in time and space of single vessels, and so about the velocity variation of a ship. By connecting the AIS data to the FIS network, fairway properties could be taken into account and the FIS graph provided tool to quantify and visualize the potential emissions on the network.

''Sub-question 3. Can we apply this method on simulated data and to what extent can we reproduce the AIS-based t0 emission scenario? What explains the differences between the two outcomes, if any?"
By making use of AIS data, we were able to give insight in the current potential emission distributions of inland shipping along the Rotterdam-Antwerp corridor. But in the context of reducing emissions, there is also demand for getting insight into the impact of alternative emission reduction policies. To use the developed method for this objective, a model has been developed. The aim was to have this model reproduce the 't0 emission scenario' resulting from the AIS data (addressed in this sub-question), and subsequently assess alternative scenario's (addressed in Sub-question 4).

To simulate the fleet on the Rotterdam-Antwerp corridor in a proper way, input was required considering the vessel characteristics, as well as the fairway properties. To define the characteristics of the vessels in the fleet, we made use of an origin-destination (OD) matrix, obtained from the AIS dataset. In this OD matrix, each ship trajectory in the AIS dataset of one day was determined. For each ship, the ship dimensions, the start and end point of the route of the ship, intermediate route points, the time the vessel starts to sail and the average vessel speed of the route were specified. To take into account the fairway properties, the simulation has been linked to the same FIS network as used in the AIS 't0 emission scenario', describing the geometry and the water depth variations of the inland waterway network. Lock simulation elements were implemented in the FIS network at

the main lock locations on the corridor, to simulate lock passages in the model.

Combining the information of the OD-matrix and the FIS network, the model simulation could be performed. This resulted in a simulated time series of one day of the fleet on the Rotterdam-Antwerp corridor. The developed algorithms to estimate the energy consumption and potential emission of a single ship, could subsequently be applied to the simulated time series, in the same way as the algorithms were applied to the observed AIS time series. For each ship, for each time step, on a certain geographical location, the energy consumption and potential emissions were computed. These emissions could be assigned to the edge of the FIS network were the ship is sailing at that moment. By summing up the emissions on each edge of the fairway network, the potential emission distributions resulting from the model simulation could be visualized on the inland waterway network. This output is the simulated 't0 emission scenario'.

Now is the question if the model is able to reproduce the 't0 emission scenario' resulted from AIS data: therefore the model simulation output has been compared to the AIS t0 case. The total output (total required power and potential emissions of the whole fleet of one day) of the model deviates just 0.3% - 3.8% from the AIS 't0 case'. Besides the total output, we have analyzed and compared the emission distribution of the model simulation versus the AIS 't0 emission scenario': a difference map was created, to show the absolute percentage difference of each edge along the FIS network. On the main waterways of the corridor (Nieuwe Maas, Oude Maas, Dortsche Kil, Hollands Diep, Zuid-Beveland route, Scheldt-Rhine canal), the absolute percentage difference of the potential emission distribution between AIS and model output lies between 0 and 20 percent. In regions around locks and in ports, the distribution of emissions over the network is less consistent when comparing the AIS output to the model output. This can mainly be explained by the fact that the 't0 emission scenario' resulting from AIS data contains detailed information about velocity variation and the geographical position of a ship as a function of time. Because of this, the spreading of emission can be projected quite well. The model works with constant speeds, and when vessels are stationary (at locks), the emissions are assigned to one single edge, instead of mapping the spreading. This is the reason why the emission distributions of the AIS t0 output and the model output do not match so well in lock and harbor areas. Summarizing, we can conclude that the model reproduces almost the same total output as the 't0 emission scenario', and that the emission distribution on the main waterways shows deviations from 0 to 20%, with outliers at locations where ships are regularly stationary.

''Sub-question 4. Can we subsequently apply the developed algorithm to simulate alternative emission reduction policies and evaluate the effectiveness of different measures?''
The model is able to reproduce the 't0 emission scenario', by making use of the developed algorithms. Subsequently, the model can be used to simulate alternative scenarios, to perform a very first assessment of different emission reduction policies. Alternative measures can be implemented by making adjustments to the input of the model (for example the OD-matrix) or by post-processing the output of the model.

At first, the emissions at locks were addressed. From the 't0 emission scenario' resulted high potential emission levels around locks. Especially considering environmental pollutants such as particulate matter and nitrogen oxides, the local effect is of importance for the environment. Therefore, first the emission rates of different types of vessels at locks were computed, to indicate how much is emitted by a single vessel in terms of grams per hour. Subsequently, a model simulation has been performed to assess the effectiveness of a 'zero emission policy' at locks, where skippers are for example required to sail on batteries in lock areas, or have to connect to shore power. The simulation showed that the local effect of this policy is significant (the emission hotspots around locks disappear), but considering the total emissions, it only leads to a reduction of a few percent.

The second policy assessed was fleet renewal. Newer engines are significantly cleaner and therefore fleet renewal can contribute to the transition towards more sustainable inland shipping. The current distribution of engine ages of the fleet was based on a Weibull function developed by TNO. To implement the fleet renewal policy in the model, this engine age distribution has been manipulated: all ships with an engine age from the year 2007 or older (CCR1 or older), have been replaced by the newest Stage V engines from 2020. The simulation output of this scenario has been compared with the 't0 emission scenario', and the following conclusions could be drawn: the effect on CO_2 emissions is limited (5% reduction), but the effect of on the environmental pollutants PM_{10} and NO_x is significant: the potential emission reduction of PM_{10} is 67%. For NO_x the potential reduction is 33%.

The final policy assessed is a speed limit. The sailing speed of inland vessels is one of the most determining factors in the energy consumption and emission calculations, since the relationship between speed and required power is exponential. A speed limit of 12 and 13 km/h was implemented in the model. It has to be noted that

this is a very first assessment of a speed limit: reality is much more complex, and since the model works with average vessel speeds, this is a limitation of the assessment. A speed limit of 12 km/h resulted in a potential CO_2, PM_{10} and NO_x emission reduction of 27%, 19% and 24% respectively. For a less strict speed limit of 13 km/h, this was 22%, 17% and 20% respectively. These results shows that a speed limit can certainly be effective, but more research is needed to assess the feasibility in practice.

To conclude, the developed method can be used to perform model simulations of different alternative scenarios to assess emission reduction policies. The three measures that were assessed in this research serve as an example of what tools the current model provides to use it in support and development of emission policy. Further research is needed for in-depth assessment of the effectiveness of such policy measures in inland navigation.

By answering the four sub-questions, the main research question of this study could be answered:

''How to develop a method that can map the CO_2, NO_x and PM_{10} emission potentials of inland shipping on an inland waterway network as a function of time and space, which can be used in support of the development and evaluation of emission policies?"

By combining different literature, a bottom-up method was developed that estimates the potential CO_2, NO_x and PM_{10} emissions of a single inland vessel as a function of time and space, taking into account the ship dimensions, vessel speed, water depth and engine age as main input parameters. By making use of AIS data to describe the fleet, and incorporating fairway properties loaded from Fairway Information Services (FIS), the developed method could can be applied and the potential emissions of a fleet can be computed and visualized on an inland waterway network ('t0 emission scenario'). A model has been developed that is able to reproduce the 't0 emission scenario', and provides a tool to simulate alternative emission reduction measures and assess the effectiveness of future policies.

11

Recommendations

Based on the limitations discussed in Chapter 9, a number of recommendations can be made for further research, which will be addressed in this chapter.

Implement velocity variations in the model
The AIS data contains detailed information about the velocity variations of inland vessels, but the developed model works with an average speed per ship trajectory. This is a limitation of the model, and it is recommended to implement velocity variations in the model in further research. In this research, a python code was already developed by van der Werff (2021) that connects the AIS data to the FIS network. This connection already provides a possibility to get insight into the average velocity per edge. A next possible step is to calculate the average speed per ship per edge. When you incorporate this information in the OD matrix, which is used as input for the model, you can describe the route of each vessel by means of a sequence of edges, with an average speed at each edge. Since the speed has a lot of influence on the energy and potential emission, implementing this velocity variation improves the mapping of the emission distribution over the network.

Take into account the effects of currents
In the development of the algorithm, the assumption was made that there are no currents along the fairway network. The velocity relative to water, which is input of the calculation method, is therefore assumed to be equal to the velocity relative to the ground. But in reality, there are currents along an inland waterway network. At some waterway sections, the effects of currents can be significant, and therefore it is recommended for further research to take into account currents. When information is available about the actual currents along the inland waterway network, this can be implemented in the FIS network. When the current per edge is quantified on the graph, you can calculate the speed relative to water at each edge, which can then be used as input in the developed algorithms.

Use IVS-next data to incorporate reliable draft data
The AIS data contains inaccurate and incomplete information about the drafts of the vessels in the fleet. Therefore, we neglected this information and we made rough assumptions based on the vessel class and average loading rates. For follow-up research, it is recommended to better map the draft of inland vessels. It is recommended to use IVS-next data for this. In the IVS-next system, the skipper registers its ship and cargo data at the start of the trip. It provides accurate information about the draft of a ship. This way, you can for example get insight into the draft distribution of all ships passing a certain lock. By linking this information to the AIS data, containing all other relevant information of the fleet, this really improves the input of the calculations to estimate emissions.

Collect empirical data of the energy consumption of stationary vessels
We have made a rough assumption regarding to the energy consumption of ships in a stationary stage (e.g. when ships are waiting at a lock or a harbor area), based on an estimation of Hulskotte (2009). Due to a lack of available data on the energy consumption of stationary ships, we have not been able to further validate this assumption. Because the high emission levels around locks and in port areas are mainly caused by stationary ships that do not turn off their engine, it is important to gain more insight into the emissions of stationary ships. Therefore it is recommended to collect empirical data of the energy consumption of stationary ships, for different types of vessels and different engine ages, and subsequently improve the assumptions.

Further development of the algorithms: distinguish between different vessel types
The developed algorithms to estimate the energy consumption and potential emissions of a single inland vessel, are now used for all different vessel types. The method does not distinguish between motor vessels, barges or convoys. In reality, these ships types differ from each other. Barges are for example much more block shaped

and lie deep in the water, which could result in different resistance curves compared to a general motor vessel. The developed algorithm takes into account the draft, and the shape of the ship is taken into account by means of the block coefficient. But a limitation of the method is that it is applicable when the block coefficient is smaller than 0.85. It is recommended for future research to perform an additional literature study, to look into the possibility to distinguish the method of estimating emissions between different types of vessels. It might be also interesting to see if the algorithms can be adapted so that it can be used for higher block coefficients, which might give a better estimate for more block shaped vessels.

Describing the exact routes of ship trajectories
The developed model uses an OD-matrix resulting from AIS data as input. The OD-matrix describes the start point (origin), end point (destination) and possible in between points of the route a vessel is sailing. Based on this information, the Dijkstra algorithm computes the shortest path. But this approach does not provide 1-to-1 route simulation of the ship. To determine the exact route in the model with 100% certainty, it is recommended for feature research to use the Python code that has been developed to project the AIS data onto the FIS network graph, to compute the exact path of the ship. The code already defines per ship trajectory, on which sequence of edges the ship is sailing. When computing the path (so the sequence of these edges) for each ship trajectory, and implementing this in the OD-matrix, you do not require the Dijkstra algorithm to estimate the path, because it already has been defined in detail. This would improve the simulation of traffic intensities along the inland waterway network.

List of Figures

List of Tables

Appendices

A

Appendix A: Method comparison

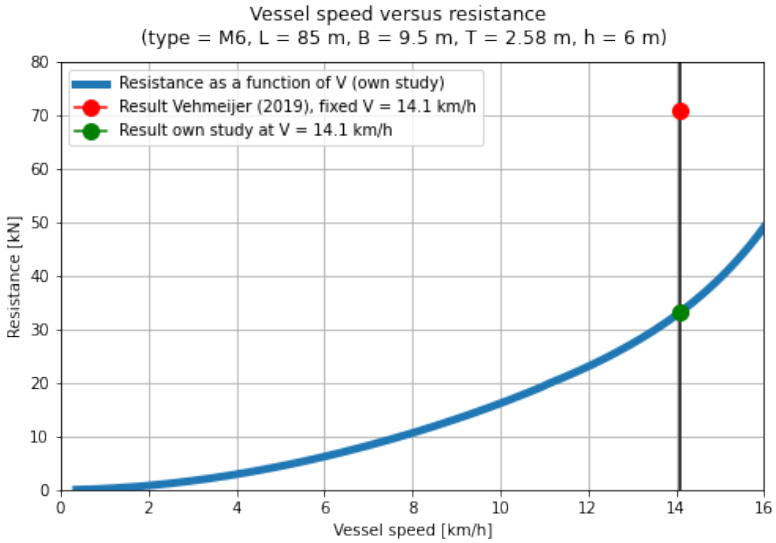

Figure A.1: Comparison of resistance output of a M6 motor vessel: the method of Vehmeijer (2019) compared to the algorithm developed in this study

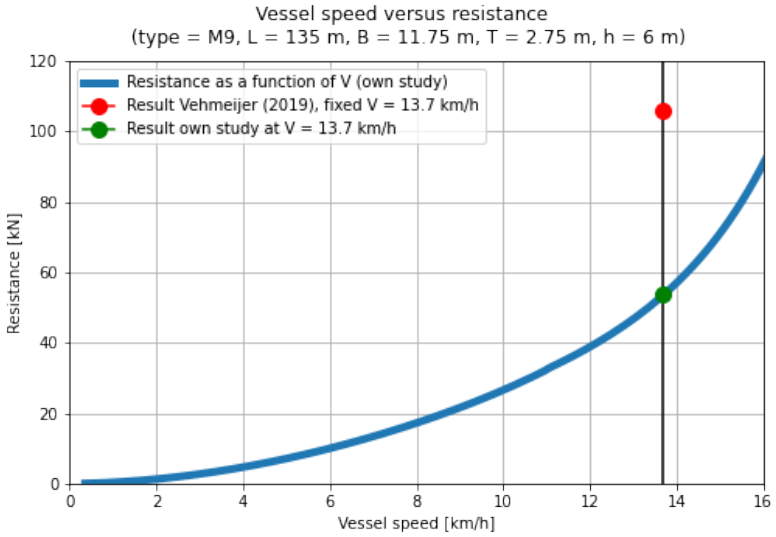

Figure A.2: Comparison of resistance output of a M9 motor vessel: the method of Vehmeijer (2019) compared to the algorithm developed in this study

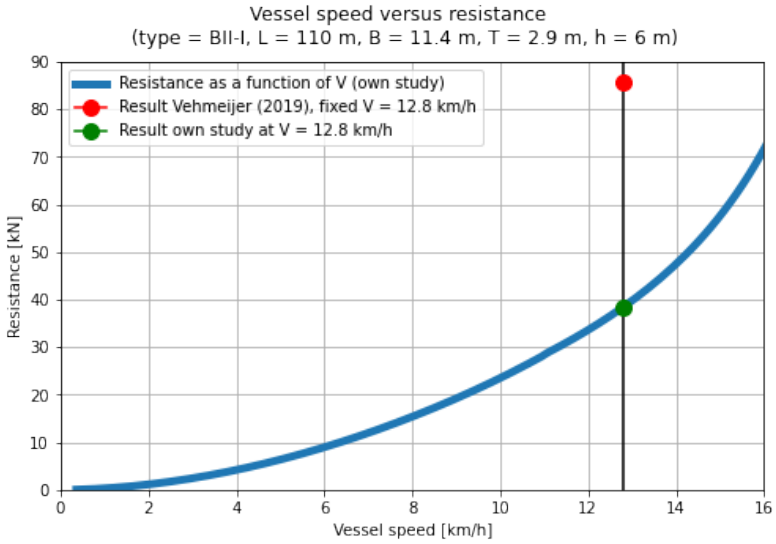

Figure A.3: Comparison of resistance output of a BII-1 barge: the method of Vehmeijer (2019) compared to the algorithm developed in this study

B

Appendix B: Karpov approximation curves

In the following figures the Karpov approximation curves are visualized for different h/T ratios: on the x-axis of these graphs the depth Froude number is presented, on the y-axis the α_{**} value, which is applied to the initial sailing speed V_0. This velocity correction is applied to take into account the asymptotic effect on the resistance when entering shallow water.

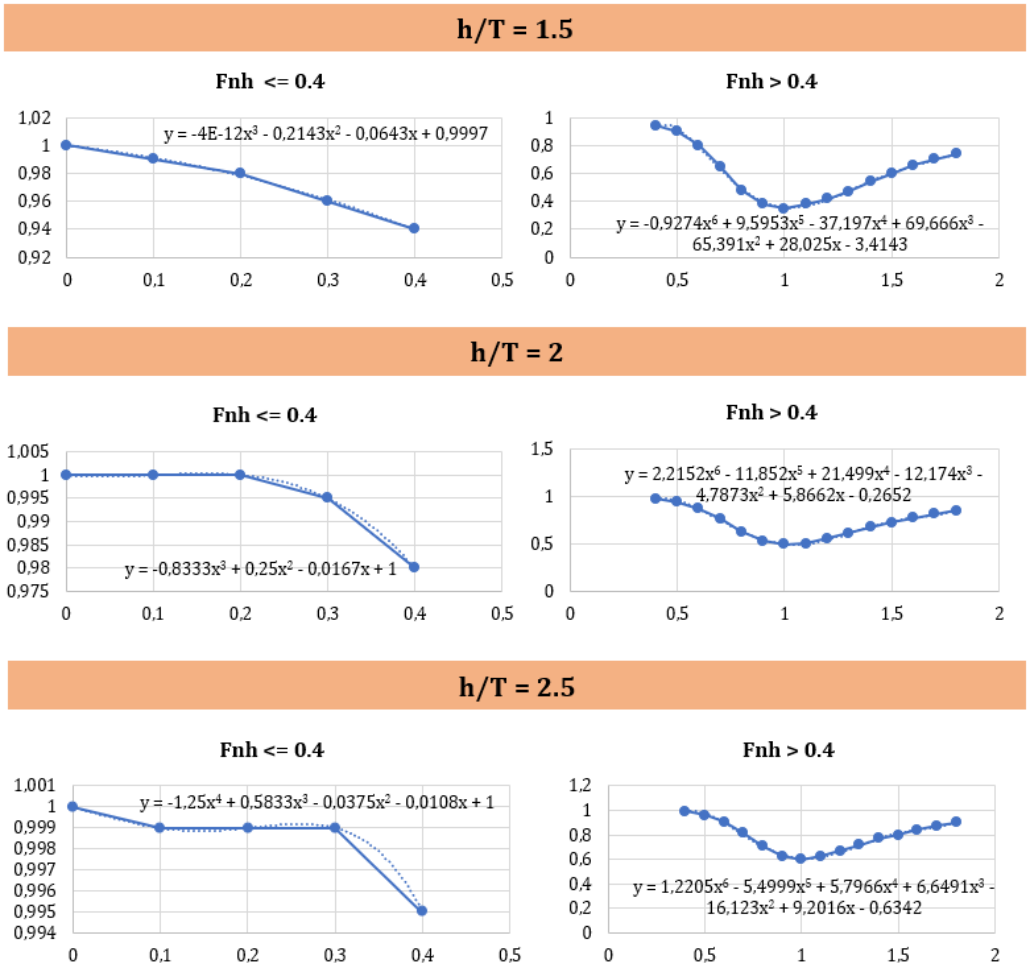

h/T = 3

Fnh <= 0.4 $\alpha_{**} = 1$

Fnh > 0.4

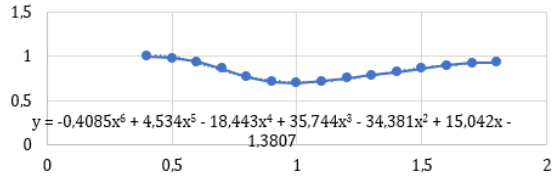

h/T = 3.5

Fnh <= 0.4 $\alpha_{**} = 1$

Fnh > 0.4

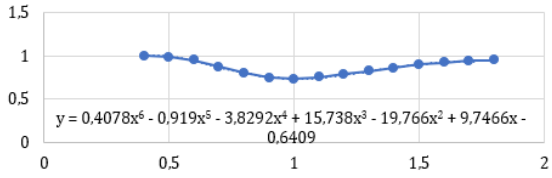

h/T = 4

Fnh <= 0.4 $\alpha_{**} = 1$

Fnh > 0.4

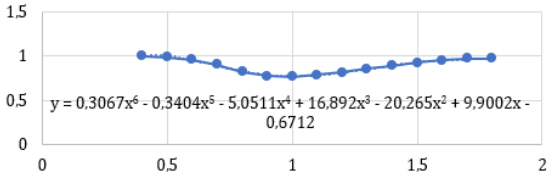

h/T = 5

Fnh <= 0.4 $\alpha_{**} = 1$

Fnh > 0.4

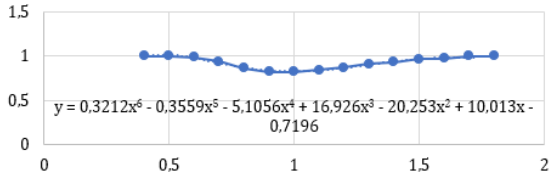

h/T = 6

Fnh <= 0.4 $\alpha_{**} = 1$

Fnh > 0.4

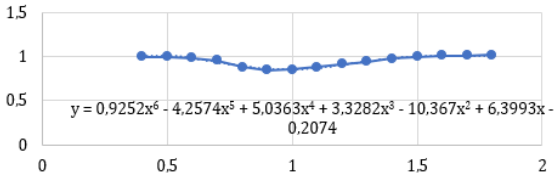

h/T = 7

Fnh <= 0.4 $\alpha_{**} = 1$

Fnh > 0.4

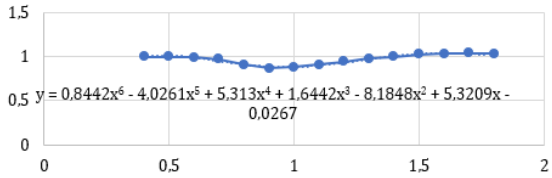

h/T = 8

Fnh <= 0.4 $\alpha_{**} = 1$

Fnh > 0.4

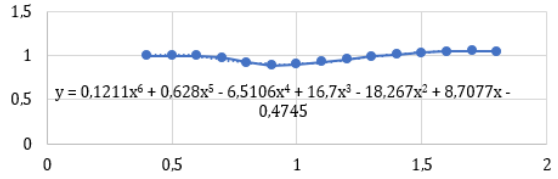

h/T = 9

Fnh <= 0.6 $\alpha_{**} = 1$

Fnh > 0.6

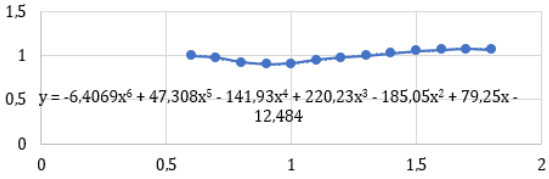

h/T = 10

Fnh <= 0.6 $\alpha_{**} = 1$

Fnh > 0.6

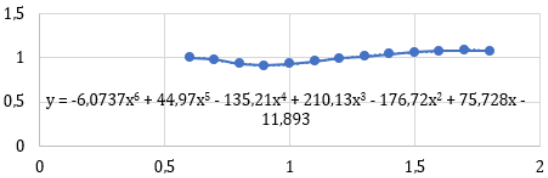

C

Appendix C: Algorithms

C.1. Hull efficiency

In a literature review of van Terwisga (1989) an empirical method of Papmel is described to determine the wake fraction. The expressions can be found in this section.

$$w = 0,11\frac{0,16}{x}C_B\sqrt{\Delta^{1/3}/D_s} - \Delta w \tag{C.1}$$

The water displacement Δ can be determined using the block coefficient:

$$\Delta = C_B * L * B * T \tag{C.2}$$

A first estimation of the screw diameter D_s can be made using a rule of thumb. For single screw ships 0.7-0.8T is common. For double screw ships this is 0.6-0.7T. In this case 0.7T is assumed (van Terwisga, 1989).

Δw is the velocity correction coefficient. This can be determined by knowing the Froude number:

$$F_n = \frac{V_0}{\sqrt{gL}} \tag{C.3}$$

In which:
F_n = Froude number [-]
V_0 = vessel speed [m/s]
L = vessel length [m]

If the Froude number is smaller than 0.2, then Δw is equal to zero. In the case that the Froude number is larger then 0.2, Δw becomes 0.1. In general, the Froude number will be smaller than 0.2 for inland shipping, so the velocity correction coefficient is negligible in that case.

With this information, the wake fraction (w) can be determined according the Formula C.1 of van Terwisga (1989). The thrust deduction factor (t) is determined by the wake fraction and the number of screws:

In case of a single screw vessel:

$$t = 0,6w(1 + 0,67w) \tag{C.4}$$

In case of a double screw vessel:

$$t = 0,8w(1 + 0,25w) \tag{C.5}$$

In which:
x = number of screws [-]
C_B = block coefficient[-]
Δ = the water displacement [m^3]

D_s = diameter of the screw [m]
Δw = velocity correction coefficient [-]

C.2. Wave resistance

For estimating the wave resistance, a distinction is made between different ranges of Froude numbers. The Froude number used in these calculations is based on the corrected velocity V_2, which takes into account the effect of shallow water, as explained in Section 3.2.4.

$$F_{n,V_2} = \frac{V_2}{\sqrt{gL}} \tag{C.6}$$

The following wave resistance calculation methods are based on the Holtrop and Mennen method, discussed in literature from Sarris (2003).

Wave resistance in case F_{n,V_2} < 0.4
When the Froude number is lower than 0.4, the wave resistance is determined according to the following expression:

$$R_{W1} = c_1 c_2 c_5 \Delta \rho g e^{\left(m_1 F_{n,V_2}^{-0.9} + m_4 cos(\lambda F_{n,V_2}^{-2})\right)} \tag{C.7}$$

In which:
R_{W1} = wave resistance ($F_n < 0.4$) [N]
$c_{1,2,5}$ = coefficients [-]
Δ = water displacement [m^3]
F_{n,V_2} = Froude number, based on V_2 [-]
m_1, m_4 = coefficients [-]
λ = wave-making length [−]

The water displacement Δ can be calculated according to Formula C.2.

Coefficient c_1 can be determined according to:

$$c_1 = 2223105 c_7^{3.78613} \frac{T}{B}^{1.07961} (90 - i_E)^{1.37165} \tag{C.8}$$

In which i_E is the half angle of entrance in degrees, which represents the angle of the waterline at the bow. It can be estimated by the following formula:

$$i_E = 1 + 89 exp\left(-\left(\frac{L}{B}\right)^{0.80856} (1 - C_{wp})^{0.30484} (1 - C_p - 0.225 lcb)^{0.6367} \left(\frac{L_R}{B}\right)^{0.34574} \left(\frac{100\Delta}{L^2}\right)^{0.16302}\right) \tag{C.9}$$

In which C_{wp} is the waterplane coefficient, which can be determined according to Formula 3.12. The longitudinal position of the centre of buoyance (lcb) can be determined with Formula 3.25 and the length of the run (L_R) with Formula 3.24.

The coefficient c_7 depends on the ratio B/L:

For B/L < 0.11:

$$c_7 = 0.229577 \left(\frac{B}{L}\right)^{0.33333} \tag{C.10}$$

For 0.11 < B/L < 0.25:

$$c_7 = \frac{B}{L} \tag{C.11}$$

For B/L > 0.25:

$$c_7 = 0.5 - 0.0625 \frac{L}{B} \tag{C.12}$$

The wave making length λ depends on the ratio L/B:

For L/B < 12 holds:

$$\lambda = 1.446C_p - 0.03\frac{L}{B} \tag{C.13}$$

For L/B > 12 holds:

$$\lambda = 1.446C_p - 0.036 \tag{C.14}$$

C_p is the prismatic coefficient and can be determined from Formula 3.23.

The coefficient c_2 acounts for the effect of the bulbous bow, but since a bulbous bow is mostly not present at inland vessels, c_2 is assumed to be equal to 1.

The coefficient c_5 takes into account the effects of the immersed transom on the wave resistance:

$$c_5 = 1 - \frac{0.8A_T}{BTC_M} \tag{C.15}$$

The immersed part of the transverse area of the transom, A_T, is assumed to be 0.2*B*T. C_M is the midship coefficient, and can be determined with Formula 3.11.

The coefficients m_1 and m_4 can be estimated with:

$$m_1 = 0.0140407\frac{L}{T} - 1.75254\frac{\Delta^{1/3}}{L} - 4.79323\frac{B}{L} - c_{16} \tag{C.16}$$

$$m_4 = 0.4c_{15}exp(-0.034F_{n,V_2}^{3.29}) \tag{C.17}$$

The coefficientc_{16} depends on the prismatic coefficient. If C_p < 0.8:

$$c_{16} = 8.07981C_p - 13.8673C_p^2 + 6.984388C_p^3 \tag{C.18}$$

If C_p > 0.8:

$$c_{16} = 1.73014 - 0.7067 * C_p \tag{C.19}$$

The coefficient c_{15} depends on the ratio L^3/Δ. If $L^3/\Delta < 512$, c_{15} = -1.69385. If $L^3/\Delta > 1727$, c_{15} is 0. If L^3/Δ is in between 512 and 1727 the following formula can be used:

$$c_{15} = -1.69385 + \frac{\left(\frac{L}{\Delta^{1/3}} - 8\right)}{2.36} \tag{C.20}$$

With all the information above, the wave resistance R_{W1} for $F_{n,V_2} < 0.4$ can be calculated.

Wave resistance in case F_{n,V_2} > 0.55
If the Froude number becomes higher than 0.55, the approximation of the wave resistance becomes different.

$$R_{W2} = c_{17}c_2c_5\Delta\rho g e^{\left(m_3F_{n,V_2}^{-0.9} + m_4cos(\lambda F_{n,V_2}^{-2})\right)} \tag{C.21}$$

There are two new coefficients in this formula:

$$c_{17} = 6919C_M^{-1.3346}\left(\frac{\Delta}{L^3}\right)^{2.00977}\left(\frac{L}{B} - 2\right)^{1.40692} \tag{C.22}$$

$$m_3 = -7.2035\left(\frac{B}{L}\right)^{0.326869}\left(\frac{T}{B}\right)^{0.605375} \tag{C.23}$$

Wave resistance in case 0.4 < F_{n,V_2} < 0.55
In case the Froude number is in between 0.4 and 0.55, a combination of R_{W1} and R_{W2} is used to calculate the wave resistance:

$$R_{W3} = R_{W1} + \frac{(10F_{n,V_2} - 4)(R_{W2} - R_{W1})}{1.5} \tag{C.24}$$

D

Appendix D: Emissions

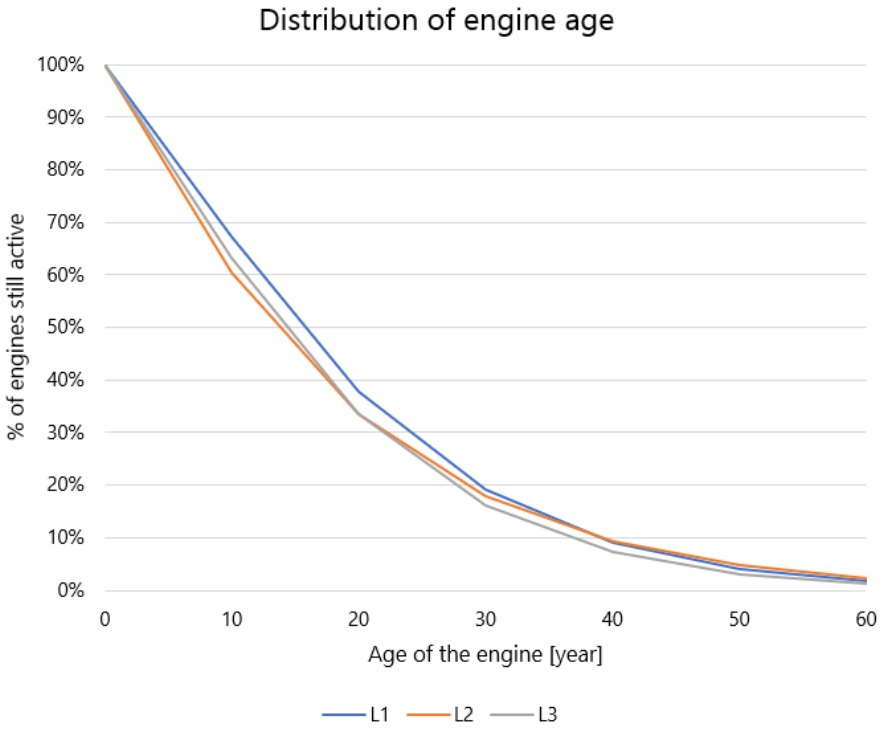

Figure D.1: Distribution of age of engines and the part of these engines that is still active

Construction year classes	2020		
	L1	L2	L2
1900 - 1974	5,85%	6,43%	4,56%
1975 - 1979	2,87%	2,57%	2,39%
1980 - 1984	4,08%	3,53%	3,50%
1985 - 1989	5,70%	4,81%	5,03%
1990 - 1994	7,76%	6,50%	7,08%
1995 - 2002	17,80%	15,20%	17,03%
2003 - 2007 CCR-1	14,84%	13,41%	14,94%
2008 - 2018 CCR-2	37,80%	41,70%	41,37%
2019 - 2019 CCR-2	2,53%	4,11%	3,09%
2019 - 20xx stage V	0,00%	0,00%	0,00%

Table D.1: Distribution of construction year classes of marine engines of the year 2020, based on Weibull-function (Ligterink, 2019)

% Partial engine load	NOx				Diesel fuel, CO2, SO2, metal	PM10	VOS and methane	CO
	<= CCR-1	CCR-2 / Stage IIIa	IWP/IWA-v /c-3	IWP/IWA-v /c-4	All classes			
5	1,83	2,02	3,99	4,79	1,25	2,44	8,00	4,00
10	1,34	1,42	2,63	3,07	1,21	1,63	4,46	5,22
15	1,17	1,27	2,12	2,42	1,18	1,32	2,74	3,51
20	1,10	1,19	1,85	2,08	1,15	1,19	2,02	2,66
25	1,06	1,15	1,69	1,88	1,13	1,12	1,65	2,14
30	1,04	1,13	1,58	1,73	1,11	1,08	1,42	1,80
35	1,03	1,11	1,50	1,63	1,09	1,05	1,27	1,56
40	1,02	1,09	1,44	1,56	1,07	1,03	1,16	1,38
45	1,01	1,08	1,39	1,50	1,05	1,01	1,09	1,23
50	1,00	1,07	1,35	1,45	1,04	1,01	1,03	1,12
55	1,00	1,07	1,32	1,41	1,03	1,00	1,00	1,06
60	0,99	1,06	1,29	1,37	1,02	1,00	0,98	1,00
65	0,99	1,06	1,27	1,35	1,01	0,99	0,95	0,94
70	0,98	1,05	1,25	1,32	1,01	0,99	0,92	0,88
75	0,98	1,05	1,24	1,30	1,00	0,98	0,89	0,82
80	0,97	1,05	1,22	1,28	1,00	0,98	0,87	0,76
85	0,97	1,04	1,21	1,27	1,00	0,97	0,84	0,70
90	0,97	1,04	1,20	1,25	1,01	0,97	0,85	0,70
95	0,97	1,04	1,19	1,24	1,02	0,97	0,86	0,70
100	0,97	1,04	1,18	1,23	1,02	0,97	0,87	0,70

Table D.2: Correction factors of emission factors depending on the partial engine load of marine engines (Ligterink, 2019)

E

Appendix E: Sensitivity analysis

Input	**Base case**	**Case: ρ**		**Case: x**		**Case: η_0**		**Case: η_r**		**Case: η_t**		**Case: η_g**	
ρ [kg/m^3]	1000	**1025**	**2,5%**	1000	0%	1000	0%	1000	0%	1000	0%	1000	0%
x [-]	2	2	0%	**1**	**-50,0%**	2	0%	2	0%	2	0%	2	0%
η_0 [-]	0,6	0,6	0%	0,6	0%	**0,7**	**16,7%**	0,6	0%	0,6	0%	0,6	0%
η_r [-]	0,98	0,98	0%	0,98	0%	0,98	0%	**1**	**2,0%**	0,98	0%	0,98	0%
η_t [-]	0,98	0,98	0%	0,98	0%	0,98	0%	0,98	0%	**1**	**2,0%**	0,98	0%
η_g [-]	0,96	0,96	0%	0,96	0%	0,96	0%	0,96	0%	0,96	0%	**0,98**	**2,1%**
L [m]	135	135	0%	135	0%	135	0%	135	0%	135	0%	135	0%
B [m]	11,75	11,75	0%	11,75	0%	11,75	0%	11,75	0%	11,75	0%	11,75	0%
T [m]	2,75	2,75	0%	2,75	0%	2,75	0%	2,75	0%	2,75	0%	2,75	0%
Pinstalled [kW]	1750	1750	0%	1750	0%	1750	0%	1750	0%	1750	0%	1750	0%
C_B [-]	0,85	0,85	0%	0,85	0%	0,85	0%	0,85	0%	0,85	0%	0,85	0%
V_0[m/s]	3,5	3,5	0%	3,5	0%	3,5	0%	3,5	0%	3,5	0%	3,5	0%
h [m]	10	10	0%	10	0%	10	0%	10	0%	10	0%	10	0%
c_year [-]	2000	2000	0%	2000	0%	2000	0%	2000	0%	2000	0%	2000	0%
Output	**Base case**	**Case: ρ**		**Case: x**		**Case: η_0**		**Case: η_r**		**Case: η_t**		**Case: η_g**	
R_{tot} [kN]	42,30	43,35	2,5%	42,30	0,0%	42,30	0,0%	42,30	0,0%	42,30	0,0%	42,30	0,0%
P_{tot} [kW]	369,58	376,63	1,9%	366,05	-1,0%	329,28	-10,9%	363,94	-1,5%	363,94	-1,5%	363,82	-1,6%
CO_2 [g/km]	21840,00	22225	1,8%	21646,70	-0,9%	19655,37	-10,0%	21530,83	-1,4%	21530,83	-1,4%	21524,51	-1,4%
PM_{10} [g/km]	10,33	10,48	1,5%	10,26	-0,7%	9,57	-7,4%	10,21	-1,2%	10,21	-1,2%	10,21	-1,2%
NO_x[g/km]	300,82	305,65	1,6%	298,39	-0,8%	274,29	-8,8%	296,93	-1,3%	296,93	-1,3%	296,85	-1,3%

Table E.1: Sensitivity analysis of the algorithm to calculate resistance, power and emissions: sensitivity of ρ, x (number of screws), and the efficiencies (η. Base case: M9 motor vessel

Input	**Base case**	**Case: L +7.4%**		**Case: L +14.8%**		**Case: L +22.2%**		**Case: L +29.6%**	
ρ [kg/m^3]	1000	1000	0,0%	1000	0,0%	1000	0,0%	1000	0,0%
x [-]	2	2	0,0%	2	0,0%	2	0,0%	2	0,0%
η_0 [-]	0,6	0,6	0,0%	0,6	0,0%	0,6	0,0%	0,6	0,0%
η_r [-]	0,98	0,98	0,0%	0,98	0,0%	0,98	0,0%	0,98	0,0%
η_t [-]	0,98	0,98	0,0%	0,98	0,0%	0,98	0,0%	0,98	0,0%
η_g [-]	0,96	0,96	0,0%	0,96	0,0%	0,96	0,0%	0,96	0,0%
L [m]	135	**145**	**7,4%**	**155**	**14,8%**	**165**	**22,2%**	**175**	**29,6%**
B [m]	11,75	11,75	0,0%	11,75	0,0%	11,75	0,0%	11,75	0,0%
T [m]	2,75	2,75	0,0%	2,75	0,0%	2,75	0,0%	2,75	0,0%
Pinstalled [kW]	1750	1750	0,0%	1750	0,0%	1750	0,0%	1750	0,0%
C_B [-]	0,85	0,85	0,0%	0,85	0,0%	0,85	0,0%	0,85	0,0%
V_0 [m/s]	3,5	3,5	0,0%	3,5	0,0%	3,5	0,0%	3,5	0,0%
h [m]	10	10	0,0%	10	0,0%	10	0,0%	10	0,0%
c_year [-]	2000	2000	0,0%	2000	0,0%	2000	0,0%	2000	0,0%
Output	**Base case**	**Case: L +7.4%**		**Case: L +14.8%**		**Case: L +22.2%**		**Case: L +29.6%**	
R_{tot} [kN]	42,30	45,39	7,3%	49,13	16,1%	53,94	27,5%	60,61	43,3%
P_{tot} [kW]	369,58	390,2	5,6%	415,1	12,3%	447,21	21,0%	491,64	33,0%
CO_2 [g/km]	21840,00	22963,6	5,1%	24307,1	11,3%	26018,5	19,1%	28345,5	29,8%
PM_{10} [g/km]	10,33	10,76	4,2%	11,25	8,9%	11,88	15,0%	12,82	24,1%
NO_x [g/km]	300,82	314,86	4,7%	331,43	10,2%	352,91	17,3%	384,25	27,7%

Table E.2: Sensitivity analysis of the algorithm to calculate resistance, power and emissions: sensitivity of the vessel length (L). Base case: M9 motor vessel

Input	**Base case**	**Case: B +8.5%**		**Case: B +17%**		**Case: B + 25.5%**		**Case: B + 34.0%**	
rho [kg/m3]	1000	1000	0,0%	1000	0,0%	1000	0,0%	1000	0,0%
x [-]	2	2	0,0%	2	0,0%	2	0,0%	2	0,0%
eta_0 [-]	0,6	0,6	0,0%	0,6	0,0%	0,6	0,0%	0,6	0,0%
eta_r [-]	0,98	0,98	0,0%	0,98	0,0%	0,98	0,0%	0,98	0,0%
eta_t [-]	0,98	0,98	0,0%	0,98	0,0%	0,98	0,0%	0,98	0,0%
eta_g [-]	0,96	0,96	0,0%	0,96	0,0%	0,96	0,0%	0,96	0,0%
L [m]	135	135	0,0%	135	0,0%	135	0,0%	135	0,0%
B [m]	11,75	**12,75**	**8,5%**	**13,75**	**17,0%**	**14,75**	**25,5%**	**15,75**	**34,0%**
T [m]	2,75	2,75	0,0%	2,75	0,0%	2,75	0,0%	2,75	0,0%
Pinstalled [kW]	1750	1750	0,0%	1750	0,0%	1750	0,0%	1750	0,0%
C_B [-]	0,85	0,85	0,0%	0,85	0,0%	0,85	0,0%	0,85	0,0%
V_0 [m/s]	3,5	3,5	0,0%	3,5	0,0%	3,5	0,0%	3,5	0,0%
h [m]	10	10	0,0%	10	0,0%	10	0,0%	10	0,0%
c_year [-]	2000	2000	0,0%	2000	0,0%	2000	0,0%	2000	0,0%
Output	**Base case**	**Case: B +8.5%**		**Case: B +17%**		**Case: B + 25.5%**		**Case: B + 34.0%**	
R_{tot} [kN]	42,30	44,71	5,7%	47,18	11,5%	49,7	17,5%	52,47	24,0%
P_{tot} [kW]	369,58	385,64	4,3%	402,09	8,8%	418,93	13,4%	437,33	18,3%
CO_2 [g/km]	21840,00	22716,2	4,0%	23607,2	8,1%	24512,5	12,2%	25494,5	16,7%
PM_{10} [g/km]	10,33	10,66	3,2%	10,99	6,4%	11,32	9,6%	11,66	12,9%
NO_x [g/km]	300,82	311,78	3,6%	322,83	7,3%	333,94	11,0%	345,86	15,0%

Table E.3: Sensitivity analysis of the algorithm to calculate resistance, power and emissions: sensitivity of the vessel width (B). Base case: M9 motor vessel

Input	**Base case**	**Case: T -18.2%**		**Case: T - 9.1%**		**Case: T +9.1%**		**Case: T +18.2%**	
rho [kg/m^3]	1000	1000	0,0%	1000	0,0%	1000	0,0%	1000	0,0%
x [-]	2	2	0,0%	2	0,0%	2	0,0%	2	0,0%
eta_0 [-]	0,6	0,6	0,0%	0,6	0,0%	0,6	0,0%	0,6	0,0%
eta_r [-]	0,98	0,98	0,0%	0,98	0,0%	0,98	0,0%	0,98	0,0%
eta_t [-]	0,98	0,98	0,0%	0,98	0,0%	0,98	0,0%	0,98	0,0%
eta_g [-]	0,96	0,96	0,0%	0,96	0,0%	0,96	0,0%	0,96	0,0%
L [m]	135	135	0,0%	135	0,0%	135	0,0%	135	0,0%
B [m]	11,75	11,75	0,0%	11,75	0,0%	11,75	0,0%	11,75	0,0%
T [m]	2,75	**2,25**	**-18,2%**	**2,5**	**-9,1%**	**3**	**9,1%**	**3,25**	**18,2%**
Pinstalled [kW]	1750	1750	0,0%	1750	0,0%	1750	0,0%	1750	0,0%
C_B [-]	0,85	0,85	0,0%	0,85	0,0%	0,85	0,0%	0,85	0,0%
V_0 [m/s]	3,5	3,5	0,0%	3,5	0,0%	3,5	0,0%	3,5	0,0%
h [m]	10	10	0,0%	10	0,0%	10	0,0%	10	0,0%
c_year [-]	2000	2000	0,0%	2000	0,0%	2000	0,0%	2000	0,0%
Output	**Base case**	**Case: T -18.2%**		**Case: T - 9.1%**		**Case: T +9.1%**		**Case: T +18.2%**	
R_{tot} [kN]	42,30	42,87	1,3%	41,95	-0,8%	43,19	2,1%	44,34	4,8%
P_{tot} [kW]	369,58	357,52	-3,3%	365,41	-1,1%	377,32	2,1%	386,78	4,7%
CO_2 [g/km]	21840,00	21178,3	-3,0%	21611,9	-1,0%	22263	1,9%	22778,3	4,3%
PM_{10} [g/km]	10,33	10,08	-2,4%	10,25	-0,8%	10,49	1,5%	10,69	3,5%
NO_x [g/km]	300,82	292,47	-2,8%	297,95	-1,0%	306,12	1,8%	312,56	3,9%

Table E.4: Sensitivity analysis of the algorithm to calculate resistance, power and emissions: sensitivity of the vessel draft (T). Base case: M9 motor vessel

Input	**Base case**	**Case: Pinstalled -450 kW**		**Case: Pinstalled +450 kW**		**Case: C_B -17.6%**		**Case: C_B -11.8%**		**Case: C_B -5.9%**		**Case: C_B +5.9%**	
rho [kg/m^3]	1000	1000	0%	1000	0%	1000	0%	1000	0%	1000	0%	1000	0%
x [-]	2	2	0%	2	0%	2	0%	2	0%	2	0%	2	0%
eta_0 [-]	0,6	0,6	0%	0,6	0%	0,6	0%	0,6	0%	0,6	0%	0,6	0%
eta_r [-]	0,98	0,98	0%	0,98	0%	0,98	0%	0,98	0%	0,98	0%	0,98	0%
eta_t [-]	0,98	0,98	0%	0,98	0%	0,98	0%	0,98	0%	0,98	0%	0,98	0%
eta_g [-]	0,96	0,96	0%	0,96	0%	0,96	0%	0,96	0%	0,96	0%	0,96	0%
L [m]	135	135	0%	135	0%	135	0%	135	0%	135	0%	135	0%
B [m]	11,75	11,75	0%	11,75	0%	11,75	0%	11,75	0%	11,75	0%	11,75	0%
T [m]	2,75	2,75	0%	2,75	0%	2,75	0%	2,75	0%	2,75	0%	2,75	0%
Pinstalled [kW]	1750	**1300**	**-25,7%**	**2200**	**25,7%**	1750	0%	1750	0%	1750	0%	1750	0%
C_B[-]	0,85	0,85	0%	0,85	0%	**0,7**	**-17,6%**	**0,75**	**-11,8%**	**0,8**	**-5,9%**	**0,9**	**5,9%**
V_0 [m/s]	3,5	3,5	0%	3,5	0%	3,5	0%	3,5	0%	3,5	0%	3,5	0%
h [m]	10	10	0%	10	0%	10	0%	10	0%	10	0%	10	0%
c_year [-]	2000	2000	0%	2000	0%	2000	0%	2000	0%	2000	0%	2000	0%
Output	**Base case**	**Case: Pinstalled -450 kW**		**Case: Pinstalled +450 kW**		**Case: C_B -17.6%**		**Case: C_B -11.8%**		**Case: C_B -5.9%**		**Case: C_B +5.9%**	
R_{tot} [kN]	42,30	42,3	0%	42,3	0,0%	34,13	-19,3%	36,17	-14,5%	38,66	-8,6%	62,8	48,5%
P_{tot} [kW]	369,58	347,08	-6%	392,08	6,1%	315,29	-14,7%	328,85	-11,0%	345,41	-6,5%	506,23	37,0%
CO_2 [g/km]	21840,00	20110,8	-8%	23524,5	7,7%	18898,4	-13,5%	19632,2	-10,1%	20519,5	-6,0%	29099,9	33,2%
PM_{10} [g/km]	10,33	9,14	-12%	11,64	12,7%	9,32	-9,8%	9,56	-7,5%	9,84	-4,7%	13,12	27,0%
NO_x [g/km]	300,82	272,71	-9%	330,67	9,9%	265,27	-11,8%	274,02	-8,9%	284,4	-5,5%	394,39	31,1%

Table E.5: Sensitivity analysis of the algorithm to calculate resistance, power and emissions: sensitivity of the installed power ($P_{installed}$) and block coefficient (C_B). Base case: M9 motor vessel

Input	**Base case**	**Case: V_0 -28,6%**		**Case: V_0 -14,3%**		**Case: V_0 +14,3%**		**Case: V_0 +28,6%**	
rho [kg/m^3]	1000	1000	0%	1000	0%	1000	0%	1000	0%
x [-]	2	2	0%	2	0%	2	0%	2	0%
eta_0 [-]	0,6	0,6	0%	0,6	0%	0,6	0%	0,6	0%
eta_r [-]	0,98	0,98	0%	0,98	0%	0,98	0%	0,98	0%
eta_t [-]	0,98	0,98	0%	0,98	0%	0,98	0%	0,98	0%
eta_g [-]	0,96	0,96	0%	0,96	0%	0,96	0%	0,96	0%
L [m]	135	135	0%	135	0%	135	0%	135	0%
B [m]	11,75	11,75	0%	11,75	0%	11,75	0%	11,75	0%
T [m]	2,75	2,75	0%	2,75	0%	2,75	0%	2,75	0%
Pinstalled [kW]	1750	1750	0%	1750	0%	1750	0%	1750	0%
C_B [-]	0,85	0,85	0%	0,85	0%	0,85	0%	0,85	0%
V_0 [m/s]	3,5	**2,5**	**-28,6%**	**3**	**-14,3%**	**4**	**14,3%**	**4,5**	**28,6%**
h [m]	10	10	0%	10	0%	10	0%	10	0%
c_year [-]	2000	2000	0%	2000	0%	2000	0%	2000	0%
Output	**Base case**	**Case: V_0 -28,6%**		**Case: V_0 -14,3%**		**Case: V_0 +14,3%**		**Case: V_0 +28,6%**	
R_{tot} [kN]	42,30	21,52	-49,1%	30,7	-27,4%	57,4	35,7%	76,05	79,8%
P_{tot} [kW]	369,58	190,03	-48,6%	263	-28,8%	525,03	42,1%	739,64	100,1%
CO_2 [g/km]	21840,00	16535,6	-24,3%	18674,8	-14,5%	26306,1	20,4%	31485,5	44,2%
PM_{10} [g/km]	10,33	9,99	-3,3%	9,64	-6,7%	11,81	14,3%	12,98	25,7%
NO_x [g/km]	300,82	260,16	-13,5%	267,73	-11,0%	356,44	18,5%	435,81	44,9%

Table E.6: Sensitivity analysis of the algorithm to calculate resistance, power and emissions: sensitivity of the velocity (V_0). Base case: M9 motor vessel

Input	**Base case**	**Case: h -70%**		**Case: h -50%**		**Case: h -30%**		**Case: h +30%**		**Case: h +50%**	
rho [kg/m^3]	1000	1000	0%	1000	0%	1000	0%	1000	0%	1000	0%
x [-]	2	2	0%	2	0%	2	0%	2	0%	2	0%
eta_0 [-]	0,6	0,6	0%	0,6	0%	0,6	0%	0,6	0%	0,6	0%
eta_r [-]	0,98	0,98	0%	0,98	0%	0,98	0%	0,98	0%	0,98	0%
eta_t [-]	0,98	0,98	0%	0,98	0%	0,98	0%	0,98	0%	0,98	0%
eta_g [-]	0,96	0,96	0%	0,96	0%	0,96	0%	0,96	0%	0,96	0%
L [m]	135	135	0%	135	0%	135	0%	135	0%	135	0%
B [m]	11,75	11,75	0%	11,75	0%	11,75	0%	11,75	0%	11,75	0%
T [m]	2,75	2,75	0%	2,75	0%	2,75	0%	2,75	0%	2,75	0%
Pinstalled [kW]	1750	1750	0%	1750	0%	1750	0%	1750	0%	1750	0%
C_B [-]	0,85	0,85	0%	0,85	0%	0,85	0%	0,85	0%	0,85	0%
V_0 [m/s]	3,5	3,5	0%	3,5	0%	3,5	0%	3,5	0%	3,5	0%
h [m]	10	**3**	**-70,0%**	**5**	**-50,0%**	**7**	**-30,0%**	**13**	**30,0%**	**15**	**50,0%**
c_year [-]	2000	2000	0%	2000	0%	2000	0%	2000	0%	2000	0%
Output	**Base case**	**Case: h -70%**		**Case: h -50%**		**Case: h -30%**		**Case: h +30%**		**Case: h +50%**	
R_{tot} [kN]	42,30	95,24	125,2%	45,77	8,2%	43,98	4,0%	42,11	-0,4%	42,04	-0,6%
P_{tot} [kW]	369,58	780,49	111,2%	408,15	10,4%	381,4	3,2%	352,78	-4,5%	352,42	-4,6%
CO_2 [g/km]	21840,00	42341	93,9%	23934	9,6%	22485,3	3,0%	20917,3	-4,2%	20897,5	-4,3%
PM_{10} [g/km]	10,33	18,8	82,0%	11,11	7,6%	10,58	2,4%	9,98	-3,4%	9,97	-3,5%
NO_x [g/km]	300,82	588,56	95,7%	326,85	8,7%	308,9	2,7%	289,17	-3,9%	288,92	-4,0%

Table E.7: Sensitivity analysis of the algorithm to calculate resistance, power and emissions: sensitivity of the water depth (h). Base case: M9 motor vessel

Input	**Base case**	**Case: -20 year**		**Case: -10 year**		**Case: +10 year**		**Case: +20 year**	
rho [kg/m^3]	1000	1000	0%	1000	0%	1000	0%	1000	0%
x [-]	2	2	0%	2	0%	2	0%	2	0%
eta_0 [-]	0,6	0,6	0%	0,6	0%	0,6	0%	0,6	0%
eta_r [-]	0,98	0,98	0%	0,98	0%	0,98	0%	0,98	0%
eta_t [-]	0,98	0,98	0%	0,98	0%	0,98	0%	0,98	0%
eta_g [-]	0,96	0,96	0%	0,96	0%	0,96	0%	0,96	0%
L [m]	135	135	0%	135	0%	135	0%	135	0%
B [m]	11,75	11,75	0%	11,75	0%	11,75	0%	11,75	0%
T [m]	2,75	2,75	0%	2,75	0%	2,75	0%	2,75	0%
Pinstalled [kW]	1750	1750	0%	1750	0%	1750	0%	1750	0%
C_B [-]	0,85	0,85	0%	0,85	0%	0,85	0%	0,85	0%
V_0 [m/s]	3,5	3,5	0%	3,5	0%	3,5	0%	3,5	0%
h [m]	10	10	0%	10	0%	10	0%	10	0%
c_year [-]	2000	**1980**	**-20**	**1990**	**-10**	**2010**	**10**	**2020**	**20**
Output	**Base case**	**Case: -20 year**		**Case: -10 year**		**Case: +10 year**		**Case: +20 year**	
R_{tot} [kN]	42,30	42,30	0,0%	42,30	0,0%	42,30	0,0%	42,30	0,0%
P_{tot} [kW]	369,58	369,58	0,0%	369,58	0,0%	369,58	0,0%	369,58	0,0%
CO_2 [g/km]	21840,00	23990,4	9,8%	23452,8	7,4%	21336	-2,3%	20260,8	-7,2%
PM_{10} [g/km]	10,33	20,67	100,1%	13,78	33,4%	6,89	-33,3%	0,517	-95,0%
NO_x [g/km]	300,82	332,82	10,6%	323,22	7,4%	242,49	-19,4%	143,27	-52,4%

Table E.8: Sensitivity analysis of the algorithm to calculate resistance, power and emissions: sensitivity of the construction year of the engine (c_{year}). Base case: M9 motor vessel

F

Appendix F: RWS vessel classification

F.1. Overview of RWS vessel classification

Motor vessels									
Classification		*Characteristics*							
CEMT	RWS	B [m]	L [m]	Tunloaded [m]	Tloaded [m]	Weight class	Pinstalled [kW]	Loading rate loaded condition	% loaded km
II	M1	5,05	38,5	1,2	2,5	L1	175	75%	70%
III	M2	6,6	52,5	1,4	2,6	L1	300	75%	70%
III	M3	7,2	62,5	1,5	2,6	L1	640	75%	70%
III	M4	8,2	67	1,5	2,7	L1	640	75%	70%
III	M5	8,2	82,5	1,5	2,7	L2	640	75%	70%
IVa	M6	9,5	82,5	1,6	2,9	L2	1070	75%	70%
IVa	M7	9,5	105	1,6	3,0	L2	1070	75%	70%
Va	M8	11,4	110	1,8	3,5	L3	1750	65%	85%
Va	M9	11,4	135	1,8	3,5	L3	2200	65%	85%
Via	M10	13,5	110	2,0	4,0	L3	2400	65%	85%
VIa	M11	14,2	135	2,0	4,0	L3	2400	65%	85%
VIa	M12	17	135	2,0	4,0	L3	3000	65%	85%
Barges									
Classification		*Characteristics*							
CEMT	RWS	B [m]	L [m]	Tunloaded [m]	Tloaded [m]	Weight class	Pinstalled [kW]	Loading rate loaded condition	% loaded km
I	B01	5,2	55	1	1,9	L1	175	75%	70%
II	B02	6,6	65	1,4	2,6	L1	300	75%	70%
III	B03	7,5	80	1,4	2,6	L1	300	75%	70%
III	B04	8,2	85	1,4	2,7	L1	640	75%	70%
IVa	BI	9,5	95	1,6	3	L2	1070	75%	70%
Va	BII-1	11,4	102,5	1,8	3,5	L2	1750	65%	85%
Vb	BII-2l	11,4	180	2	3,8	L3	1750	65%	85%
VIa	BII-2b	22,8	120	2	3,9	L3	2400	65%	85%
VIb	BII-4	22,8	190	2	3,8	L3	3000	65%	85%
VIc	BII-6l	22,8	270	2	3,8	L3	4000	65%	85%
VIIa	BII-6b	34,2	195	2	3,8	L3	4000	65%	85%
Convoys									
Classification		*Characteristics*							
CEMT	RWS	B [m]	L [m]	Tunloaded [m]	Tloaded [m]	Weight class	Pinstalled [kW]	Loading rate loaded condition	% loaded km
I	C1l	5,05	79	1,3	2,5	L1	175	75%	70%
I	C1b	10,1	38,5	1,3	2,5	L1	175	75%	70%
IVb	C2l	9,5	177,5	1,6	3	L2	1070	75%	70%
Vb	C3l	11,4	180	2	3,8	L3	1750	65%	85%
VIa	C2b	19	95	1,6	3	L2	1070	75%	70%
VIa	C3b	22,8	102,5	2	3,8	L3	2400	65%	85%
VIb	C4	22,8	185	2	3,8	L3	3000	65%	85%

Figure F.1: RWS-classification of inland ships in the Netherlands

F.2. Python code to estimate RWS vessel class

In the following figures, the python code is presented that has been developed to estimate the right RWS vessel class for each ship in the AIS dataset.

```
def estimate_vessel_class(row):
    if row['vessel type'] == 'motor vessel': #If the vessel is for sure a motor vessel
        if row['length'] <= 38 or row['width'] <= 5.00:
            return 'M0'

        else:
            if 5.00 < row['width'] <= 5.10:
                return 'M1'
            if 5.10 < row['width'] <= 6.70:
                return 'M2'
            if 6.70 < row['width'] <= 7.30:
                return 'M3'
            if 7.30 < row['width'] <= 8.30:
                if row['length'] <= 74:
                    return 'M4'
                else:
                    return 'M5'
            if 8.30 < row['width'] <= 9.60:
                if row['length'] <= 86:
                    return 'M6'
                else:
                    return 'M7'
            if 9.60 < row['width'] <= 11.50:
                if row['length'] <= 111:
                    return 'M8'
                else:
                    return 'M9'
            if 11.50 < row['width'] <= 14.30:
                if row['length'] <= 111:
                    return 'M10'
                else:
                    return 'M11'
            if row['width'] > 14.30:
                return 'M12'
```

Figure F.2: Code to specify the RWS vessel class for motor vessels

```
    if row['vessel type'] == 'barge': #If the vessel is for sure a barge type
        if row['width'] <= 5.20:
            return 'B01'
        if 5.20 < row['width'] <= 6.70:
            return 'B02'
        if 6.70 < row['width'] <= 7.60:
            return 'B03'
        if 7.60 < row['width'] <= 8.40:
            return 'B04'
        if 8.40 < row['width'] <= 9.60:
            return 'BI'
        if 9.60 < row['width'] <= 15.10:
            if row['length'] <= 146:
                return 'BII-1'
            else:
                return 'BII-2l'
        if 15.10 < row['width'] <= 24:
            if row['length'] <= 146:
                return 'BII-2b'
            if 146 < row['length'] <= 200:
                return 'BII-4'
            else:
                return 'BII-6l'
        if row['width'] > 24:
            return 'BII-6b'
```

Figure F.3: Code to specify the RWS vessel class for barges

```
    if row['vessel type'] == 'convoy': #If the vessel is for sure a convoy
        if row['width'] <= 5.10:
            return 'C1l'
        if 5.10 < row['width'] <= 9.60:
            return 'C2l'
        if 9.60 < row['width'] <= 12.60:
            if row['length'] <= 80:
                return 'C1b'
            else:
                return 'C3l'
        if 12.60 < row['width'] <= 19.10:
            if row['length'] <= 136:
                return 'C2b'
            else:
                return 'C4'
        if row['width'] > 19.10:
            if row['length'] <= 136:
                return 'C3b'
            else:
                return 'C4'
```

Figure F.4: Code to specify the RWS vessel class for convoys

```
if row['vessel type'] == 'unknown': #If the vessel is not for sure a certain type, the code is a bit more complex
    if row['length'] <= 38:
        return 'M0'
    else:
        if row['width'] <= 5.20:
            if row['length'] <= 48:
                return 'M1'
            if 48 < row['width'] <= 65:
                return 'B01'
            else:
                return 'C1l'
        if 5.20 < row['width'] <= 6.70:
            if row['length'] <= 58:
                return 'M2'
            else:
                return 'B02'
        if 6.70 < row['width'] <= 7.60:
            if row['length'] <= 70:
                return 'M3'
            else:
                return 'B03'
        if 7.60 < row['width'] <= 8.40:
            if row['length'] <= 74:
                return 'M4'
            if 74 < row['length'] <= 83:
                return 'M5'
            else:
                return 'B04'
        if 8.40 < row['width'] <= 9.60:
            if row['length'] <= 86:
                return 'M6'
            if 86 < row['length'] <= 100:
                return 'BI'
            if 100 < row['length'] <= 170:
                return 'M7'
            else: # > 170
                return 'C2l'
        if 9.60 < row['width'] <= 15.10:
            if row['length'] <= 80:
                return 'C1b'
            if 80 < row['length'] <= 105:
                return 'BII-1'
```

Figure F.5: Code to specify the RWS vessel class for unknown vessel types (part 1)

```
            if 105 < row['length'] <= 115:
                if row['width'] <= 12:
                    return 'M8'
                else:
                    return 'M10'
            if 115 < row['length'] <= 160:
                if row['width'] <= 12:
                    return 'M9'
                else:
                    return 'M11'
            else:
                if row['width'] <= 12.60:
                    return 'C3l'
                else:
                    return 'BII-2l' #both have same dimensions, does not really matter
        if 15.10 < row['width'] <= 19.10:
            if row['length'] <= 110:
                return 'C2b'
            else:
                return 'M12'
        if 19.10 < row['width'] <= 24.00:
            if row['length'] <= 110:
                return 'C3b'
            if 110 < row['length'] <= 140:
                return 'BII-2b'
            if 140 < row['length'] <= 188:
                return 'C4'
            if 188 < row['length'] <= 200:
                return 'BII-4'
            else:
                return 'BII-6l'

        else:
            return 'BII-6b'
```

Figure F.6: Code to specify the RWS vessel class for unknown vessel types (part 2)

G

Appendix G: AIS data

G.1. VesseltypeERI

ERI Code			SOLAS AIS Code	
code	U	ship name	1st digit	2nd digit
8000	No	Vessel, type unknown	9	9
8010	V	Motor freighter	7	9
8020	V	Motor tanker	8	9
8021	V	Motor tanker, liquid cargo, type N	8	0
8022	V	Motor tanker, liquid cargo, type C	8	0
8023	V	Motor tanker, dry cargo as if liquid (e.g. cement)	8	9
8030	V	Container vessel	7	9
8040	V	Gas tanker	8	0
8050	C	Motor freighter, tug	7	9
8060	C	Motor tanker, tug	8	9
8070	C	Motor freighter with one or more ships alongside	7	9
8080	C	Motor freighter with tanker	8	9
8090	C	Motor freighter pushing one or more freighters	7	9
8100	C	Motor freighter pushing at least one tank-ship	8	9
8110	No	Tug, freighter	7	9
8120	No	Tug, tanker	8	9
8130	C	Tug freighter, coupled	3	1
8140	C	Tug, freighter/tanker, coupled	3	1
8150	V	Freightbarge	9	9
8160	V	Tankbarge	9	9
8161	V	Tankbarge, liquid cargo, type N	9	0
8162	V	Tankbarge, liquid cargo, type C	9	0
8163	V	Tankbarge, dry cargo as if liquid (e.g. cement)	9	9
8170	V	Freightbarge with containers	8	9
8180	V	Tankbarge, gas	9	0
8210	C	Pushtow, one cargo barge	7	9
8220	C	Pushtow, two cargo barges	7	9
8230	C	Pushtow, three cargo barges	7	9
8240	C	Pushtow, four cargo barges	7	9
8250	C	Pushtow, five cargo barges	7	9
8260	C	Pushtow, six cargo barges	7	9
8270	C	Pushtow, seven cargo barges	7	9
8280	C	Pushtow, eigth cargo barges	7	9
8290	C	Pushtow, nine or more barges	7	9
8310	C	Pushtow, one tank/gas barge	8	0
8320	C	Pushtow, two barges at least one tanker or gas barge	8	0
8330	C	Pushtow, three barges at least one tanker or gas barge	8	0
8340	C	Pushtow, four barges at least one tanker or gas barge	8	0
8350	C	Pushtow, five barges at least one tanker or gas barge	8	0
8360	C	Pushtow, six barges at least one tanker or gas barge	8	0
8370	C	Pushtow, seven barges at least one tanker or gas barge	8	0
8380	C	Pushtow, eight barges at least one tanker or gas barge	8	0
8390	C	Pushtow, nine or more barges at least one tanker or gas barge	8	0
8400	V	Tug, single	5	2
8410	No	Tug, one or more tows	3	1
8420	C	Tug, assisting a vessel or linked combination	3	1
8430	V	Pushboat, single	9	9
8440	V	Passenger ship, ferry, cruise ship, red cross ship	6	9
8441	V	Ferry	6	9
8442	V	Red cross ship	5	8
8443	V	Cruise ship	6	9
8444	V	Passenger ship without accomodation	6	9
8450	V	Service vessel, police patrol, port service	9	9
8460	V	Vessel, work maintainance craft, floating derrick, cable-ship, buoy-ship, dredge	3	3
8470	C	Object, towed, not otherwise specified	9	9
8480	V	Fishing boat	3	0
8490	V	Bunkership	9	9
8500	V	Barge, tanker, chemical	8	0
8510	C	Object, not otherwise specified	9	9

Figure G.1: VesseltypeERI identification codes to specify the inland vessel type in AIS data (Vessel Tracking and Tracing Expert Group, 2014)

	VesseltypeERI
Motor vessels	8010, 8020, 8021, 8011, 8023, 8030, 8040,8400, 8420, 8440, 8441, 8442, 8443, 8444, 8450, 8460, 8480, 8490
Barges	8150, 8160, 8161, 8162, 8163, 8170, 8210, 8220, 8230, 8240, 8250, 8260, 8270, 8280, 8290, 8310, 8430, 8500
Convoys	8050, 8060, 8070, 8080, 8090, 8100, 8110, 8120, 8130, 8140, 8410, 8470

Table G.1: Inland vessel VesseltypeERI's from AIS data, subdivided into three subgroups: motor vessels, barges and convoys (based on the RWS classification system)

H

Appendix H: Water levels and bathymetry

Figure H.1 shows the bathymetry (position of the bottom) of the inland waterway network of Rotterdam-Antwerp corridor, obtained from an online source of Rijkswaterstaat (2021a). In this first version of the bathymetry connected to FIS, not all edges had a specified bathymetry. Assumptions have been made, based on the bathymetry of surrounding edges. For secondary waterways that are not the main focus of this study, a fixed bathymetry of 15 meters w.r.t. NAP has been assumed.

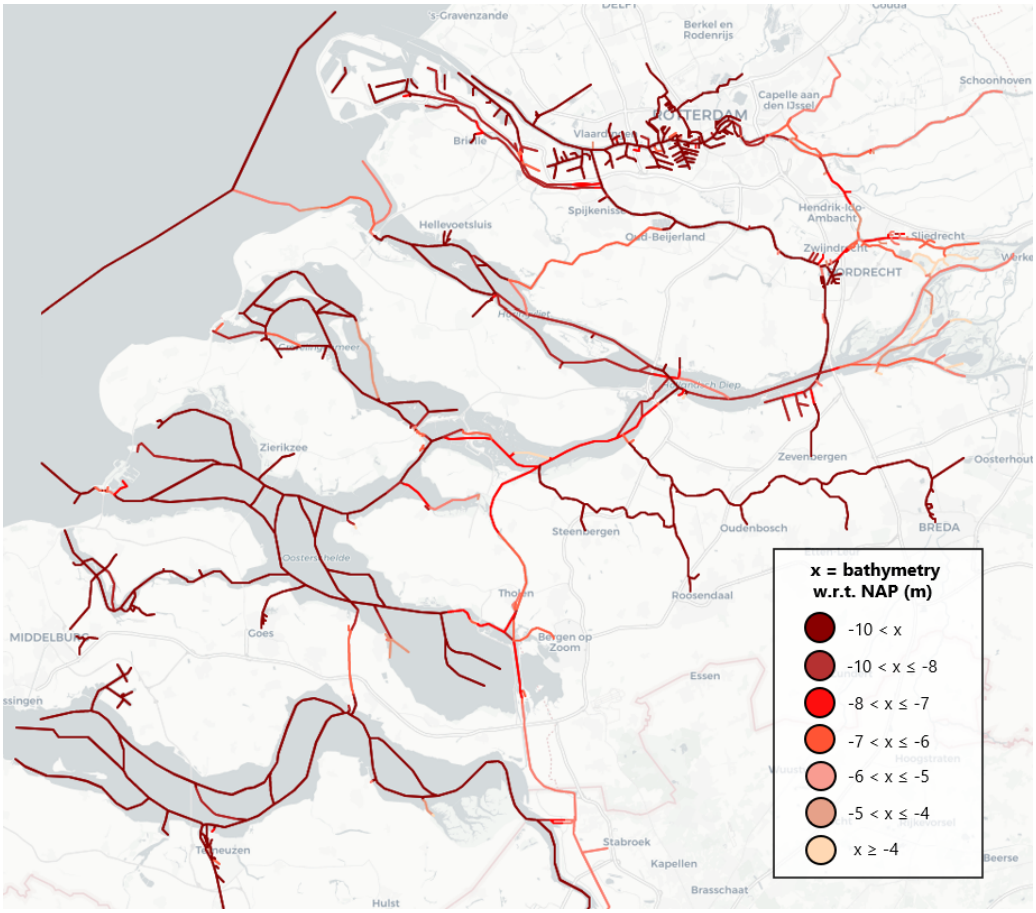

Figure H.1: The bathymetry of the Rotterdam-Antwerp corridor, expressed in meters w.r.t. NAP. (Rijkswaterstaat, 2021a)

The water level along the corridor is specified based on water level data at several measurement locations along the corridor: the blue dots in Figure H.2 show the locations that are used for this specification.

Based on three months of data of the measuring locations of Figure H.2, the water levels (w.r.t. NAP) are specified along the corridor. These water levels are visualized in Figure H.3. For secondary waterways that are not the main focus of this study, the water level is not specified per edge, but a fixed water level of 0.2 meter w.r.t. NAP has been assumed.

Figure H.2: Measurement locations of water level along the Rotterdam-Antwerp corridor: the blue dots are the measurement locations that have been taken into account.

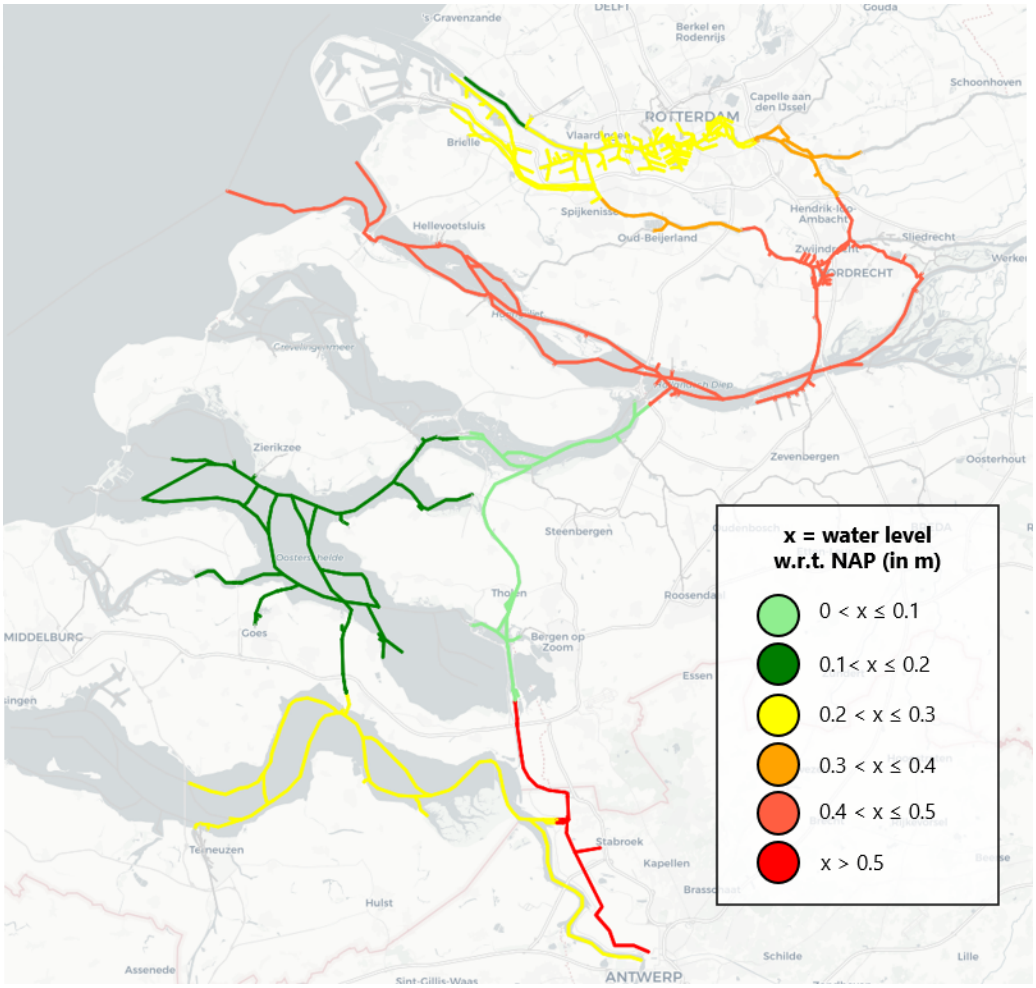

Figure H.3: Overview of the water levels w.r.t. NAP along the Rotterdam-Antwerp corridor

Appendix I: Emission heatmaps

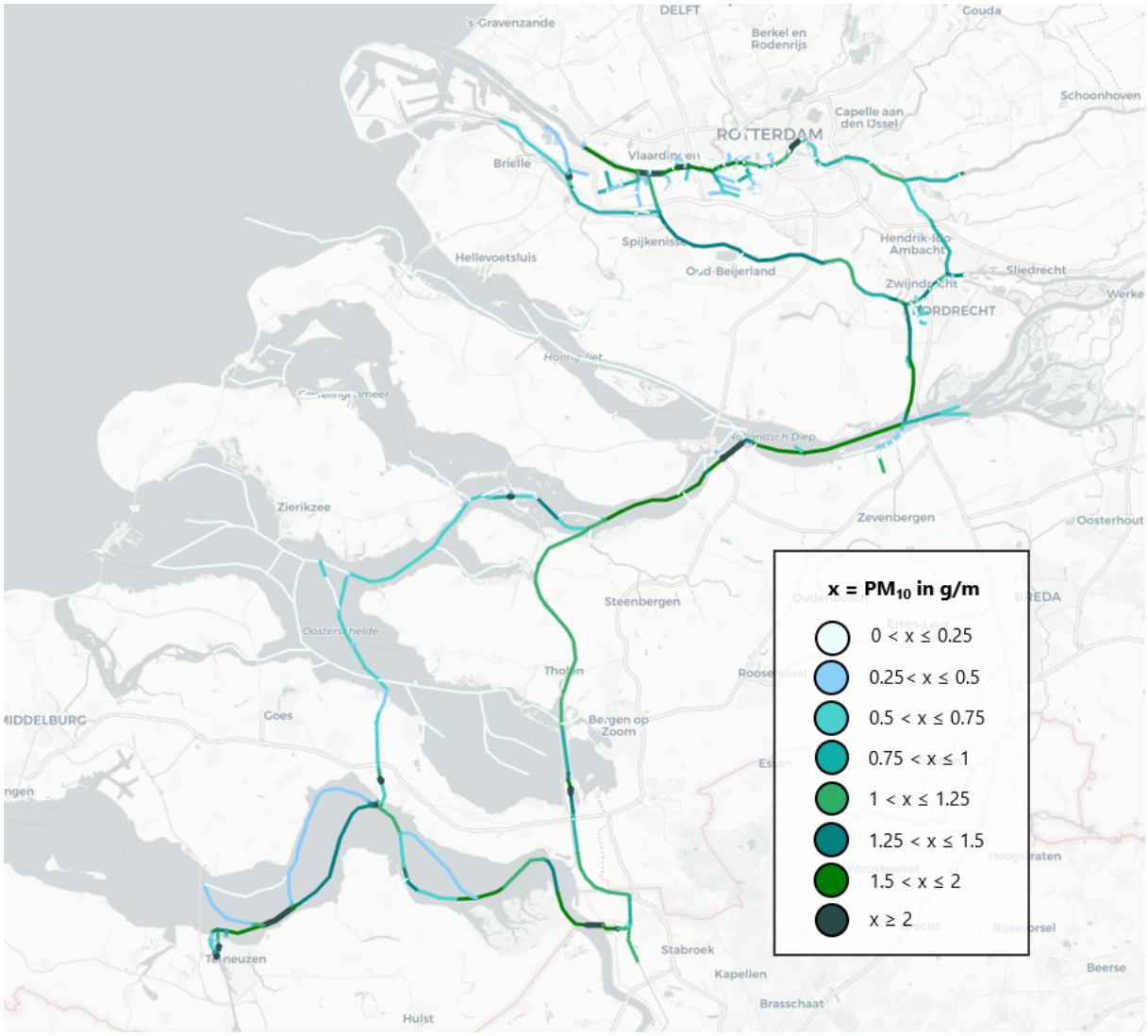

Figure I.1: AIS 't0 emission scenario': potential PM_{10} emission levels of one day (2 Sept 2019) on the Rotterdam-Antwerp corridor

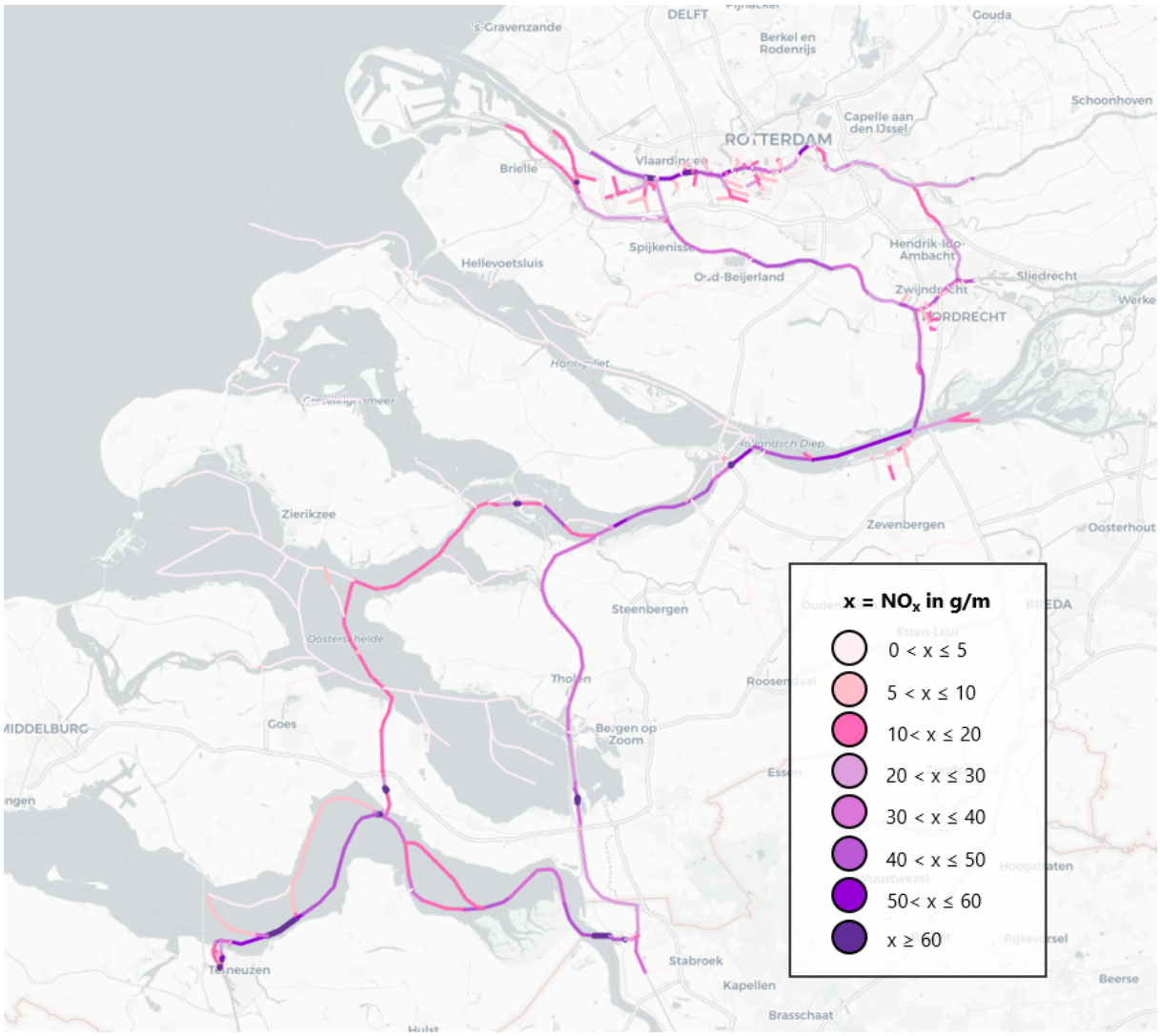

Figure I.2: AIS 't0 emission scenario': potential NO_x emission levels of one day (2 Sept 2019) on the Rotterdam-Antwerp corridor

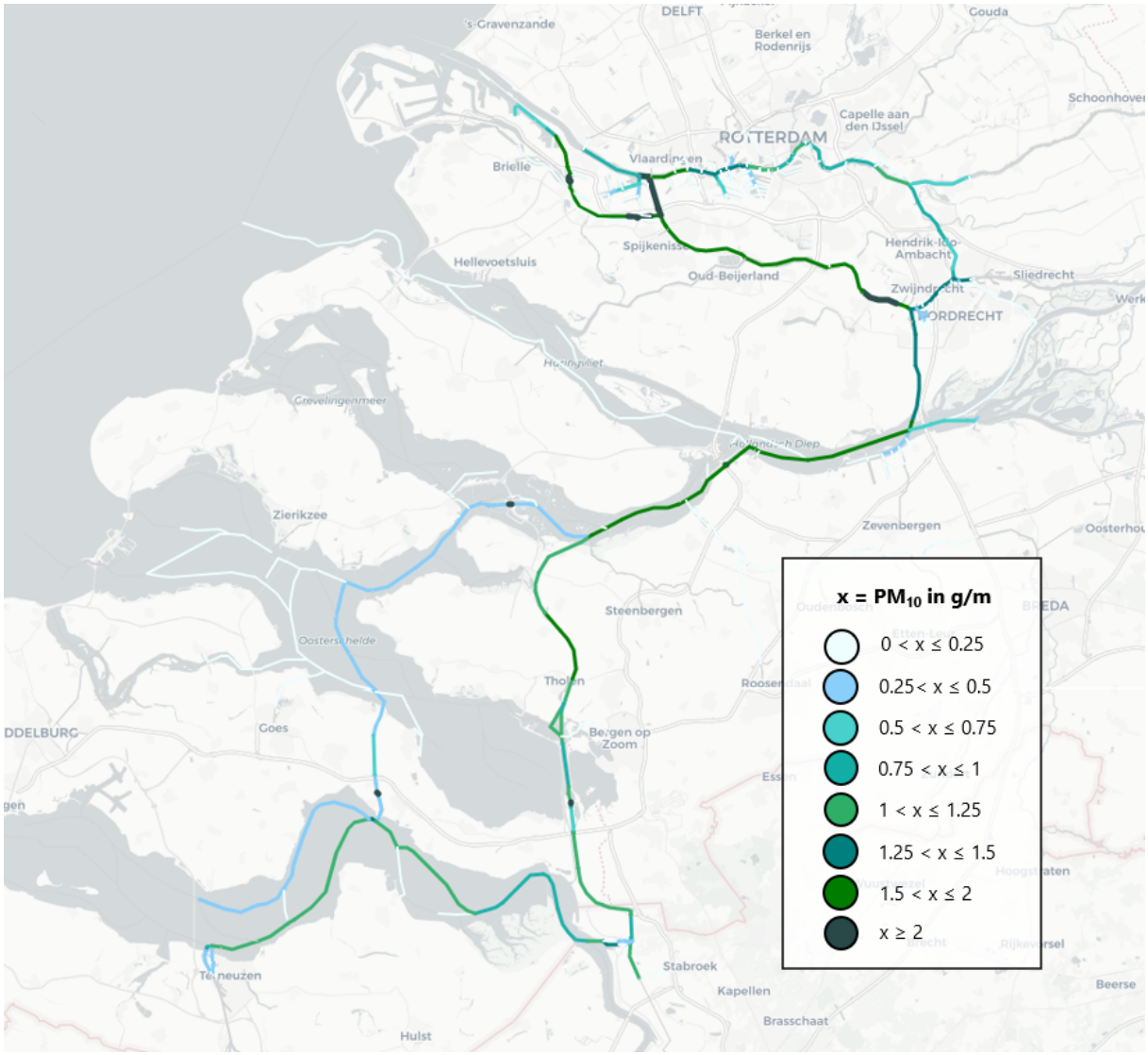

Figure I.3: Model output, simulated 't0 emission scenario': potential PM_{10} emission levels of one day (2 Sept 2019) on the Rotterdam-Antwerp corridor

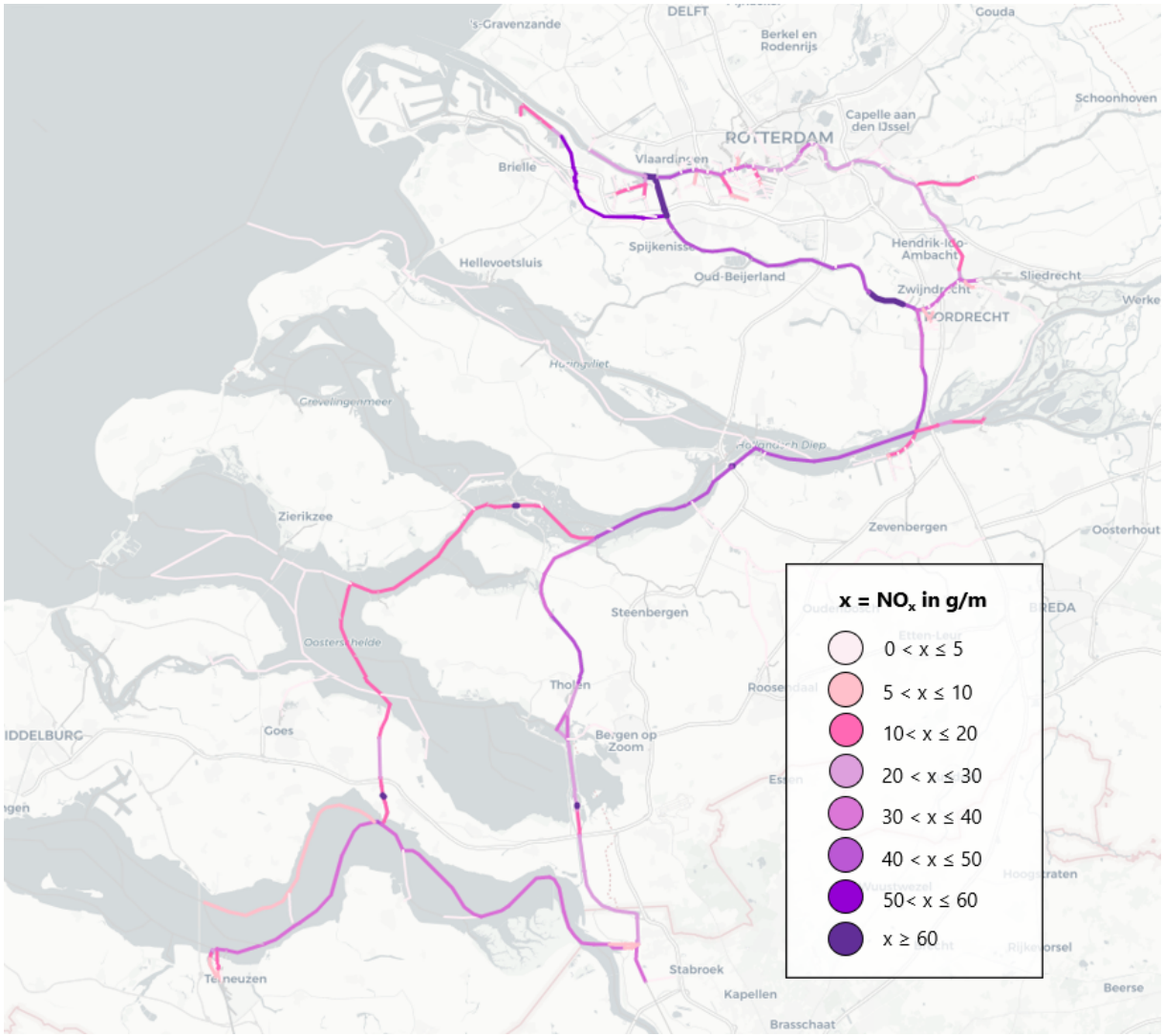

Figure I.4: Model output, simulated 't0 emission scenario': potential NO_x emission levels of one day (2 Sept 2019) on the Rotterdam-Antwerp corridor

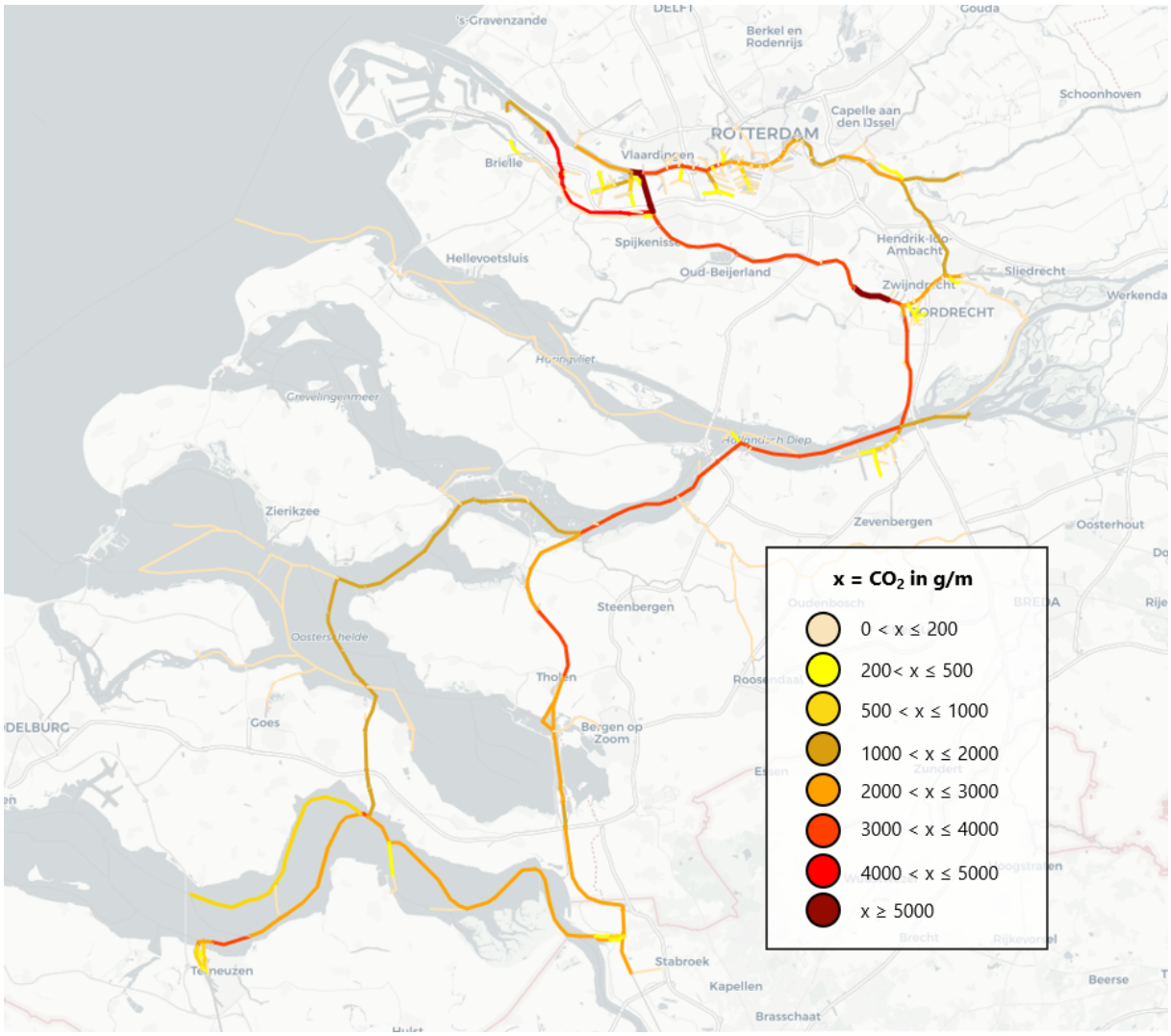

Figure I.5: Model simulation: zero emission policy at locks. Map shows potential CO_2 emission levels of one day (2 Sept 2019) on the Rotterdam-Antwerp corridor

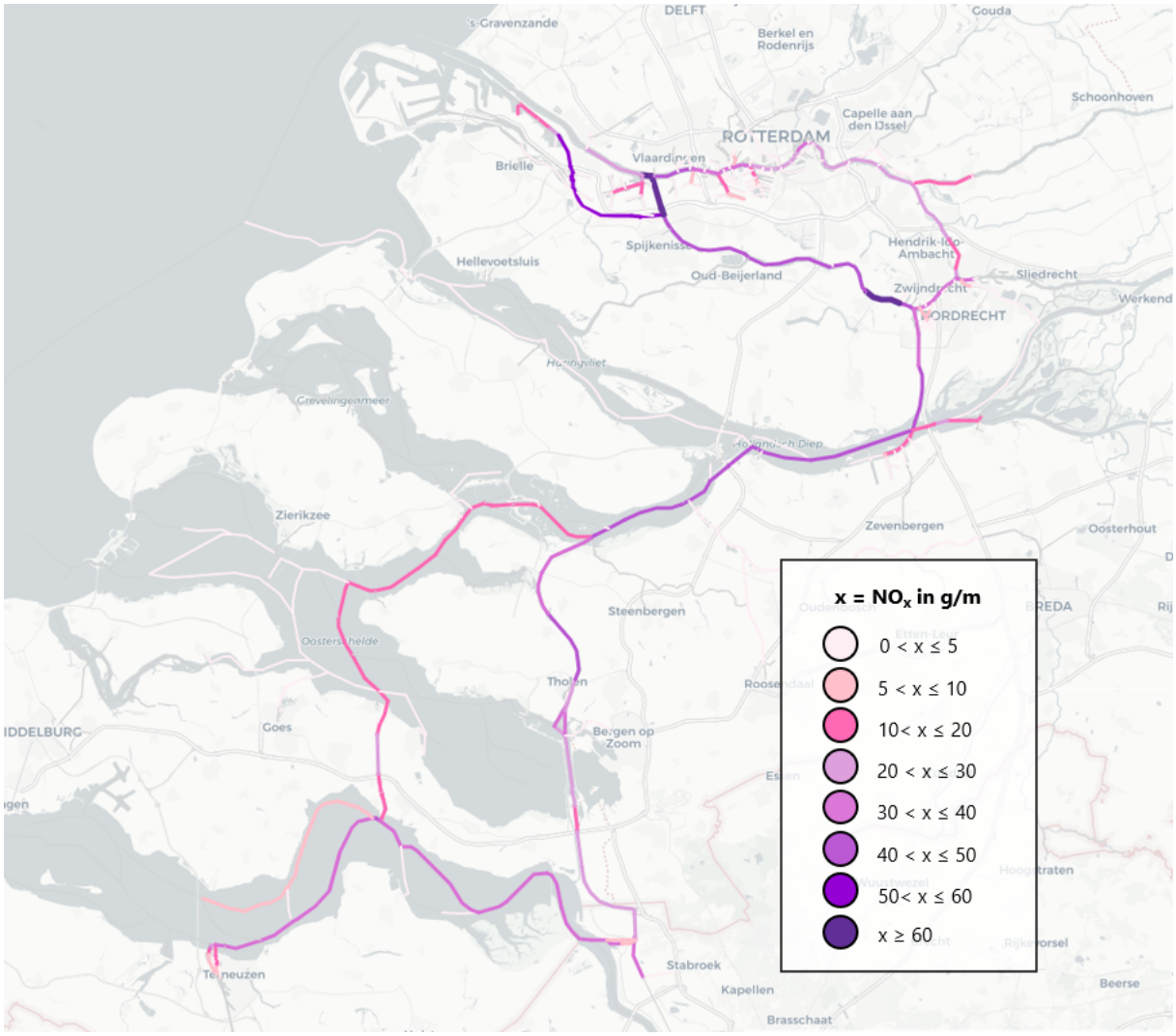

Figure I.6: Model simulation: zero emission policy at locks. Map shows potential NO_x emission levels of one day (2 Sept 2019) on the Rotterdam-Antwerp corridor

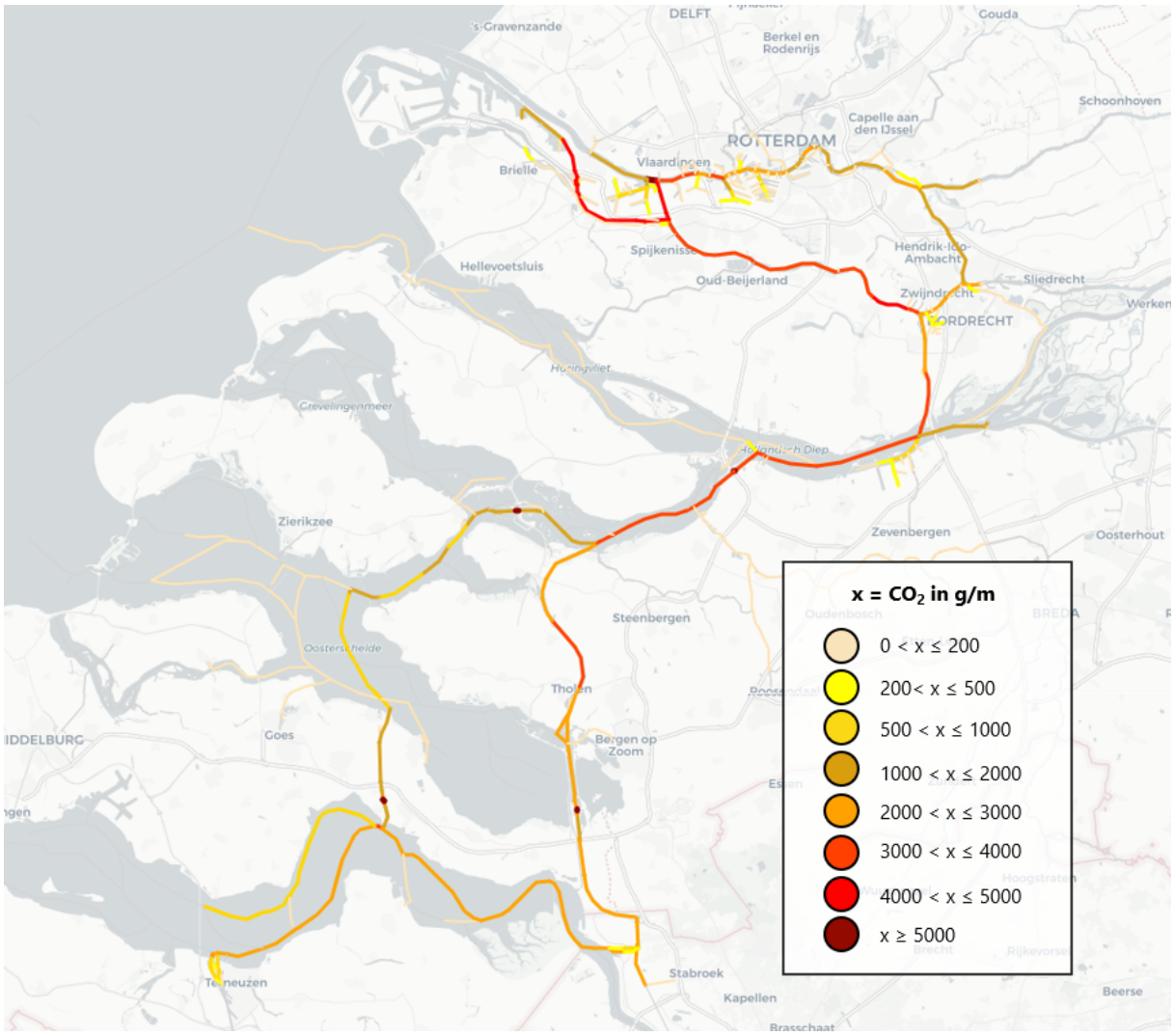

Figure I.7: Model simulation of fleet renewal policy: potential CO_2 emission distribution of one day on the Rotterdam-Antwerp corridor (2 September 2019). All engines from the year 2007 or older are replaced by new Stage V engines.

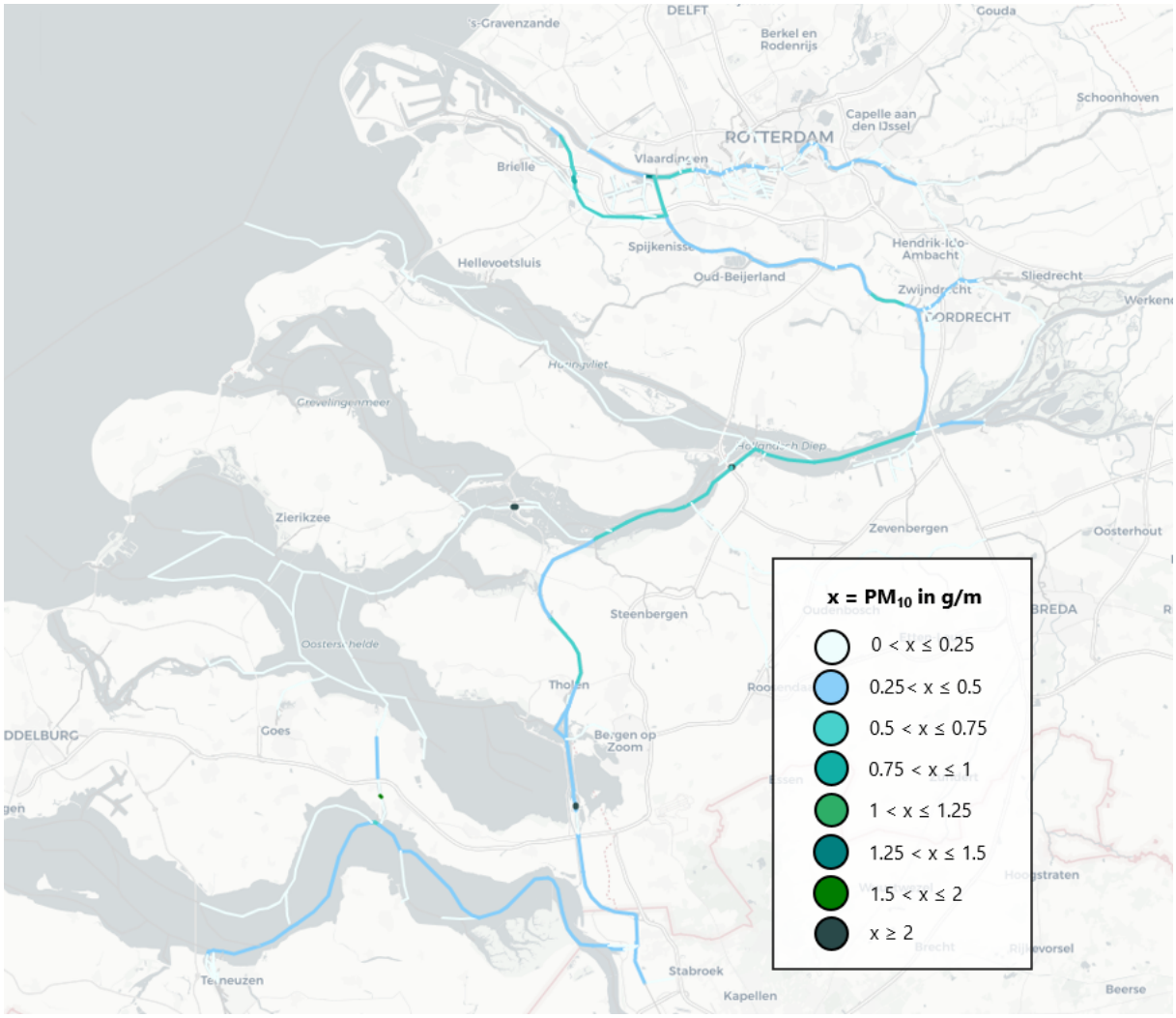

Figure I.8: Model simulation of fleet renewal policy: potential PM_{10} emission distribution of one day on the Rotterdam-Antwerp corridor (2 September 2019). All engines from the year 2007 or older are replaced by new Stage V engines.

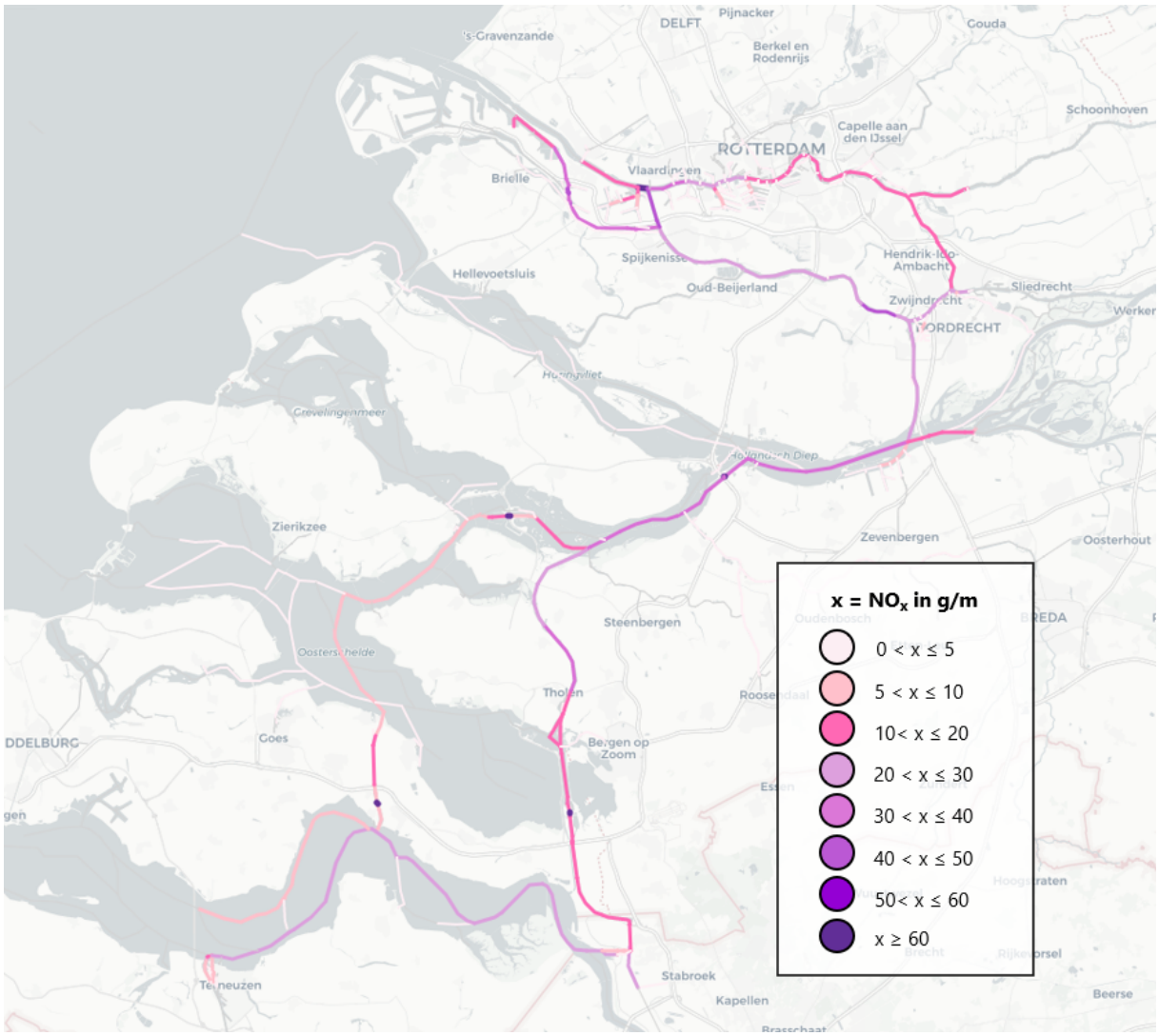

Figure I.9: Model simulation of fleet renewal policy: potential NO_x emission distribution of one day on the Rotterdam-Antwerp corridor (2 September 2019). All engines from the year 2007 or older are replaced by new Stage V engines.

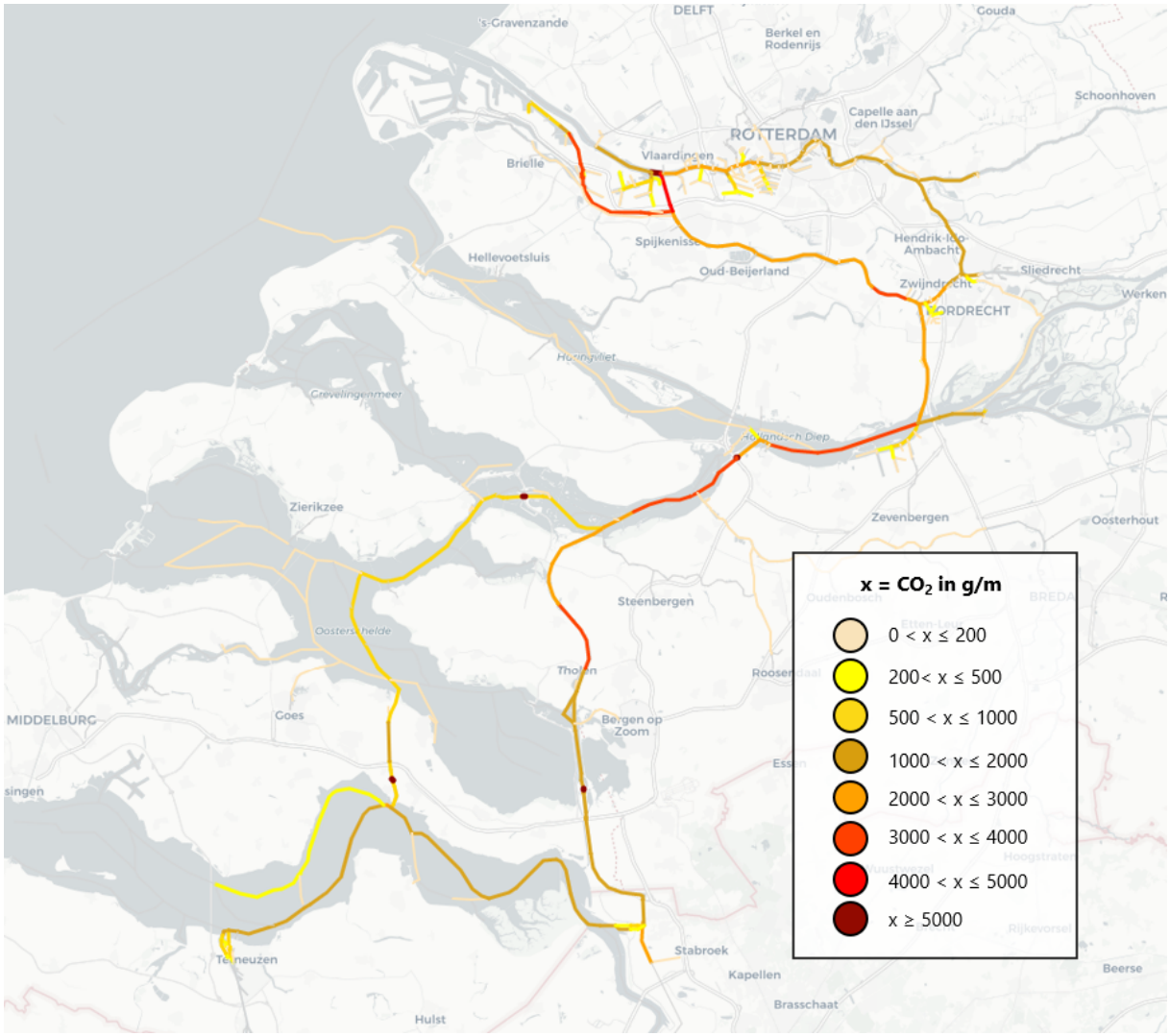

Figure I.10: Model simulation with a speed limit of 12 km/h: CO_2 emission distribution of one day (2 September 2019) along the Rotterdam-Antwerp corridor

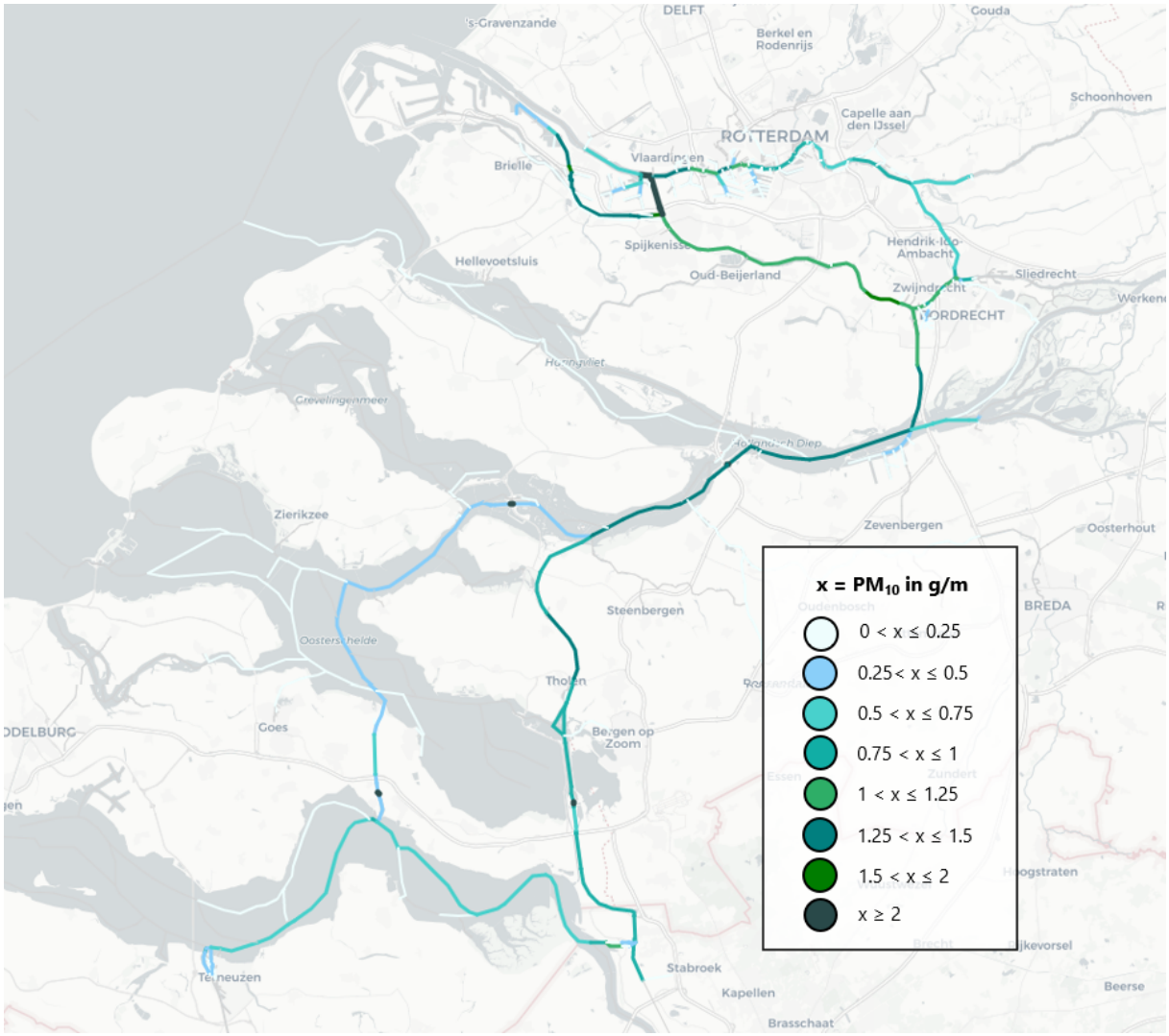

Figure I.11: Model simulation with a speed limit of 12 km/h: CO_2 emission distribution of one day (2 September 2019) along the Rotterdam-Antwerp corridor

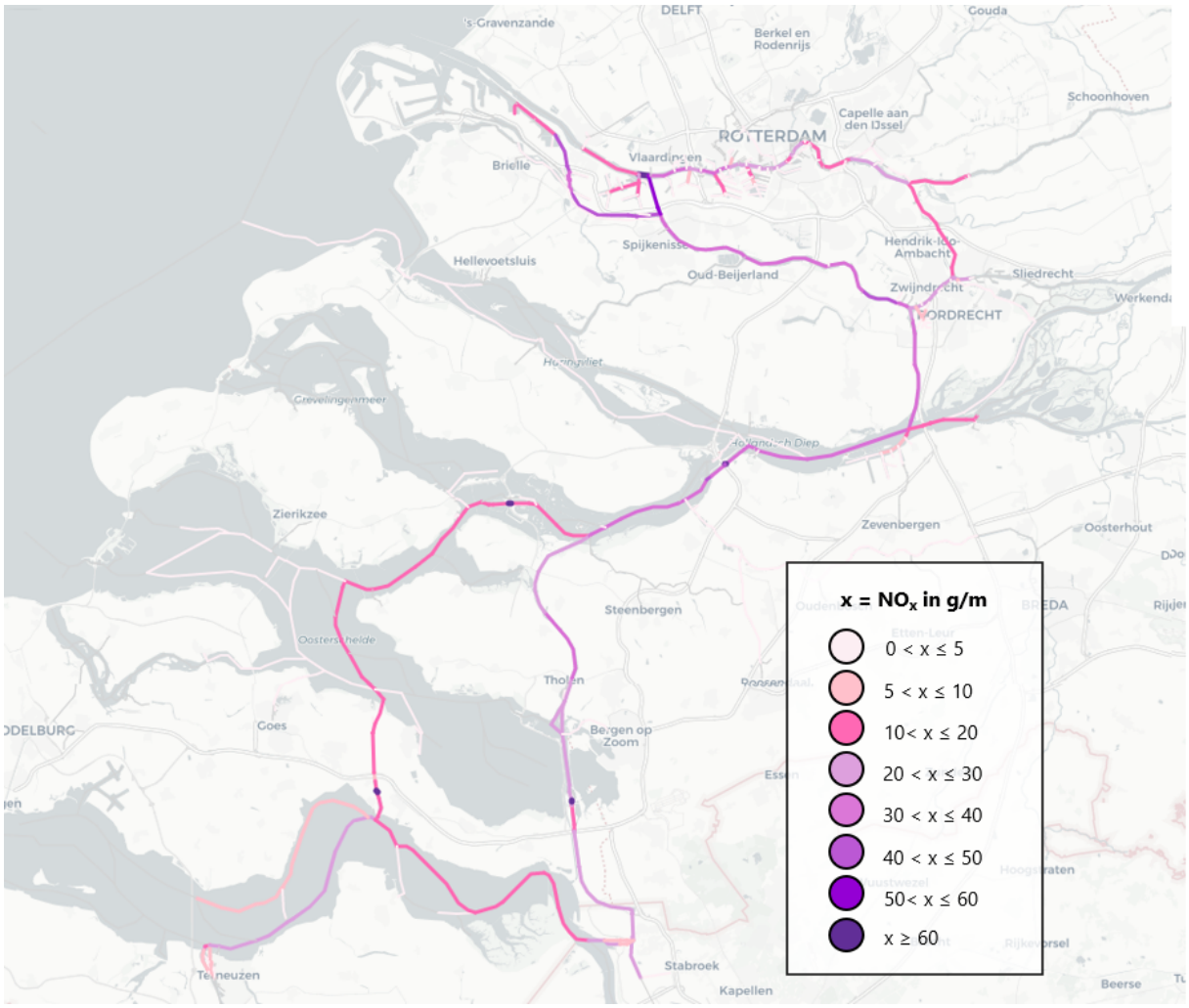

Figure I.12: Model simulation with a speed limit of 12 km/h: CO_2 emission distribution of one day (2 September 2019) along the Rotterdam-Antwerp corridor

J

Appendix J: Stationary emission rates

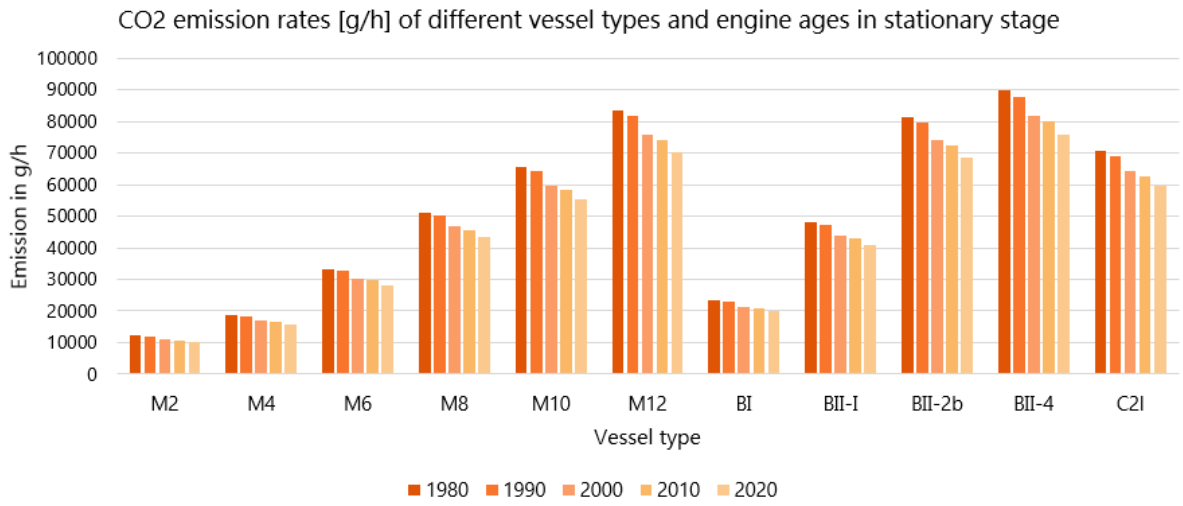

Figure J.1: CO_2 emission rates (in g/h) of different vessel types and engine ages in a stationary stages

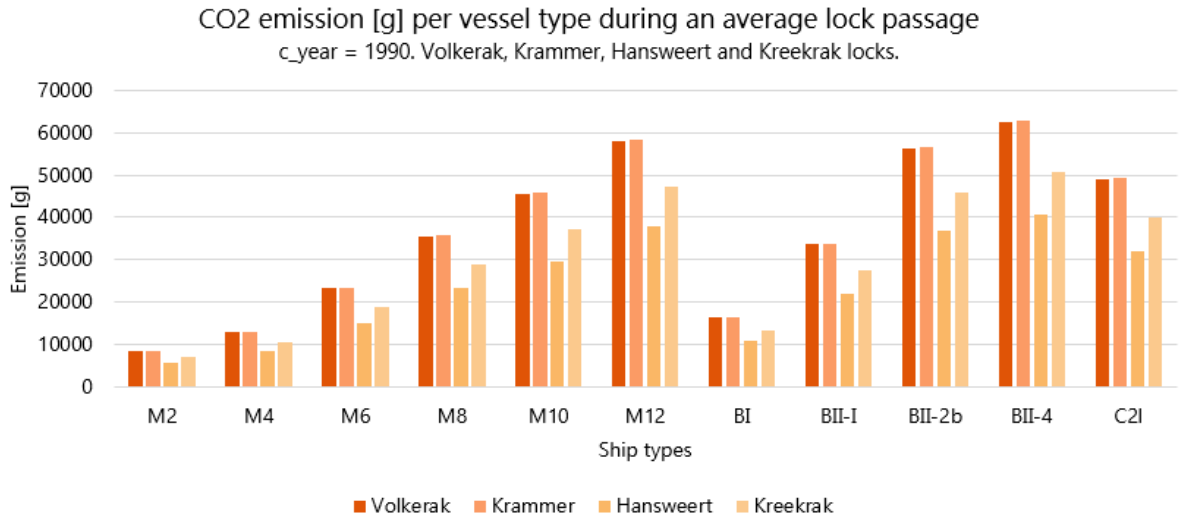

Figure J.2: CO_2 emissions during one average lock passage at different locks, for different vessel types with c_{year} = 1990.

	c_year = 1980			c_year = 1990			c_year = 2000			c_year = 2010			c_year = 2020		
	CO2	**PM10**	**NOX**	**CO2**	**PM10**	**NOX**	**CO2**	**PM10**	**NOX**	**CO2**	**PM10**	**NOX**	**CO2**	**PM10**	**NOX**
M2	12155	9,85	167,21	11883	6,56	162,39	11066	4,92	151,14	10810	3,28	131,36	10266	0,25	56,36
M4	18637	15,66	255,67	18218	10,44	248,3	16965	7,83	231,09	16574	5,22	186,59	15739	0,39	95,16
M6	33343	27,69	455,5	32596	18,46	442,36	30355	13,84	411,7	29654	9,23	332,7	28160	0,69	184,55
M8	51243	43,02	702,62	50095	28,68	682,35	46650	21,41	635,06	45573	14,34	512,8	43277	1,08	291,03
M10	65525	55,86	904,73	64057	37,24	878,63	59652	27,93	817,73	58275	18,62	659,64	55339	1,4	383,5
M12	83369	70,81	1149,2	81501	47,29	1116	75896	35,4	1038,7	74145	23,6	838,06	70408	1,77	484,31
BI	23578	21,29	334,17	23050	14,19	324,53	21465	10,64	302,04	20970	7,1	243,72	19913	0,53	152,39
BII-I	48294	41.08	666.13	47212	27,39	646,91	43965	20,54	602,08	42950	13,69	484,75	40786	1,03	281,42
BII-2b	81221	66,84	1108,9	79401	44,56	1076,9	73941	33,42	1002,3	72235	22,28	810,55	68595	1,67	425,42
BII-4	89834	75,01	1228,8	87821	50	1193,4	81781	37,5	1110,7	79894	25	879,17	75868	1,88	504,89
C2l	70438	58,03	996,4	68860	38,69	967,65	64124	29,02	900,59	62645	19,34	718,07	59488	1,45	317,92

Table J.1: Emission rates in g/h in stationary stages, for different vessel types and engine ages (c_{year})

	c_year = 1980			c_year = 1990			c_year = 2000			c_year = 2010			c_year = 2020		
	CO2	**PM10**	**NOX**	**CO2**	**PM10**	**NOX**	**CO2**	**PM10**	**NOX**	**CO2**	**PM10**	**NOX**	**CO2**	**PM10**	**NOX**
M2	8637	7,00	118,81	8444	4,66	115,39	7863	3,50	107,39	7681	2,33	93,34	7295	0,18	40,05
M4	13243	11,13	181,67	12945	7,42	176,43	12055	5,56	164,20	11777	3,71	132,58	11183	0,28	67,62
M6	23692	19,68	323,66	23161	13,12	314,32	21569	9,83	292,54	21071	6,56	236,40	20009	0,49	131,13
M8	36411	30,57	499,25	35595	20,38	484,85	33147	15,21	451,25	32382	10,19	364,37	30751	0,77	206,79
M10	46559	39,69	642,86	45516	26,46	624,32	42386	19,85	581,04	41408	13,23	468,71	39321	0,99	272,50
M12	59238	50,31	816,53	57911	33,60	792,98	53928	25,15	738,03	52684	16,77	595,49	50029	1,26	344,13
BI	16753	15,13	237,45	16378	10,08	230,60	15252	7,56	214,62	14900	5,04	173,18	14149	0,38	108,28
BII-I	34316	29,19	473,32	33547	19,46	459,67	31240	14,59	427,81	30518	9,73	344,44	28981	0,73	199,96
BII-2b	57712	47,49	787,94	56419	31,66	765,21	52539	23,75	712,18	51327	15,83	575,94	48741	1,19	302,28
BII-4	63832	53,30	873,15	62401	35,53	847,96	58110	26,65	789,19	56769	17,76	624,70	53908	1,34	358,75
C2l	50050	41,23	708,00	48929	27,49	687,57	45564	20,62	639,92	44513	13,74	510,23	42270	1,03	225,90

Table J.2: Emissions during one lock passage (in g) at Volkerak locks, for different vessel types and engine ages (c_{year}). Average passing time: 2560 s.

	c_year = 1980			c_year = 1990			c_year = 2000			c_year = 2010			c_year = 2020		
	CO2	**PM10**	**NOX**	**CO2**	**PM10**	**NOX**	**CO2**	**PM10**	**NOX**	**CO2**	**PM10**	**NOX**	**CO2**	**PM10**	**NOX**
M2	8681	7,03	119,42	8486	4,68	115,97	7903	3,51	107,94	7720	2,34	93,81	7332	0,18	40,25
M4	13310	11,18	182,59	13011	7,46	177,33	12116	5,59	165,04	11837	3,73	133,26	11240	0,28	67,96
M6	23812	19,78	325,30	23279	13,18	315,92	21679	9,88	294,02	21178	6,59	237,60	20111	0,49	131,80
M8	36596	30,72	501,79	35776	20,48	487,31	33316	15,29	453,54	32547	10,24	366,22	30907	0,77	207,84
M10	46796	39,89	646,13	45747	26,60	627,49	42601	19,95	584,00	41618	13,30	471,09	39521	1,00	273,88
M12	59539	50,57	820,68	58205	33,77	797,01	54202	25,28	741,78	52952	16,85	598,51	50283	1,26	345,88
BI	16839	15,20	238,65	16462	10,13	231,77	15330	7,60	215,71	14976	5,07	174,06	14221	0,38	108,83
BII-I	34490	29,34	475,73	33717	19,56	462,00	31398	14,67	429,99	30673	9,78	346,19	29128	0,74	200,98
BII-2b	58005	47,73	791,95	56706	31,82	769,10	52806	23,87	715,79	51588	15,91	578,87	48988	1,19	303,82
BII-4	64156	53,57	877,59	62719	35,71	852,27	58405	26,78	793,20	57058	17,85	627,87	54182	1,34	360,58
C2l	50304	41,44	711,60	49178	27,63	691,06	45795	20,73	643,17	44739	13,81	512,82	42484	1,04	227,05

Table J.3: Emissions during one lock passage (in g) at Krammer locks, for different vessel types and engine ages (c_{year}). Average passing time: 2570 s.

	c_year = 1980			c_year = 1990			c_year = 2000			c_year = 2010			c_year = 2020		
	CO2	**PM10**	**NOX**	**CO2**	**PM10**	**NOX**	**CO2**	**PM10**	**NOX**	**CO2**	**PM10**	**NOX**	**CO2**	**PM10**	**NOX**
M2	5632	4,56	77,47	5506	3,04	75,24	5127	2,28	70,03	5009	1,52	60,86	4757	0,12	26,11
M4	8635	7,26	118,46	8441	4,84	115,05	7860	3,63	107,07	7679	2,42	86,45	7292	0,18	44,09
M6	15449	12,83	211,05	15103	8,55	204,96	14064	6,41	190,75	13740	4,28	154,15	13047	0,32	85,51
M8	23743	19,93	325,55	23211	13,29	316,16	21615	9,92	294,24	21115	6,64	237,60	20052	0,50	134,84
M10	30360	25,88	419,19	29680	17,25	407,10	27639	12,94	378,88	27001	8,63	305,63	25640	0,65	177,69
M12	38628	32,81	532,44	37762	21,91	517,08	35165	16,40	481,25	34354	10,93	388,30	32622	0,82	224,40
BI	10924	9,86	154,83	10680	6,57	150,37	9945	4,93	139,95	9716	3,29	112,92	9226	0,25	70,61
BII-I	22376	19,03	308,64	21875	12,69	299,73	20370	9,52	278,96	19900	6,34	224,60	18898	0,48	130,39
BII-2b	37632	30,97	513,79	36789	20,65	498,97	34259	15,48	464,39	33469	10,32	375,55	31782	0,77	197,11
BII-4	41623	34,75	569,36	40690	23,17	552,93	37892	17,38	514,61	37018	11,58	407,35	35152	0,87	233,93
C2l	32636	26,89	461,67	31905	17,93	448,34	29711	13,45	417,27	29026	8,96	332,71	27563	0,67	147,30

Table J.4: Emissions during one lock passage (in g) at Hansweert locks, for different vessel types and engine ages (c_{year}). Average passing time: 1670 s.

	c_year = 1980			c_year = 1990			c_year = 2000			c_year = 2010			c_year = 2020		
	CO2	**PM10**	**NOX**	**CO2**	**PM10**	**NOX**	**CO2**	**PM10**	**NOX**	**CO2**	**PM10**	**NOX**	**CO2**	**PM10**	**NOX**
M2	7040	5,70	96,84	6882	3,80	94,05	6409	2,85	87,54	6261	1,90	76,08	5946	0,14	32,64
M4	10794	9,07	148,08	10551	6,05	143,81	9826	4,53	133,84	9599	3,02	108,07	9116	0,23	55,11
M6	19311	16,04	263,81	18879	10,69	256,20	17581	8,02	238,44	17175	5,35	192,69	16309	0,40	106,89
M8	29678	24,92	406,93	29013	16,61	395,19	27018	12,40	367,81	26394	8,31	297,00	25065	0,63	168,55
M10	37950	32,35	523,99	37100	21,57	508,87	34548	16,18	473,60	33751	10,78	382,04	32051	0,81	222,11
M12	48285	41,01	665,55	47203	27,39	646,35	43956	20,50	601,56	42942	13,67	485,38	40778	1,03	280,50
BI	13656	12,33	193,54	13350	8,22	187,96	12432	6,16	174,93	12145	4,11	141,15	11533	0,31	88,26
BII-I	27970	23,79	385,80	27344	15,86	374,67	25463	11,90	348,70	24875	7,93	280,75	23622	0,60	162,99
BII-2b	47040	38,71	642,24	45986	25,81	623,72	42824	19,36	580,49	41836	12,90	469,44	39728	0,97	246,39
BII-4	52029	43,44	711,70	50863	28,96	691,17	47365	21,72	643,26	46272	14,48	509,19	43940	1,09	292,42
C2l	40795	33,61	577,08	39881	22,41	560,43	37138	16,81	521,59	36282	11,20	415,88	34453	0,84	184,13

Table J.5: Emissions during one lock passage (in g) at Kreekrak locks, for different vessel types and engine ages (c_{year}). Average passing time: 2085 s.

References

[1] Atlas Leefomgeving. Fijnstof. Accessed at 4-8-2020, from https://www.atlasleefomgeving.nl/meer-weten/lucht/fijnstof.

[2] E. Bolt. “Schatting energiegebruik binnenvaartschepen”. In: Rijkswaterstaat Adviesdienst Verkeer en Vervoer, Rotterdam (2003).

[3] Bureau Telematica Binnenvaart. “Wat is AIS? Een introductie van AIS voor de binnenvaart”. In: (2009).

[4] Bureau Voorlichting Binnenvaart. “„The power of inland navigation: The future of freight transport and inland navigation in Europe“”. In: (2017).

[5] Bureau Voorlichting Binnenvaart. Over de binnenvaart: Milieu. Accessed at 5-8-2020, from https://www.bureauvoorlichtingbinnenvaart.nl/over/milieu.

[6] Bureau Voorlichting Binnenvaart. Vaarwegen. Accessed at 21-10-2020, from https://www.bureauvoorlichtingbinnenvaart.nl/over/basiskennis/vaarwegen.

[7] CBS. Emissies naar lucht op Nederlands grondgebied; mobiele bronnen, 1990-2018. Accessed at 4-8-2020, from https://www.cbs.nl/nl-nl/cijfers/detail/7062. 2020.

[8] CBS. Vervoerd gewicht per modaliteit. Accessed at 21-10-2020, from https://binnenvaartcijfers.nl/vervoerd-gewicht-per-modaliteit/. 2020.

[9] CE Delft. “STREAM Goederenvervoer 2020: Emissies van modaliteiten in het goederenvervoer”. In: CE Delft (2020).

[10] CE Delft. “STREAM Goederenvervoer: Emissies van modaliteiten in het goederenvervoer”. In: CE-publicaties (2016).

[11] P. de Vos and R. van Gils. “„Walstroom versus generatorstroom“”. In: Delft University of Technology (2011).

[12] European Commission. Inland navigation: What do we want to achieve? Accessed at 20-10-2020, from https://ec.europa.eu/transport/modes/inland$_e$n. 2020.

[13] European Commission. Paris Agreement. Accessed at 11-05-2020, from https://ec.europa.eu/clima/policies/international/negotiations/paris$_e$n. 2020.

[14] G.C. Gillmer and B. Johnson. “Introduction to Naval Architecture”. In: (1982).

[15] Green Deal. Green Deal Zeevaart, Binnenvaart en Havens. Accessed at 5-8-2020, from https://www.greendeals.nl/green-deals/green-deal-zeevaart-binnenvaart-en-havens. 2019.

[16] R.G. Hekkenberg. “Inland ships for efficient transport chains”. PhD thesis. Delft University of Technology, 2013.

[17] J Holtrop and GGJ Mennen. “A statistical power prediction method”. In: International shipbuilding progress 25.290 (1978).

[18] J. Holtrop and G.G.J. Mennen. “An approximate power prediction method”. In: International Shipbuilding Progress 29.335 (1982), pp. 166–170.

[19] J.H.J. Hulskotte. “„Toelichting Rekenapplicatie PRELUDE versie 1.1“”. In: TNO (2013).

[20] J.H.J. Hulskotte. “Korte verkenning van enkele opties voor uitstootbeperking in de binnenvaart in de periode 2010-2020”. In: TNO (2009).

[21] J.H.J. Hulskotte. “Modules voor sluis- en lig-emissies voor BIVAS”. In: TNO (2011).

[22] J.H.J. Hulskotte and E. Bolt. “EMS-protocol Emissies door binnenvaart: verbrandingsmotoren, version 4, 15 December”. In: Taakgroep Verkeer en Vervoer (in Dutch) (2012).

[23] O.C. Koedijk. “„Richtlijnen Vaarwegen 2020“”. In: Rijkswaterstaat (2020).

[24] N.E. Ligterink. “Emissiefactoren wegverkeer - Actualisatie 2019”. In: TNO (2019).

[25] MAN Energy Solutions. Basic principles of ship propulsion. 2018.

[26] Ministerie van Economische Zaken en Klimaat. "„Klimaatakkoord"". In: (2019).

[27] Ministerie van Infrastructuur en Waterstaat. Van Nieuwenhuizen: Miljoenenimpuls duurzame binnenvaart. Accessed at 19-2-2021, from https://www.rijksoverheid.nl/actueel/nieuws/2021/01/29/van-nieuwenhuizen-miljoenenimpuls-duurzame-binnenvaart. 2021.

[28] Natura2000. Natura-2000 gebieden. Accessed at 1-2-2021, from https://www.natura2000.nl/gebieden. 2020.

[29] NetworkX. Software for complex networks. Accessed at 09-01-2021, from https://networkx.org/documentation/stable/index.html. 2020.

[30] Pierre-Jean Pompée. "About modelling inland vessels resistance and propulsion and interaction vessel-waterway: Key parameters driving restricted/shallow water effects". In: Proceeding of Smart Rivers 2015 (2015).

[31] Jacques Resing. "Discrete-Event Simulation". In: Eindhoven University of Teechnology (2013).

[32] Rijksoverheid. Werken aan een schone binnenvaart. Accessed at 1-12-2020, from https://www.rijksoverheid.nl/onderwerp en-havens/verduurzaming-scheepvaart-en-havens/werken-aan-een-schone-binnenvaart. 2020.

[33] Rijkswaterstaat. "„Scheepvaartinformatie hoofdvaarwegen"". In: Ministerie van Verkeer en Waterstaat (2009).

[34] Rijkswaterstaat. Bathymetry Nederland. Accessed at 18-2-2021, from https://maps.rijkswaterstaat.nl/geoweb55/index.html?viewer=Bathymetrie$_Nederland$. 2021.

[35] Rijkswaterstaat. BIVAS applicatie: emissies. Accessed at 06-02-2021, from https://bivas.chartasoftware.com/Home/BIVASApplicatie/Documentatie/Emissies/. 2021.

[36] Rijkswaterstaat. Verkeersinformatie: AIS. Accessed at 14-12-2020, from https://www.rijkswaterstaat.nl/zakelijk/verkeersmanagement/scheepvaart/scheepvaartverkeersbegeleiding/river-information-services/automatic-identification-system/index.aspx. 2014.

[37] Rijkswaterstaat. Waterhoogte t.o.v. NAP. Accessed at 18-2-2021, from https://waterinfo.rws.nl/!/kaart/waterhoogte-t-o-v-nap/. 2021.

[38] RIVM. AERIUS, rekeninstrument voor de leefomgeving. Accessed at 06-02-2021, from https://www.aerius.nl/nl/factsheets/emissieberekening-binnenvaartschepen/16-09-2019. 2019.

[39] RIVM. Stikstof - Stikstofoxiden (NO_x). Accessed at 5-8-2020, from https://www.rivm.nl/stikstof/stikstofoxiden-nox.

[40] Royal HaskoningDHV. iReport: Gebiedsfoto Rotterdam-Antwerpen. Accessed at 28-10-2020, from http://rhk.maps.arcgis.com/apps/MapSeries/index.html?appid=15b6c016adeb4f359fdeaf378dc5b6cb. 2018.

[41] G.K. Saha and A.K. Sarker. "Optimization of ship hull parameter of inland vessel with respect to regression based resistance analysis". In: Proceedings of MARTEC–The International Conference of Marine Technology. 2010.

[42] E. Sarris. "Naval Ship Propulsion and Electric Power Systems Selection for Optimal Fuel Consumption". In: Hellenic Naval Academy (2003).

[43] H. Tijms. "OPtimalisatie in Netwerken". In: Afdeling Econometrie Operationale Research, VU Amsterdam (2008).

[44] D. Toscano and F. Murena. "Atmospheric ship emissions in ports: A review. Correlation with data of ship traffic". In: Atmospheric Environment: X 4 (2019), p. 100050.

[45] United States Naval Academy. United States Naval Academy - Course 'Principles of Ship Performance' - Lecture Notes Ch7 - Resistance and Powering of Ships. Accessed at 21-7-2020, from https://www.usna.edu/NAOE/academics/en400.php.

[46] Vaarweginformatie.nl. "Vaarwegen en objecten". In: (2020).

[47] T. van Terwisga. "„Weerstand en voortstuwing van bakken, een literatuurstudie"". In: Maritime Research Institute Netherlands, Wageningen (1989).

[48] L.M.J. Vehmeijer. "Measures for the reduction of CO_2 emissions, by the inland shipping fleet, on the Rotterdam-Antwerp corridor". In: TU Delft (2019).

[49] Vessel Tracking and Tracing Expert Group. "„Guidelines on the Installation of the Inland Automatic Identification System (Inland AIS)"". In: (2014).

[50] D.G.M. Watson. Practical ship design. Vol. 1. Elsevier, 1998.

[51] Q. Zeng et al. “A modification of the ITTC57 correlation line for shallow water”. In: Journal of Marine Science and Technology 24.2 (2018), pp. 642–657.